AFRL-RQ-WP-TR-2012-0280

AIR VEHICLE INTEGRATION AND TECHNOLOGY RESEARCH (AVIATR)

Delivery Order 0023: Predictive Capability for Hypersonic Structural Response and Life Prediction: Phase II - Detailed Design of Hypersonic Cruise Vehicle Hot-Structure

Brian Zuchowski

Lockheed Martin Aeronautics Company
Lockheed Martin Corporation

MAY 2012
Final Report

AIR FORCE RESEARCH LABORATORY
AEROSPACE SYSTEMS DIRECTORATE
WRIGHT-PATTERSON AIR FORCE BASE, OH 45433-7542
AIR FORCE MATERIEL COMMAND
UNITED STATES AIR FORCE

NOTICE AND SIGNATURE PAGE

Using Government drawings, specifications, or other data included in this document for any purpose other than Government procurement does not in any way obligate the U.S. Government. The fact that the Government formulated or supplied the drawings, specifications, or other data does not license the holder or any other person or corporation; or convey any rights or permission to manufacture, use, or sell any patented invention that may relate to them.

This report was cleared for public release by the USAF 88th Air Base Wing (88 ABW) Public Affairs Office (PAO) and is available to the general public, including foreign nationals.

Copies may be obtained from the Defense Technical Information Center (DTIC) (http://www.dtic.mil).

AFRL-RQ-WP-TR-2012-0280 HAS BEEN REVIEWED AND IS APPROVED FOR PUBLICATION IN ACCORDANCE WITH ASSIGNED DISTRIBUTION STATEMENT.

*//Signature//

THOMAS G. EASON
Project Engineer
Sustainable Structures Branch
Structures Division

//Signature//

MICHAEL P. CAMDEN, Acting Chief
Sustainable Structures Branch
Structures Division

//Signature//

DAVID M. PRATT, Technical Advisor
Structures Division
Aerospace Systems Directorate

This report is published in the interest of scientific and technical information exchange, and its publication does not constitute the Government's approval or disapproval of its ideas or findings.

*Disseminated copies will show "//Signature//" stamped or typed above the signature blocks.

REPORT DOCUMENTATION PAGE

Form Approved
OMB No. 0704-0188

1. REPORT DATE *(DD-MM-YY)*	2. REPORT TYPE	3. DATES COVERED *(From - To)*
May 2012	Final	18 August 2010 – 29 February 2012

4. TITLE AND SUBTITLE
AIR VEHICLE INTEGRATION AND TECHNOLOGY RESEARCH (AVIATR)
Delivery Order 0023: Predictive Capability for Hypersonic Structural Response and Life Prediction: Phase II - Detailed Design of Hypersonic Cruise Vehicle Hot-Structure

5a. CONTRACT NUMBER
FA8650-08-D-3858-0023

5b. GRANT NUMBER

5c. PROGRAM ELEMENT NUMBER
62201F

6. AUTHOR(S)
Brian Zuchowski

5d. PROJECT NUMBER
2401

5e. TASK NUMBER
N/A

5f. WORK UNIT NUMBER
Q03Y

7. PERFORMING ORGANIZATION NAME(S) AND ADDRESS(ES)
Lockheed Martin Aeronautics Company
Lockheed Martin Corporation
1011 Lockheed Way
Palmdale, CA 93599

8. PERFORMING ORGANIZATION REPORT NUMBER

9. SPONSORING/MONITORING AGENCY NAME(S) AND ADDRESS(ES)
Air Force Research Laboratory
Aerospace Systems Directorate
Wright-Patterson Air Force Base, OH 45433-7542
Air Force Materiel Command
United States Air Force

10. SPONSORING/MONITORING AGENCY ACRONYM(S)
AFRL/RQSS

11. SPONSORING/MONITORING AGENCY REPORT NUMBER(S)
AFRL-RQ-WP-TR-2012-0280

12. DISTRIBUTION/AVAILABILITY STATEMENT
Approved for public release; distribution unlimited.

13. SUPPLEMENTARY NOTES
PA Case Number: 88ABW-2012-4769; Clearance Date: 06 Sep 2012. This report contains color.

14. ABSTRACT
Structural design of hypersonic vehicles requires additional considerations and effort, relative to conventional subsonic and low-supersonic aircraft, because of the wide Mach number range and the associated heating effects at high Mach numbers. At high temperatures, conventional structural materials, such as metals, suffer from reduced strength, reduced stiffness, increased creep, increased oxidation, increased thermal stresses, and other detrimental effects that impact structural design; many of these effects are of limited concern for aircraft with more conventional Mach number range and so hypersonic vehicles require a different approach to structural design. Four panels of a representative hypersonic cruise vehicle with state-of-the-art standard methods and tools to verify structural response and life predictive capabilities.

15. SUBJECT TERMS
hypersonic performance, predictive capability, hypersonic service life, hypersonic simulation, coupled analyses, hypersonic environment, structural testing, combined environments, thermal analysis, stress analysis, acoustic analysis, flutter, fatigue,, thermal loads

16. SECURITY CLASSIFICATION OF:			17. LIMITATION OF ABSTRACT:	18. NUMBER OF PAGES	19a. NAME OF RESPONSIBLE PERSON (Monitor)
a. REPORT	b. ABSTRACT	c. THIS PAGE			Thomas G. Eason
Unclassified	Unclassified	Unclassified	SAR	198	19b. TELEPHONE NUMBER *(Include Area Code)* N/A

TABLE OF CONTENTS

LIST OF FIGURES

LIST OF TABLES

1.0 EXECUTIVE SUMMARY

This document describes the results of the Phase II Hypersonic Predictive Capability – Detailed Design of Hypersonic Vehicle Hot-Structure effort as administered by the Air Force Research Lab (AFRL) as part of their efforts with the Midwest Structural Sciences Center (MSSC).

The AFRL is interested in developing a technology base for the future design of reusable long duration cruise hypersonic aircraft. Such aircraft will likely possess gross takeoff weight magnitudes over 300,000 pounds, fly without re-fueling for over 2000 nautical miles, and cruise at speeds between Mach 5-7 (M5-7). These speeds will subject skin surface structures to temperatures over 1000°F for the majority of the anticipated multi-hundred to thousands of hours of service life of the aircraft. To meet these requirements and be viable, the vehicle structure must be able to have accurate service life prediction capability methods in place in ensuring mission reliability, maintainability, and viability, along with an overall guide to reduced structural mass fraction. These issues must be fully addressed before a M5-7 Hypersonic Cruise Vehicle (HCV) becomes a reality. Today, new standards and criteria are being established in the areas of service life predictability to meet the flight performance requirements of future AFRL programs.

The overall objective of this Phase II program is to build upon the efforts of the Phase I program in order to continue to identify gaps in structural analysis and life prediction methods as applied to reusable, integrated structures for sustained operations in a hypersonic environment. The charter of the Phase II program is to exploit these gaps through detailed design and analyses exercises on four individual zones of a conceptual M5-7 Hypersonic Cruise Vehicle (HCV) that meet the objectives of the analyses areas that the Air Force is focused upon. The objectives of this report are to address the products of the Phase II effort:

1. Provide the background on the flight environments that the individual panel designs will be designed for structural integrity against.
2. Provide a detailed review of the individual vehicle study area screening phase, preliminary design phase, and critical design phase tasks in the design of the four individual panels during the course of the Phase II program.
3. Provide recommendations for testing and draft test plans for the Phase II delivered panel designs in the Phase III program.

2.0 INTRODUCTION

2.1 BRIEF RE-CAP OF PHASE I PROJECT

The Phase I Hypersonic Predictive Capability – Identification of Knowledge Gaps program delivered a Lockheed Martin (LM) generated report (Ref. 1) which provided a review of critical gaps in structural analysis and life prediction methods that had been identified. Major re-useable hypersonic vehicle programs were researched. Areas where state-of-the-art methods are incapable of predicting the response and life of structure were identified. Uncertainties due to predictive capabilities have been major issues that affected the success or failure of hypersonic programs.

As a brief review the Phase I results, strength sizing of hypersonic vehicles requires the inclusion of temperature as that additional critical variable. At high Mach numbers, aerodynamic and propulsion limitations restrict the maneuverability of hypersonic aircraft and increasing Mach number radically reduces the aerodynamic efficiency of wings. In turn, the external loads on the airframe are reduced but because of the higher temperatures, which also reduces the strength of conventional structural materials, it is unclear as to which of these loading conditions actually size the structure. A further complication is the fact that for many materials the yield and ultimate strength vary differently with temperature, so both limit and ultimate loading conditions, which correspond respectively to yield and ultimate material strengths, require consideration.

As determined through the course of the Phase II program, the most important heat transfer problem in flight at high supersonic and hypersonic speeds is that of determining skin temperature magnitudes since the skin temperatures will normally be the boundary condition for internal heat transfer problems. Not only is the skin temperature influenced by such external conditions as radiation from other surfaces and solar heat load but by such internal factors as conduction through structures, convection to fuel and gases, radiation to fuel and structure, and transient effects.

In addition, as the vehicle design Mach number increases to the hypersonic range, that above Mach 5.0, new physical phenomena become progressively of greater importance to the hypersonic airframe structural analysts, making hypersonic flow much more complex than supersonic flow. These phenomena include: 1) fluid dynamics effects that limit the validity of boundary-layer approximations, and 2) high-temperature effects that introduce chemical reactions with the structure.

2.2 PRE-PHASE II TASKS COMPLETED DURING PHASE I

During the latter stages of the Phase I program LM Aero investigated the usage of the DARPA Falcon program developed HTV-3X loft (***Figure 2.2.1***) for its translation into an operational vehicle, the Hypersonic Cruise Vehicle (HCV), capable of carrying adequate fuel load for the target of at least a 30 minute cruise profile. The vehicle geometry was arrived at by "growing" the HTV-3X loft and generating a flight trajectory to meet this cruise profile.

The trajectory development for the HCV was completed during the latter phases of the Phase I program in preparation for the Phase II program. The Phase II program premise was to investigate a vehicle that was capable of a sustained cruise level of Mach 5+ for a period of at least 30 minutes in order to achieve its operational range requirement. Concurrent with this effort was an LM Aero program entitled HSMAR (or High Speed Mission Analysis Research) that studied the loft of such a Mach 5+ cruise vehicle.

Figure 2.2.1 DARPA Falcon Program HTV-3X Vehicle

The trajectory of the HTV-3X vehicle followed that of a steady climb to Mach 6.0 with a brief one minute cruise at Mach 6.0 followed by powered descent. With the completion of the HCV trajectory generation the cruise phase arrived at per the trajectory resulted in 46 minutes of cruise at a sustained velocity of Mach 5.2 which met the vehicle requirements, with the associated environments, for the Phase II study. The HCV resulted, for the given propulsion system, in a 378,413 lb. Take Off Gross Weight (TOGW) vehicle that could take off, climb to 90,000 feet and cruise at Mach 5.2 for 46 minutes, descend, and land. The nominal landing weight was 180,484 lb. with an assumed 5% fuel reserve at touchdown. At a maximum cruise velocity of Mach 5.2 the radiation temperature maps developed resulted in temperature levels that could possibly employ the use of Titanium alloys for Outer Mold Line (OML) hot skin structure.

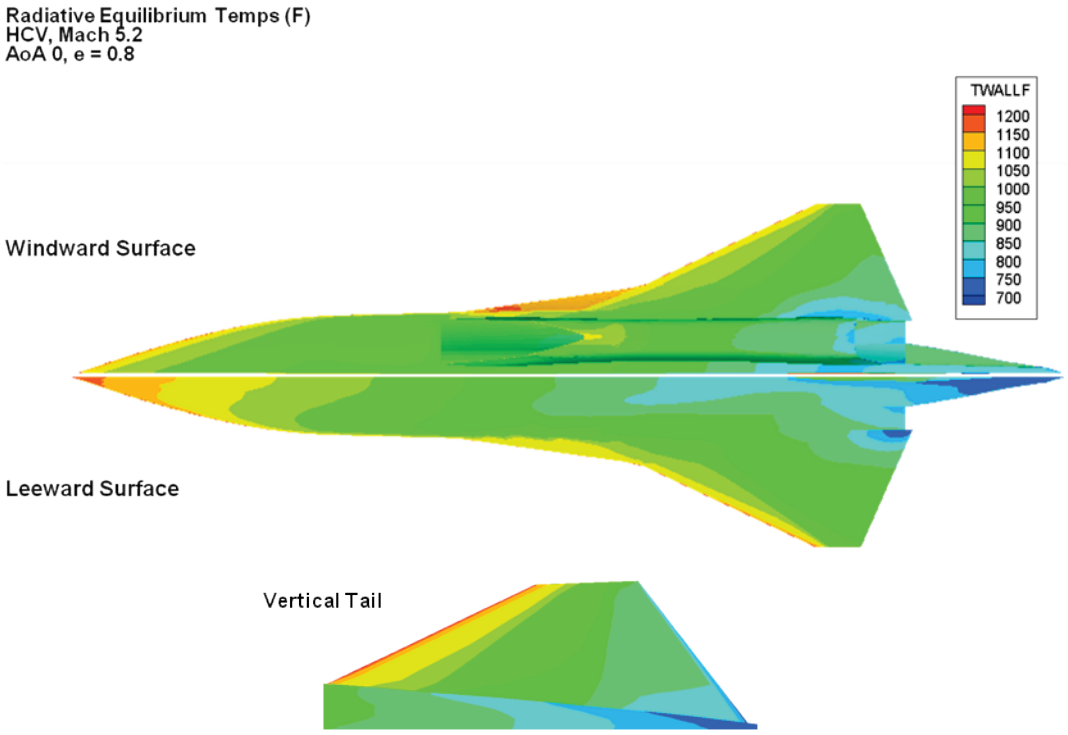

Figure 2.2.2 HCV Radiation Equilibrium Temperature (RET) Map at Mach 5.2 Cruise Condition

In meeting these requirements while "scaling up" the HTV-3X loft into the HCV it was decided to retain the HTV-3X propulsion layout of a "four over two" propulsion system, that being a propulsion flow path design of four turbine engines over two inward turning scramjets. As the study of the OML panels was the target of the program's scope, this linear scaling of the vehicle's

propulsion system was viewed to have no impact on the overall vehicle outer skin environment. In addition, the LM Aero team decided to, in the course of scaling up the complex fuel tank design, design a centerline structural bulkhead for the revised fuel tank design as the HTV-3X demonstration program's conceptual level fuel tank truss design had not been adequately analyzed by the time of the HTV-3X program cessation in late 2008.

The initial structural design requirements for the HTV-3X specified an airframe capable of withstanding the higher extreme temperatures of Mach 6.0 flight, as that vehicle was primarily designed for propulsion demonstration purposes, which were calculated to range up to 1400ºF for the forward fuselage and tail leading edge structure. Structural trades performed during the HTV-3X conceptual design phase focused on selecting the lightest weight and most cost-effective material capable of withstanding these temperatures, with candidate materials including various stainless steel alloys, titanium alloys, and nickel-based alloys such as Inconel as well as cobalt based alloys such as in the Haynes family of materials. High temperature composite materials were also considered in the initial stages of these trades, but were rejected due to high development and manufacturing costs that could not be incurred within the schedule of that program.

The HCV flight regime, designed for the Mach 5.2 cruise condition as opposed to the Mach 6.0 design of the demonstrator vehicle, was a platform affording an increased number of hot structure options as its acreage temperatures primarily centered around 1000ºF as opposed to the higher temperature requirements of Mach 6.0 flight, as illustrated in ***Figures 2.2.2 and 2.2.3***.

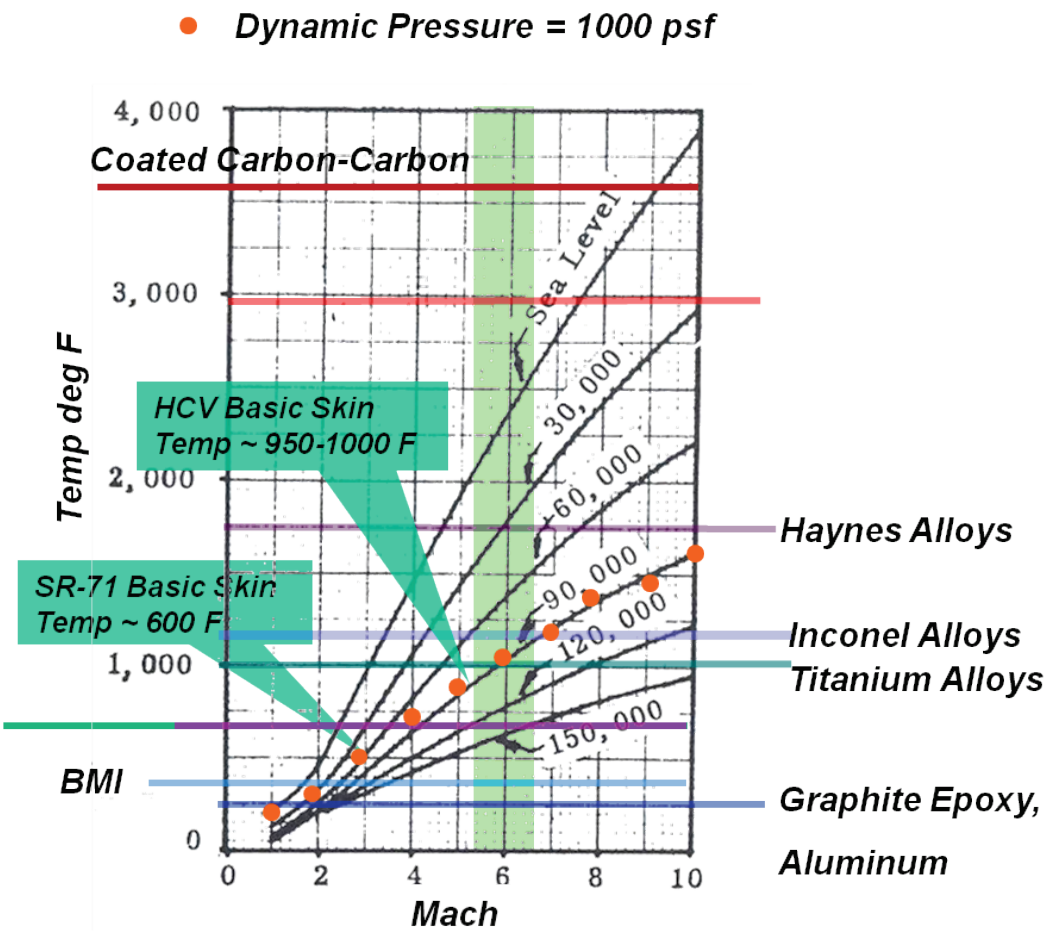

Figure 2.2.3 Generalized Mach vs. Temperature Range

2.3 INITIAL PANEL SELECTION FOR PHASE II STUDY

During the course of the Falcon program the structural design of the HTV-3X Demonstration Vehicle presented several unique challenges, largely related to the temperatures and pressures associated with the high supersonic and hypersonic environments, which carried over to the study of the HCV.

A challenging element of the HTV-3X structural analysis effort, as well as the HCV structural analysis of the Phase II program, involved accurately predicting the thermal stresses resulting from temperature gradients within the airframe structure. The primary sources of these temperature gradients were two-fold; the non-uniform nature of the aerodynamic and propulsion system heating, for example leading edge and engine bay structure being generally hotter than other areas, combined with the cooling effect of fuel that was in close proximity to the fuselage structure. Fuselage structure in contact with fuel maintained a relatively lower temperature as compared to the non-fuel areas that reached maximum temperatures of 700°F and greater. In addition, these thermal gradients and resulting thermal stresses were time-dependent, as illustrated in ***Figure 2.3.1***.

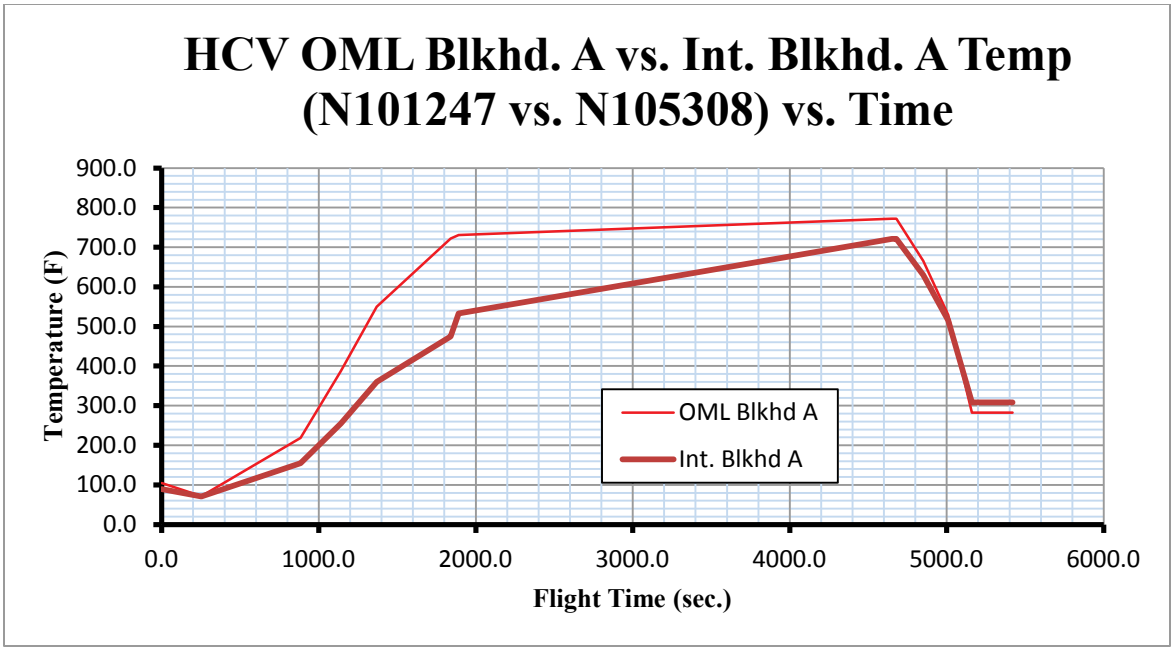

Figure 2.3.1 HCV OML Point Over Internal Bulkhead vs. Fuel Laden Internal Point Temperature vs. Flight Time

Temperature differences within the HCV structure resulted in thermally induced loads and stresses as shown in Figure 2.3.1. In this example, the hot "dry" skins of the mid-body try to expand but are constrained by cooler fuel floor and "wet" skins. This condition results in a force fight between the different structures as they strive to reach a state of strain equilibrium, with compression loads in the hotter structure and tension loads in the cooler structure.

To meet the scope and goals of the Phase II panel study the panel selection process followed a review of the outer skin environment investigated during the HTV-3X program which was suitable as a screening method for the selection of the HCV panels. For the selection of each of the four panels two candidate panels in each of the four vehicle study zones were selected for screening.

Panel 1

The study goal for the Panel 1 design and analysis effort was to investigate a vehicle region where material property changes and aero-acoustic/high frequency fluctuating pressures resulting from turbulent separated flow and shock-interaction were of primary concern. The first area investigated in order to meet this panel study goal centered around the HCV nozzle/fuselage exhaust washed areas due to the effects of heavily driven thermal loading from exhaust as well as aero induced effects as well as an estimated 169db OASPL acoustic field. Two candidate panels from this particular vehicle zone were screened for suitability within this investigation, as illustrated in ***Figure 2.3.2***. Panel stress levels (***Figure 2.3.3***) were compared and Panel 1A was first down-selected as it was closer to the plume impingement effects that would trigger higher instabilities in flow.

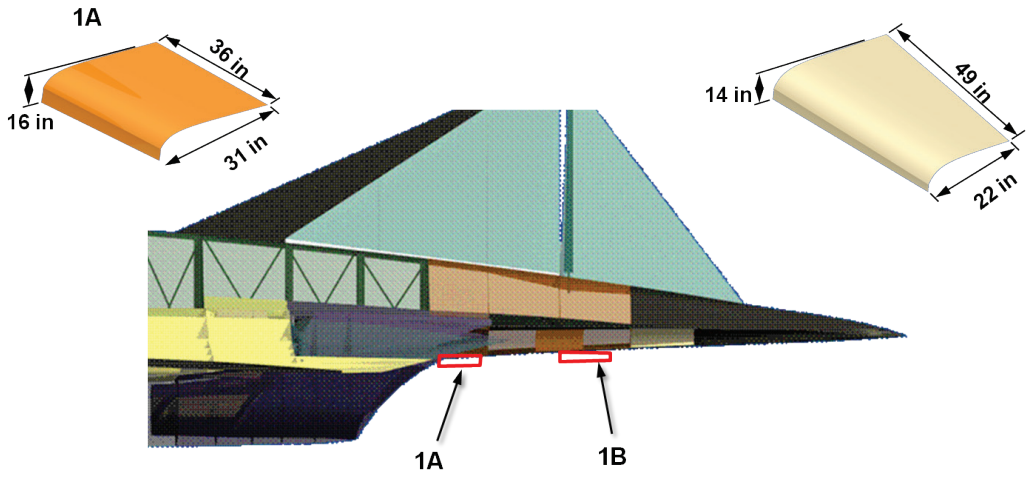

Figure 2.3.2 Panel 1 Initial Areas Investigated

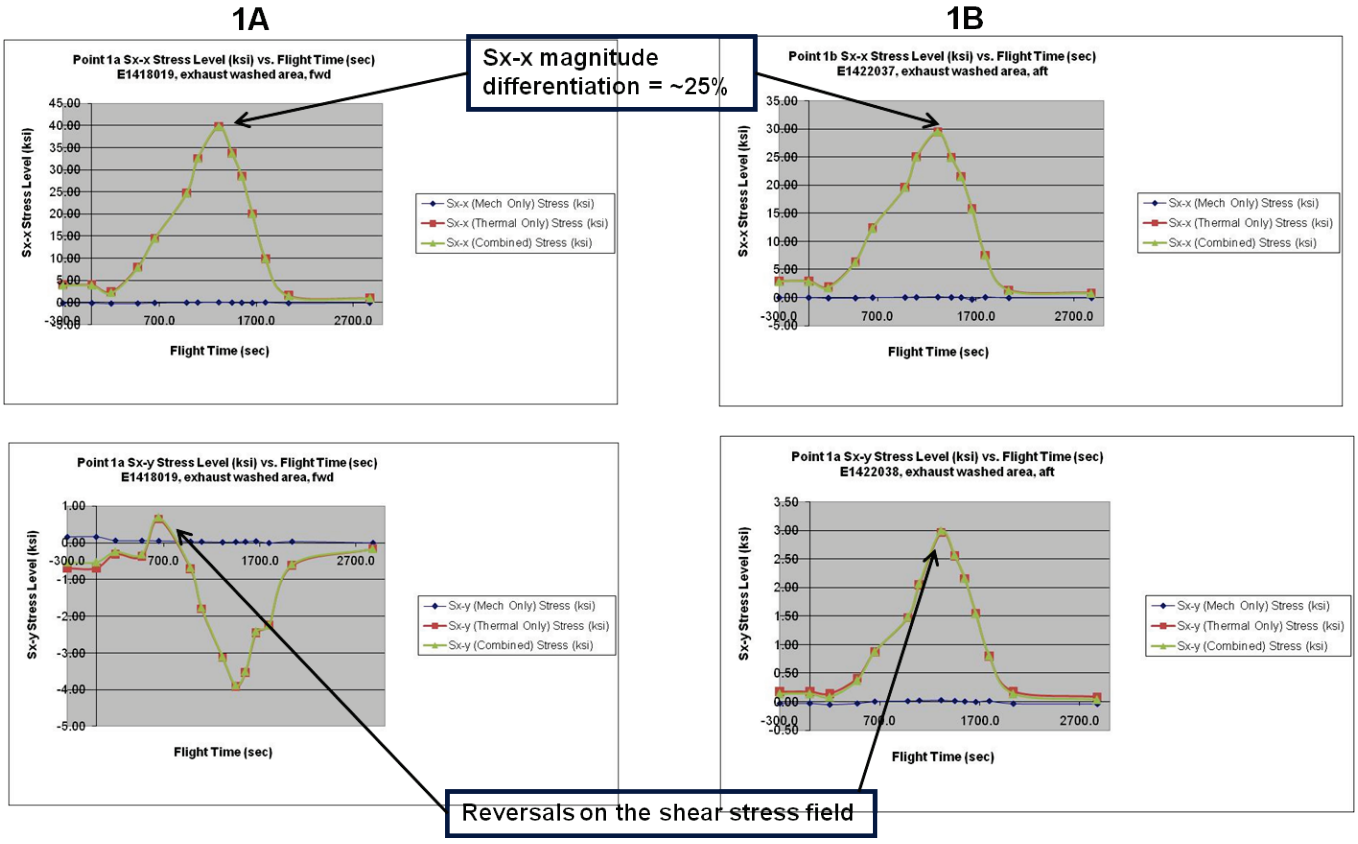

Figure 2.3.3 Panel 1A and 1B Stress Level vs. Flight Time Screening

Upon further investigation the LM Aero team felt that a vehicle study zone that would lend itself more readily to the goals of the panel 1 study would center upon a panel at the base root of the vertical tail, where shock effects from the vertical tail and rudder cove joint, as well as from control surface movement, would be triggered, as shown in ***Figures 2.3.4 and 2.3.5***.

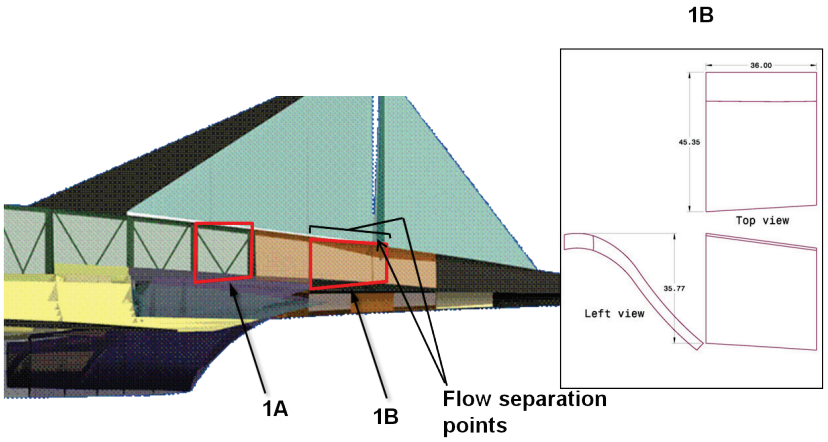

Figure 2.3.4 Revised Panel 1 Areas Investigated

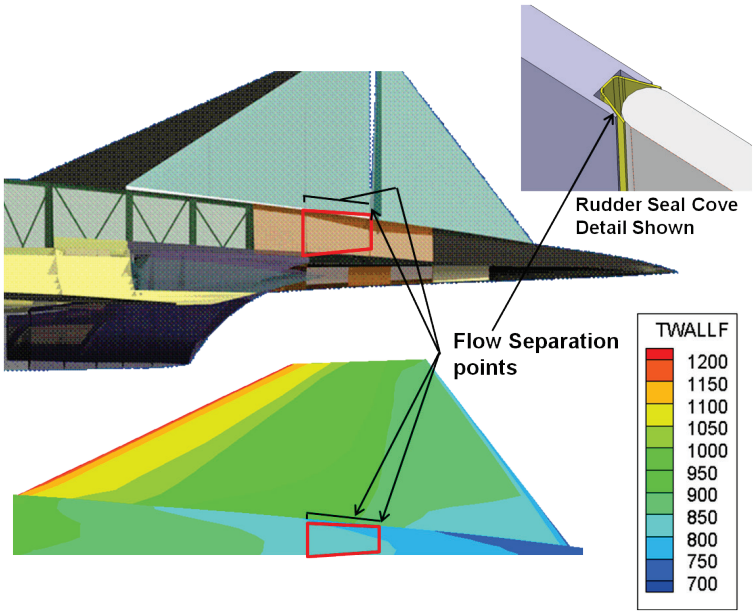

Figure 2.3.5 Panel 1B Area Investigated

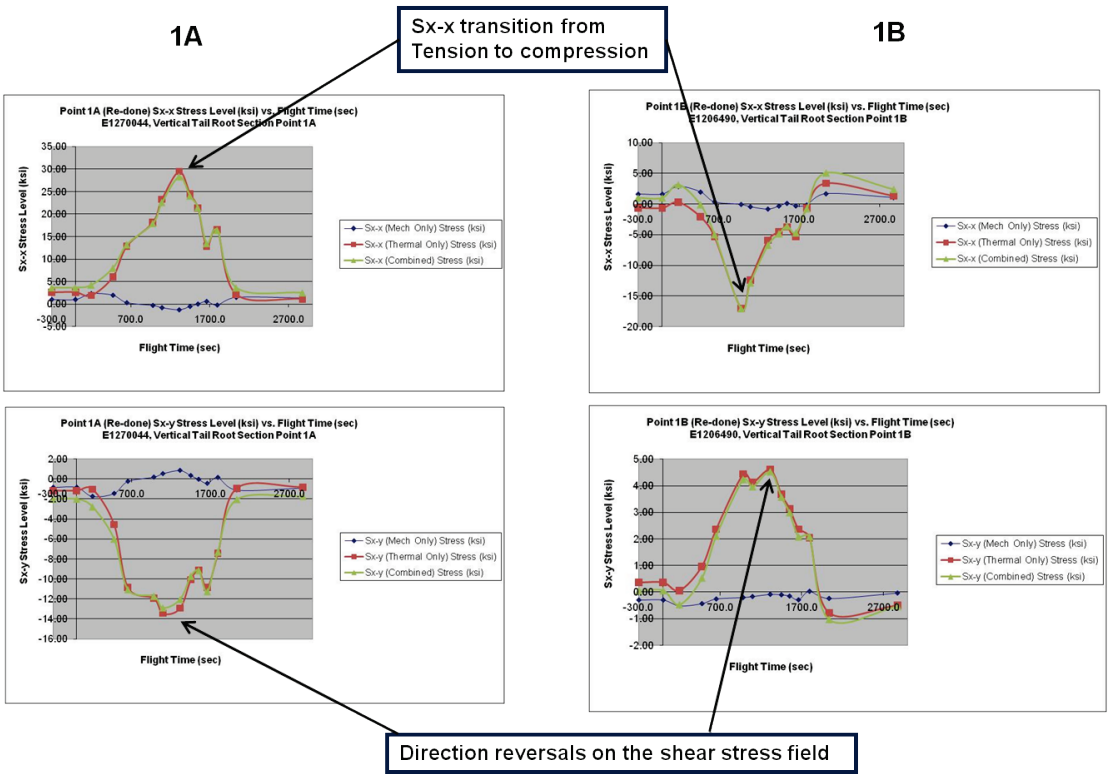

Figure 2.3.6 Revised Panels 1A and 1B Stress Levels vs. Flight Time Screening

Subsequently, Panel 1B was down-selected from the screening process as it was observed to be subjected to stronger thermal field contributions due to fuel burn-down. More importantly, the flow transition around the vertical tail to aft fuselage joint and rudder cove will have a very high level of complexity.

Panel 2

The study goal for the Panel 2 design and analysis effort was to investigate a vehicle region where transient, quasi-static thermal and mechanical loading and material property changes drive the design.

For this study area the mid-body fuselage areas centering upon the thermal fluctuations stimulated by fuel burn down were screened, as illustrated in ***Figure 2.3.7***.

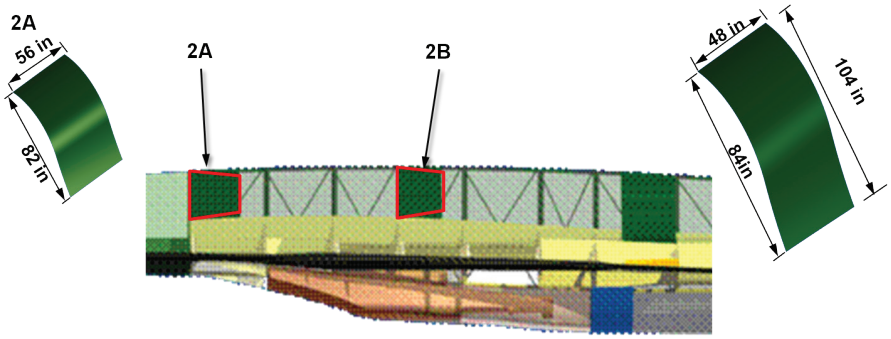

Figure 2.3.7 Panel 2 Vehicle Areas Investigated

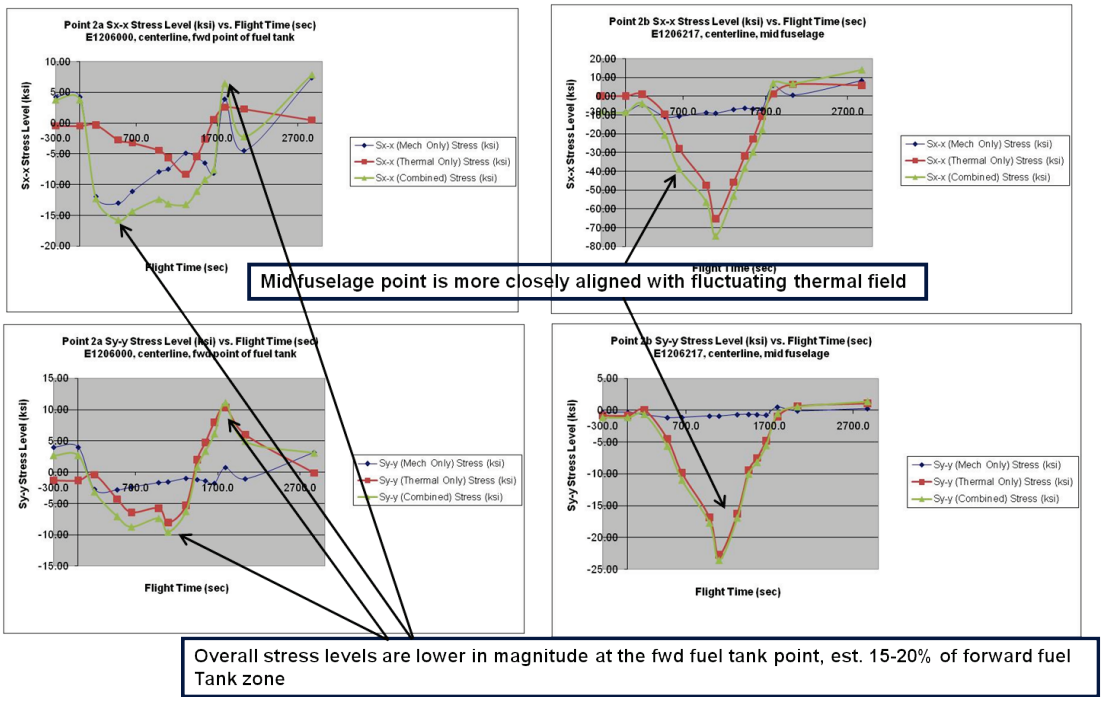

Figure 2.3.8 Panels 2A and 2B Stress Levels vs. Flight Time Screening

Upon review of the results shown in ***Figure 2.3.8*** it is evident that the mid-fuselage Panel 2B overall stress levels show closer correlation to the thermal stress activity from fuel tank, and thermal sink, effects, as these mid-fuselage Panel 2B point stress magnitudes are roughly 80-85% higher than at the fwd fuel tank location, Panel 2A. In addition, the larger Panel 2B will be associated with complexity if testing evaluations are conducted. Upon these reasons, Panel 2B was selected for the Phase II study area.

Panel 3

The study goal for the Panel 3 design and analysis effort was targeted toward a vehicle region where a combination of high dynamic pressure, thermally induced stress, and material property change cause aero-elastic stability to be of primary concern. For this study area the areas just aft of the wing leading edge, that being relatively flat skin structure, were investigated as to their posing a high chance of aero-elastic instability, or panel flutter, condition. Two vehicle areas were looked

at for the goal of this panel study as illustrated in ***Figure 2.3.9***. The results of the panel stress levels as screened are illustrated in ***Figure 2.3.8.***

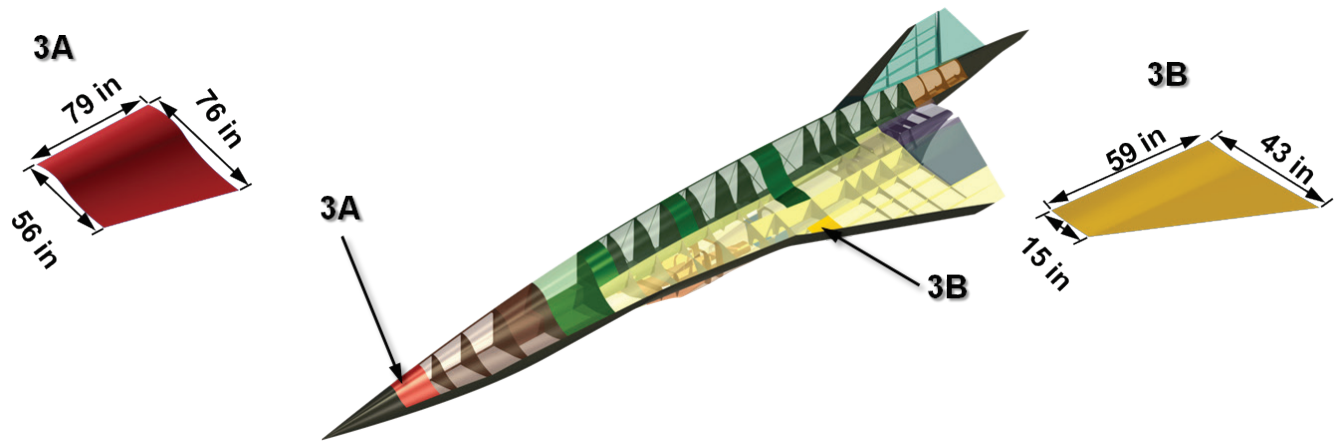

Figure 2.3.9 Panel 3 Vehicle Areas Investigated

Upon review of the results of the panel stress levels as screened, Figure 2.3.10, it was thought that the temperature induced stability value magnitude change on the upper wing surface will most likely be of high concern for aero-elastic stability due to its relative "flatness" as compared to the forward chine zone. In addition, the strength sizing of the wing section will drive toward thin gauge but aero-elastic stability might drive it toward a thicker section, more stiffeners, a combination, etc. The fwd chine zone, Panel 3A, with its inherent 2-D curvature, will be somewhat stiffer based on its OML geometry alone. The overall Sx-x, Sy-y, and Sx-y stress levels were comparable between the two zones but with more positive and negative fluctuation observed in Panel 3B. With these considerations taken into account Panel 3B was down-selected for the Panel 3 study.

At this time the baseline concept for the Panel 3 hot structure was for a thin gauge multi-stiffener approach. However, as the study phase progressed the Panel 3 hot structure concept evolved into a honeycomb structure upon the results of a structure trade study in the preliminary design phase of the program, which is discussed in Section 5.4 of this report.

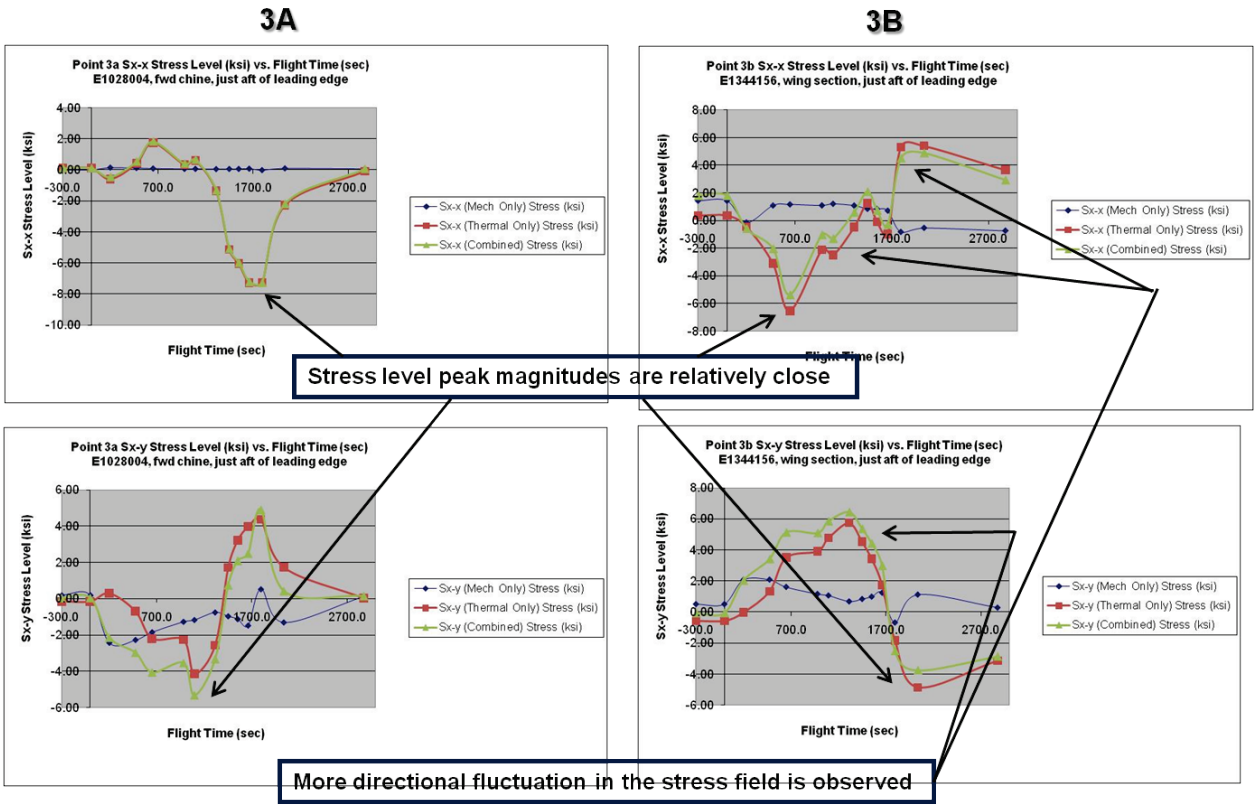

Figure 2.3.10 Panels 3A and 3B Stress Levels vs. Flight Time Screening

Panel 4

The study goal for the Panel 4 design and analysis effort was targeted toward a vehicle region where the combination of all extreme-environments (aero-elastic loading, material property change, thermally induced stress, mechanical loading) were anticipated to drive the design. For this Panel 4 study area the engine shroud, or fairing, in very close proximity (approximately 2" away from the scramjet walls at a number of clearance points) to the scramjet engines with their excessively high acoustic energy distribution around this hot structure, was investigated, as illustrated in ***Figure 2.3.11***. In addition, an area aft of the fairing, that being in the exhaust washed zone of the vehicle similar to the Panel 1 study, was also investigated.

The engine fairing baseline design for the HTV-3X, as well as the HCV, was metallic honeycomb sandwich as opposed to a skin stringer or isogrid structure due to lack of allowable clearance between the lower engine and the OML requirement. This vehicle area will witness heavy acoustic field effects and upon the HTV-3X program studies, magnitudes forecasted ranged up to 172db OASPL. The mechanically induced stress magnitudes along the length of the fairing were generally consistent but due to those stress levels being dominated by transient thermal effects upon mode transition, which per the vehicle trajectory occurred at the Mach 2.5 vehicle velocity level, this structure was viewed with high criticality as one that needed to be understood. As a result, the Panel 4 selection was down-selected to a forward section of the scramjet engine fairing.

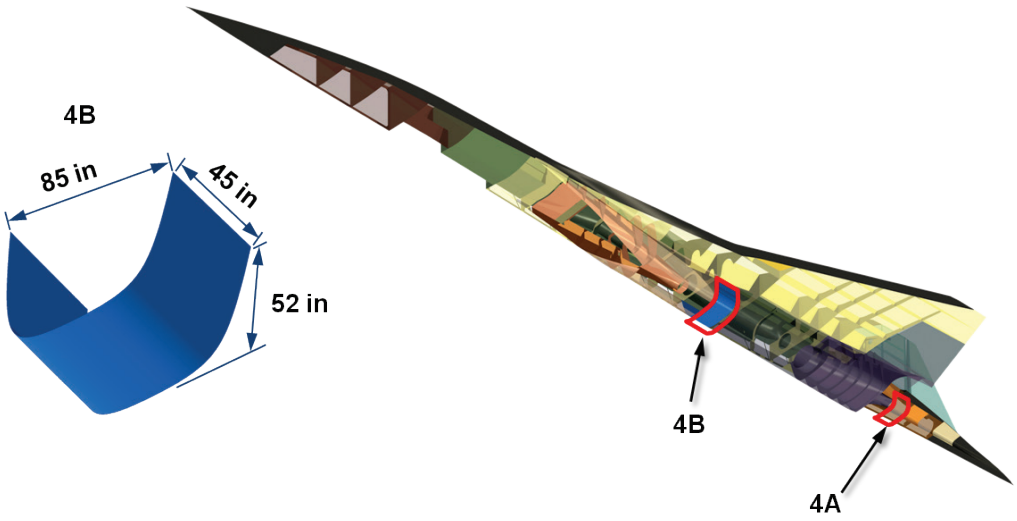

Figure 2.3.11 Panel 4 Vehicle Areas Investigated

3.0 FINAL SELECTION OF OML PANELS FOR STUDY

An illustration summarizing the four OML panels as down-selected for the Phase II is found in ***Figure 3.0.1***

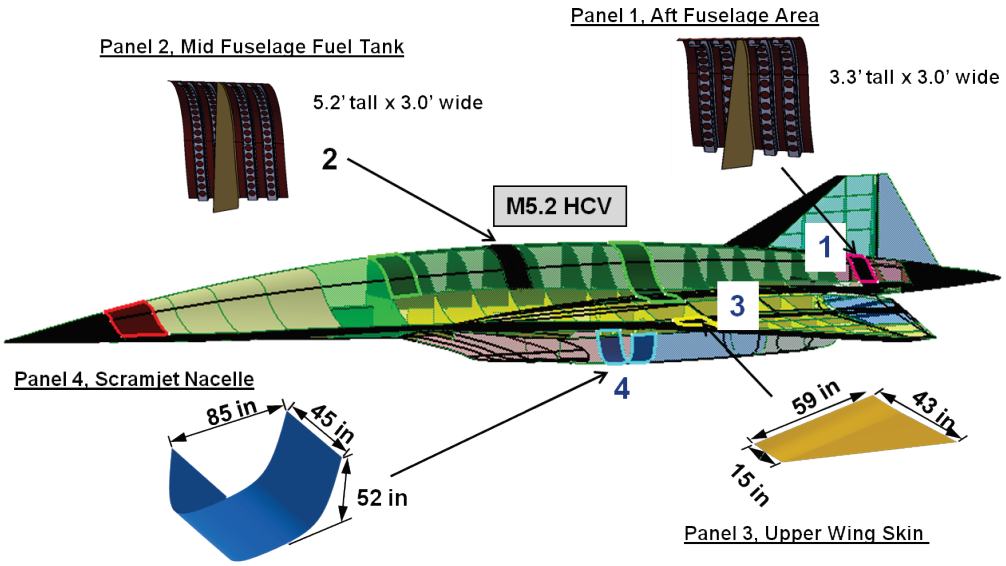

Figure 3.0.1 HCV OML Panels Down-Selected for Phase II Program

3.1 MATERIAL SELECTION

One of the fundamental structural trades performed during conceptual design of the HTV-3X vehicle involved selection of the airframe material. The material selection had far-reaching impacts on the subsequent design and fabrication approach that was to be employed on HTV-3X, and as a result, would have also greatly influenced the selection of vendors responsible for fabrication of airframe components. The most important parameter in the material selection process, during the course of the conceptual design phase, was the thermal environment to which the HTV-3X airframe would be exposed during high speed flight. As the HTV-3X vehicle was designed for demonstration flight up to Mach 6.0 material trades for an X-vehicle metallic alloy based hot structure airframe were conducted for the relatively short duration temperature 1000-1200ºF environments that were anticipated, and four material properties that were screened are illustrated in Figure 3.1.1. Data results shown were based upon Mil-HdBk data (Ref. 2) as well as LM Aero material testing. As mentioned previously, high temperature carbon fiber reinforced Ceramic (CMC) Matrix Composite materials were also considered in the initial stages of these trades, but were rejected due to high development and manufacturing costs that could not be incurred within the schedule of the program.

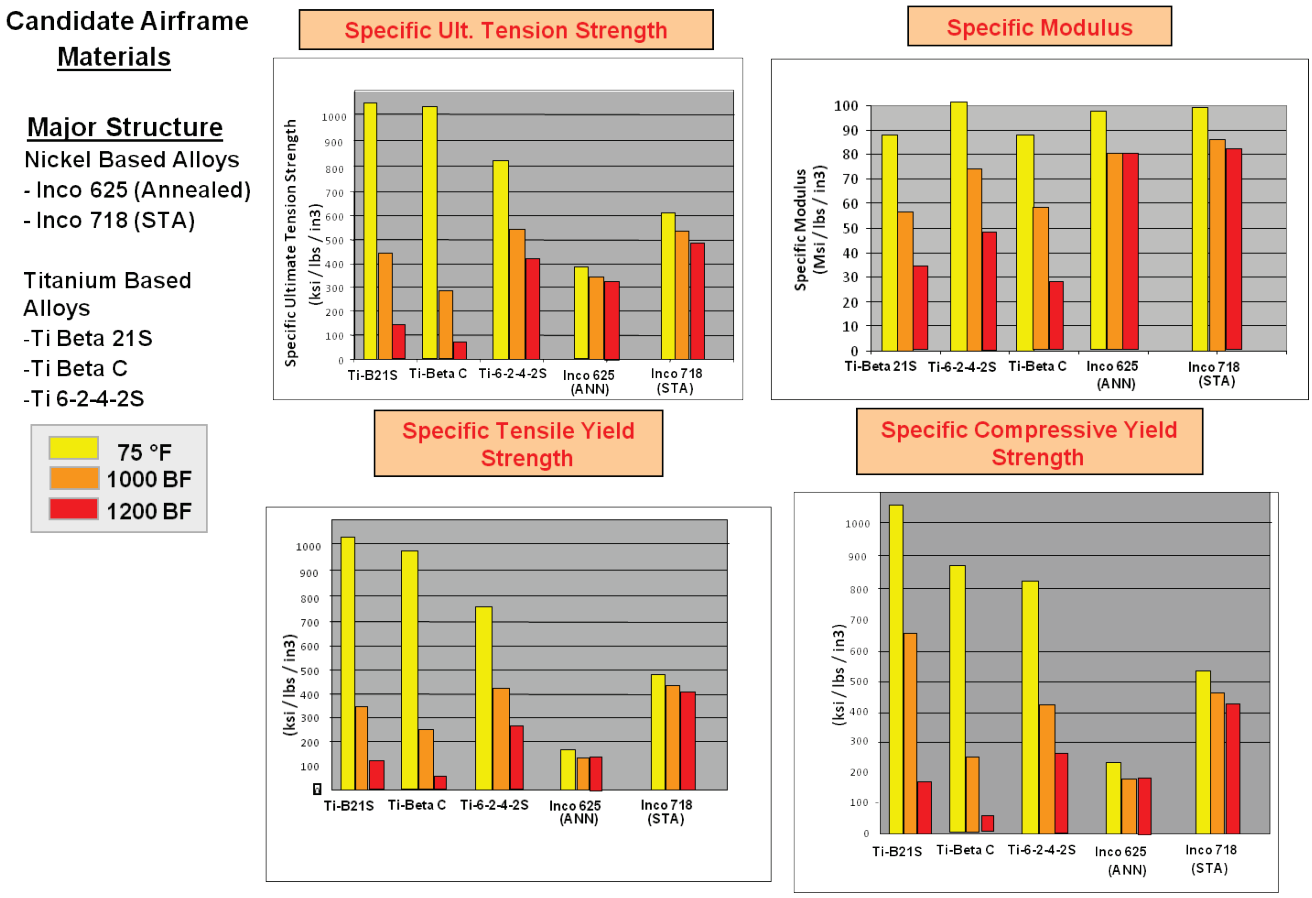

Figure 3.1.1 Metallic Alloy Screening for the Hypersonic Flight Environment

As per the HCV flight trajectory of Mach 5.2 max velocity, the environment is extremely harsh. At Mach 5 (approx. 3,700 mph) skin temperatures exceeding 1000°F are highly likely, as are cyclic thermal and mechanical loading all within a high sonic energy environment. These conditions pose high risks if structural materials are not up to the task. Materials must possess excellent strength-to-weight ratios for optimum weight savings, be thermally stable, oxidation resistant, and have the ability to endure extended times at temperature without creep deformation. Just as important materials must be producible, i.e., they must possess the ability to be formed, joined and assembled into adjacent structure cost effectively. An ever present "maxim" in the design of modern aircraft is that as needed materials become stronger, tougher and more thermally resistant for use in the particular design environment, they become more difficult to fabricate and assemble, and thus manufacturing costs become more exorbitant.

On a strength-to-weight basis (i.e. specific strength) only two alloy systems come to mind for metallic structural materials that could be used for the majority of the airframe design within this Mach 5.0+ environment, and that which can be readily supplied for panel construction within the next few years: titanium and nickel base alloys. Titanium alloys offer superior strength-to-weight ratios up to about 1000-1100°F. By and large the near-alpha titanium alloys possess the best high

temperature properties of any of the titanium alloy families (Table 3.1.1), as they possess excellent strength, crack growth, creep, thermal stability and oxidation resistance, and offer the lightest weight compared to alpha, alpha-beta, or beta titanium alloys. Additionally, titanium alloys are also producible through efficient structural design which also requires elevated temperature processing. As noted in the previous Phase I report (Ref.1), the Titanium 6-2-4-2S (with the "S" designation referring to the additional silicon content) alloy has seen service on the exhaust tailpipe of the U2 high altitude surveillance aircraft for the past 20 years without issue. This application sustains operating temperatures of 940°F and maintains a 10,000 hour service life.

Table 3.1.1 List of Near-Alpha Alloys in Consideration for Aircraft Structure

Alloy	Density	Year of	Max. Use Temp.		Chemical Composition, w/o							
	(lb/in^3)	Intro.	°C	°F	Al	Sn	Zr	Mo	Nb	V	Si	Other
Ti-811	0.158	1961	425	800	8			1		1		
IMI-679	0.175	1961	450	840	2	11	5	1			0.2	
Ti-6242	0.164	1967	450	840	6	2	4	2				
IMI-685	0.161	1969	520	970	6		5	0.5			0.25	
Ti-11	0.162	1972	540	1000	6	2	1.5	1			0.1	0.3Bi
Ti-6242S	0.164	1974	520	970	6	2	4	2			0.1	
IMI-829	0.164	1976	580	1080	5.5	3.5	3	0.3	1		0.3	
IMI-834	0.164	1984	590	1100	5.5	4	0.3	1			0.5	0.06C
Ti-1100	0.163	1987	590	1100	6	2.75	4	0.4			0.45	
Beta 21S	0.178	1988	590	1100	3			15	2.75		0.25	

Above the 1000-1100°F range of temperatures nickel based alloys, primarily INCONEL 718, or IN718, offer superior performance to about 1200°F. IN718 offers considerable advantage over other nickel and cobalt based alloys since it is precipitation harden-able. This ability allows for high strength levels, excellent modulus and ductility, good thermal stability, and good creep and oxidation resistance. IN718 is producible but the associated manufacturing and assembly costs are, arguably and per vendor, slightly higher than those for titanium manufacturing. In light of their excellent properties, ready availability, excellent service records, both titanium and nickel base alloys were considered the most viable and thus were base-lined at the onset of the preliminary design phase of this Phase II program study.

4.0 HTV-3X PROGRAM SUPPLIED DATA FOR HCV

As stated earlier, the DARPA Falcon HTV-3X program consisted of a very detailed conceptual design phase of a hypersonic platform for flight testing in the lower hypersonic (Mach 5.0 – 6.0) velocity range. These previous studies were able to provide a number of parameters, environments, and vehicle Finite Element Models (FEMs) that were utilized for the Phase II program.

4.1 HTV-3X STRUCTURAL MODEL SCALE-UP

In order to eventually create detailed sub-models of the four Phase II panels of interest, a full vehicle loads model was required to obtain the full picture of the load conditions at each panel location. A Patran/Nastran based loads model was previously created for the HTV-3X program (***Figure 4.1.1***), and this FEM was scaled up for the HCV study.

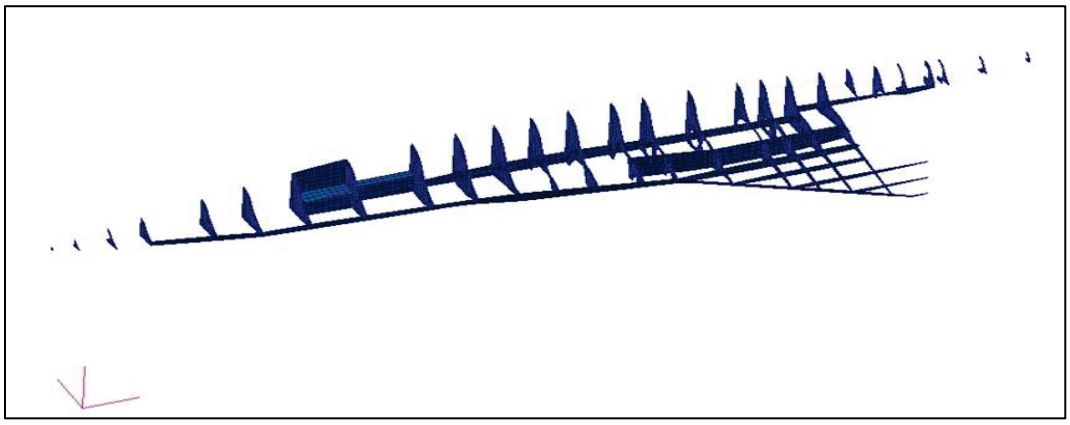

Figure 4.1.1 HTV-3X FEM Original Internal Structure

The existing structure was first photo-scaled up by 3x in all dimensions. The element density remained the same, thus the element size grew by 3x in all dimensions as well. The scaling up of the vehicle FEM left large unsupported skin regions between bulkheads. Therefore, additional internal structure had to be created to keep the unsupported skin panel spans to approximately 30 +/- 6 inches so as to mitigate any potential panel flutter concerns. ***Figure 4.1.2*** is a view of the internal structure after scale up and with the additional bulkheads that were inserted. The number of structural bulkheads nearly tripled as a result. Another addition to the internal structure was a centerline keel web that runs along the fuel tank region and through the centerline of the main body of the vehicle. This keel was added to eliminate the need for the more complex system of tension rods base-lined in the original HTV-3X vehicle, which was never adequately analyzed during the course of the HTV-3X conceptual design phase. The keel design provides a more proven design approach and reduces complexity in the model, but could result in increased vehicle rigidity in this region, and less compliance to thermal loads (Panel 2 only).

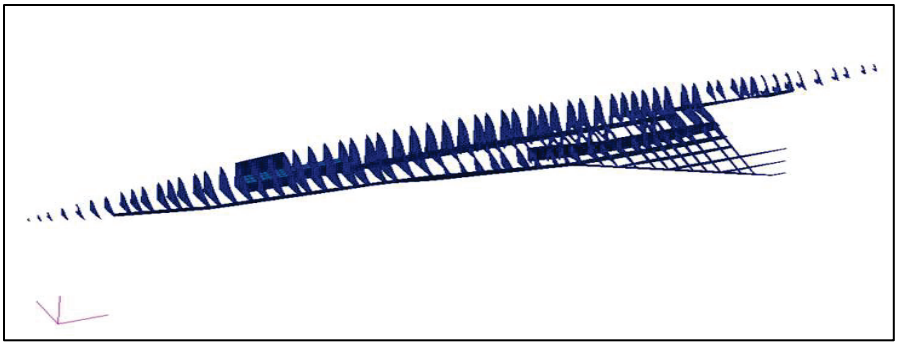

Figure 4.1.2 Scaled Up HCV FEM Internal Structure With New Bulkheads Added

Additionally, the fuel pans which spanned from a forward fuselage bulkhead to an aft fuselage bulkhead in the original HTV-3X vehicle structure were now unequally divided by the new bulkheads. It was required to rebuild the fuel pans in order to attach them at each new bulkhead location, as shown below in ***Figure 4.1.3***.

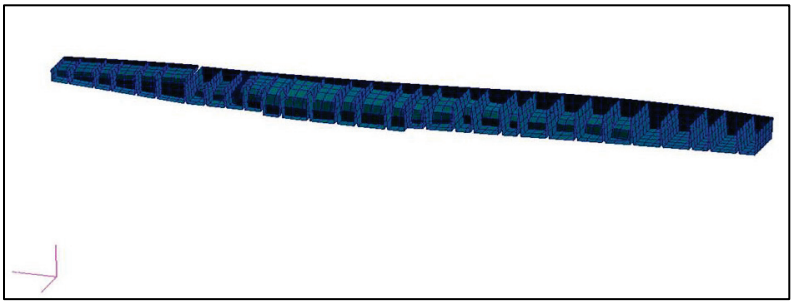

Figure 4.1.3 Updated Fuel Pan Layout

Once the loads model had been scaled up the FEM was validated using structural load cases created for the scaled up geometry. These structural load cases and how they were determined is discussed in Section 4.2 of this report. The displacements from one of the load cases tested are shown in ***Figure 4.1.4*** below and the investigation showed the model to be behaving appropriately. Displacements of the body region of the vehicle appear to be appropriate for this bending mode. The elevon displacements were disregarded for this study as they were large due to a necessary recalibration study of the actuator models and Nastran spring elements.

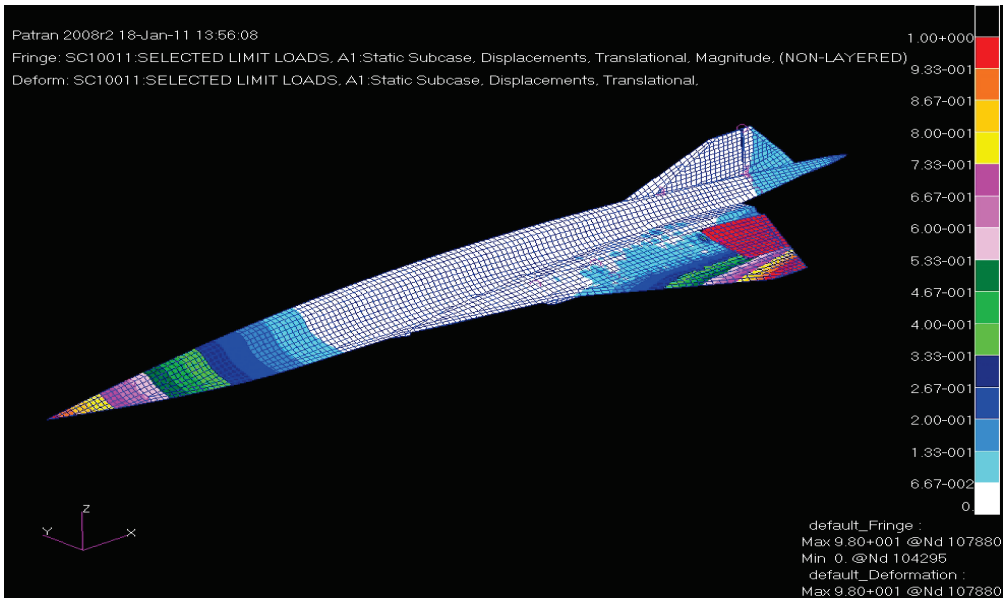

Figure 4.1.4 Structural Load Case Runs to Validate FEM Behavior

During the HTV-3X analysis phase, thermal models were created based on that geometry. This thermal data was able to be applied to the new HCV FEM (coordinates adjusted by 3x), however, the new structural regions created in this model did not have corresponding temperatures available from the old data. Therefore, a conduction thermal analysis run was performed with MSC/Nastran in order to let the model simply use the existing temperatures available as a thermal boundary condition in which to let the temperatures, through conduction, fill in the revised structural zones. This is a reasonable approximation that was necessary due to time and resource constraints that prevented a new scaled up detailed thermal analysis model to be created and mapped on to the scaled up model. An example of temperatures at Mach 5.2 is shown in ***Figure 4.1.5***.

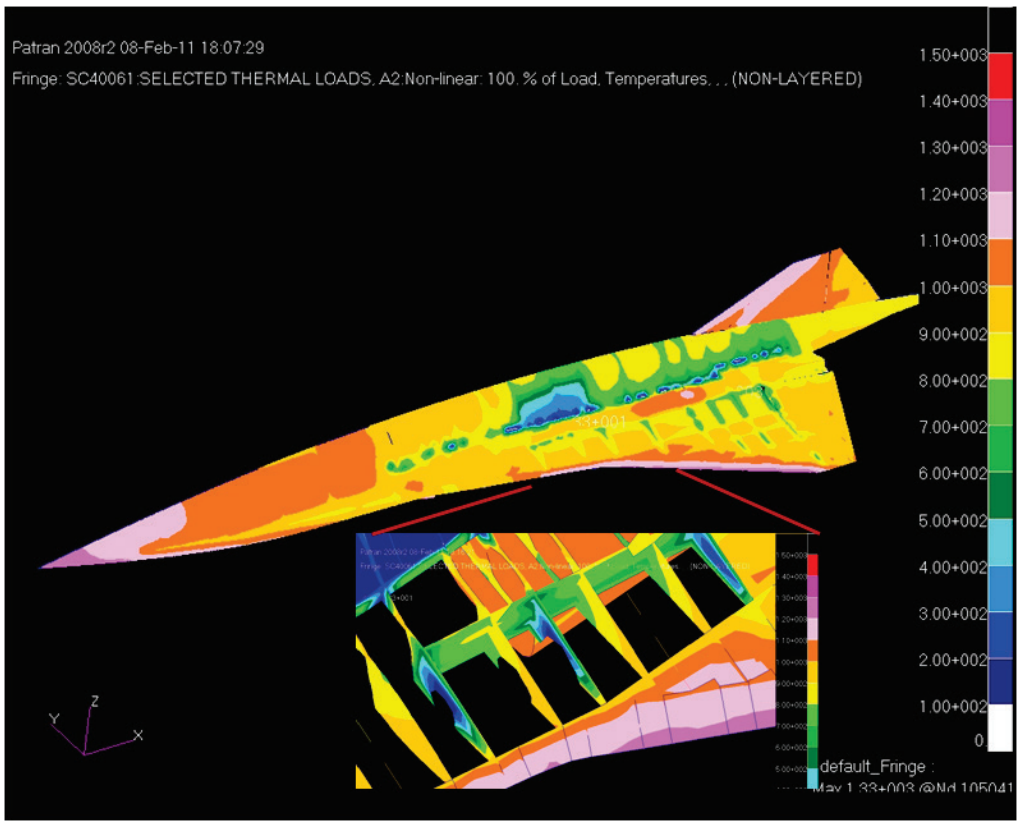

Figure 4.1.5 Mach 5.2 Temperature Results on HCV Model

The resultant internal temperatures show where the conduction approximation shortfalls are most evident. Previous boundary conditions such as cooled zones for landing gear in the detailed thermal model did not get accounted for. Instead, the temperatures between the top and bottom skins had to be conducted between to achieve the unknown bulkhead temperatures. The ***Figure 4.1.5*** insert shows the cooler blue bulkheads of the original geometry in contrast to the hotter new bulkheads in between. These new bulkhead temperatures were derived from the conduction approximation solution, which does not take into account the cooled region. These small differences were deemed acceptable for these studies since they are very localized, and were not directly connected to any of the panels analyzed.

This thermal analysis approach was used for all HCV thermal load conditions (a more idealized approach is summarized in Section 11.0). These thermal conditions were then combined with their corresponding structural load cases as described in Section 4.2. All structural load cases were run for completeness, but only a select handful were investigated further in order to extract panel load conditions. This process is described further in Section 5.1 of this report.

4.2 EXTERNAL LOAD CASE GENERATION

At this time, no customer structural design criteria exists for hypersonic vehicles, which operate in a speed regime above that of high-supersonic, manned reconnaissance aircraft, such as the SR-71, and below that of orbital launch and reentry vehicles, such as the Space Shuttle Orbiter. Whether manned or unmanned, it is unlikely the performance requirements of hypersonic vehicles will call

for high-maneuverability at hypersonic flight conditions because of inlet flow constraints, which limit the transient flow excursions necessary for maneuvers from the carefully designed steady-state flow conditions. These flow constraints force integrated design of the vehicle forebody and inlet for hypersonic flow conditions and maneuvers upsetting these conditions which risk an engine un-start; where a flowing inlet and high-thrust instantly, and violently, change to a non-flowing inlet and high-drag. Engine un-starts at hypersonic speeds abruptly change the force and moment balance of a hypersonic vehicle and can lead to a departure from the flight path. For this reason, it is unlikely hypersonic vehicles will require high-maneuverability at hypersonic speeds, at least per the level of scramjet technology as it is today.

In lieu of government agency structural criteria specifically for hypersonic vehicles (i.e. horizontal takeoff and landing hypersonic vehicles), the MIL-A-8860 (Ref. 3) series offers reasonable criteria for maneuvers (i.e. strategic bombers), gust, landing impact, taxi, ground conditions, and miscellaneous loads. Any horizontal takeoff and landing hypersonic vehicle will have to function on the ground as any other aircraft and will encounter the same gust environment, so it makes sense to use the MIL-A-8860 series structural criteria. At this time, it is likely any hypersonic vehicle developed will be a military vehicle, so the MIL-A-8860 series is more appropriate than structural criteria for civil aircraft, such as the FAA's FAR 23 or 25.

On the detail level, a potential problem with using the MIL-A-8860 series is the discrete runway single and double one-minus-cosine bumps. Hypersonic vehicles typically have very high wing loading, which means the takeoff and landing speeds are very high (i.e. approximately 200 knots). Taxiing over the one-minus-cosine bumps at high speeds could be more severe than landing impact, so taxiing will likely determine the required gear stroke to avoid excessive loads.

Rudder-kick loads are another potential problem with using the MIL-A-8860 series. The MIL-A-8860 series assumes pilot force limits in determining rudder deflection; criteria that might be more applicable are the NATO structural criteria for unmanned aerial vehicles (UAV), STANAG 4671.

For the panel detailed sizing tasks of the Phase II program a set of structural design margins were established, as illustrated in ***Figure 4.2.1***. The referenced margins reflect design factors and margins of safety employed on other unmanned high speed and hypersonic flight vehicles under study by LM Aero as agreed upon with their respective customers.

Load Condition	Ultimate Factor-of-Safety	Ultimate Margin-of-Safety
Taxi, Ground Handling	1.5	0.00
Free Flight		
Aero/Inertia/Dynamic Loading	1.25	0.00*
Internal Pressure (fuel tank / inlet system)	1.67**	0.00
Thermal Stresses	1.25	0.25

*Vehicle Structural Proof Test would normally be used for confirmation of structural loads at critical vehicle areas

**1.25 x 1.33 (on tank pressure) – for internal loading on fuel tank area panels

Figure 4.2.1 Baseline HCV Structural Factors and Margins of Safety

Figure 4.2.2 illustrates a flat-plate aerodynamic model of a hypersonic vehicle. This is the type of model used to create steady (i.e. zero reduced frequency) Aerodynamic Influence Coefficient (AIC) matrices at a variety of Mach numbers to cover the flight regime of a hypersonic vehicle. This is necessary because at different Mach numbers, the aerodynamic loading shifts, which thereby loads the vehicle differently. In addition, the temperature of the structure increases with increasing Mach number thereby reducing the material allowable. The structure must be capable of supporting all of these loading conditions.

However, these flat-plate models do not model the three-dimension aspects of the vehicle as these are literally a flat plate for calculating the pressure differential across aerodynamic surfaces (i.e. wings, control surfaces, lifting bodies, etc.). This is adequate for generating structural loading distributions for designing primary structure, but not for generating pressures on the vehicle's surface for designing individual skin panels. Generating surface pressures requires using aerodynamic theories with a higher level of sophistication. MSC/Nastran provides three flat-plate aerodynamic modeling methods for generating AICs, one for each Mach number range:

- Doublet lattice, $0 \leq M \leq 1.0$
- ZONA51, $1.0 \leq M \leq 3.0$
- Piston Theory, $3.0 \leq M \leq 7.0$

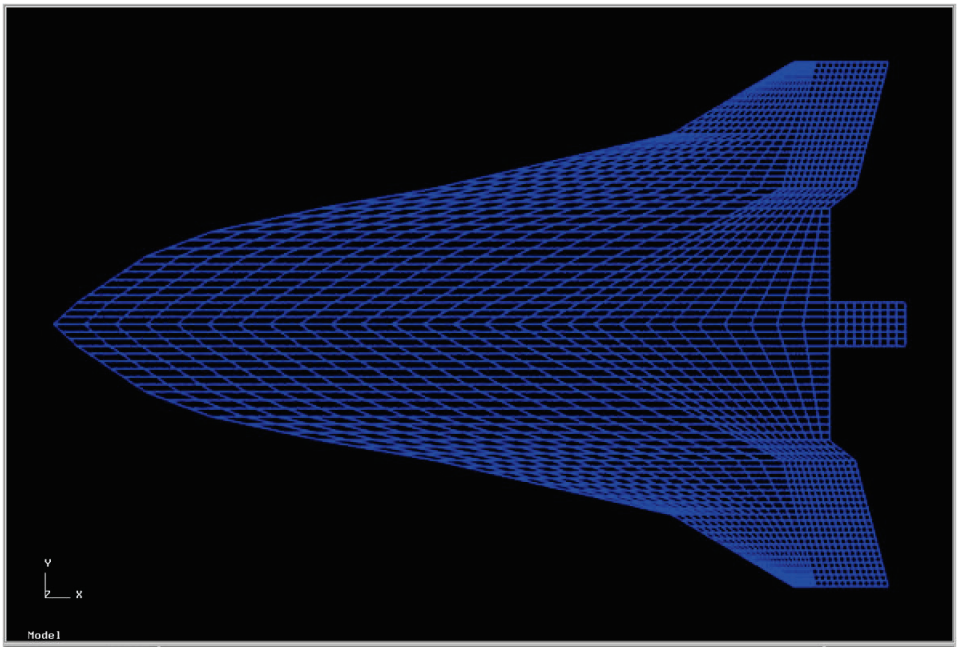

Figure 4.2.2 Example of Aerodynamic Panel Modeling for Generating AIC Matrices for Aerodynamic Loads

The AIC is a square matrix relating the local aerodynamic box normal force per unit dynamic pressure per local box angle-of-attack. At subsonic speeds, all boxes influence all other boxes; at supersonic speeds, only boxes in the upstream Mach cone influence a given box; at hypersonic speeds, no box influences any other box, each box influences only itself. For loads calculations, it is convenient to resolve this normal force into force distributions per aerodynamic state variable, such as lift and side-force distributions per vehicle angle-of-attack and angle-of-sideslip. Also necessary are force distributions per control surface deflection for each control surface.

It is convenient in the process of generating external load sets to map the hypersonic vehicle's inertia distribution to the same mesh as the aerodynamic model. Generally, the Mass Properties organization is responsible for distributing the vehicle's inertia on the aerodynamic model grid and they have proprietary tools specifically for that purpose.

Load calculation involves using linear unit loading distributions for aerodynamic and inertia loads. Aerodynamic loading distributions for symmetric maneuvers are angle of attack and elevon deflection,
and obvious unit conditions are per radian or per degree. Inertia loading distributions for symmetric maneuvers and gust are normal acceleration and pitch acceleration and obvious unit conditions for these are per normal acceleration or per normal load factor and per pitch acceleration (i.e. either rad/sec^2 or deg/sec^2). If using unnatural units, caution is strongly advised to include all necessary conversion factors.

Other aerodynamic load distributions can include camber distributions to more accurately model moment distributions. Hypersonic vehicles often have propulsion related moments that affect trim,

such as the momentum of the inlet capture air turning as it enters the inlet, or the momentum of air turning in other parts of the propulsion system.

It is convenient if the aerodynamic and inertia unit forces are on the same mesh or grid, such as the aerodynamic mesh or grid (***Figure 4.2.2***). This allows adding the forces from the two sources without having to go though intermediate transformations.

Before generating loading distributions, it is important to know whether the loads are for a full- or half-model. For vehicles with a plane of symmetry, it is possible to build a half-structural model on only one side of the plane of symmetry and use appropriate constraints on the plane of symmetry to represent the other half. Full-model loads are simpler to generate and apply to structural models for strength sizing, but require approximately four-times more storage and computer runtime than half-model loads do. Half-model loads require breaking the force distributions into symmetric (i.e. F_X, F_Z, & M_Y) and anti-symmetric (i.e. F_Y, M_X, & M_Z) components. In half-models, centerline constraint loads are an important and significant contribution to the vehicle loading, even for perfectly balanced load distributions. In full-models, constraint loads should be zero for perfectly balanced load distributions. Asymmetric loading conditions for half-models require combining a symmetric and an anti-symmetric solution to get the final answer. For these cases, the savings in storage and computer runtime is approximately a factor of two over the equivalent full model. The external load case set generation for the HCV was that for a half-structural model.

Balancing the loads requires solving for the unknown load scale factors that result in the aerodynamic and inertia forces and moments being equal or balanced. As an example, for a symmetric maneuver, usually the normal acceleration and the pitch acceleration are the known variables and the unknown variables are angle-of-attack and elevon deflection. Roughly speaking, the angle-of-attack balances the normal forces and the elevon deflection balances the pitching moment. Balancing the normal force and pitching moment are necessary to satisfy the free-free beam boundary conditions at the ends of the fuselage or at the wingtips. In other words, the vertical shear and bending moment being zero at the nose and tail of the vehicle or at the wingtips are a result of the forces and moments being in balance.

After balancing the forces and moments from the applicable force distributions, it is possible to integrate beam-type loads, such as shear, bending moment, and torsion. As a check, all of these should go to zero at the ends of the structure. These beam-type loads are adequate to strength size certain beam-like structures, but for analyses using finite element models (FEM), the force distributions must be splined to the FEM GRID points.

Structural FEMs require force distributions at the model GRID points. For MSC/Nastran, forces are input using FORCE cards. A collection of FORCE cards is necessary to load the FEM in an approximately balanced loading condition. Usually, the GRID points are at different locations from the forces in the load distribution, so some method is necessary to move the forces to the appropriate GRID points.

In general, not all GRID points should be loaded and the fidelity of the Loads Model is usually less than the fidelity of the FEM. The fidelity of the Loads model is usually not increased to correspond to the fidelity level of the structural FEM, but it is still possible to get a representative loading of

the FEM at the scale of the Loads Model by splining or mapping the forces from the Loads Model to GRID points on significant structure. By the term "significant structure", this means points on the FEM that can sustain large loads without significant deflections. It is usually a mistake to generate FORCE cards for skin elements since they will have excessive deflections, sometimes several feet. It is better to use only FEM points where major structural elements intersect, such as frames and longerons or spars and ribs. These will generate correct far-field stresses and correctly load the FEM although locally to the loaded GRID the stresses will be too high.

There are many methods for splining or mapping forces from one mesh or grid to another. Nastran's Harder and Demaris spline is one example, but almost any function that generates highly spiked distributions, as shown in ***Figure 4.2.3***, will work.

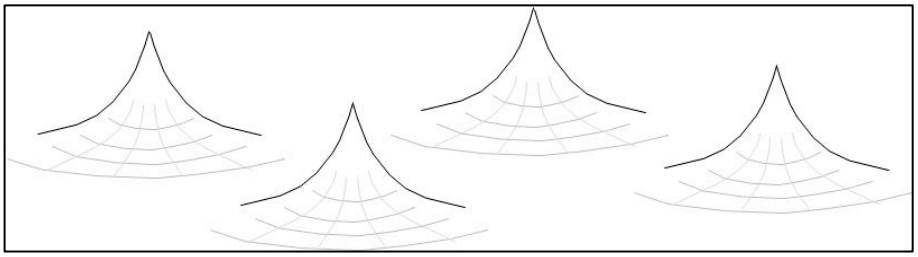

Figure 4.2.3 Individual Logarithmic Load Distributions for Mapping Loads From a Loads Grid to GRID Points

Figure 4.2.3 displays logarithmic loading distributions around several forces on the Loads grid; the goal will be to assign a portion of that force to each GRID. ***Figure 4.2.4*** shows a close-up view of one of those spikes, the center of which is the load point and the height is a unit force at the Load point. In ***Figure 4.2.4***, the distribution assigns most of the unit force to the two nearest GRIDs, which is appropriate. As long as the distribution is sufficiently "spiky", very little of the force will spill over onto any GRID other than the ones very close. Normalizing this force distribution on the GRIDs to a unit value gives a distribution for any force at that Load point to all appropriate GRIDs.

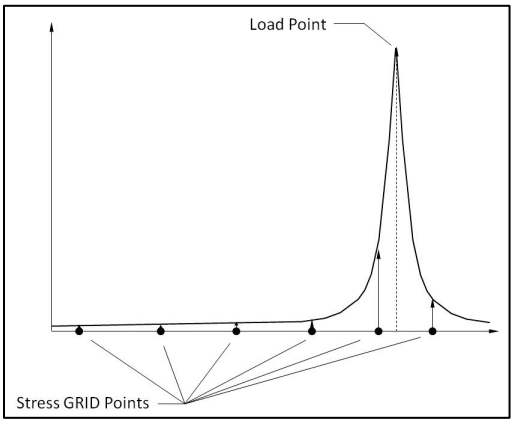

Figure 4.2.4 Single Load Mapping to Several Stress GRID Points

Following this procedure for all Load points gives a matrix mapping of forces at the Load points to the GRIDs, and this transformation matrix is applicable for all load cases. Intuitively, it makes sense to assign most of the force at each Load point to the nearest GRIDs. The normalization process guarantees a force balance between the loads and the GRIDs, but it does not guarantee a moment balance, which is apparent in ***Figure 4.2.4***. If there are a large number of load points and a large number of GRIDs, then it will preserve the moment balance approximately.

To correct the moment imbalance, it is possible to force the distribution by applying an arbitrary distribution of forces, scaled to match the moment imbalance. The least intrusive distributions places forces at the greatest distance from the vehicle's CG, but if an accurate loading is necessary at those points, then it will be necessary to pick other points. Forcing distributions in the least intrusive manner is a science unto itself and usually requires using both a force and moment distribution to guarantee the arbitrary moment distribution which is truly only a moment distribution (i.e. by combining two arbitrary distributions, it is always possible to generate a moment, only distribution).

In the area of hypersonic vehicle structural design and analysis special treatment needs to be given to the phenomena of engine un-start loads and their bearing upon hypersonic vehicle airframe sizing and design, and certainly on the system level early in the preliminary design phase. Such un-start conditions can have far ranging impacts upon both the static as well as dynamic condition sizing of inlet and isolator support as well as fore-body and forward fuselage structure.

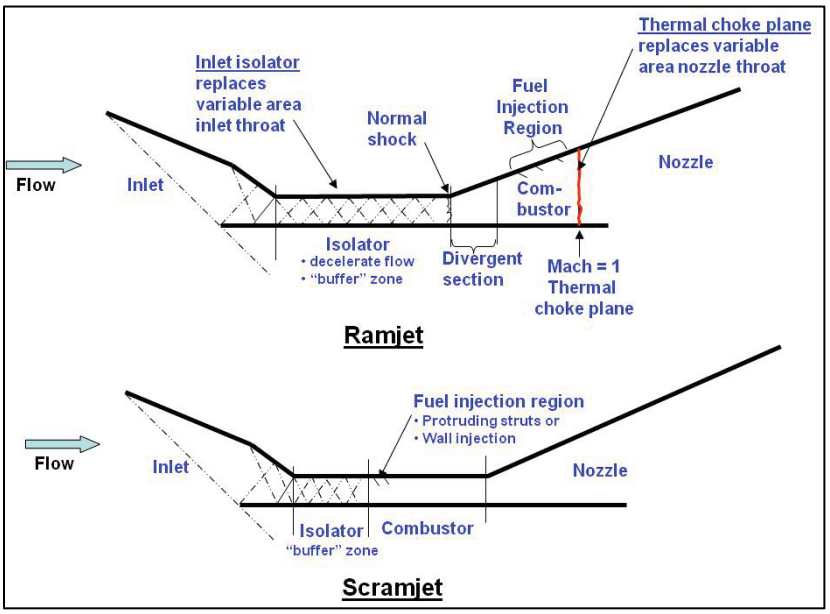

Figure 4.2.5 Dual-Mode Ramjet Configuration

Engine un-starts can occur in supersonic and hypersonic flows if the internal normal shock moves upstream into the inlet where it must continue moving upstream until disgorged from the mouth of the inlet. The inlet duct and its supporting structure must be able to withstand the high pressures behind the moving shockwave. During engine flow conditions when a normal shock exists (***Figure 4.2.5***), if flow conditions in the engine force the normal shock to move forward, beyond

the isolator and into the downstream end of the inlet, then it is impossible for the shock to reenter the isolator. In this case, the shock must move forward until disgorged from the mouth of the inlet, and only then can the flow reestablish itself. Unfortunately, the highest pressures occur downstream of the normal shock, so this requires designing the entire isolator and inlet duct for the moving pressure load on the duct.

Moving loads can generate higher stresses than static loads, as nineteenth-century railway bridge designers discovered the hard way. Consequently, designing isolator and inlet ducts for static un-start pressures is risky. Calculating the speed of the moving shockwave and the pressure behind it requires an unsteady flow solution to capture the transient flow conditions, which is more complex than a static analysis. As a first approximation, ignoring the deflections of the duct on the moving shockwave would be appropriate and would uncouple the unsteady flow problem from the duct dynamic response problem. The unsteady duct pressures, of course, are necessary as the forcing function for the duct dynamic response as the small duct deflections would have only a secondary effect on the unsteady duct pressures. Solving a dynamics problem as a statics problem is inappropriate and, in the case of hypersonic vehicles with engine un-starts, can lead to catastrophic loss of the vehicle from a duct failure.

Concurrent with the scaling up of the HTV-3X model into the HCV FEM for the Phase II study was the HCV external load case set generation. As mentioned previously, this was performed upon the half structural FEM configuration.

The C310 configuration loads required scaling for this effort. Scaling the inertia loads, at the direction of the Mass Properties representative, involved a scale factor formed from the empty and full-fuel weights of the two vehicles. The inertia was per aerodynamic box, so the application point of the scaled inertia was at the box center, as with the previous model.

Scaling the aerodynamic loads for angle-of-attack and flaperon load distributions was geometric. The modification of the geometry for each aerodynamic box was merely a lengthening in two-dimensions to match the new vehicle length and wingspan. This increased the area of each box accordingly. Each of the seventeen Mach number distributions in the database had this scaling.

Each of the 171 load cases (163 flight maneuver cases, 4 landing cases, and 4 nose-wheel taxi steering cases) required rebalancing, reintegrating the loads, and redistributing to the FEM GRID points. The entire listing of HCV external load cases is found in Appendix A of this report.

As an aside, note that geometric or “photo” scaling flying vehicles is not a rigorous engineering approach to aircraft design. These tasks were performed in accordance with the schedule and constraints of the Phase II program, however, oftentimes in conceptual level vehicle studies, it is an adequate and sound approach for load path layout and early design structural sizing activities and trade studies.

As with anything, there are penalties in every process and method. Since weight increases by approximately the cube of the scale factor and wing area, which determines the lift necessary to carry the weight, increases only by approximately the square of the scale factor, on a scaled up

aircraft, it will have too little wing area to operate at the same lift coefficient and speed. The propulsion system, which as the wing, scales by approximately the scale factor squared, will likewise be too small. Operating at a higher lift coefficient than that for the original design will reduce the lift-to-drag ratio in cruise and that increased drag will further make the propulsion system underpowered. For flying vehicles, the structure will also have problems with "photo" scaling as operating at the same load factor will cause normal and shear stresses to increase by the scale factor. Unless the material thicknesses grow faster than the scale factor, the structural weight could grow even faster than the cube of the scale factor. In short, there are issues with "photo" scaling aircraft, but, in general, the wing and control surfaces, propulsion system, and structural material thicknesses have to grow at a rate greater than the scale factor for the aircraft to fly.

4.3 INITIAL ENVIRONMENTS DEFINITION

As the HCV FEM scale up and external load case set tasks were proceeding, the HCV thermal environment across the trajectory was investigated. The first step was to generate a series of RET maps of thermal contours, in the same format as displayed in ***Figures 4.3.1 and 4.3.2***, per the various HCV trajectory points.

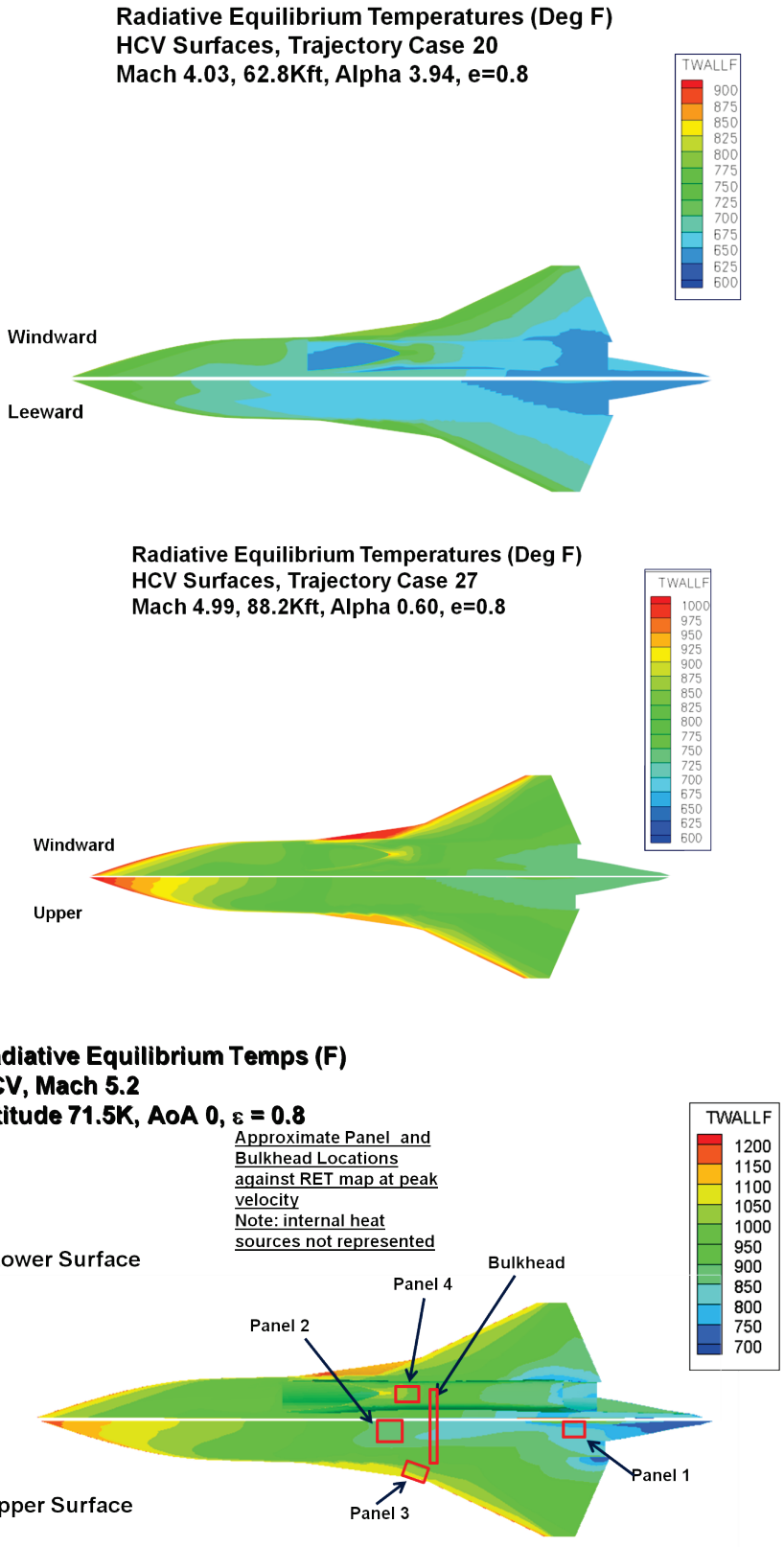

Figure 4.3.1 HCV RET Maps at the Mach 4.03 and 4.99 Flight Conditions

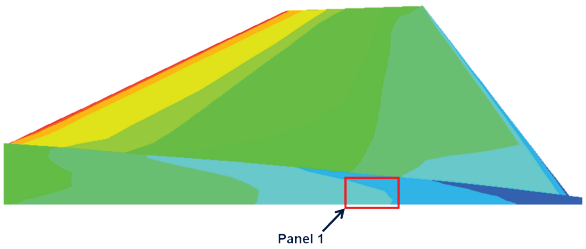

Figure 4.3.2 Preliminary Design Level Panel Temperature Environments

These RET maps were used to establish the initial panel structural trade studies that were conducted in the Panel 1-4 Preliminary Design Phase.

5.0 PRELIMINARY DESIGN PHASE

The sizing of the vehicle was broken into preliminary and detailed design phases, each of which is illustrated in ***Figure 5.0.1***.

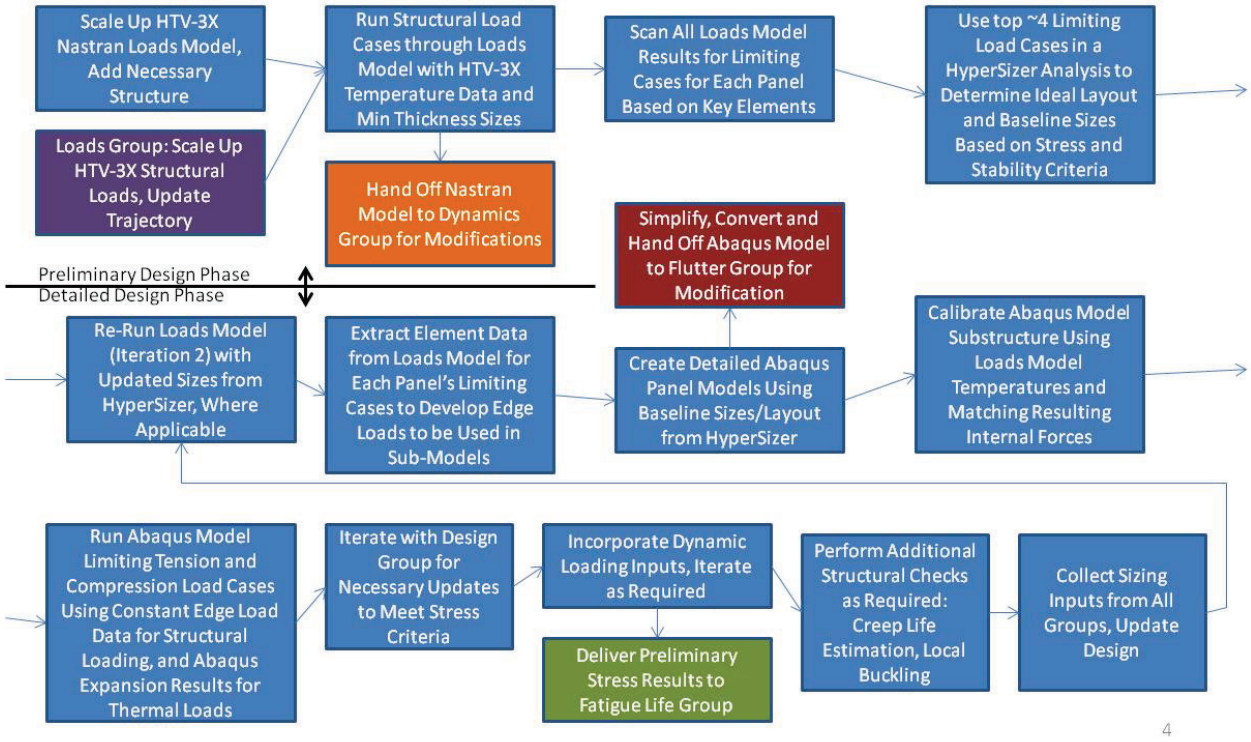

Figure 5.0.1 Phase II Analysis Process

5.1 PANEL STRUCTURAL CONCEPT STUDIES (HYPERSIZER)

In the first phase of panel sizing, the commercially available tool HyperSizer was implemented to perform the basic layout and material decisions. HyperSizer is a structural optimization software code that performs large numbers of iterations on structure within the parameters provided. HyperSizer will optimize each panel based on a minimum weight resultant metric. The Preliminary Design Phase comprised a trading of parameters including stiffening concepts (honeycomb sandwich, hat Stiffened, z stiffened, blade stiffened, etc), stiffener thickness sizing, panel sheet thickness sizing, stiffener spacing, and materials.

The basic sizing criteria applied for all sizing studies in the Phase II program are summarized in ***Figure 5.1.1***, and were maintained for both preliminary and detailed design phases.

1. LIMIT Loads Applied to Model and are Compared to Yield Stress of Material and Local Buckling
2. Ultimate Loads = (1.25 * LIMIT Loads), and are Compared to Ultimate Strength of Material (Maintaining 0.25 Margin for Thermal Loads) and Global Buckling
3. Aero-smoothness Checks Per Table (Waviness only)

LOCATION	FORWARD FACING STEP (INCH)	AFT STEP (INCH)	GAP (INCH)	WAVINESS (HEIGHT/LENGTH) (INCH/INCH)
NOSE/CHINES				
FALCON	None Allowed	0.05	0.055	0.004
NASP	None Allowed	<0.1	0.3 on sliding joints for CTE motion	0.004
X-33	0.03	0.05	0.055	0.004
WINDWARD– MIDBODY				
FALCON	0.04	0.04	0.075	0.007
NASP	<0.020	0.04	0.3 on sliding TPS joints	0.007
X-33	0.04	0.075	0.075	0.007
LEEWARD-MIDBODY				
FALCON	0.1	0.15	0.1	0.02
NASP	0.15	0.15	0.3 on sliding joints	0.02
X-33	0.1	0.15	0.1	0.02
WINDWARD-CANTED FIN				
FALCON	None Allowed	0.05	0.03	0.004
NASP	None Allowed	<0.1	0.3 on sliding joints	0.004
X-33	0.03	0.05	0.03	0.004

HCV aero-smoothness requirements are based upon conservative interpretation of Space Shuttle Orbiter values defined by Rockwell Int'l, "Orbiter Entry Heating Prediction Methods and Data Base", STS83-0948, Rev. 1, July 1988

Figure 5.1.1 Sizing Criteria Assumptions

HyperSizer can be supplied input data in two different ways. The optimization studies can be linked directly to a structural FEM to obtain geometry and loads, or this data can be entered manually. In order to have greater flexibility and control over the input, the data is supplied manually to HyperSizer for the panel studies that follow. For each panel the basic dimensions and curvature were measured from the CATIA models and entered in to the software, along with the boundary conditions associated. A simple support at the edges is assumed for conservatism in a buckling limited condition, which is expected. Each panel was optimized for each of six stiffening layouts, depicted in ***Figure 5.1.2*** (with the exception of the Panel 4 engine fairing, which was only studied as a honeycomb structure). The minimum weights for each design were then compared upon completion, and were factored into the design decision for each panel.

A trade study approach for each of the four panels was laid out early in the Preliminary Design Phase, and these input assumptions are listed in Appendix B of this report.

Within each panel stiffening concept, many parameters were adjusted for optimization. These parameters include materials, thicknesses, stiffener direction and spacing, and various heights, widths and other dimensions. The materials assumed in the trade studies, per the listed assumptions in Appendix B, were IN 600, IN718, Ti 6-4 and Ti 6-2-4-2S. Each panel was also analyzed individually for each of a few selected limiting loadcases, as described below. The loads were applied as constant running loads along the edges of the panels in the X and Y directions, as well as the shear components and pressure loads being incorporated if applicable (Panel 2 - fuel tank structure). For each load case, the maximum temperature within the panel was assumed for

the entire panel, which sets the material properties used by HyperSizer. The thermal stresses were already accounted for in the data extracted from the FEM loads model which was applied to the panel edges. Each panel was checked for various failures including stress limits and buckling for every design iteration within the specified parameters. A sample output graphical representation is shown below in ***Figure 5.1.3*** for panel buckling failure in Panel 1.

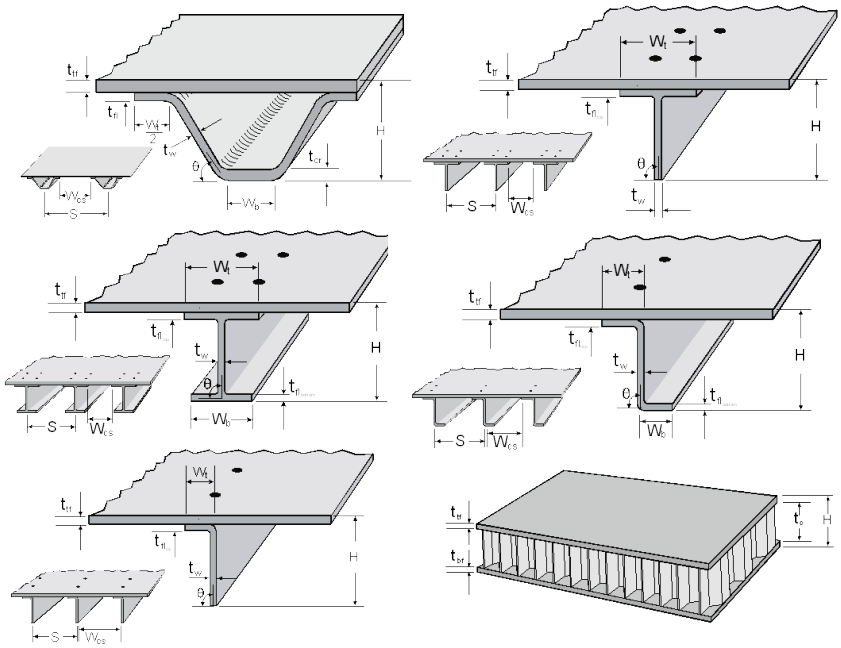

Figure 5.1.2 Hypersizer Panel Design Options

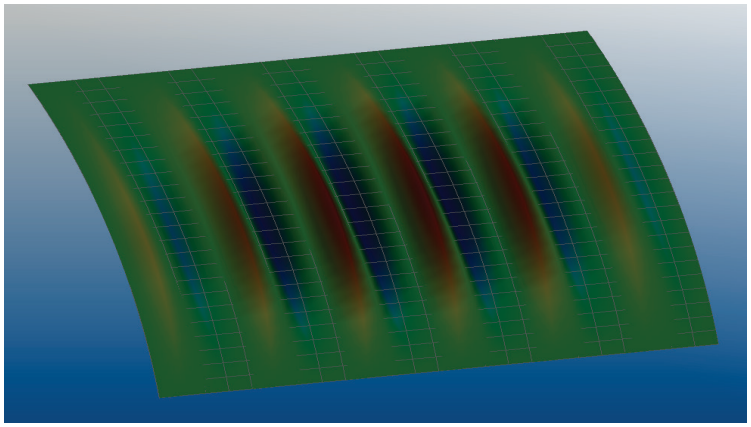

Figure 5.1.3 HyperSizer Graphical Buckling Result

Once all structural checks were performed, the lowest weight solution meeting all criteria was reported in the HyperSizer output for each configuration and load case.

As mentioned above, the HyperSizer optimization requires loading data to be supplied for all edges of the panels. Using the FEM data from the Patran/Nastran loads model, loads were able to be extracted for each panel for any load case. An initial scan of all 171 load cases run provides

indicators of which load cases may be limiting for each panel based on maximum loads produced. Once a few of the most limiting cases were determined, detailed data for each element of the panel location was further studied. The running loads in the X and Y directions, along with the shear loads, were extracted for every corresponding panel element in the loads model. This data was then imported into Excel for each load case indicated in the initial screening, in order to determine load case sub sets to be used in the HyperSizer optimization studies. The Panel 1 elements from the Loads Model to be queried for data are shown in ***Figure 5.1.4***.

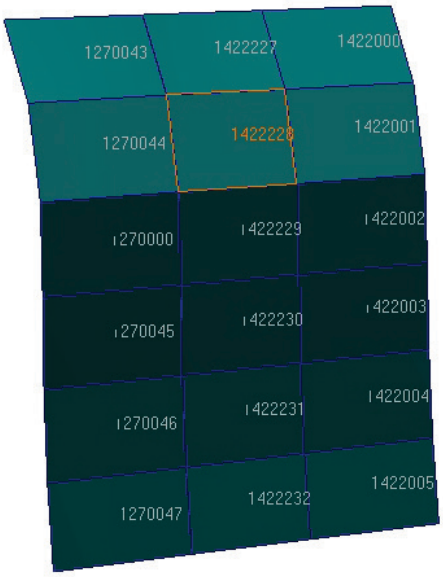

Figure 5.1.4 Panel 1 Loads Model Elements

A sample load case sheet, using the data from each element above, is shown in ***Figure 5.1.5*** for Panel 1. All corresponding element numbers are shown in the left-most boxes at their proper relative locations. The three data sets to the right illustrate the running loads in X, running loads in Y, and the XY shear loads, respectively. The HyperSizer studies are a simplistic first cut at panel sizing, and therefore will use more uniform loading than the FEM results imply. Therefore, the maximum values for each type of loading is taken from the Excel data and are combined into sub cases.

ELEM Locations				Membrane Forces in X				Membrane Forces in Y				Membrane Forces in XY			
1270043	1422227	1422000		-73.9	40.0	602.1		116.4	-177.6	85.8		-184.2	91.7	188.4	
1270044	1422228	1422001		711.8	860.5	788.6		-380.7	16.9	-13.6		-353.1	452.4	457.4	
1270000	1422229	1422002		746.7	816.8	554.0		-124.6	-32.5	22.1		161.3	-6.3	238.5	
1270045	1422230	1422003		-116.0	-198.6	-100.7		-102.3	153.5	-19.0		-9.8	249.9	161.4	
1270046	1422231	1422004		-26.2	0.7	-968.1		-11.5	393.5	-216.6		45.5	47.2	-151.0	
1270047	1422232	1422005	"-------> X"	-721.8	-1856.4	-1919.6	"-------> X"	49.5	-48.1	-21.2	"-------> X"	355.2	-709.7	-530.6	"------->

Figure 5.1.5 Excel Formatting of FEM Data for Hypersizer Studies

The maximum values for tension and compression of each of the X and Y running loads, as well as the shear loads, were combined in every possible combination, as shown in Table 5.1.1.

Table 5.1.1 Sizing Sub Cases

Subcase	Nx	Ny	Nxy
1	Compressive X	Compressive Y	Positive XY
2	Compressive X	Compressive Y	Negative XY
3	Compressive X	Tensile Y	Positive XY
4	Compressive X	Tensile Y	Negative XY
5	Tensile X	Compressive Y	Positive XY
6	Tensile X	Compressive Y	Negative XY
7	Tensile X	Tensile Y	Positive XY
8	Tensile X	Tensile Y	Negative XY

Table 5.1.2 Limiting Load Cases

	LC #	Type	Therm Cond	Mach	Nz	Fuel %
Panel 1	60020	Positive Manuever	M5 Ascent	5.546	1.50	33.2
	60126	Positive Gust	M2 Descent	1.563	2.71	0.0
	60148	Negative Gust	M2 Descent	1.563	-0.71	0.0
	LC #	Type	Therm Cond	Mach	Nz	Fuel %
Panel 2	60014	Positive Manuever	M4 Ascent	4.246	1.75	55.9
	60170	Landing Full 2 pt	M1 Ascent	0.450	1.00	100.0
	60172	Landing Hot 2 pt	M0.3 Hot Land	0.450	1.00	0.0
	LC #	Type	Therm Cond	Mach	Nz	Fuel %
Panel 3	60009	Positive Manuever	M2 Ascent	2.335	2.00	68.9
	60061	Negative Manuever	M2 Descent	1.059	-1.00	0.0
	60076	Negative Manuever	M5 Descent	5.197	-0.20	0.0
	LC #	Type	Therm Cond	Mach	Nz	Fuel %
Panel 4	60172	Landing Hot 2pt	M.3 Hot Land	0.450	1.00	0.0
	60126	Positive Gust	M2 Descent	1.563	2.71	0.0
	60062	Negative Manuever	M2 Descent	1.161	-1.00	0.0
	60041	Negative Manuever	M5 Ascent	5.197	-0.20	33.2

These eight sub-cases were used for each of the pre-selected loadcases determined for each panel. The loads used for the HyperSizer based studies included both thermal and structural effects from the loads model. HyperSizer analyzes all the sub-cases in the same design iteration. Therefore, when a load case solution is obtained, that solution meets all structural criteria for each of the sub-cases.

The top limiting load cases for each panel, that were to be used in Hypersizer as well as the detailed Abaqus models in the critical design phase of the project are listed in Table 5.1.2.
For each panel, the lightest weight solution that met all load case structural criteria was reported, and each design type was compared to determine a going forward design approach that was to be analyzed in the detailed design and analysis phase.

Panel 1 results are assembled in Table 5.1.3 below. These results are from the maximum temperature load case, which also represents the maximum loading seen in the panel. These results indicate that a honeycomb sandwich panel solution would be the lightest option per the prescribed input and boundary conditions. However, other factors such as tooling and manufacturing costs for such a large acreage region had to be taken into account. Upon taking all design criteria into consideration, the Ti-6-2-4-2S hat stiffened sheet (ranked #2) was ultimately chosen for the Panel 1 design. Using the HyperSizer data from the hat stiffened concept analysis, optimum stiffener spacing, dimensions, and skin thickness were extracted as a baseline for the design.

Table 5.1.3 Panel 1 HyperSizer Weight Optimization Results

Overall ranking	Weight (lbs/sq ft)	Temp at sizing load (deg F)	Max service temperature (deg F)	Panel Component 1 Primary Failure Mode	Panel component 1 Primary Failure Mode load case	Panel Component 2 Primary Failure Mode	Panel Component 2 Primary Failure Mode Load Case	Structural Concept	Max depth (in.)	Primary Sheet Gage (in.)	Material
1	1.765	900	900	MS = 1.16 (Isotropic Strength (yield criterion))	M5 ascent, pos. Manuever; (Subcase 4)	MS = .29 (Panel buckling)	M5 ascent, pos. Maneuver; (Subcase 1)	Honeycomb (.375" core)	0.6057	0.032	Ti 6-2-4-2 sheets with IN 718 core
2	1.992	900	900	MS = .01 (Local buckling interaction)	M5 ascent, pos. Manuever; Subcase 2)	MS = .06 (Crippling)	M5 ascent, pos. Maneuver; (Subcase 1)	Hat Stiffened Sheet	1.25	0.049	Ti 6-2-4-2
3	2.090	900	900	MS = .16 (Crippling)	M5 ascent, pos. Manuever; (Subcase 2)	MS = .02 (Crippling)	M5 ascent, pos. Maneuver; (Subcase 1)	I Stiffened Sheet	1.5	0.0615	Ti 6-2-4-2
4	2.176	900	900	MS = .16 (Crippling)	M5 ascent, pos. Manuever; (Subcase 2)	MS = .07 (Crippling)	M5 ascent, pos. Maneuver; (Subcase 1)	Z Stiffened Sheet	1.5	0.0615	Ti 6-2-4-2
5	2.538	900	900	MS = .27 (Crippling)	M5 ascent, pos. Manuever; (Subcase 2)	MS = .10 (Crippling)	M5 ascent, pos. Maneuver; (Subcase 1)	T Stiffened Sheet	1.5	0.0615	Ti 6-2-4-2
6	2.538	900	900	MS = .27 (Crippling)	M5 ascent, pos. Manuever; (Subcase 2)	MS = .10 (Crippling)	M5 ascent, pos. Maneuver; (Subcase 1)	L Stiffened Sheet	1.5	0.0615	Ti 6-2-4-2

Other load cases with higher loading at lower temperatures proved to be less limiting. For Panel 2, the results indicated that a honeycomb sandwich panel solution would be the lightest option, similar to the findings in the Panel 1 trade. However, the tooling and manufacturing costs for such a large acreage region must again be considered, as well as the fact that this is a fuel tank region that must contain tank pressure. Taking all design criteria into consideration at that time, the Ti-6-2-4-2S hat stiffened sheet (ranked #2) was ultimately chosen for the Panel 2 design. Using the

HyperSizer data from the hat stiffened concept analysis, optimum stiffener spacing, dimensions, and skin thickness were extracted as the baseline for the design.

Table 5.1.4 Panel 2 HyperSizer Weight Optimization Results

Overall ranking	Weight (lbs/sq ft)	Temp at sizing load (deg F)	Max service temperature (deg F)	Panel Component 1 Primary Failure Mode	Panel component 1 Primary Failure Mode load case	Panel Component 2 Primary Failure Mode	Panel Component 2 Primary Failure Mode Load Case	Structural Concept	Max depth (in.)	Primary Sheet Gage (in.)	Material
1	1.862	1000	1000	MS = .49 (Isotropic strength against limit)	M4 ascent, pos. Manuever; (Subcase 3)	MS = .25 (Isotropic strength against ultimate)	M4 ascent, pos. Manuever; (Subcase 3)	Honeycomb (.375" core) (max .5" core height)	0.814	0.032	Ti 6-2-4-2
2	2.387	1000	1000	MS = .02 (Local buckling interaction against limit)	M4 ascent, pos. Manuever; (Subcase 1)	MS = .44 (Crippling - buckling interaction against ultimate)	M4 ascent, pos. Manuever; (Subcase 1)	Hat Stiffened Sheet	1.25	0.066	Ti 6-2-4-2
3	3.940	1000	1000	MS = .81 (Local buckling interaction against ultimate)	M4 ascent, pos. Manuever; (Subcase 1)	MS = .05 (Crippling - buckling interaction aginst ultimate)	M4 ascent, pos. Manuever; (Subcase 1)	I Stiffened Sheet	2.00	0.1205	Ti 6-2-4-2
4	3.940	1000	1000	MS = .44 (Local buckling - longitududinal direction, against limit)	M4 ascent, pos. Manuever; (Subcase 3)	MS = .03 (Crippling - buckling interaction against ultimate)	M4 ascent, pos. Manuever; (Subcase 1)	Z Stiffened Sheet	2.000	0.1205	Ti 6-2-4-2
5	4.192	1000	1000	MS = .07 (Local buckling - longitudinal direction, against limit)	M4 ascent, pos. Manuever; (Subcase 3)	(Crippling - buckling interaction, against ultimate)	M4 ascent, pos. Manuever; (Subcase 1)	T Stiffened Sheet	2.000	0.1205	Ti 6-2-4-2
6	4.192	1000	1000	MS = .07 (Local buckling - longitudinal direction, against limit)	M4 ascent, pos. Manuever; (Subcase 3)	MS = .01 (Crippling - buckling interaction, against ultimate)	M4 ascent, pos. Manuever; (Subcase 1)	L Stiffened Sheet	2.000	0.1205	Ti 6-2-4-2
7	5.565	1000	1000	MS = .42 (Isotropic strength - exceeding yield criterion, against limit)	M4 ascent, pos. Manuever; (Subcase 3)	MS = .05 (Panel buckling, against ultimate)	M4 ascent, pos. Manuever; (Subcase 1)	Honeycomb (.375" core) (max .25" core height)	0.3744	0.062	IN 600 alloy

Ultimately, the discrete stiffener approach was eliminated based on a desire to limit the depth of the panel to allow more space in the wing. This left the honeycomb design, which was later updated to a new material option not present in the HyperSizer trades, as a non-optimal approach at first. As shown below, the honeycomb design was originally not shown be a low weight solution. However, studies were updated to allow the honeycomb depth to be increased to 0.65” (instead of the artificial limit of 0.25” originally used to decrease panel depth as per the demonstration vehicle wing cross-sectional depth), which decreased the weight per square foot significantly to 1.36 which was lighter than the other solutions. An all titanium honeycomb core sandwich was eventually down-selected, per the Panel 3 trade study (Section 5.4 of this report) as the baseline design for the detailed analysis of Panel 3, assuming dimensions that were dictated by the current availability of the product.

Table 5.1.5 Panel 3 HyperSizer Weight Optimization Results

Overall ranking	Weight (lbs/sq ft)	sizing load (deg F)	Max service temperature (deg F)	Component 1 Primary Failure Mode	component 1 Primary Failure Mode load case	Component 2 Primary Failure Mode	Component 2 Primary Failure Mode Load Case	Structural Concept	Max depth (in.)	Primary Sheet Gage (in.)	Material
1	2.897	1100	1100	MS = .17 (Panel buckling against ultimate)	M2 ascent, pos. Manuever; (Subcase 1)	n/a	n/a	Hat Stiffened Sheet	1.5	0.066	Ti 6-2-4-2
2	3.754	1100	1100	MS = .05 (Local buckling, against limit)	M2 ascent, pos. Manuever; (Subcase 1)	n/a	n/a	Hat Stiffened Sheet	1.25	0.049	IN718
3	5.257	1100	1100	MS = .07 (Panel buckling against ultimate)	M2 ascent, pos. Manuever; (Subcase 1)	n/a	n/a	Blade Stiffened Sheet, longitudinal direction	2	0.049	IN718
3	5.697	1100	1100	MS = .02 (Panel buckling, against ultimate)	M2 ascent, pos. Manuever; (Subcase 1)	n/a	n/a	I Stiffened Sheet	2.00	0.2	Ti 6-2-4-2
5	6.461	1100	1100	MS = .00 (Panel buckling, against ultimate)	M2 ascent, pos. Manuever; (Subcase 1)	n/a	n/a	Honeycomb (max .25" core height)	0.3896	0.07	IN 600 alloy
6	7.035	1100	1100	MS = .04 (Panel buckling, against ultimate)	M2 ascent, pos. Manuever; (Subcase 1)	n/a	n/a	I Stiffened Sheet	2.00	0.1	IN600 alloy
7	7.889	1100	1100	MS = .05 (Panel buckling, against ultimate)	M2 ascent, pos. Manuever; (Subcase 1)	n/a	n/a	Blade Stiffened Sheet, transverse direction	2.00	0.0	IN718
8	7.986	1100	1100	MS = .04 (Panel buckling, against ultimate)	M2 ascent, pos. Manuever; (Subcase 1)	n/a	n/a	L Stiffened Sheet	2.00	0.2	Ti 6-2-4-2

The Panel 4 trade approach was somewhat different from the approach employed for the Panels 1, 2, and 3 trade studies. As Panel 4 is a fairing that was not subject to large edge loads, but does see high acoustic loading from the engines, a honeycomb sandwich design had already been selected based on the engine clearances allowable within the engine fairing. Hypersizer was again used to determine the optimum dimensions for the core thickness, material (IN718 alloy), and facesheet thickness. These results are shown in Table 5.1.6 for the more limiting maximum temperature load case.

Table 5.1.6 Panel 4 HyperSizer Weight Optimization Results

Overall ranking	Weight (lbs/sq ft)	Temp at sizing load (deg F)	Max service temperature (deg F)	Panel Component 1 Primary Failure Mode	Panel component 1 Primary Failure Mode load case	Panel Component 2 Primary Failure Mode	Panel Component 2 Primary Failure Mode Load Case	Structural Concept	Max depth (in.)	Primary Sheet Gage (in.)	Material
1	2.796	1200	1200	MS=.69 (Panel buckling against ultimate)	2 Point Landing, Hot; (Subcase 2)	n/a	n/a	Honeycomb (.375" core) (max 1.0" core height)	0.189	0.032	IN718

Using the HyperSizer studies as a basis for each panel's basic design and dimensions, the CATIA CAD models were updated, and detailed analyses were to now be commenced using the commercial Abaqus software structural analysis code.

5.2 PANEL FLUTTER ASSESSMENT

Upon the Hypersizer trade study results for panel structure baseline designs it was necessary to perform a preliminary design level check of the flutter margins of the four panels for the high speed flight regime. This had also been performed upon OML panels during the Conceptual Design Phase of the HTV-3X program and had been considered vital as a cross-check on the gauge thickness as well as the stiffener spacing for the thin gauge metallic alloy construction of the four panels. Flutter is a dynamic instability that occurs in flight where the elasticity of the structure plays an essential part in the instability. In it, vibration can amplify into structural damage. Panel flutter is unstable oscillatory motion that occurs in a panel or can occur in an array of panels.

During the preliminary design portion of Phase II, a LM Aero developed spreadsheet-based empirical panel flutter analysis was performed, and the technique was based upon NASA report CR-2801, "Design Procedures for Flutter-Free Surface Panels" (Ref. 4). The report developed a series of parameters involving aspect ratio, speed, Mach number, etc., to use to determine the required thickness of flat or simply curved rectangular panels to evaluate panel flutter. These parameters were empirical results from a series of tests and which extend into the hypersonic range.

For the study, the fuselage panels were analyzed at ambient temperature, 1000ºF and 1200ºF, with the Mach 1.2 condition considered to be the critical part of the flight envelope. The panel temperatures at that flight condition, on the descent phase of the flight after the high heating soak effects of the cruise portion of flight had been experienced, were conservatively estimated to remain at the max temperature level of the appropriate panel for this preliminary level analysis check. A 4 inch panel was selected as the starting point, corresponding to the airstream distance between the stiffeners. Likewise, 3 inch panels were also analyzed for the Ti cases.

For this spreadsheet approach six different panels strips were examined. Refer to the locations as shown in

Figure 5.2.1: 1) a 4" × 58" Ti 6-2-4-2S, simply supported 0.049-in thick panel with a 150-inch radius of curvature; 2) a 4" × 92" Ti 6-2-4-2S, simply supported 0.049-in thick panel with a 240-inch radius of curvature; 3) a 36" × 4" IN 718, simply supported 0.049-in thick flat panel; 4) a 4" × 58" Ti 6-2-4-2S, simply supported 0.032-in thick panel with a 150-inch radius of curvature; 5) a 4" × 92" Ti 6-2-4-2S, simply supported 0.032-in thick panel with a 240-inch radius of curvature; and 6) a 4" × 45" IN718, simply supported 0.049-in thick flat panel. In all cases, the stream-wise length is the first dimension and the width is the second, and the sizes represent the spacing between stiffeners on full panels 1 (strips 1 and 4), 2 (strips 2 and 5), and 3 (strips 3 and 6). Each panel was analyzed at 644 knots equivalent airspeed (keas) at the standard 15% flutter margin for ambient temperature (70°F) and flight temperatures ranging from 900°F to 1100°F. Panels 1 and 4 are the same rough shape except for the thickness; similarly, panels 2 and 5 only differ in thickness. Panels 3 and 6 are of the same panel with a different stiffener arrangement.

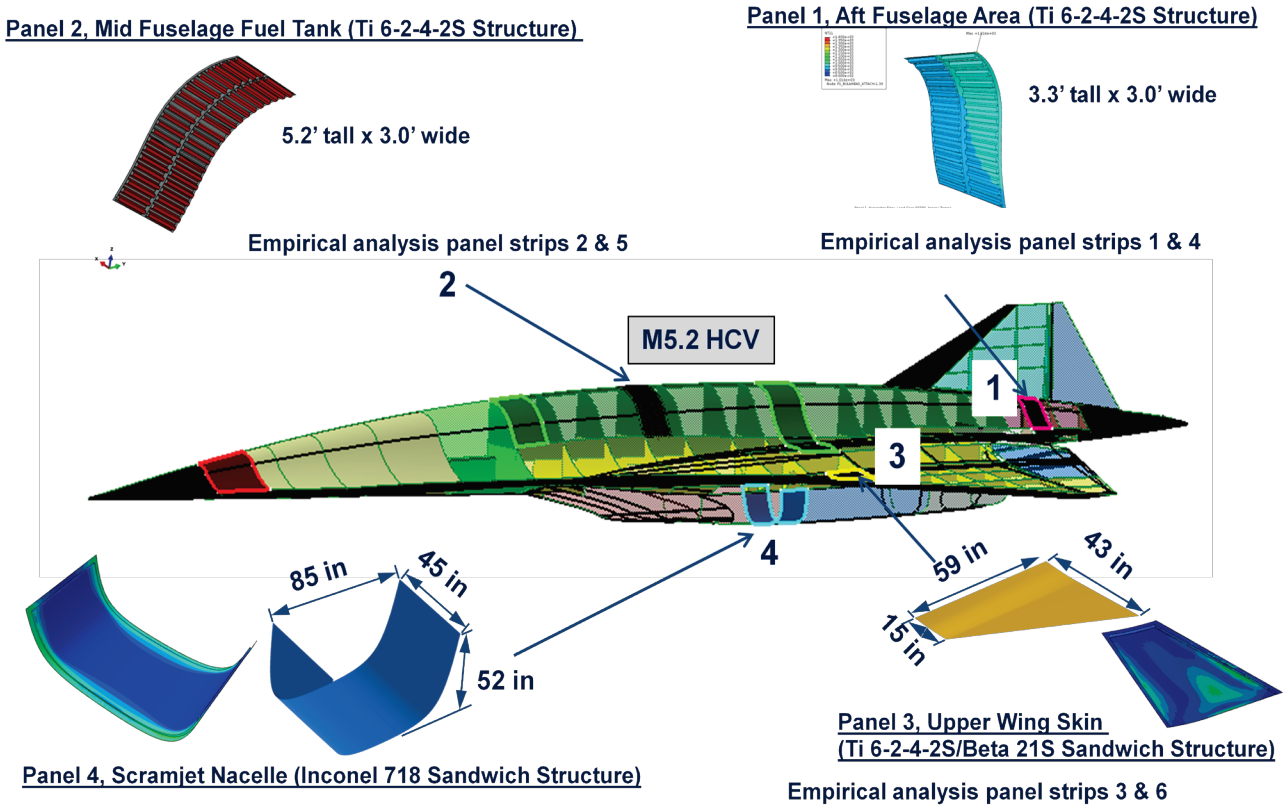

Figure 5.2.1 Panel Locations and Their Corresponding Panel Strip Sizes

Each panel was analyzed at loads ranging from 25% to 100% of the panel buckling load (P_{cr}), starting at 100% P_{cr} as a conservative load, and then reducing the load. If the actual panel thickness was greater than that analyzed to 100% Pcr, panel flutter should be precluded. The results are shown in Table 5.2.1.

Table 5.2.1 Results From Preliminary Design Level Empirical Panel Flutter Analysis

Panel strip	Corresponding panel #	streamwise length (in)	width (in)	panel thickness (in)	required thickness at 100% buckling (in)	required thickness at 50% buckling (in)
1	1	4.0	58.0	0.049	0.0451	
2	2	4.0	92.0	0.049	0.0460	
3	3	36.0	4.0	0.049	0.0613	
4	1	4.0	58.0	0.032	0.0451	0.0297
5	2	4.0	92.0	0.032	0.0460	0.0303
6	3	4.0	45.0	0.049	0.0360	

Figure 5.2.2 through Figure 5.2.7 illustrate the results for the preliminary design phase using the empirical method. The first, second, and sixth panel strips are free from flutter as designed as there is margin in the actual thicknesses. Panel strips 4 and 5, which are the same as strips 1 and 2 except for thickness, do not have margin at 100% $P_{cr,}$ but do at 50% $P_{cr.}$ Panel strip 3 does not have margin

at 100% $P_{cr,}$ but this was mitigated when it was decided to change the orientation of the stiffeners of Panel 3. Per the preliminary design phase Panel 3 trade study, its configuration was later changed to a Ti honeycomb sandwich design. Panel 4 was not run using the spreadsheet as the program is not adaptable to honeycomb structure.

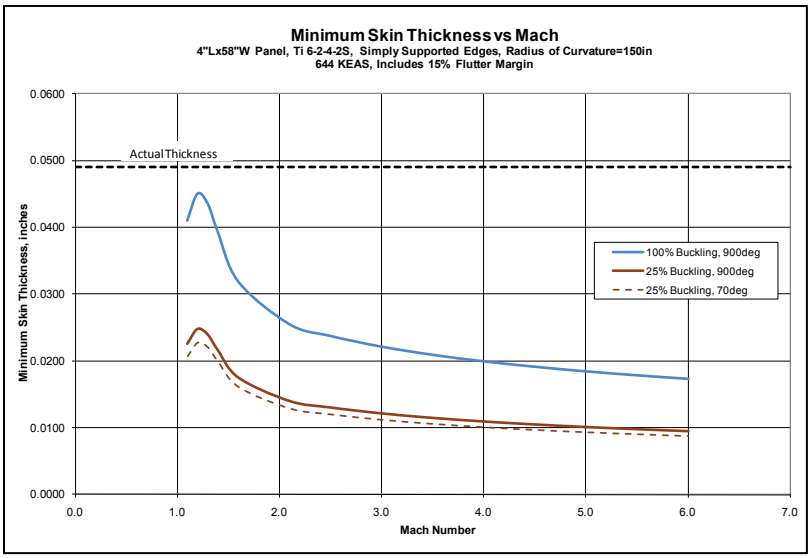

Figure 5.2.2 Minimum Skin Thickness to Prevent Flutter in 4" × 58" Ti 6-2-4-2S, Simply Supported 0.049-in Thick Panel with 150-inch Radius of Curvature at 644 keas (Corresponding to Panel 1)

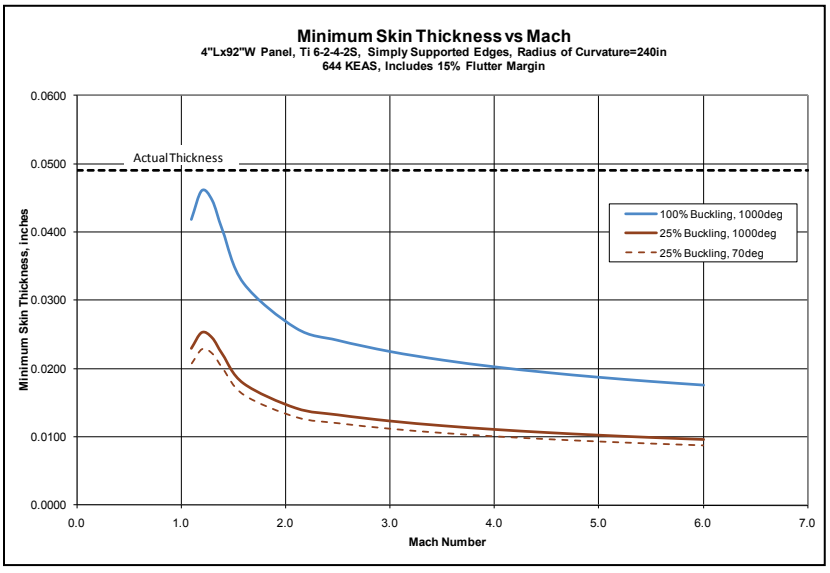

Figure 5.2.3 Minimum Skin Thickness to Prevent Flutter in 4" × 92" Ti 6-2-4-2S, Simply Supported 0.049-in Thick Panel with 240-inch Radius of Curvature at 644 keas (Corresponding to Panel 2)

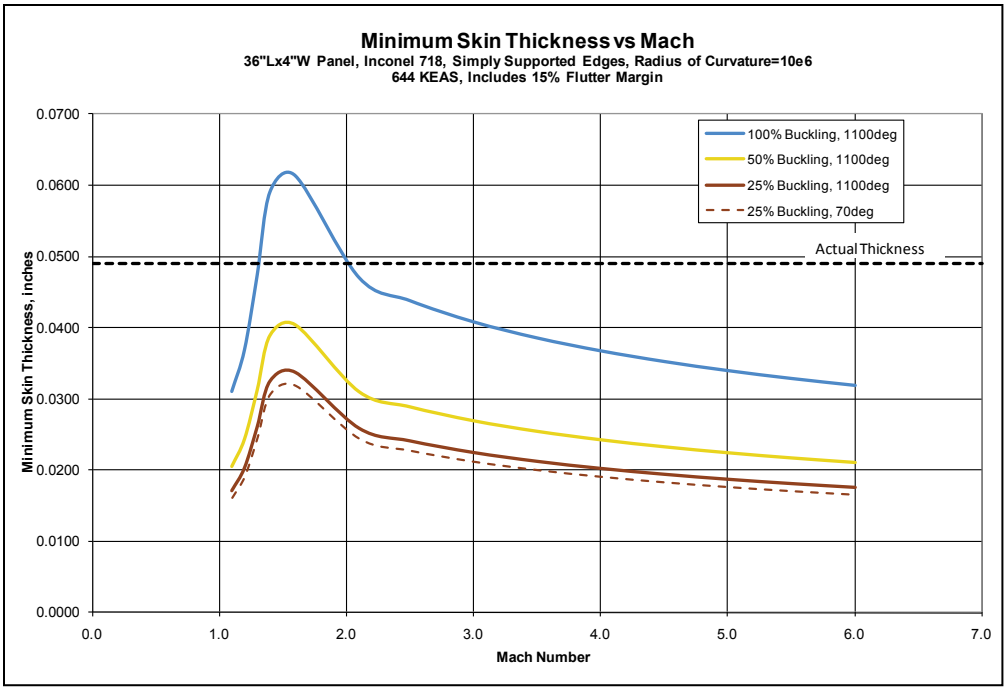

Figure 5.2.4 Minimum Skin Thickness to Prevent Flutter in 36" × 4" Inconel 718, Simply Supported 0.049-in Thick Flat Panel at 644 keas (Corresponding to the First Panel 3 Configuration)

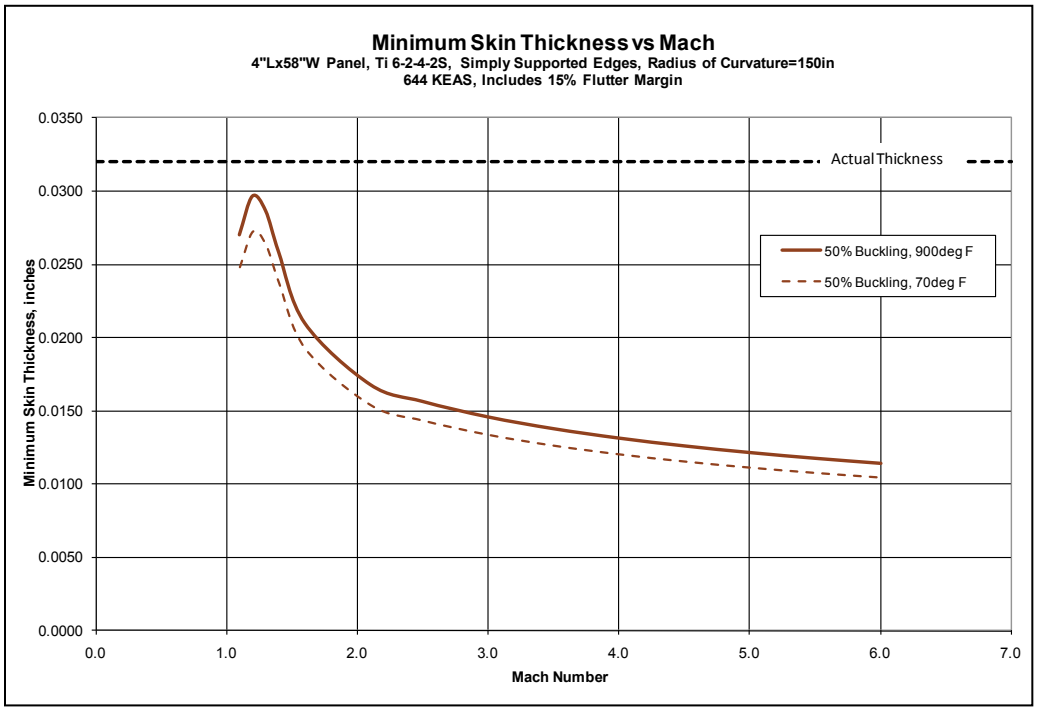

Figure 5.2.5 Minimum Skin Thickness to Prevent Flutter in 4" × 58" Ti 6-2-4-2S, Simply Supported 0.032-in Thick Panel with 150-inch Radius of Curvature at 644 keas (Corresponding to Panel 1)

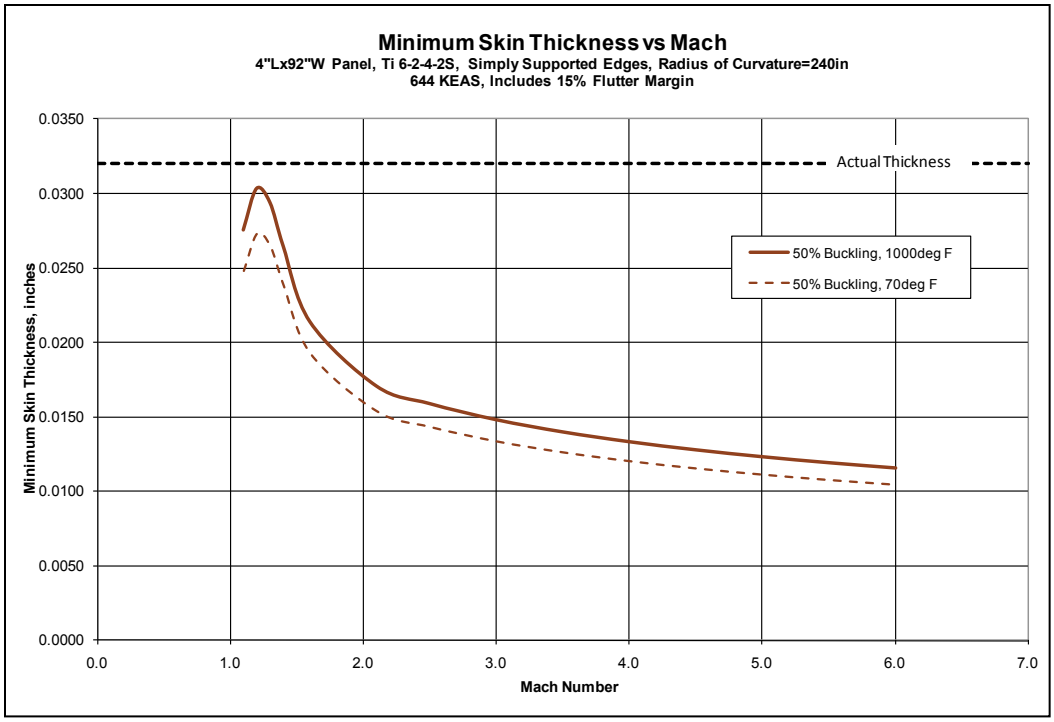

Figure 5.2.6 Minimum Skin Thickness to Prevent Flutter in 4" × 92" Ti 6-2-4-2S, Simply Supported 0.032-in Thick Panel with 240-inch Radius of Curvature at 644 keas (Corresponding to Panel 2)

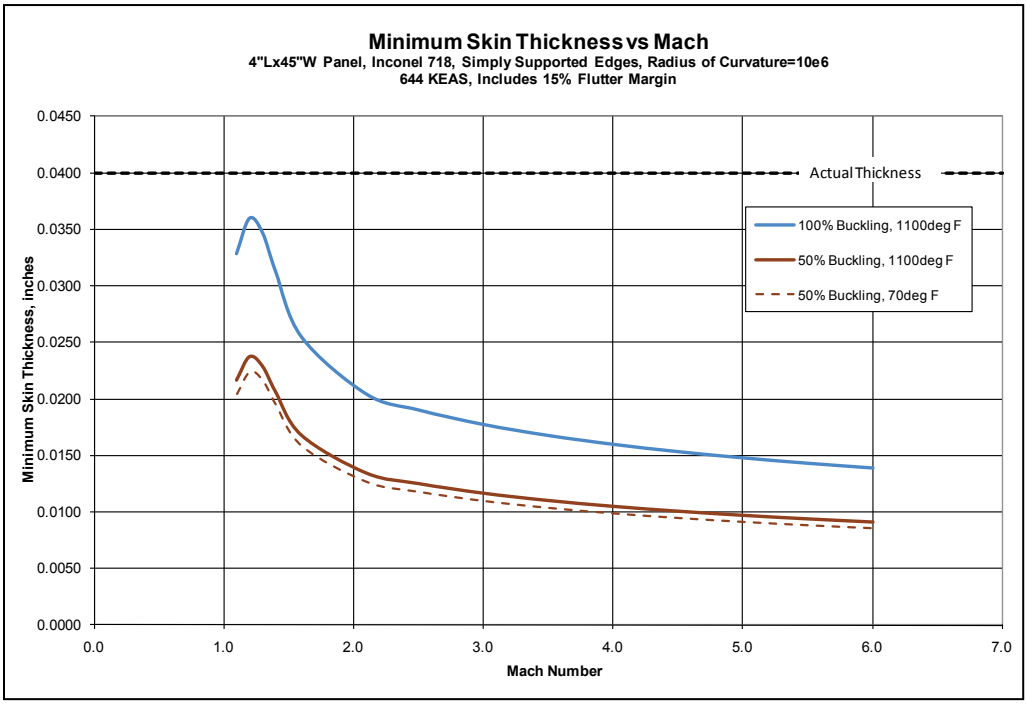

Figure 5.2.7 Minimum Skin Thickness to Prevent Flutter in 4" × 45" Inconel 718, Simply Supported 0.049-in Thick Flat Panel at 644 keas (Corresponding to the First Panel 3 Configuration)

As a summary of the preliminary design level flutter analyses, no negative margins were determined as per the baseline structural concepts as outlined, ***Figures 5.2.8 and 5.2.9***.

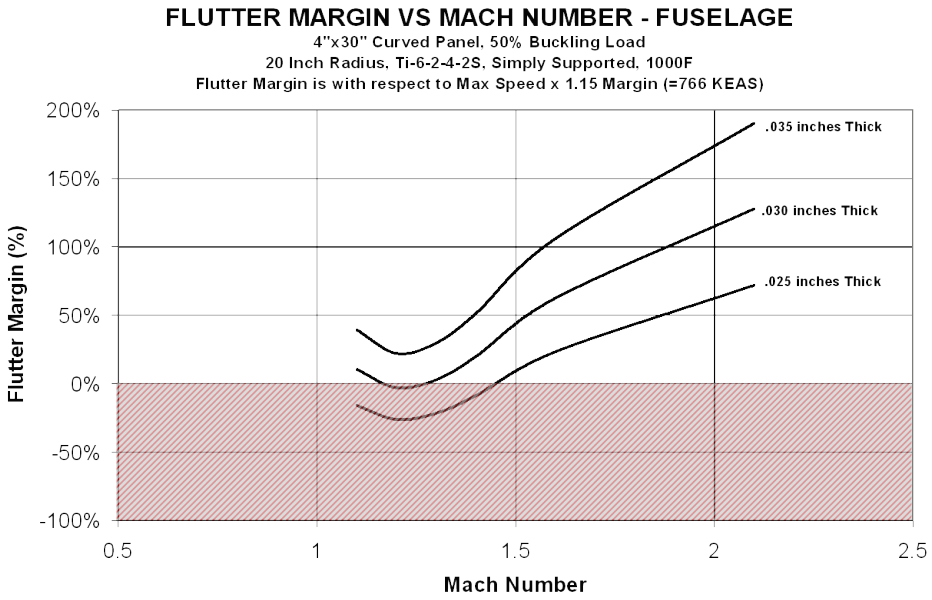

Figure 5.2.8 Flutter Margins vs. Mach Number per Three Thicknesses of Metallic Skin at 1000°F

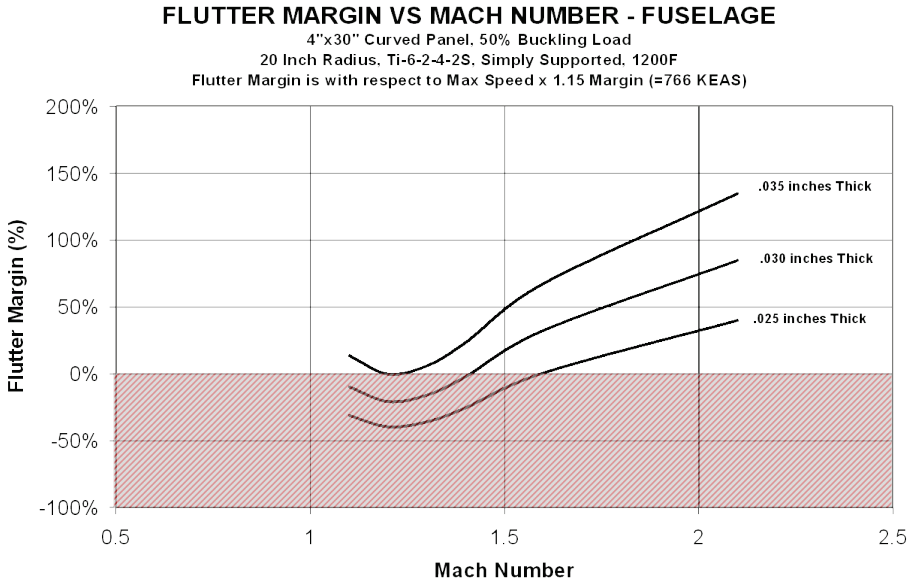

Figure 5.2.9 Flutter Margins vs. Mach Number per Three Thicknesses of Metallic Skin at 1200°F

5.3 PANEL DETAILED CFD WORK FOR THERMAL RESPONSE

Aerodynamic heating rates and the resultant surface temperatures are critical when analyzing structural behavior at Mach 5-7 speeds. Not only is material strength degraded during high Mach flight, but over the life of the vehicle, creep can become significant. In addition, thermal stress can become the dominant stress for some vehicle components and must be accurately accounted for. Aerodynamic analysis provides pressure loads, skin friction levels, and aerodynamic heating rates which are used as inputs for structural loads analysis. Although approximations can be made

through the use of geometrically based impact methods for pressure loads, and Reynolds number-based flat plate analysis for both friction forces and temperatures, the most accurate approach for obtaining aerodynamic forces and heating rates is through the use of three dimensional Navier-Stokes equations.

The pre-Phase II tasks performed during the Phase I project provided RET maps over the outer surface of the vehicle using impact methods and the Reynolds analogy, and these were highlighted in Section 4.3 of this report. This method provided pressure and temperature data at the vehicle surfaces and the heating rates were extracted. This approach is sufficient for the acreage of the vehicle but does not account for the nonlinear effects, such as boundary layer state and or shock interactions, both of which can be locally significant for thermal and pressure loads.

RET maps were utilized in the initial screening material phase as well as the preliminary design phase
of the individual panels. Higher fidelity temperature maps of the panels were required for detailed design and this work is described in Section 6.4 of this report.

5.4 PANEL 3 TRADE STUDY

Upon completion of the Hypersizer code based Panel 3 (***Figure 5.4.1***) preliminary design results (***Figure 5.4.2***) further investigations were made into previous studies conducted by LM Aero on Mach 5 airframe structures, and especially for upper wing skin compression critical design areas of high speed and hypersonic aircraft. Metallic honeycomb structures, while intuitively thought as providing enough stiffness for compression and buckling critical structure, were not acceptable for the wing skin structure of the HTV-3X vehicle per the thin cross section of the wing design. However, with the thickness of the HCV wing and sections just aft of the vehicle leading edge ranging between 11-12” in depth depending upon the point on the span, honeycomb sections were considered to be very viable candidates for upper wing structure. The outboard wing structural box of the HCV, following on the wingbox studies performed under the HTV-3X program, was base-lined as a multi-rib design with ribs and spars for honeycomb skin to mechanically attach to. As the vehicle design did not rely upon fuel laden wings the mechanically attached panel design was also base-lined.

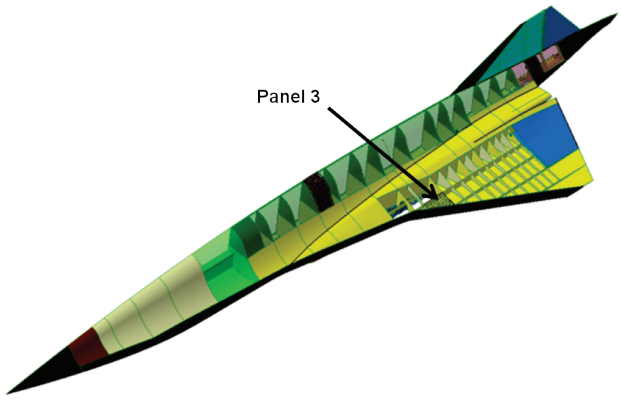

Figure 5.4.1 Panel 3 Upper Wingskin Structure in the Aero-Elastic Critical Zone

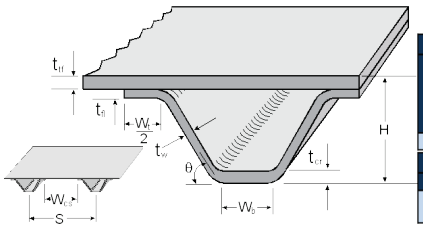

Component Dimensions													
Component ID	t_{tf} (in)	t_w (in)	H (in)	S (in)	w_b (in)	θ (°)	w_t (in)	w_{cs} (in)	t_{fl} (in)	t_{cr} (in)	Unit Weight (lb / ft²)	Area (ft²)	Weight (lb)
1	0.049	0.032	0.75	4	1.5	75	1	1.141	0.032	0.032	3.425	1	3.425

Component Margin of Safety Summary					
Component	MS	Load Case	Lim/Ult	AID	Analysis
1	.09	1	Limit	43	Local Buckling-Interaction

Weight: 3.425 lbs / sqft
Matl: IN 718
Temp: 1000 deg
LoadCase: 60009, subcase 1
Stiffener Orientation: Chord-wise

Figure 5.4.2 Panel 3 Preliminary Design Structural Concept Baseline

During the course of the Hypersizer based structural trade study results showed strong weight advantages even with using a more conservative but lower service temperature capable Ti 3-2.5V panel structure. This amounted to weight savings up to 60% per square foot of the entire upper wing structure. As a whole, the material property screening reinforced earlier assessments of the Ti 6-2-4-2 and Ti 6-2-4-2S alloys as offering strong lower weight potential options for stiffness critical structure for design areas up to 1000°F and possibly even over 1000°F.

The Panel 3 trade study was conducted through the following approach steps:

1. Definition of the trade study purpose and approach methodology
2. Initial temperature field determination
3. Material screening for the $\geq 1000^0$F environment
4. Review of previous Ti sandwich panel work (1980s-1990s)
5. Panel 3 Hypersizer addendum runs (to the initial runs per the blade stiffened design, Table 5.1.5 results)
6. In-plant discussions with potential vendors on the bond/weld technologies to date and determination of the manufacturability of panels with 1-D and 2-D curvature

In general, the structural panel design in this vehicle zone was driven by stiffness requirements over material strength requirements as the leeward, or upper, side wing structure would be designed primarily for compression and buckling failure drivers. A honeycomb core/sandwich panel that could be designed to carry both spanwise and chordwise bending loads, while providing a light weight structural concept option, appeared highly lucrative during the course of preliminary design. The honeycomb structure would be designed to transmit the wing surface loads into the structural wingbox through the ribs that the honeycomb panel is joined to and the biaxial strength capability of the honeycomb itself. However, a honeycomb core structure might potentially pose a greater thermal stress risk which deemed that it should be studied further with an available structural database. Nonetheless, as hypersonic airframes evolve through design the gaps in the study of these structural concepts should be studied with the analysis gaps capabilities fully

identified and exploited. On a detailed level, the facesheet failures that would drive the design would center upon in-plane strength, wrinkling, and dimpling while the core failures would comprise its capability of shear strength, shear crimping, cell buckling, and its avoidance of core crushing.

Based on prior LM Aero research the following assumptions were made:

1.) The Mach 5 vehicle invoked reference, was a blended wing-body and in a configuration with suitable applications for new materials and structural concepts to permit usage in this study. 2.) The wing box structure was similar enough for use in this study; 3.) An adequate joint design, i.e., panel-to-panel, panel-to-rib, and panel-to-spar could be made to enable the joining of titanium H/C sandwich to high temperature wing structure; 4.) An oxidation resistant coating would be needed to prevent deterioration of the mechanical properties of the titanium skins for prolonged service above 1000^{o}F. In house research has shown the alloy is susceptible to surface initiated cracking under short time exposures at 1200^{o}F in air atmosphere (***Figure 5.4.3***).

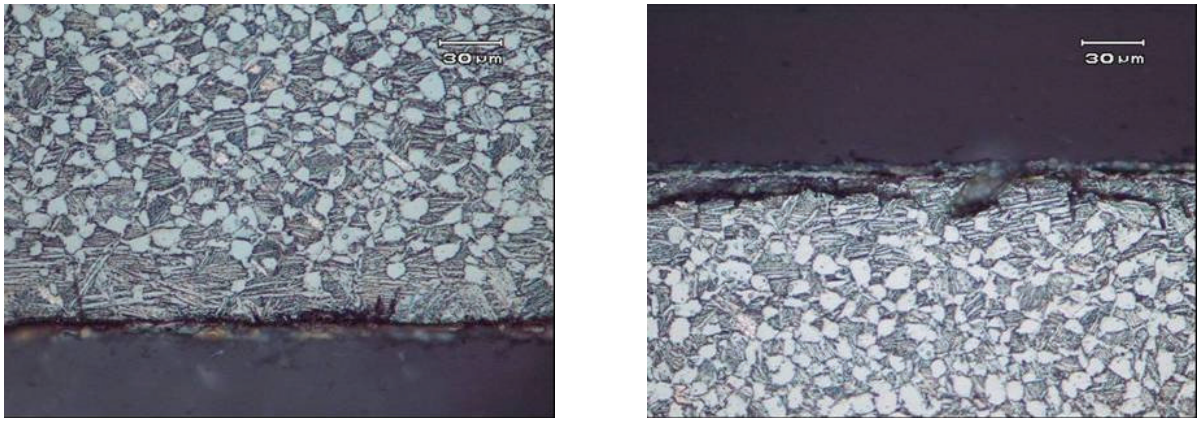

Figure 5.4.3 Ti-6-2-4-2 Sheet After 1200^{o}F Exposure for 50 Hours (left) and 200 Hours (right)

LM Aero has a long-standing relationship with DOD and NASA-LaRC personnel in the development of advanced materials and high temperature structures. Assisting LM Aero in these endeavors has been Goodrich Aero-Structures (previously known as Rohr Industries, of Chula Vista, CA) and GKN Manufacturing (formerly ASTECH, of Santa Ana, CA). These are two of the foremost manufacturers of titanium and nickel based honeycomb (H/C) sandwich structure in the United States. LM Aero has worked together with both companies on many research projects over the past 30 years including the production of flight hardware.

Goodrich Aero-structures has extensive experience in the design, fabrication, and assembly of engine nacelle covers using their patented Liquid Interface Diffusion (LID) brazing process. A furnace operation is used to melt the braze alloy which then forms a eutectic with the substrate and upon cooling joins the honeycomb core to face sheets. The process allows for flat or contoured panel design and manufacture. A superior, more efficient part fabrication and assembly method is made available by combining super-plastic forming (SPF) facesheets and then assembling with LID bonding. Complex shapes are more easily attained though tooling is more expensive than the GKN process. LID is a capable and proven technology for joining titanium based alloys, and the

LID process has stood the test of time for it continues to be used in bonding titanium alloys into metallic sandwich for superior light weight primary structure. Some of the more salient structural applications include the aircraft engine nacelle structures cited below in ***Figure 5.4.4***.

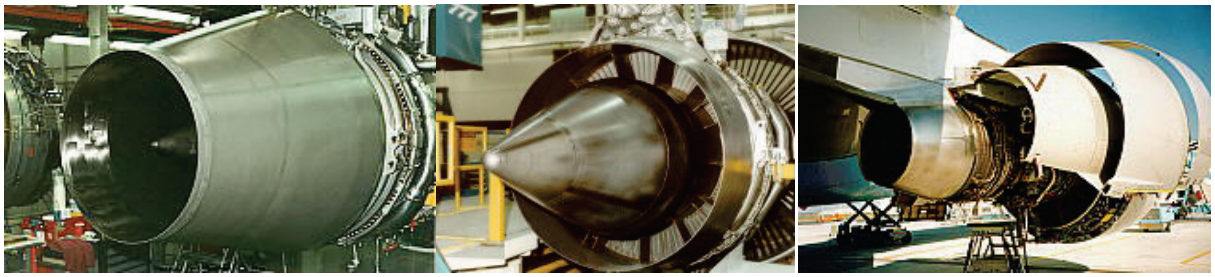

Figure 5.4.4 Examples of Uses of Titanium Honeycomb Sandwich Structures in Engine Nacelle Areas.

Goodrich has also been instrumental in the design, development and use of nickel honeycomb sandwich structure dating back to the early 1970's. Design applications have since included the programs as the X-33, and many high temperature engine ducts.

GKN Manufacturing is another company with considerable expertise in this area. The GKN process incorporates fabrication of the core and face sheet using an in situ core H/C forming and spot welding process to make honeycomb sandwich structure. Shaping the final product is possible much like what is done in stretch forming sheet metal parts. Welds at the nodes of the thin core hold up extremely well. The GKN designs can accommodate cutouts, attach fittings (incl. crushed core), and bosses for attaching the adjacent structure to the assembly. The GKN honeycomb sandwich process was used extensively in the engine exhaust area of the F-117 Nighthawk. The engine exhaust duct called the "Platypus" (See ***Figure 5.4.5***, below), consists of thin gage IN617 honeycomb core brazed to nickel face sheets. This type of technology is mature and is presently used in the engine nacelle areas of the major engine companies.

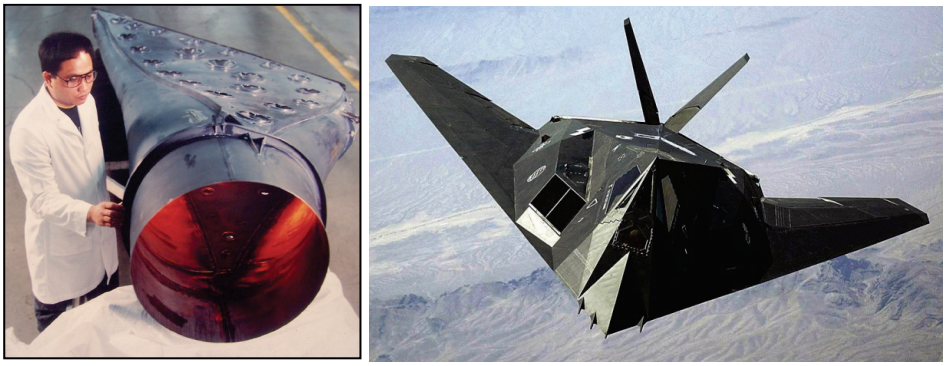

Figure 5.4.5 IN617 Exhaust Tailpipe "Platypus" for F-117 Nighthawk Program

In the early-to-mid 1980's Lockheed undertook several studies to develop advanced high temperature materials and structural concepts. Funding agencies were DOD, in general, and the NASA-Langley Research Center, Hampton, Virginia. Early efforts addressed the development and characterization of the new (as of 1981) TI-6Al-2Sn-4Zr-2Mo alloy (Ref.5) with additions of 0.10-0.15 w/o silicon. Minor additions of silicon were found to enhance the creep resistance of the alloy. The baseline panel design consisted of two outer facesheets of Ti 6-2-4-2S, diffusion bonded to Ti 6-4 honeycomb core. The study was undertaken as there was considerable interest in the alloy

for use in honeycomb sandwich structure for high speed aircraft and spacecraft. The alloy was tested in tension, bend, lap shear, creep, fatigue, fatigue crack growth, and honeycomb sandwich tests at room and elevated temperature (900°F). The effects of processing variables, e.g., TIG welding, LID bonding, and heat treatment of the parent metal, were examined. Favorable results were obtained and the material was subsequently selected for use in design and fabrication trials of titanium honeycomb core sandwich structure. The program looked at the design, development, and test of bi-axially stiffened Titanium honeycomb sandwich panels and the sub-component tests consisted of shear tests, bending tests, and static tension and compression tests at room and elevated temperature. During the program experimentally determined stresses that were applied in the upper facesheet were found to be within 10% of predicted levels. Component testing to that time had not indicated any core-to-facesheet dis-bonding as the panels had withstood the expected thermal stress levels. Results were promising enough to fabricate demonstration articles like those in Figure 5.4.6. The success of these efforts led to the inclusion of such technology for use in a Mach 5 hypersonic aircraft in a subsequent LM study and the primary use of the sandwich structure was for the vehicle upper wing skin layout as shown in ***Figure 5.4.6*** below.

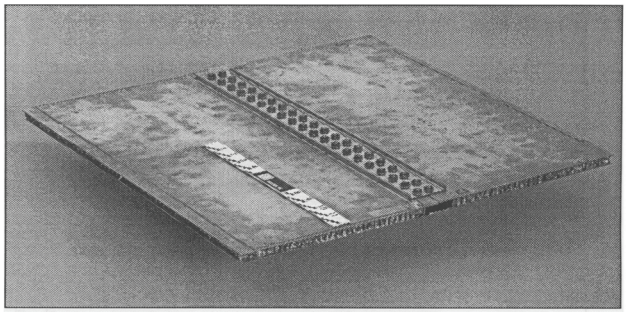

Figure 5.4.6 Demonstration Upper Ti Wing Panel

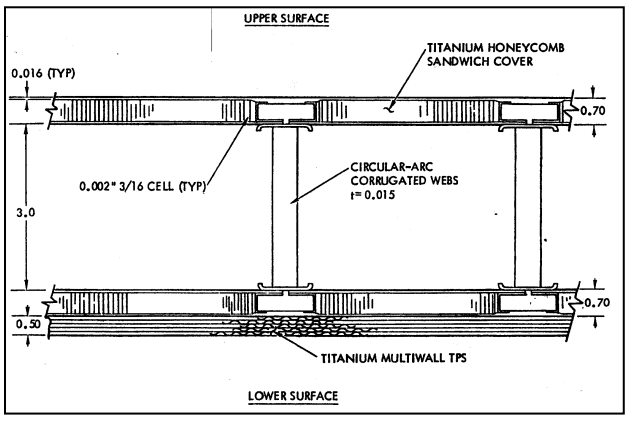

Figure 5.4.7 Typical Outboard Wing Structure

During the course of the Phase II project LM Aero personnel paid visits to both companies to: 1.) solicit the latest technology developments that may merit inclusion into the Phase II portion of the program; 2.) determine the availability of any design data on the predictive nature of alpha case for titanium alloys, e.g., the alpha case thickness as a function of temperature and time exposure in air, and subsequent effects on design properties; and 3.) determine possible teaming arrangements should schedule and cost data warrant inclusion into the program.

LM Palmdale Engineering visited Goodrich in May 2011 and met with several members of the Engineering and Management staff. LM personnel gave them a review of prior joint research and development work and requested its pertinence towards using in the current program. Considerable discussion centered on the effects of alpha case on mechanical properties and accessing company proprietary data for the same. After some back and forth discussions with management it was decided not to team with Goodrich. Goodrich had the data that LM requested, but it could not be utilized since considerable internal development costs were involved as Goodrich was not amenable to divulging such information especially for a relatively small research program.

In June 2011 LM Engineering paid a visit to GKN/Astech and reviewed with them more the same issues. GKN expressed an interest in participating in Phase II of the program and Phase III if it was awarded. GKN/Astech did offer considerable information leading into the effects of alpha case on mechanical properties. More specifically, there was interest in acquiring information on alpha case versus temperature and time, coatings development to curtail the development and growth, and affect on mechanical properties. ***Figure 5.4.8 and Figure 5.4.9*** provide samples of this data.

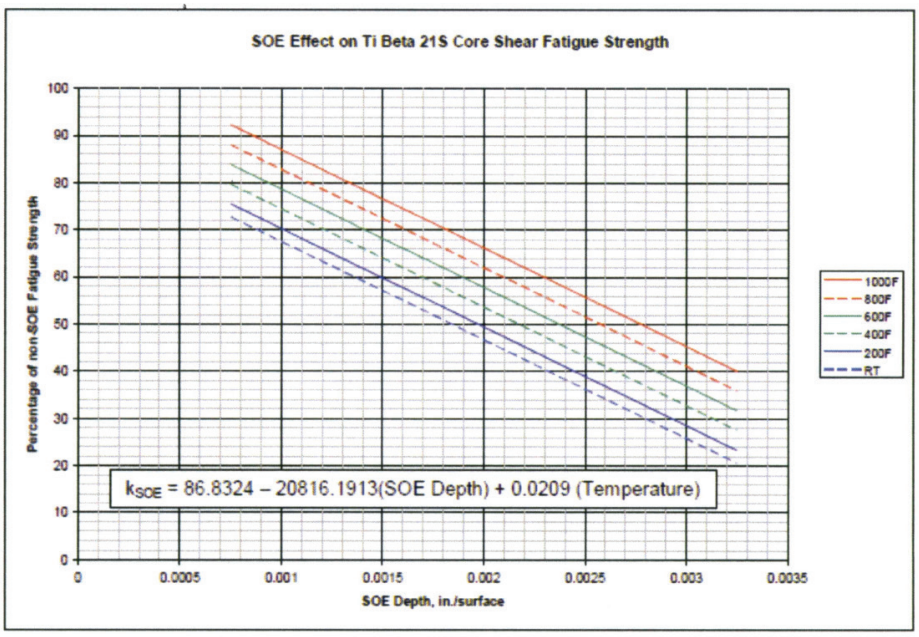

Figure 5.4.8 Effect of SOE Accumulation on Ti Beta 21S Core Shear Fatigue Strength

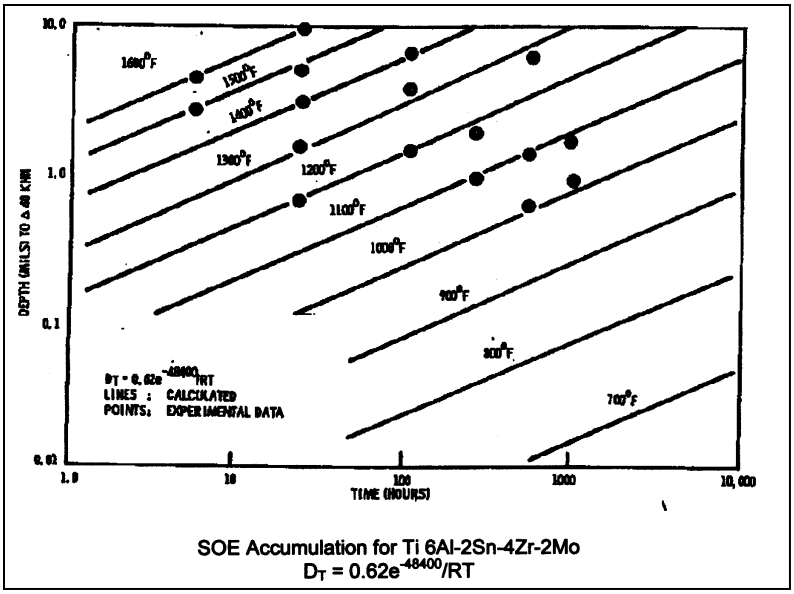

Figure 5.4.9 Oxide Depth as a Function of Time and Temperature

There was some discussion about Ti-6-2-4-2S sheet being capable of withstanding 1200°F for long time exposures on the order of hundreds of hours, as considerable investment in this area had been made by both GKN/Astech and Goodrich. Upon closer examination of the Ti alloy sandwich structures that were being developed by both companies it was determined that indeed, the engine nacelle structures were being exposed briefly to these ~1200°F temperatures just from engine run-up prior to take-off and departure. However, the exposure times were very brief and, if all totaled, the aggregate time at temperature was considered short, as in tens of hours. Thus, upon discussion of the honeycomb sandwich structures it was apparent that these structures had sustained thermal exposure to temperatures much higher than previously thought possible, but only for a very brief total time period. This was in stark contrast to Lockheed's very own data which showed severe micro-cracking at exposure temperatures of 1200°F for 50 and 100 hours (Figure 5.4.3). Although static properties would fare reasonably well, these fine cracks would cause severe reduction in fatigue and fracture properties.

The GKN/Astech high temperature Titanium panel uses Ti 6-2-4-2S facesheets with Beta 21S core structure and the structure is currently flying on the 747-8 exhaust nozzles and was nearing FAA certification at the time of the visit to GKN/Astech. In addition, similar structure has been flying on the A330 Airbus sine 1993 with 30,000-40,000 hours at over 1200°F service temperature. Upon discussions with GKN/Astech LM was highly advised that strong consideration must be given to the close-out design of the panel and that this must be well thought out in advance. Core crushing for closeouts was one concept that was discussed at this time.

It was at this point in the program where it was decided that the alpha case data needed for actively determining the affect on mechanical properties with time on the aircraft, it was determined that this subject was extensive and way outside the scope of this program. Thus it was mutually decided that the alpha case issues would be disregarded for the remainder of the program.

The initial concept of the Panel 3 design is as shown in ***Figures 5.4.10 - 5.4.11*** and consisted of blade stiffeners per the Hypersizer code based preliminary design level trade studies. Closer examination of the thermal boundary conditions were made per the thermal model results of the HTV-3X program which displayed results for flight up to Mach 5 plus. The temperature levels of several points of the OML of the panel were tracked and plotted per the flight trajectory. In short, the thermal field showing a predominance of > 1000ºF in service temperatures at the Panel 3 location denoting a departure from industry acceptable Ti 6-2-4-2S utilization for long term service and operations was seen as a risk in pursuing Ti honeycomb panel structure for Panel 3. However, in discussions with both Goodrich and GKN/ASTECH it appeared that the Ti 6-2-4-2S alloy in general is acceptable for prolonged temperature spikes to 1100ºF and 1200ºF.

Upon examination of the HTV-3X trajectory at the Mach 5+ environment the results for the leading edge points of Panel 3 temperatures over 1000^0F were observed. Peak temperature levels aft of the leading edge points in the chord wise direction reached levels below the customary design limit of 1000^0F. In the case of an actual wing design effort and until further exposure testing at the anticipated temperature levels would be performed the design of the leading edge structure to acreage hot structure joint would be moved aft toward the near and below 1000^0F acreage temperatures zone. For the purposes of the HCV and Phase II panels study it was decided to continue to look at 1000ºF – 1100^0F area exposure of the Ti honeycomb concept for the upper wing structure as a great weight advantage over heavier heat resistant alloy based design could, and might, be realized.

As a conclusion to the trade study the recommendations that were made were to proceed with welded Ti 6-2-4-2S sheet/Beta 21S core sandwich structure as the baseline concept for the Panel 3 critical design phase.

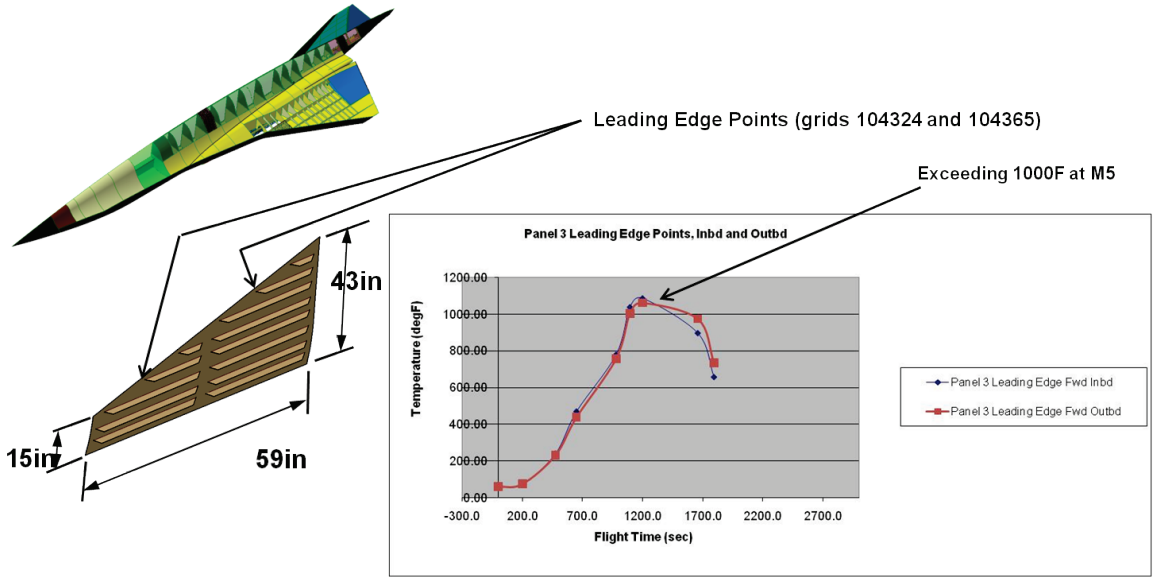

Figure 5.4.10 Panel 3 Leading Edge Points Temperature vs. Flight Time

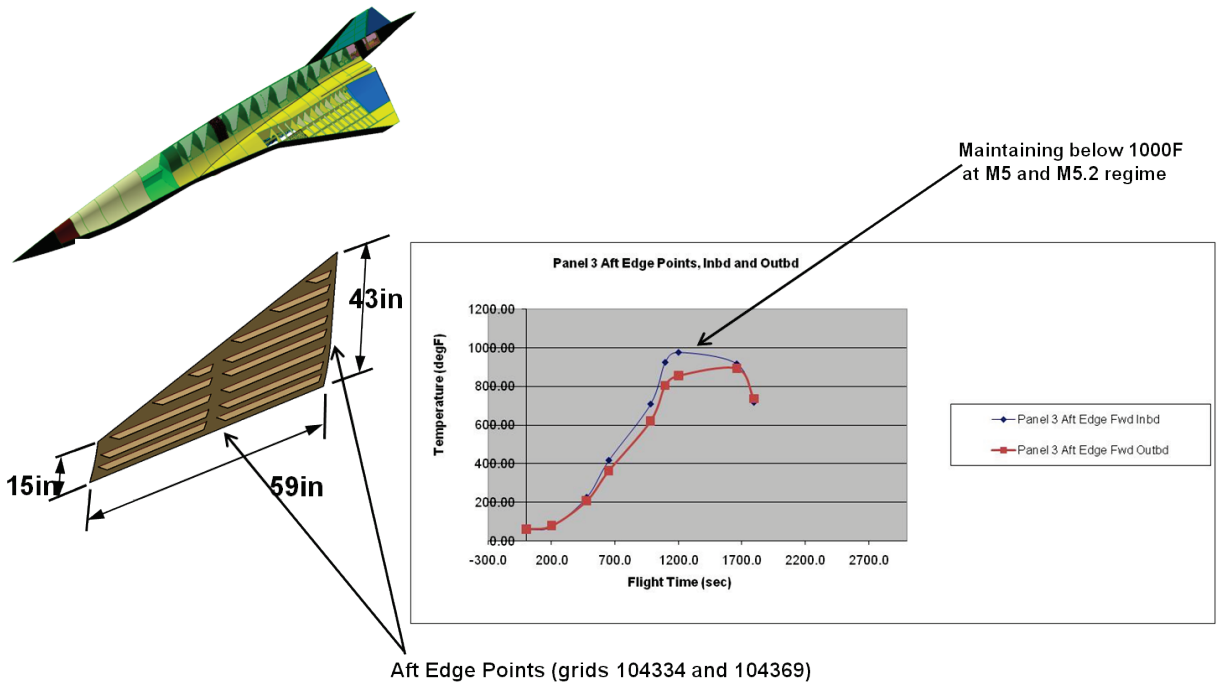

Figure 5.4.11 Panel 3 Aft Edge Points Temperature vs. Flight Time

5.5 FINAL DOWN-SELECT OF PANEL STRUCTURAL CONCEPTS PER PRELIMINARY DESIGN PHASE

At the conclusion of the preliminary design phase Panel 1-4 results were briefed to Air Force Research Lab for concurrence and approval to proceed with the baseline panels into the critical design phase of the Phase II program.

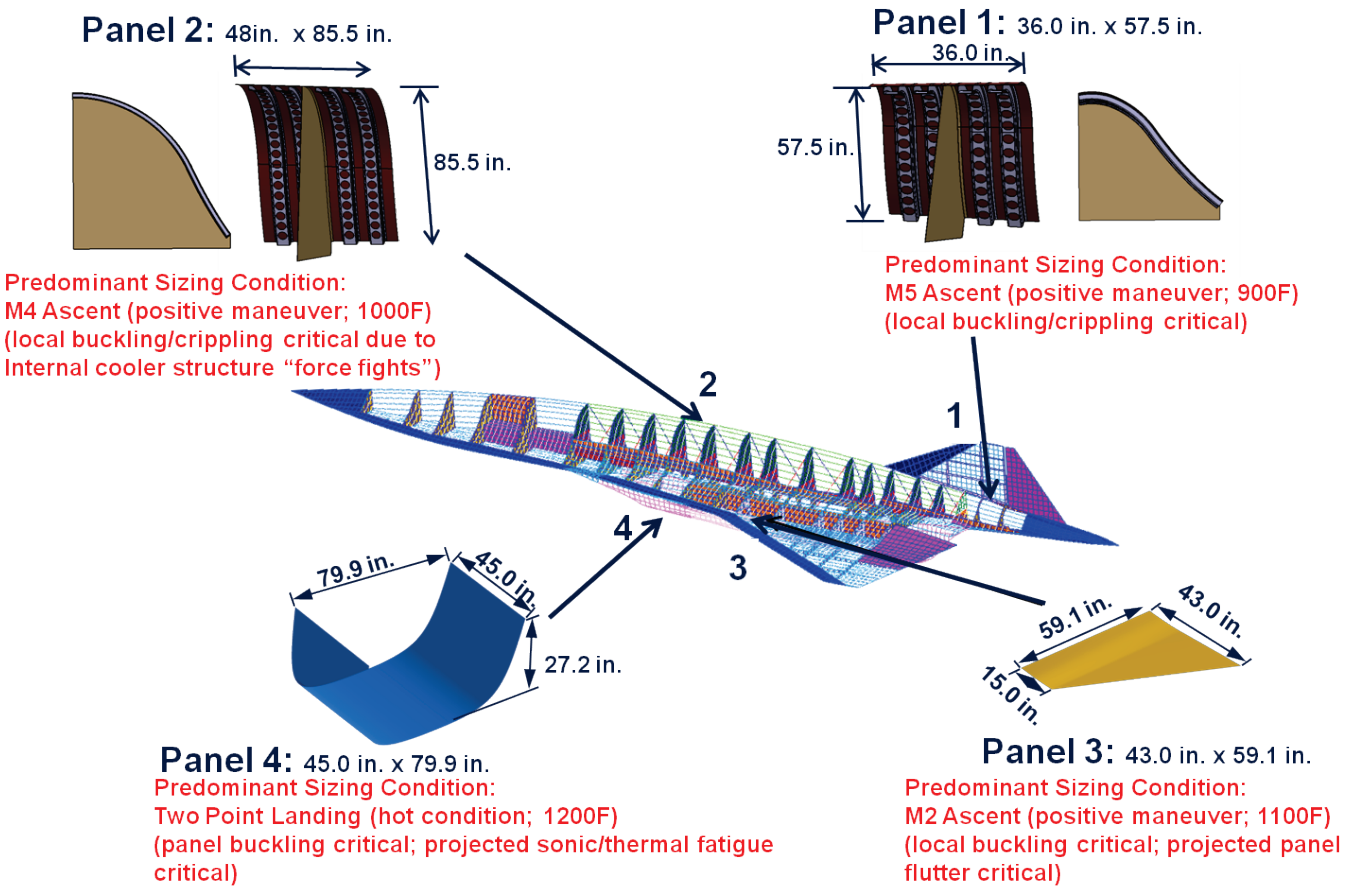

Figure 5.4.12 Down-selected HCV Panels 1-4 per Design Criteria: 3D Solids for Preliminary Design Phase Component Study

6.0 CRITICAL DESIGN PHASE

Upon completion of all design and analysis tasks for the four panels during the Preliminary Design Phase critical design of the panels, for static response as well as service life prediction, was commenced.

6.1 PANELS RESPONSE PREDICTION (STATIC SIZING)

Using the preliminary sizing from HyperSizer as the starting point, each panel was analyzed in further detail using the Abaqus Finite Element Analysis (FEA) software suite as the pre and post processor, as well as the solver. Abaqus FEA was chosen for this study due to its strength in non-linear analyses, as well as assembly features which allow more parametric options in combining parts, such as fastener spacing independent of node locations, and "tie" constraints which allow a welded boundary condition without having node locations from each part lined up exactly.

Since the Phase II project required starting with a legacy model from another software package, making a true "sub-model" of each panel was not straightforward. If project schedule time had allowed, a recreation of the loads model in Abaqus FEA with the full load case spectrum run would have been ideal. This would have allowed for easy sub-modeling within Abaqus FEA to better capture the effects of the substructure on each panel, and especially in thermal conditions. Lacking this option in this phase, a best effort was made to recreate a small amount of the substructure associated with each panel, and to utilize loads from the Patran model and apply them to the substructure in order to account for the remainder of the vehicle. Having substructure to attach each panel to allowed a more accurate thermal expansion analysis to be performed. Detailed temperatures were then able to be applied to both the panels and substructure, allowing the fastening scheme to be loaded as well as providing more accurate results of the thermal effects within the panels.

Each modeled part such as skin and stiffeners was modeled independently and then assembled in Abaqus FEA. When possible, all parts were modeled with 2D elements to allow sizing studies to be performed by iterating on sheet thicknesses. Only honeycomb core was modeled as solid elements, which is shown later for Panels 3 and 4. The basic model construction process for each panel consisted of the panel sheets and stiffener concept being assembled, and then that subassembly was attached to the substructure. For Panel 1, the hat stiffeners were first assembled onto the skin sheet shown in ***Figure 6.1.1.1***.

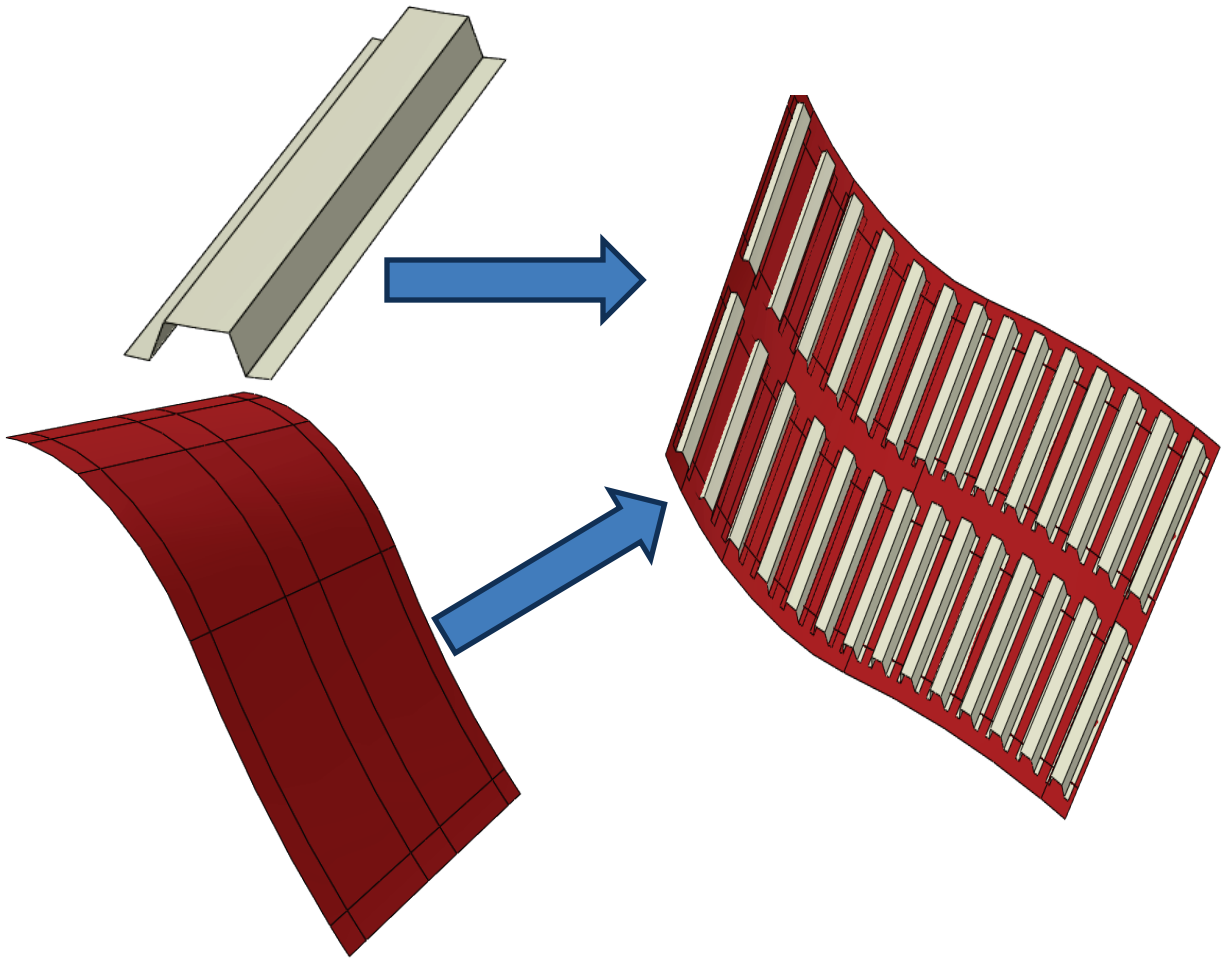

Figure 6.1.1.1 Panel 1 Sub-Assembly

Once the panel was assembled, it was then attached to a selection of keels and bulkhead partial pieces which were used to represent the underlying substructure of the vehicle, as shown in ***Figure 6.1.2***. Once all parts were assembled, the fastening scheme was implemented. The baseline fastening scheme for Panel 1 is discrete fasteners. Using a fastener boundary condition available in Abaqus FEA, the green crosses represent the desired fastener locations. A sample of the fastener location is shown in the close-up section in ***Figure 6.1.3***.

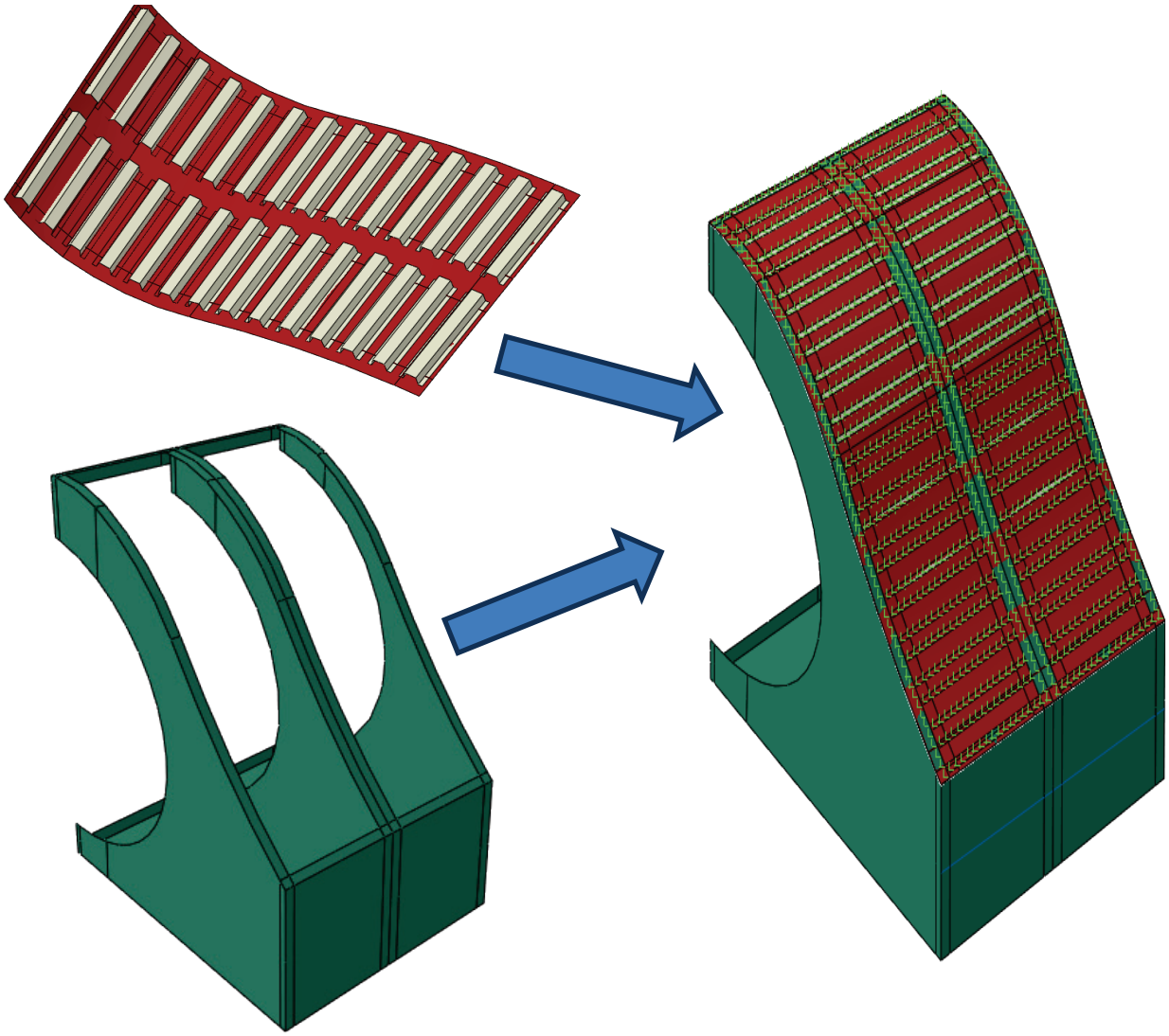

Figure 6.1.2 Panel 1 to Sub-Structure Attachment

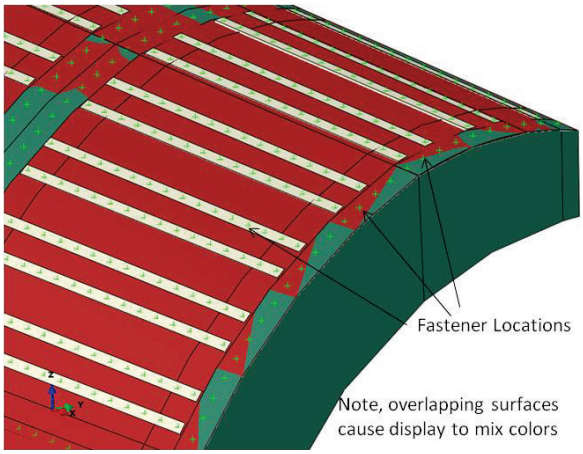

Figure 6.1.3 Fastener Location Sample

Panel 2 was very similar to Panel 1 in the model construction, and the final assembly is illustrated in ***Figure 6.1.4***. The main difference between Panels 1 and 2, aside from the size and shapes, is the baseline attachment scheme. As Panel 2 is located in a wetted fuel zone, a welded approach was base-lined. For the attachment of the stiffeners to the skin, a spot welding scheme was used and was attached analytically similar to the fastener attachment used for Panel 1. For the perimeter attachment of the panel to the substructure, an e-beam weld was base-lined. The simplest way to incorporate this into the model, while still leaving the option to go back to fasteners if desired, is to simply model the joint as fastened similar to the spot welds, except to make the make the fastener spacing smaller than the element size, thus attaching every coinciding node similar to a weld.

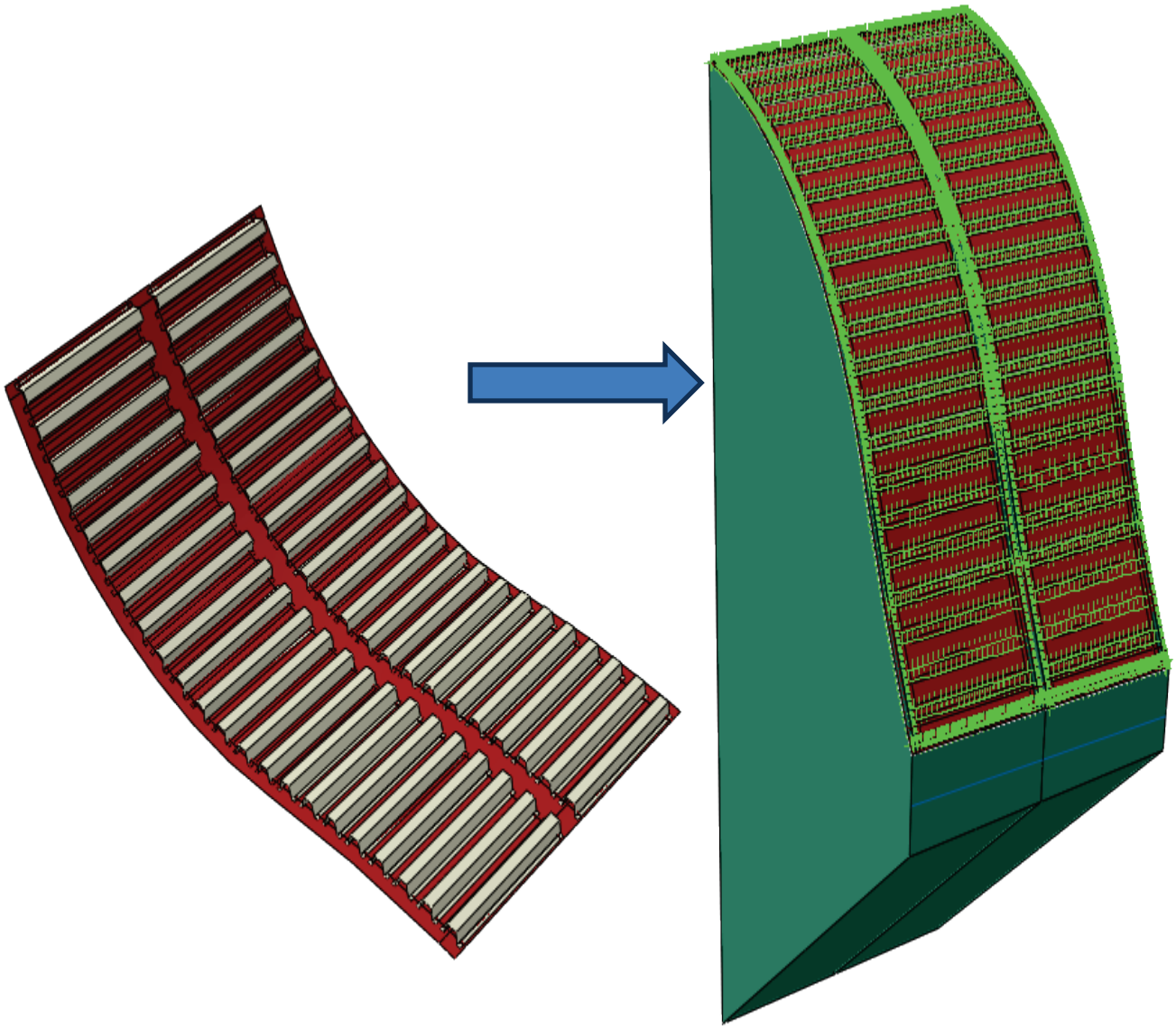

Figure 6.1.4 Panel 2 to Sub-Structure Attach

Panels 3 and 4 are of honeycomb sandwich structure and thus required a different type of modelling and assembly technique effort. The honeycomb skin panel consisted of a top and bottom skin. The honeycomb core was modelled as solid elements and a “frame” part, which holds all the

other parts together by providing a 90 degree connection between the sidewalls with an “L” shape. The core was connected to the top and bottom skins via a “tie” constraint in Abaqus FEA, which acted as a weld. The frame was then tied onto one leg of the L, onto the bottom of the top skin, onto the downward leg of the L to the sides of the core, and, finally, onto an edge of the bottom skin. This Panel 3 assembly is shown in ***Figure 6.1.5***.

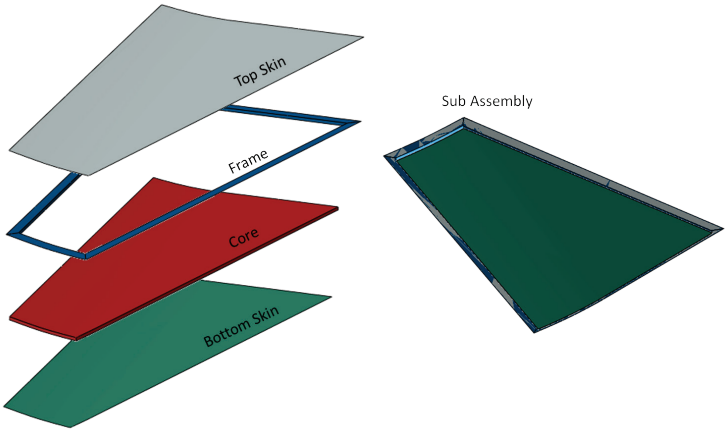

Figure 6.1.5 Panel 3 Assembly

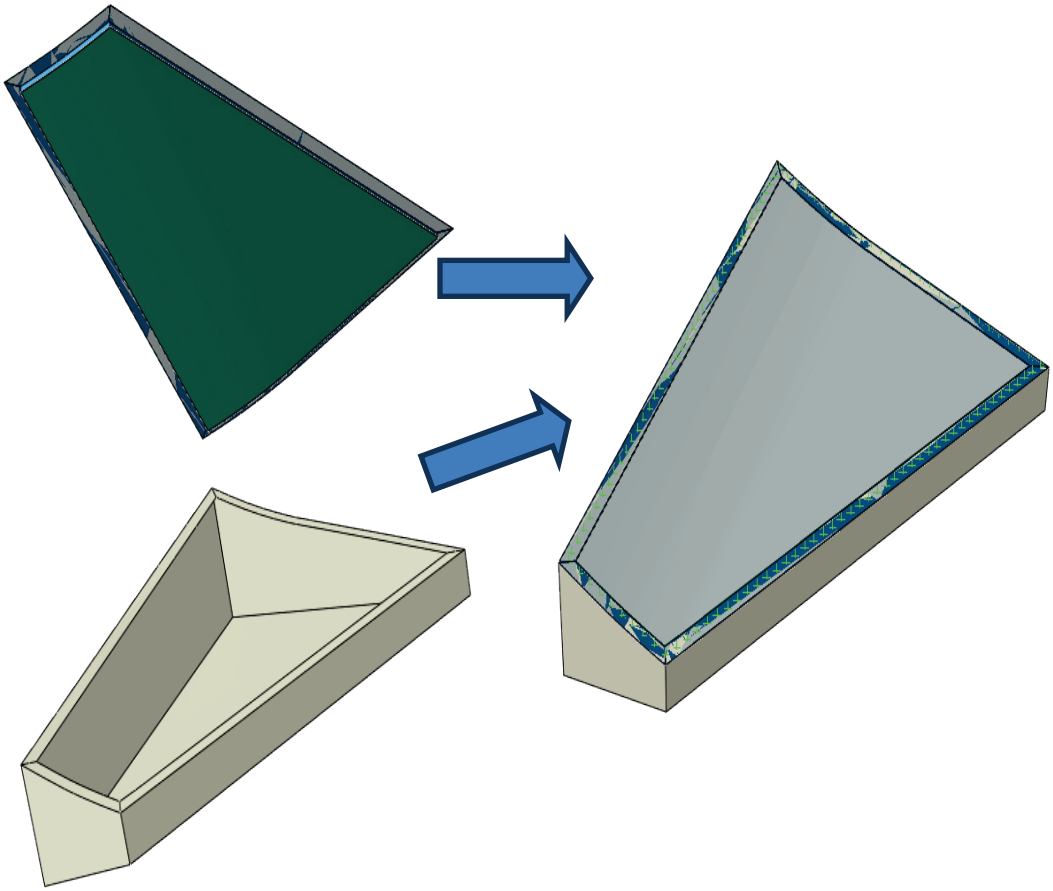

Figure 6.1.6 Panel 3 to Sub-Structure Attach

Once the stiffened panel was assembled, it was then attached to substructure (***Figure 6.1.6***). Panel 3 was then attached to the wing substructure via discrete fasteners, similar to Panel 1.The Panel 4 fairing sub-assembly was put together similar to Panel 3, consisting of inner and outer sandwich skins along with a solid core and frame. ***Figure 6.1.7*** shows each part of the panel along with the final results of the sub-assembly.

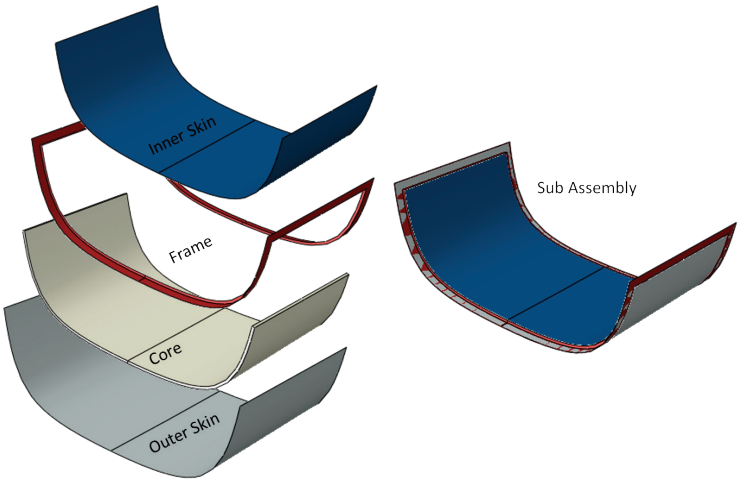

Figure 6.1.7 Panel 4 Sub-Assembly

The Panel 4 attachment scheme was slightly more complicated than other panels since this vehicle region had not previously been designed in great detail. U-shaped beams were assumed to be attached to the vehicle, and to allow a landing for the Panel 4 sub assembly to attach to. This approach allowed for a fully removable section to accommodate engine installation and repairs. This final assembly of the panel to the U-frames, and to the substructure, is shown in ***Figure 6.1.8***. The sub-assembly is attached to the U-frame via fasteners, similar to Panel 3.

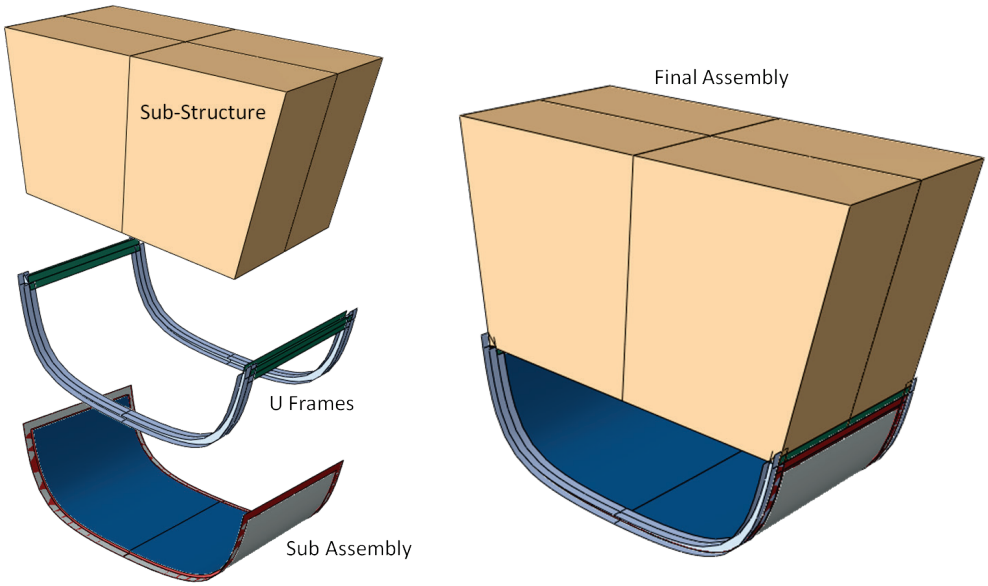

Figure 6.1.8 Panel 4 to Sub-Structure Attach

For Panels 1 and 2, one additional parameter that needed to be considered was which direction the stiffeners were to be aligned to. Previous designs were normally baselined with the stiffeners running parallel to fuselage stations. However, the loading from the Patran Loads Model indicated a much larger loading in the longitudinal direction than in the inboard/outboard direction. Therefore, it would seem that stiffeners running in the longitudinal direction would be advantageous. A simplified version of Panel 1 was constructed using beam elements for the stiffeners rather than the discretely modelled hats. These stiffeners were oriented in two different conditions, resulting in panels of approximately the same total weight. Each panel design was then loaded identically with a loads model worst case compression acting on both panel directions. The results of this study are shown in ***Figure 6.1.9***, and show a clear advantage to orienting the stiffeners in the longitudinal direction, which had become the baseline design.

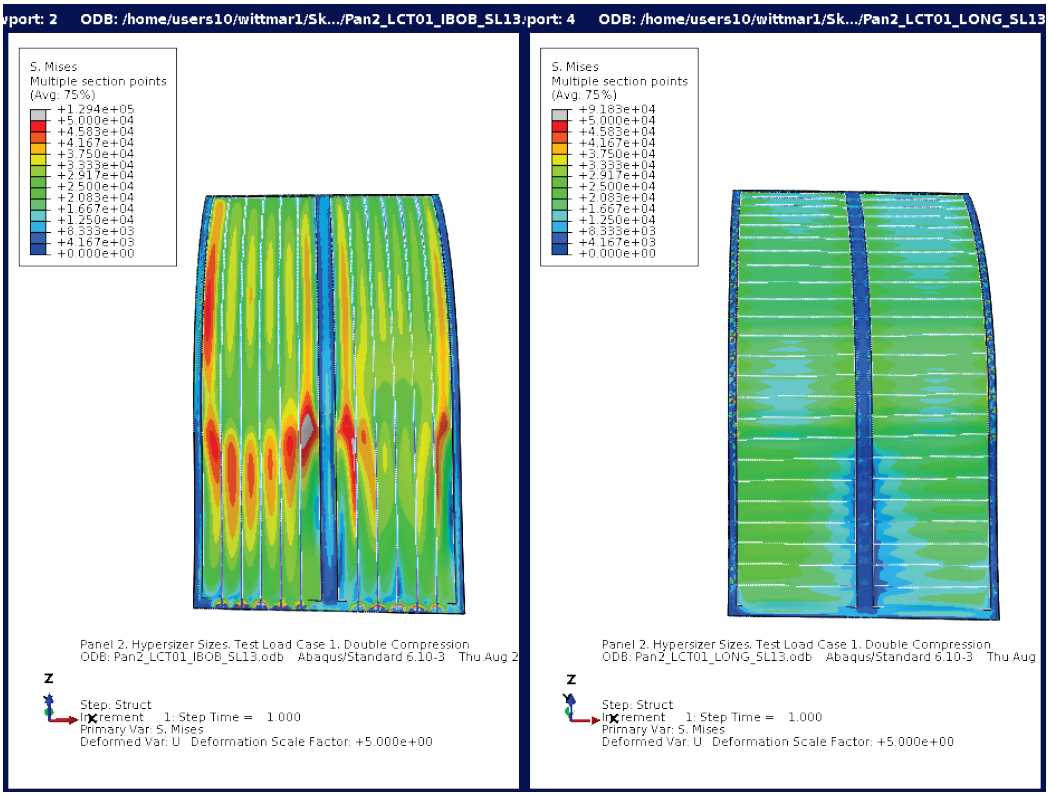

Figure 6.1.9 Stiffener Direction Trade Study

Each panel design was iterated until all structural criteria were met, and a summary is given in Table 6.1.1. These main criteria included limit loads compared to yield stress, buckling stability, panel deformation limits, and bearing stress at the fasteners. Some sizing iterations were later refined when the creep and fatigue life calculations required lower stress levels to meet requirements. Some of the detailed model results such as maximum tensile and compressive stresses are reported in Section 7.3 as they are the input to the fatigue lifetime analyses. The design margins for each panel is presented later in this section. Flatness and waviness requirements, (Appendix C), are not addressed in Section 7.3 and therefore are reported below. “Flatness” is defined as out of plane deflections across a panel divided by the span of that deflection (inch/inch), as shown for Panel 1 in ***Figure 6.1.10*** as an example. All flatness requirements were met for each panel.

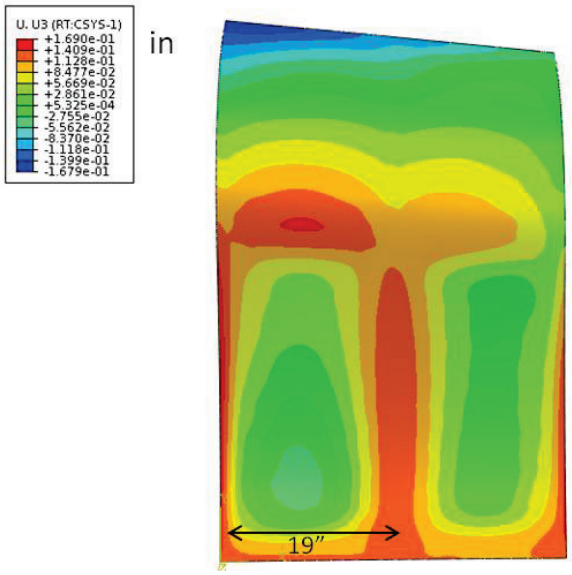

Figure 6.1.10 Flatness Check Example, Panel 1

Table 6.1.1 Panel Static Response Sizing Results Summary

Note: In order to close the design and have all Margins Calculated based on the exact same design, Another Iteration of the Process Must be Performed Starting With Loads Model

	Margin			
Criteria	**Panel 1**	**Panel 2**	**Panel 3**	**Panel 4**
Limit Stress	0.29	0.50	0.42	0.50
Ultimate Stress	0.25	0.33	0.29	0.30
Bearing Stress	0.71	0.96	0.91	0.90
Local Buckling/Stability (LIMIT)	0.02 (0.01)[1]	0.69 (0.07)[1]	N/A [3]	N/A [3]
Panel Buckling (Ultimate)	0.20[1]	0.29[1]	0.56	0.69[1]
Waviness Check	0.011" [2] (<0.020")	0.007" [2] (<0.020")	0.006" [2] (<0.020")	0.004" [2] (<0.007")

1. Result from HyperSizer, Needs to be Updated to Final Design of First Iteration, Conservative
2. Needs to be Updated to Final Design of First Iteration, Conservative
3. Covered by Sandwich Panel Checks in HyperSizer (Dimpling, Wrinkling, etc.)

The most limiting load cases for each panel were previously summarized in Section 5.2, and were used to obtain the stress margin results. The comparison of the limit stresses in each panel to the allowable (yield) limits of that material at the load condition temperature determined the design margin for the panels. In the plots below, ***Figures 6.1.11 through 6.1.14***, for each panel the maximum limit stress at the load condition was divided by the allowable stress of the material at

the local temperature during that load condition. When this ratio equaled 1.0, zero margin remained, shown by red on the contour plot scale. The allowable stress (yield stress for limit loads) is temperature dependent, and was calculated by Abaqus at each element based on the temperature at that element and the temperature dependent material data supplied to Abaqus. As can be seen for each panel, the stress levels were well below their structural limits as they were limited by stability and creep/fatigue concerns. The regions nearing stress limit in the FEM occur in two types of anomaly regions. These regions were fastener regions where the bearing stress was calculated independently and the peaks are exaggerated on the panel, and at a thickness discontinuity region, which in reality would be tapered thus eliminating the stress peak.

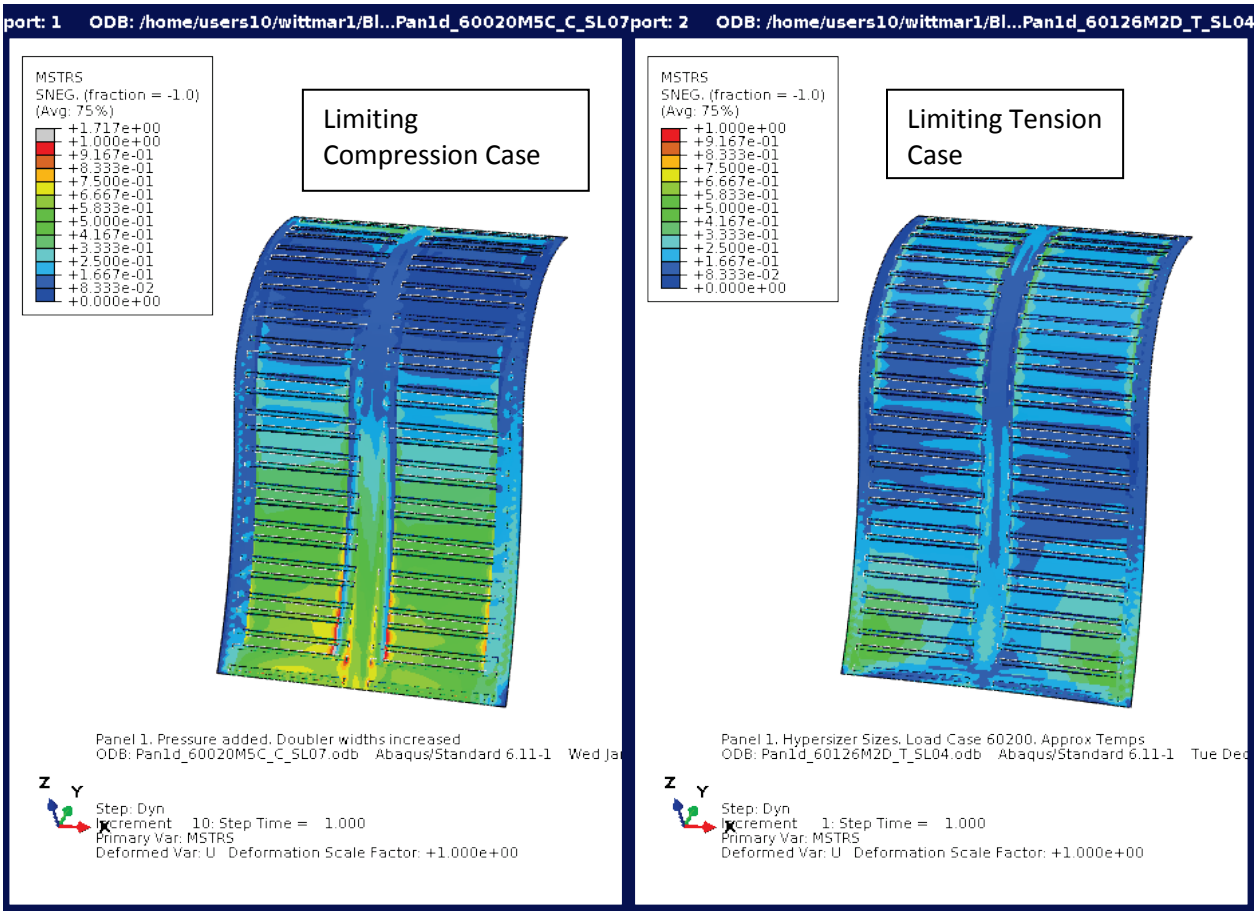

Figure 6.1.11 Panel 1 Margin to Material Allowable

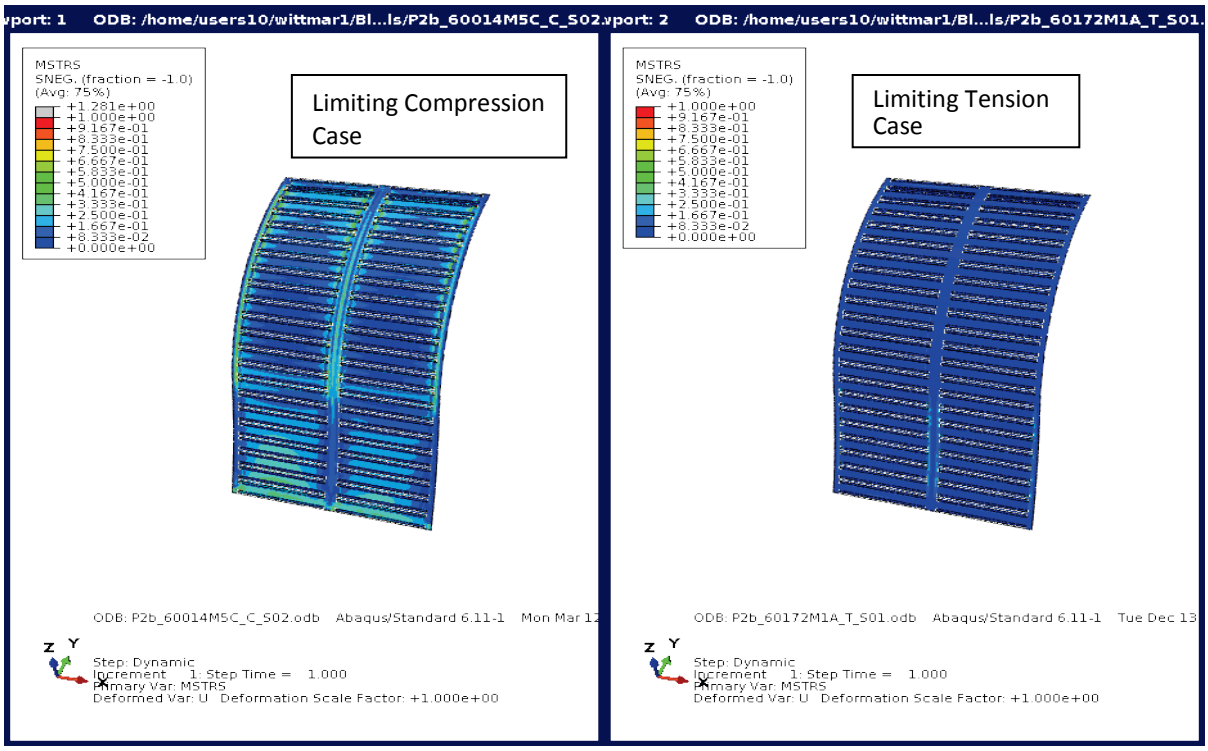

Figure 6.1.12 Panel 2 Margin to Material Allowable

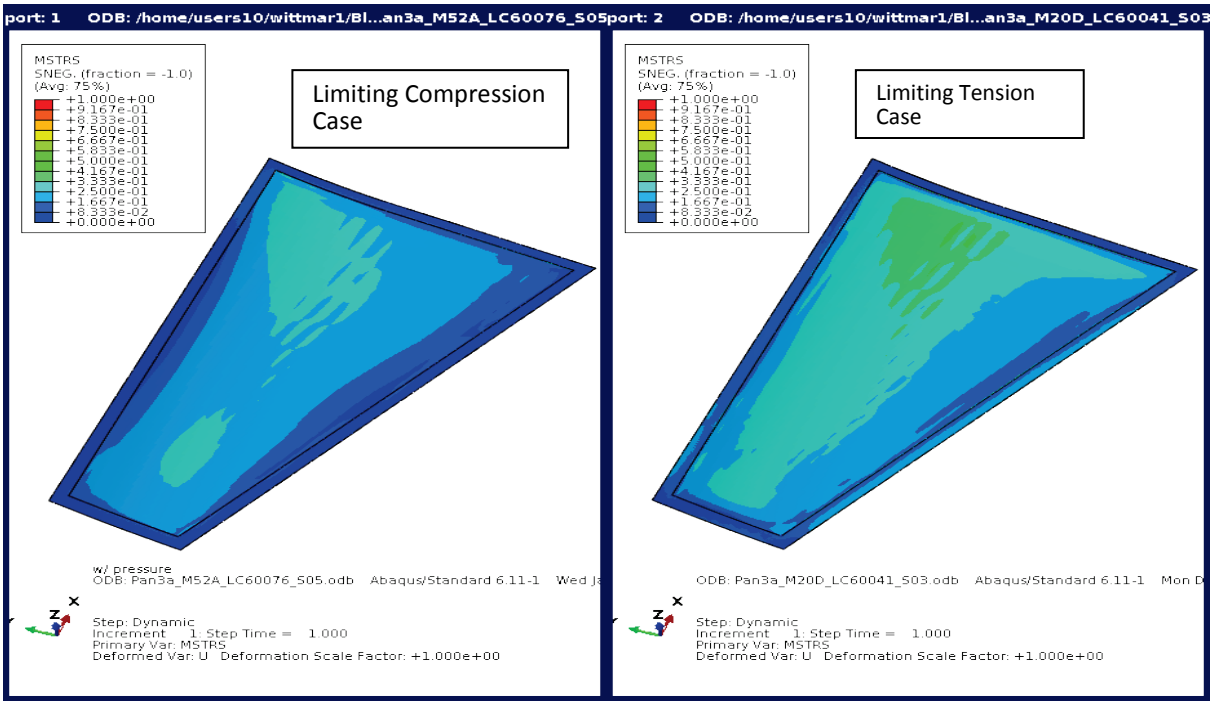

Figure 6.1.13 Panel 3 Margin to Material Allowable

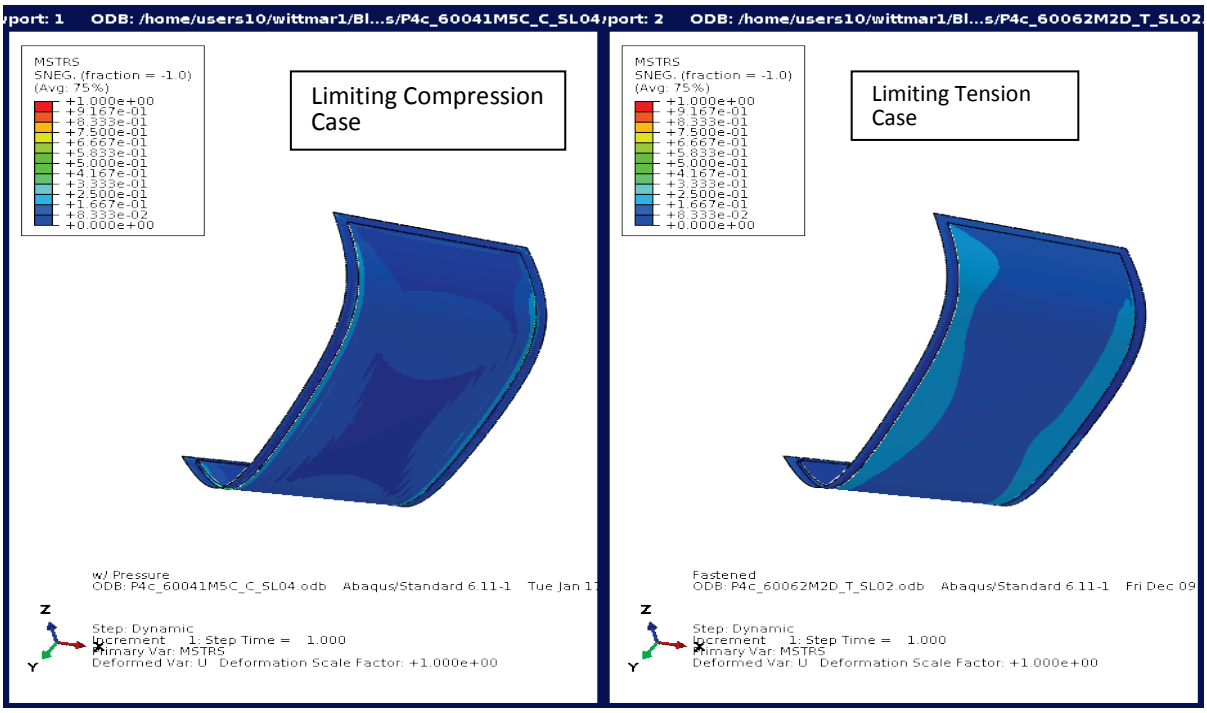

Figure 6.1.14 Panel 4 Margin to Material Allowable

Global buckling of each basic panel was also performed in the HyperSizer checks. This was considered to be sufficient for Panels 3 and 4 as they are honeycomb with no obvious local buckling modes. Panels 1 and 2 were checked for local buckling with a simplified version of the detailed models without the substructure, and fixed edge supports. The critical edge load to cause the local buckling was compared to the internal forces produced in the detailed model runs for Panels 1 and 2. If the critical edge load was larger than the maximum internal running loads (lbs/in) of the limiting compression load case, then local buckling should not occur. These buckling results were also verified with non-linear analysis runs at ultimate loads again using the less complex model (no substructure). The buckling and non-linear result pairs are shown below. When buckling concerns arose from local buckling runs (Panels 1 and 2), stiffener thickness was increased and verified with non-linear analysis. Detailed results are shown in ***Figure 6.1.15 through 6.1.20***.

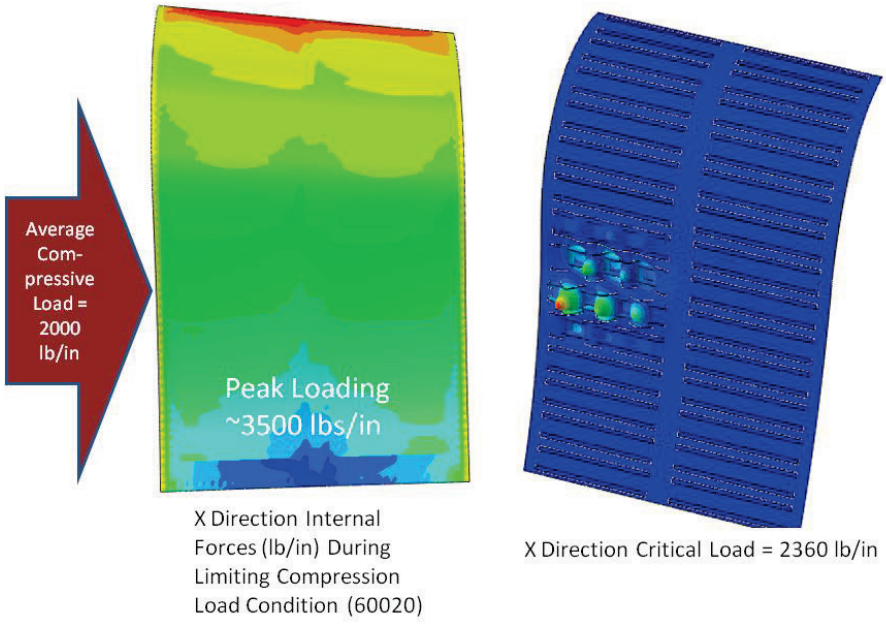

Figure 6.1.15 Panel 1: Local Buckling Analysis

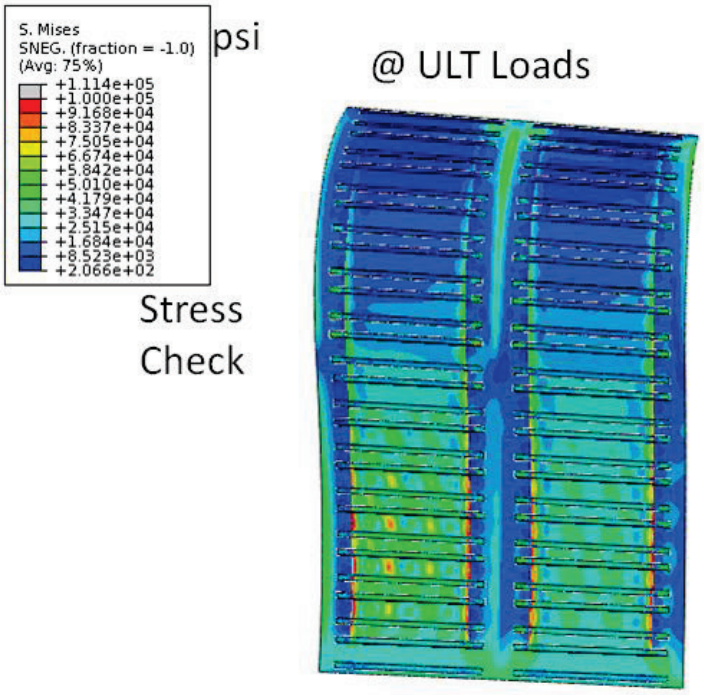

Figure 6.1.16 Panel 1: Non-Linear Von Mises Stress, Ultimate Loads

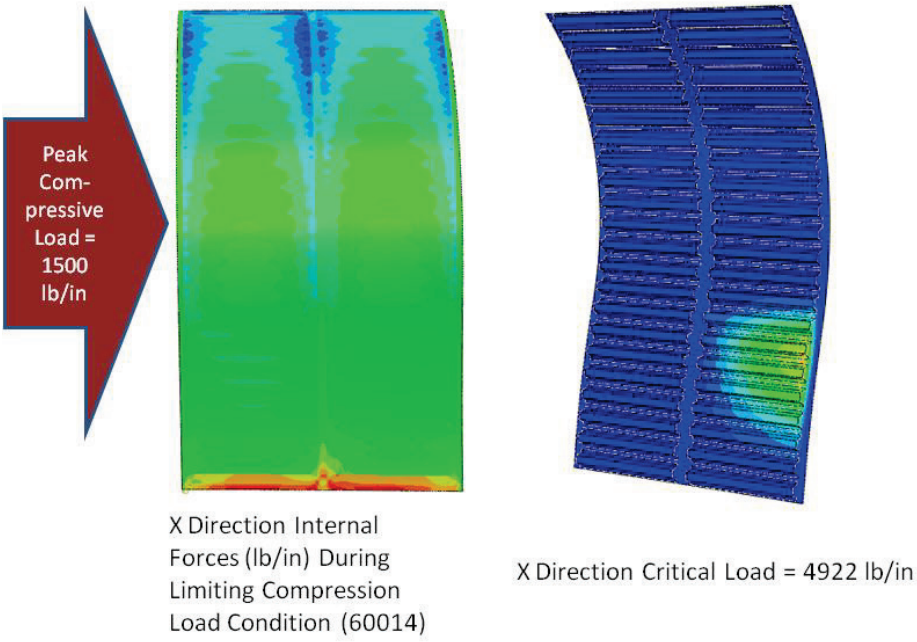

Figure 6.1.17 Panel 2: Local Buckling Analysis

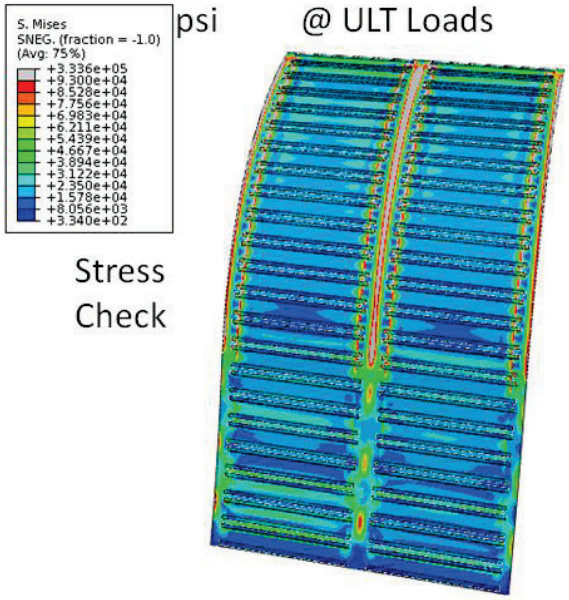

Figure 6.1.18 Panel 2: Non-Linear Von Mises Stress, Ultimate Loads

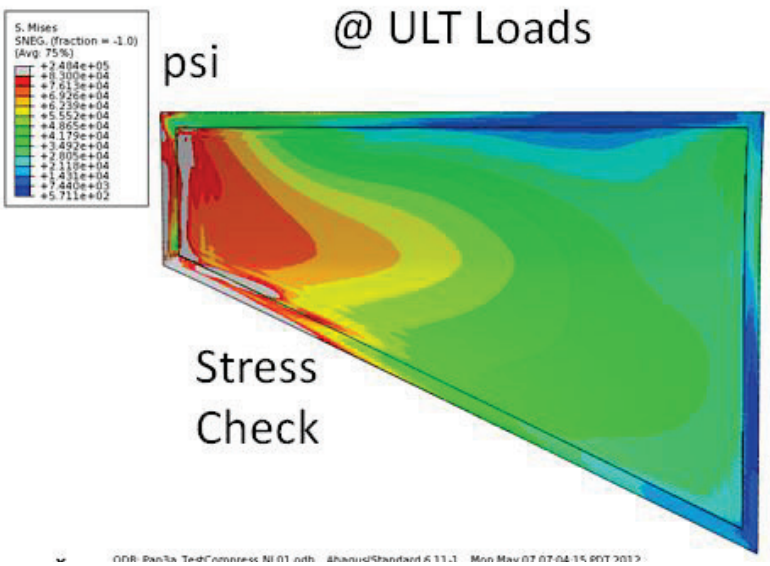

Figure 6.1.19 Panel 3: Non-Linear Von Mises Stress, Ultimate Loads

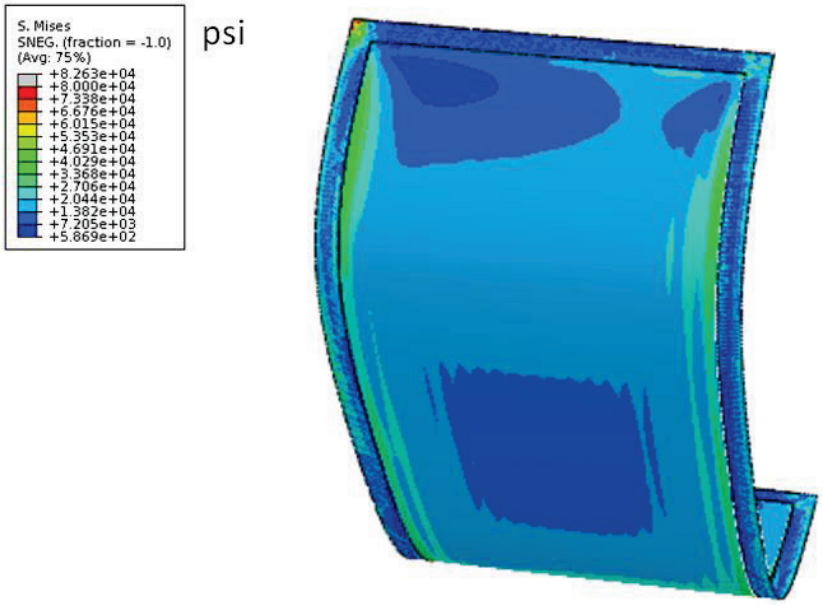

Figure 6.1.20 Panel 4: Non-Linear Von Mises Stress, Ultimate Loads

The loading on each panel consisted of 3 basic types; thermal, structural, and dynamic. These loads were all developed and accounted for in very different ways. The details of the dynamic load development are documented in Section 6.2. For both the structural and dynamic loads, MSC/Patran Loads Model data were used to extract running load forces. The detailed edge load mapping between the two FEM software packages is tedious and was simplified for this study to be a constant value. This assumption was reasonable given the relatively low (~10%) loading

contribution of the structural loads. A more ideal approach to this method is summarized in Section 5.0. The maximum tension or compression running load at any point along an edge in the Loads Model is assumed to be the running load for the entire edge. Therefore, the running loads in the X and Y directions are constant for structural and dynamic loading. Each running load is applied to the panel edge through the substructure edge, and the load is transferred into the panel through the fasteners or welds. The loads are reacted at the opposite edge, again by the substructure, Figure . In addition to the running loads, pressure loads were applied normal to the panel to represent aero loading and tank pressures where appropriate. External pressure loads were predicted for a few specific trajectory points as shown in Section 6.4. The design maximum operational internal fuel tank pressure was set to 10 psi. All vertical loads were reacted by the bottom skin of the substructure and some rotational constraints were also used on keels to limit the bending of the substructure.

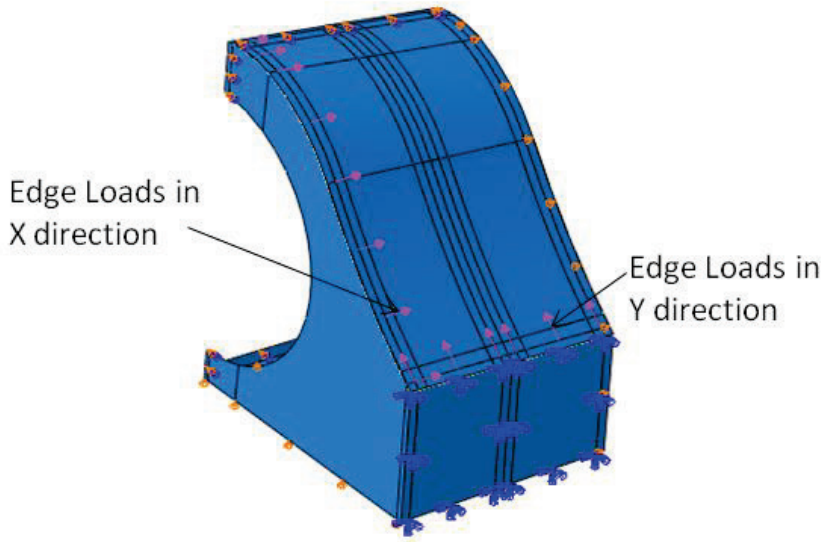

Figure 6.1.21 Panel 1 Structural and Dynamic Loading Scheme

The structural and dynamic loads were applied after the thermal load step was complete. The thermal loading scheme was significantly more complex. The Loads Model gives a good approximation of thermal expansion induced loads which occur assuming the baseline structure sizing. However, these thermal loads change drastically as skin thickness increases, leading to larger expansion forces at the same temperatures. Therefore, the thermal loading from the Loads Model cannot be directly applied to the detailed model. As a starting point, the detailed model was run with the same baseline sizing assumptions as the loads model. Temperatures are applied to the detailed model using varying heat fluxes on the top and bottom skins, along with other starting temperature data to account for cooler fuel, etc, shown in ***Figure 6.1.22***.

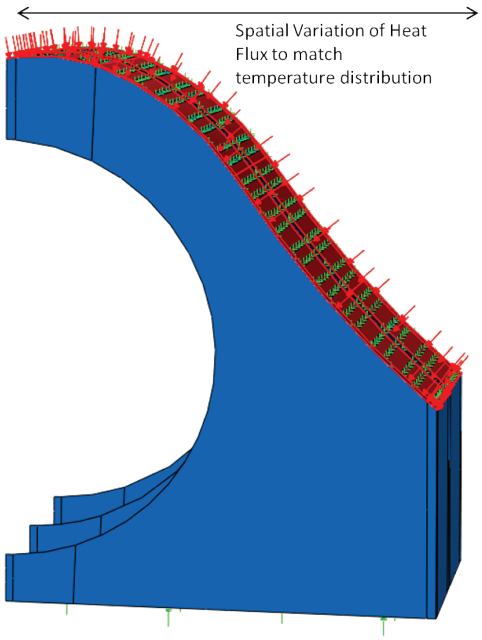

Figure 6.1.22 Panel 1 Heat Fluxes

These fluxes are adjusted in order to obtain the temperatures from the Loads Model thermal data. The Abaqus thermal model approach was a simplified conduction analysis used to closely achieve the more accurate Loads Model temperatures. The Abaqus model thermal inputs were surface heat flux and initial temperatures. The idealized process for thermal inputs is summarized in Section 5.0. The Mach 5+ temperature case was applied to the detailed model for comparison to the Loads Model. The conduction thermal case results for the Detailed Model were compared with the Loads Model results, and consistent temperatures are shown in ***Figure 6.1.23***.

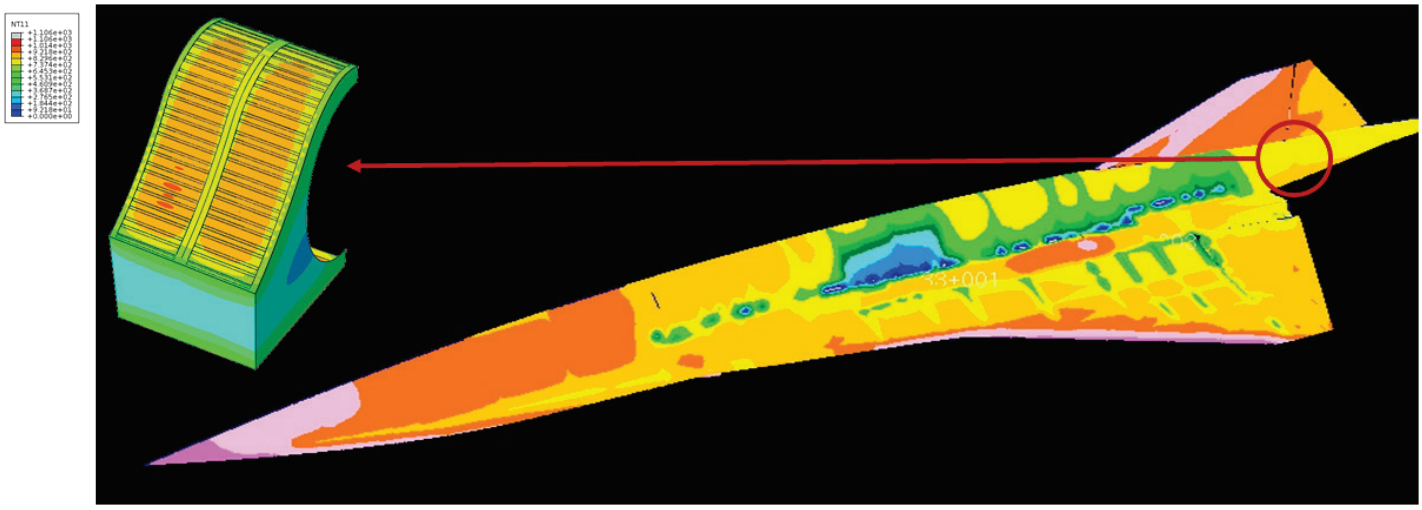

Figure 6.1.23 Panel 1 Loads Model to Detailed Model Temperature Comparison

The detailed model thermal approach was able to more accurately reflect thermal details that the coarse Loads Model was not. For example, the heat sink nature of the substructure at joints

between the skin and bulkheads is evident. Fasteners were also assigned a thermal mass to account for the small effects that might arise in certain conditions. Given that the thermal model details are primarily at the joint regions, the best verification of temperatures between models, throughout the flight trajectory, occurs in the center of each panel, as shown below for Panel 1 in ***Figure 6.1.24***. The desired temperatures, as scaled from HTV-3X data accounting for the updated trajectory are on the chart in the top left. The new detailed model temperatures are shown in the chart on the top right.

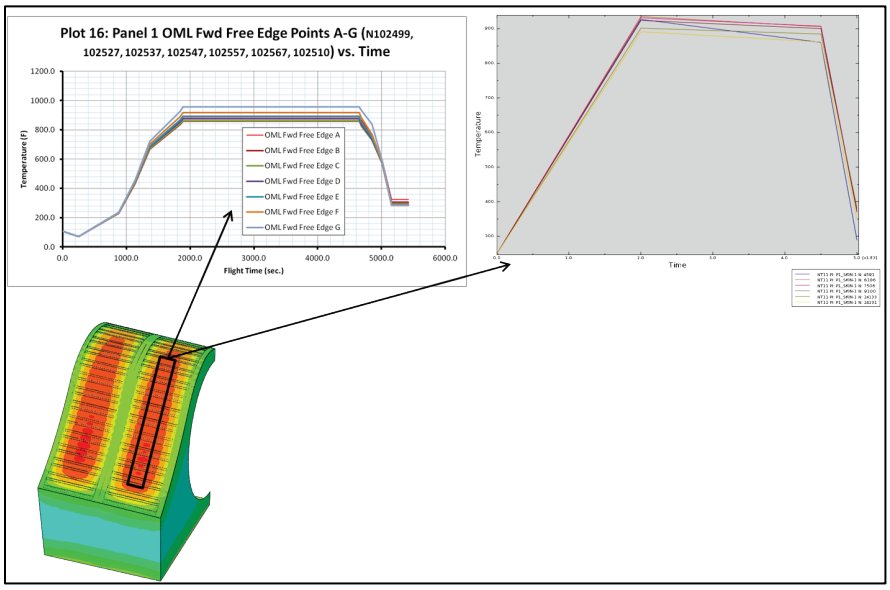

Figure 6.1.24 Detailed Temperature Comparisons

Once that satisfactory temperature results were shown as comparable between the two models, the resulting thermal loads must now be calibrated. The detailed model substructure was adjusted as needed to achieve a good correlation between the two. Adjustments involved certain boundary conditions such as allowing a keel to bend at an intersection with a bulkhead and sub structure panel thicknesses. The panel section forces in the X direction between the Loads baseline model and the detailed model are compared in ***Figure 6.1.25*** and are similar.

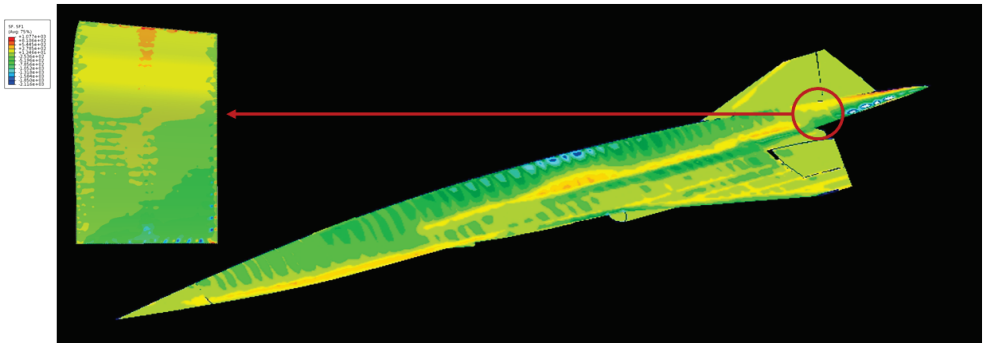

Figure 6.1.25 Panel 1 Section Forces in X Comparison

Once the resistance of the substructure was calibrated, the panel thicknesses could be sized and the temperatures updated as required in the detailed model for each trajectory temperature case from the Loads Model (***Figure 6.1.23***), and the resulting thermal loads in the panels should be correct.

The model was then updated to the HyperSizer results panel and hat thicknesses and subsequently re-run for each limiting load case. In order to run all applicable structural load cases, multiple thermal loading conditions had to be analyzed. Temperature states for various phases of flight are shown below in ***Figure 6.1.26***.

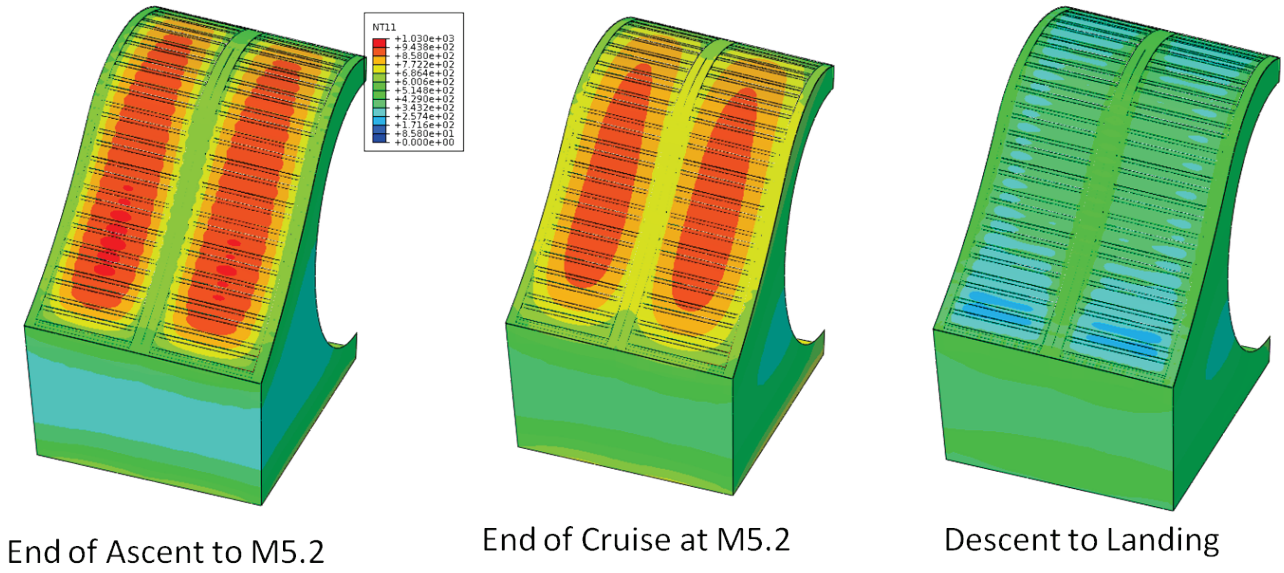

Figure 6.1.26 Panel 1 Flight Phase Temperature Conditions

In combining maneuver loads with their corresponding thermal load condition for each panel, the most limiting tensile and compressive load cases were analyzed in detail. In general, the maximum compression cases occurred at the higher temperature panel conditions at the end of ascent and during cruise, as the sub-structure is relatively cooler than the panel, which constrains the panel growth. This thermal condition was combined with the flight maneuver which causes the maximum compressive force addition (Section 6.1). Cooler conditions during initial ascent or landing led to the highest tension thermal forces. This thermal condition was then combined with the maneuver which causes the highest tensile loads in the panel, and these were analyzed in detail.

The dynamic loads supplied were in raw form, and had to be factored up to meet the 3 sigma criteria (Section 6.2). For simplicity the dynamic load was applied as a constant edge running load, similar to the structural loads mentioned above. The highest running load value from the Loads Model was used when possible. As discussed in Section 6.2, the acoustic loading from the dynamics models was extremely high for Panels 1 and 2. As a result assumptions were made that these loads would be able to be reduced in the future. In the interim and for the purposes of this analysis, the Panel 4 dynamic load levels were assumed to act on Panels 1 and 2 as well.

Each panel design was iterated using the limiting tension and compression load case, until basic structural criteria were met. The panel heating effects from the CFD model are accounted for in the detailed model analysis thermal runs. The RET maps were used as data for the skin temperatures in the conduction analyses. Aerodynamic pressure was also extracted from the CFD model to be applied to the panels. The aerodynamic pressure did not have a significant impact on the panel sizing.

6.2 PANEL DYNAMIC AND ACOUSTIC ANALYSES

The dynamics environments were developed using the mission profile and trajectory of the HCV. The profile was separated into several phases; transonic, supersonic acceleration, hypersonic cruise, and de-acceleration & landing. The supersonic acceleration phase was further divided into several sub-phases due to the function of the propulsion system and temperature: room temperature turbojet, room temperature mixed mode, elevated temperature mixed mode, and elevated temperature DMRJ.

Transonic Phase

Takeoff and transonic phase was defined as M=0.9 to 1.1. The time duration of this phase is 100 Seconds, turbojet powered, maximum Q is 1,300 Psf, and with the exception of the propulsion components, the airframe temperature is approximately ambient temperature. The external acoustic level can be estimated using well established methods prescribed in Mil-Standard 810.

Supersonic Acceleration Phase

Supersonic acceleration phase was defined as M>1.1 to M<4.5. The time duration of this phase is 1,220 seconds, with a maximum and constant Q at 1,500 Psf. The airframe experiences a gradual increase of temperature during this phase. Panel 1 temperature will go from ambient at M = 1.1, to over 900^0F at M = 4. The propulsion system switches from pure turbojets, to mixed mode (above M=2.5), then to the SCRAM jets when the Mach number is above 3.5. The external or attached turbulent boundary layer acoustic level (A/TBL OASPL) can be estimated report AFRL-RB-WP-TR-2010-3068, V1, Equation 4.1.1 (Ref. 6). The overall structural model did not have sufficient details to predict the separated boundary layer acoustic level (S/TBL OASPL).

Hypersonic Cruise Phase

Hypersonic phase was defined as M>4.5 cruise climb. The time duration of this phase is 54 minutes, with a constant Q at 1,400 Psf, and the altitude changes from 80,000 to 100,000 ft. The airframe is at elevated temperature during this phase. The propulsion system is in pure SCRAM mode. The external or attached turbulent boundary layer acoustic level (A/TBL OASPL) can be estimated using the report, AFRL-RB-WP-TR-2010-3068, V1, Equation 4.1.1. The hypersonic cruise phase turn out to is a major design driver due to the severe acoustic environment caused by the SCRAM jet.

De-Acceleration to Landing Phase

De-acceleration to Landing phase was defined as the HCV exit from hypersonic cruise, rapid de-acceleration to subsonic stage, shutdown of the SCRAM jet and the restart of the turbojet engine. It was an examination of the dynamic load effect of a hot structure (reduced stiffness) response to the turbojet propulsion.

Excitation

There are mainly two major sources of dynamic excitation for an aerospace vehicle during flight, external and internal acoustics. The external aero-acoustics were caused by the attached and separated turbulent boundary layer, as the vehicle flies within the atmosphere. The internal acoustics were mainly caused by propulsion noise. There were other sources for internal noise and vibration, but these excitations are normally orders of magnitude below the propulsion and aero-acoustic excitation.

Transonic External Excitation

The aero-acoustic excitation was determined using Mil-Std-810G Method 515.5, Table 515.5A-I, overall pressure levels and duration, and Lockheed Martin's RATTLRS aero-acoustic analysis. Mil-Std 810 (Ref.7) basically states, for aero-vehicles that flies in a dynamic pressure (q) < 1,200 psf, the OASPL test level, with 0 dB margin, for aero-acoustic is 150 dB. For a q < 1,800 Psf, the sound level increases to 165 dB. The HCV transit shows the transonic range at a q that varies from 700 to 1,400 psf (see Figure 6.2.2). Using Equation 6.1, the attached turbulent boundary layer acoustic level during the transonic phase can be roughly estimated to be 148 or 154 dB. Figure 6.2.1 illustrates the results of Equation 6.1 during the transonic phase in decibels.

$$P_{rms} = 0.015 * \frac{Q}{144}$$

Equation 6.1

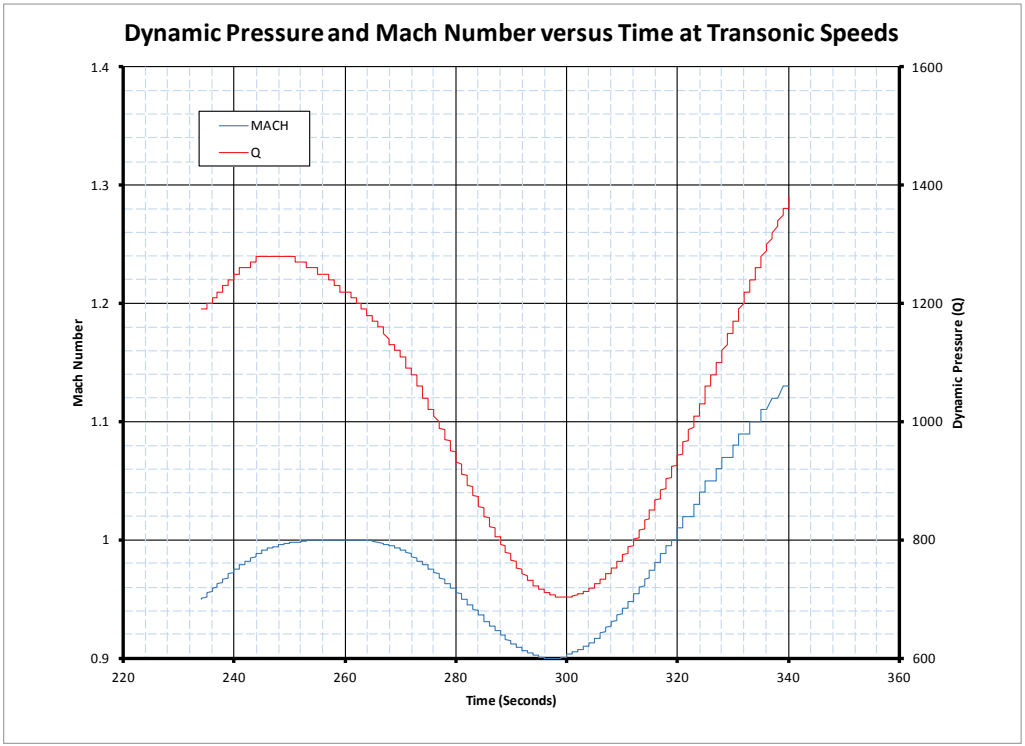

Figure 6.2.1 Dynamic Pressure and Mach Number Versus Flight Time – Transonic Phase

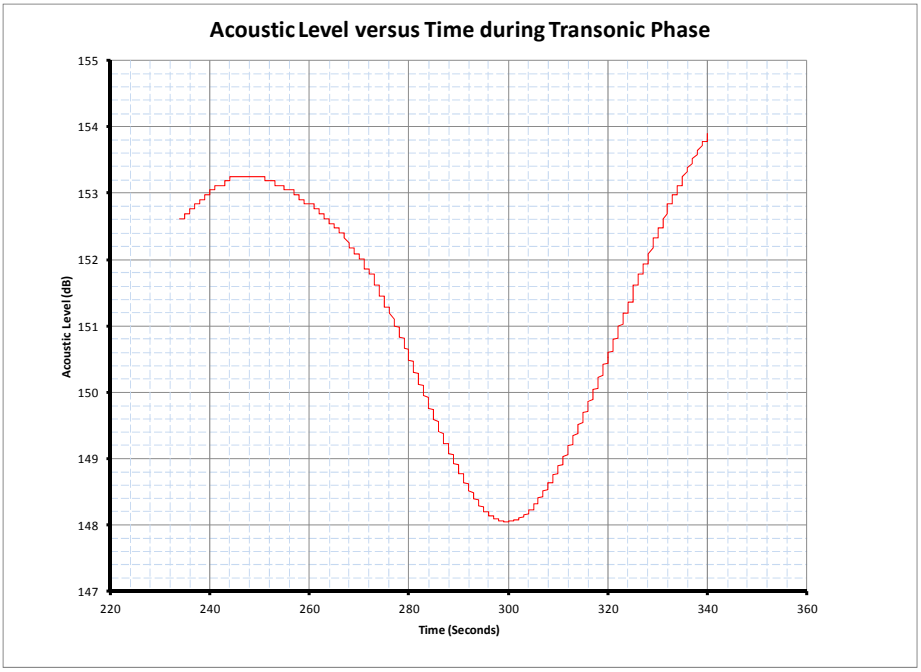

Figure 6.2.2 External Acoustic Versus Flight Time – Transonic Phase

Margins are added to the predicted aero-acoustic level at specific panel locations to address the leading edge and inlet shocks, and the proximity to the engine exhaust. Table 6.2.1 illustrates the margins added.

Table 6.2.1 External Acoustic Margins – Transonic Phase

Panel	Location	Margin (dB)	Notes
Panel 1	Aft Section, Over Engine Exhaust	6	Control Surface + Nozzle Effect
Panel 2	Fuselage, Over Fuel Tank	0	Fuselage
Panel 3	Wing Forward Leading Edge	3	Minor Turbulence rom Wing and Body Interface
Panel 4	Inlet	9	Inlet Shock

Transonic Internal Excitation

The internal propulsion induced vibration environment was determined using Mil Std 810G Method 514.6, Category 7, using a V_c = 1,500 ft/sec:

Engine Induced Vibration: $W_j = \left[\frac{0.48*a*d*cos^2(\theta)}{R}\right] * \left[D_c * \left(\frac{V_c}{V_r}\right) + D_f * \left(\frac{V_f}{V_r}\right)\right]$

Equation 6.2.1

Where:

W_0: Total Exposure Levels (G^2/Hz)
W_a: Aerodynamic Induced Vibration (G^2/Hz)
W_j: Engine Induced Vibration (G^2/Hz)
n: Number of Engines (In This Case: n=1)
q: Dynamic Pressure (psf)
a: Platform / Material Interaction Factor (In This Case: a=0.25)
b: Proportionality factor between vibration level and dynamic pressure (In This Case: b=1.4 X 10^{-7})
c: Mach Number Correction (c=1.0 Mach<= 0.9 M, (c=-4.8*M+5.32) 0.9<Mach<=1.0, c=0.52 Mach>1.0)
d: Afterburner factor (In This Case: d=1)
R: Vector Distance from Center of Engine to Material CG
D_c: Diameter of Core (ft)
D_f: Diameter of Fan (ft), (In This Case: D_f=0)
V_c: Engine Core Exit Velocity (ft/sec)
V_f: Fan Exit Velocity (ft/sec), (In This Case: V_f=0)
V_r: Reference Velocity (1,850 ft/sec)

Figure 6.2.3 illustrates the results of the vibration energy input to the engine mounts.

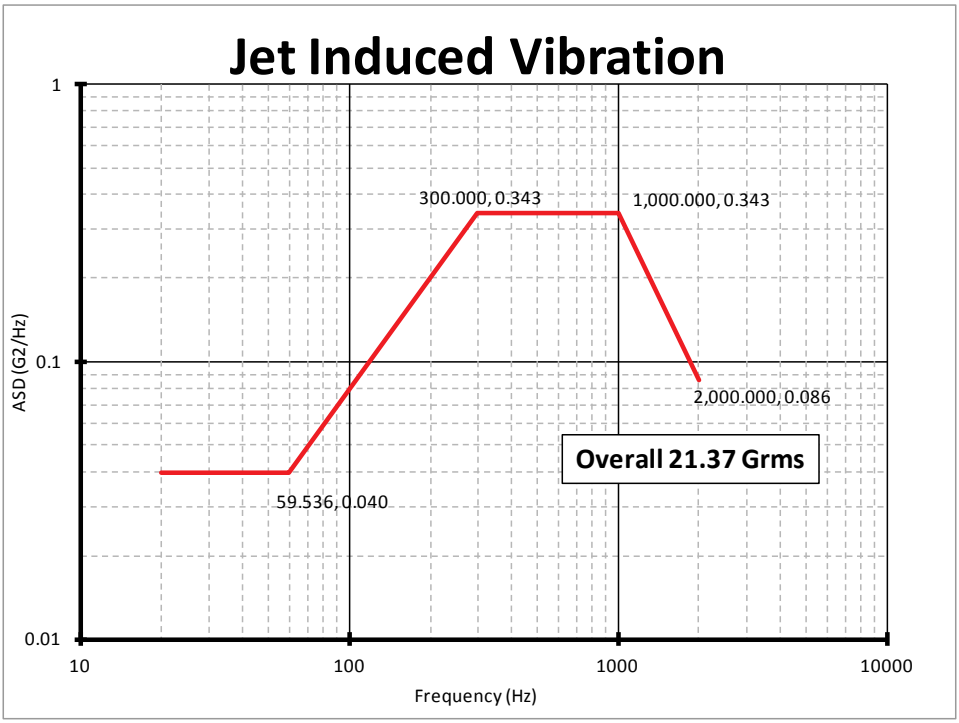

Figure 6.2.3 Vibration Input to the Engine Mounts

Supersonic Acceleration External Excitation:
The acoustic environments were developed primary using the HCV mission trajectory. The external acoustics were a function of the Mach number and altitude and these methods were

detailed in an AFRL report AFRL-RB-WP-TR-2010-3068, V1. The attached acoustics were governed by Equation 6.2.2.

$$A/TBL\ OASPL = 16.153 * Ln(Mach) + (150. - Alt * 0.0004)$$

Equation 6.2.2

Where:

A/TBL OASPL: Attached Turbulent Boundary Layer OASPL, dB
Mach: Mach number
Alt: Altitude, feet

Attached Turbulent Boundary Layer equation was used because the current model does not provide adequate details to evaluate the separation flow region. ***Figures 6.2.4 through 6.2.6*** illustrate the results.

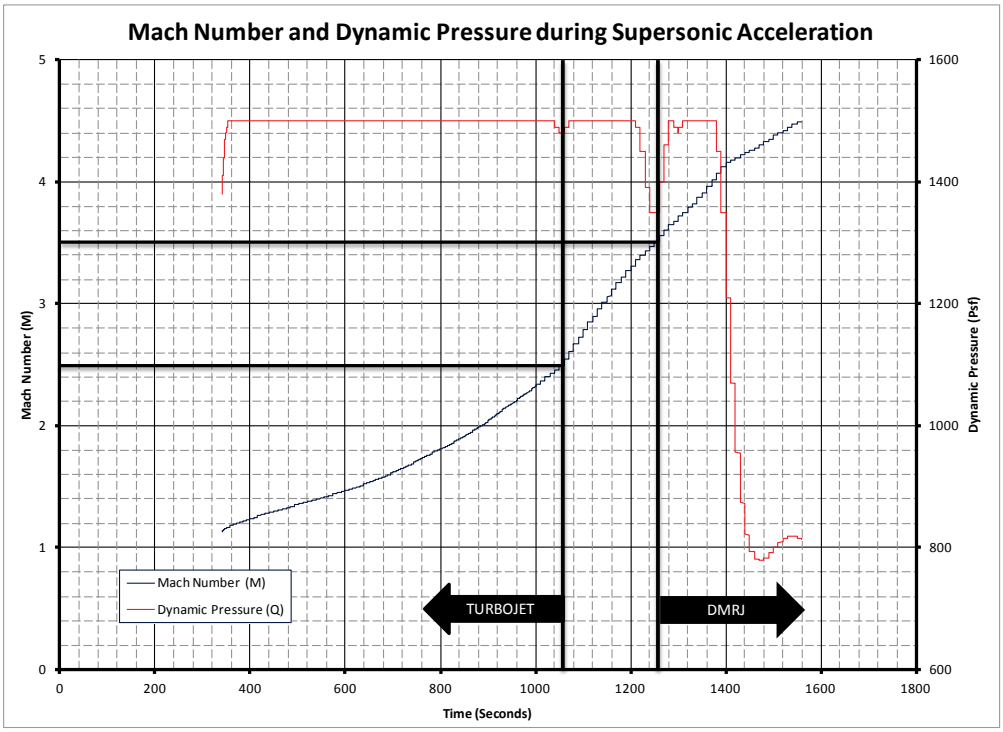

Figure 6.2.4 Mach Number and Dynamic Pressure Versus Flight Time

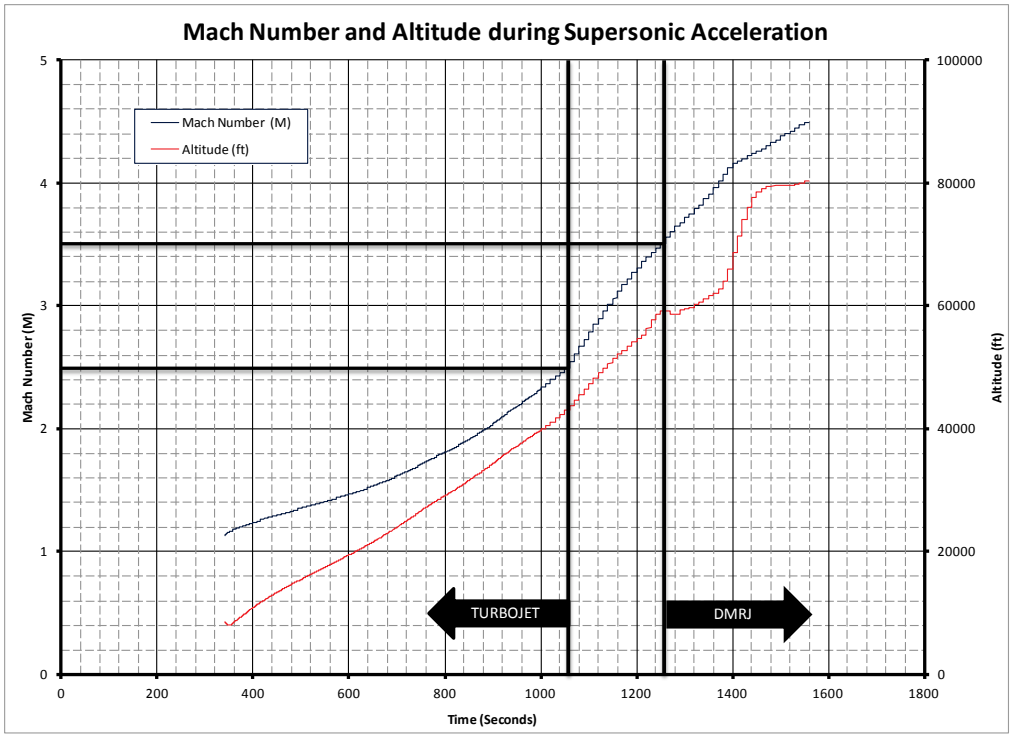

Figure 6.2.5 Mach Number and Altitude Versus Flight Time

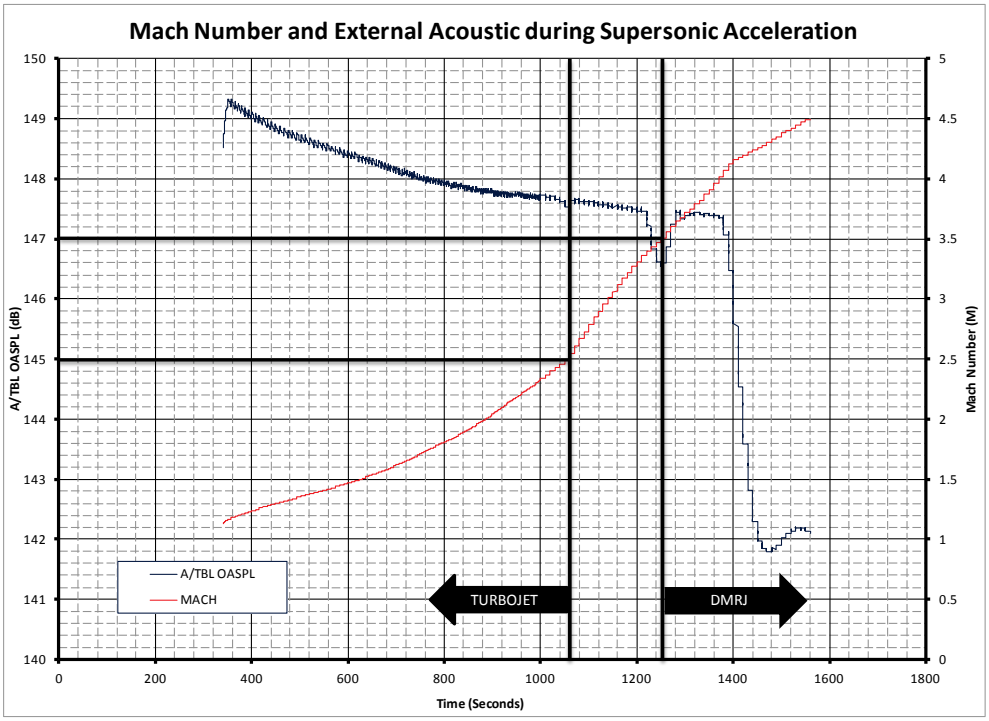

Figure 6.2.6 Mach Number and Attached External Acoustic Versus Flight Time

Supersonic Acceleration Internal Excitation:
The internal excitation during the supersonic stage was a bit more complex than the transonic stage. Below Mach = 2.5, the primary propulsion are the turbojets, and above Mach = 3.5, the primary propulsion are the SCRAM jets. In between Mach = 2.5 to Mach = 3.5, the propulsion is a mix between the turbojets and the SCRAM jets.

For the turbojet propulsion, the process is the same methods described in the transonic internal excitation.

For the SCRAM jet, the processes involved developing the pressure mapping along the inlet and the exhaust of the SCRAM jet assembly using VA One, and apply the pressure mapping along the finite element model for the response analysis.

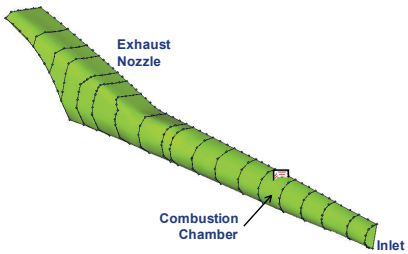

Figure 6.2.7 VA One ScramJet SEA Model

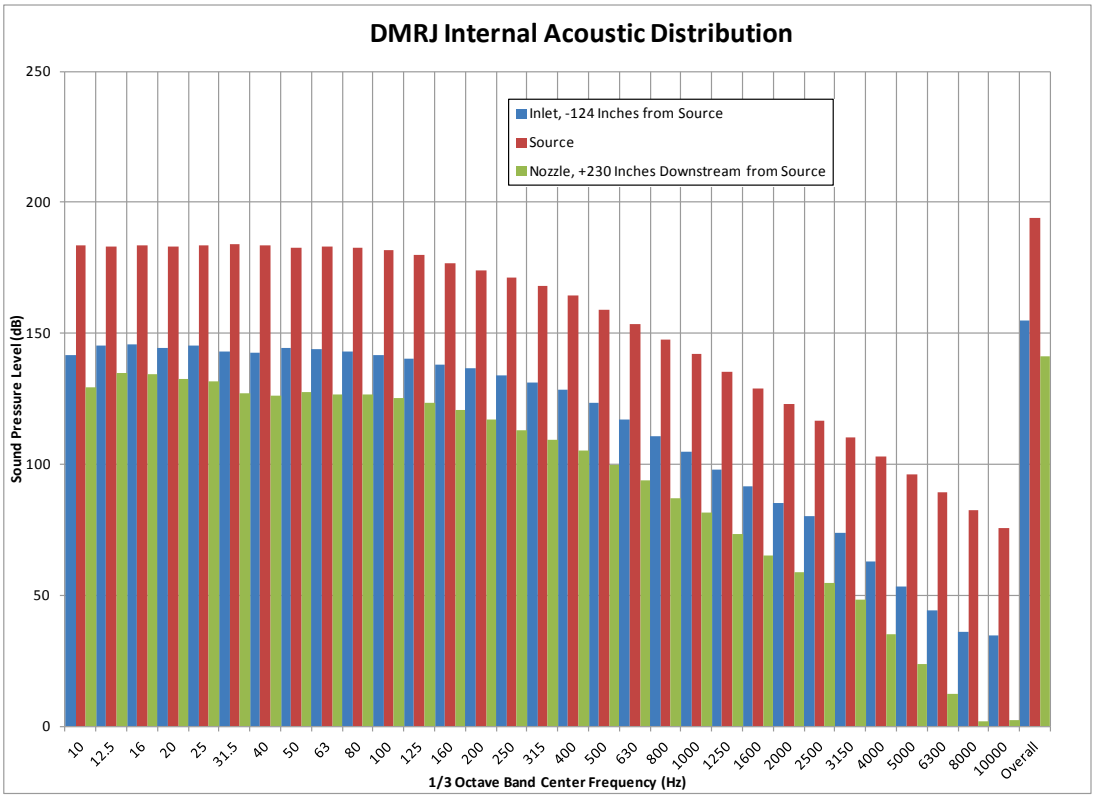

Figure 6.2.8 VA One ScramJet SEA Results

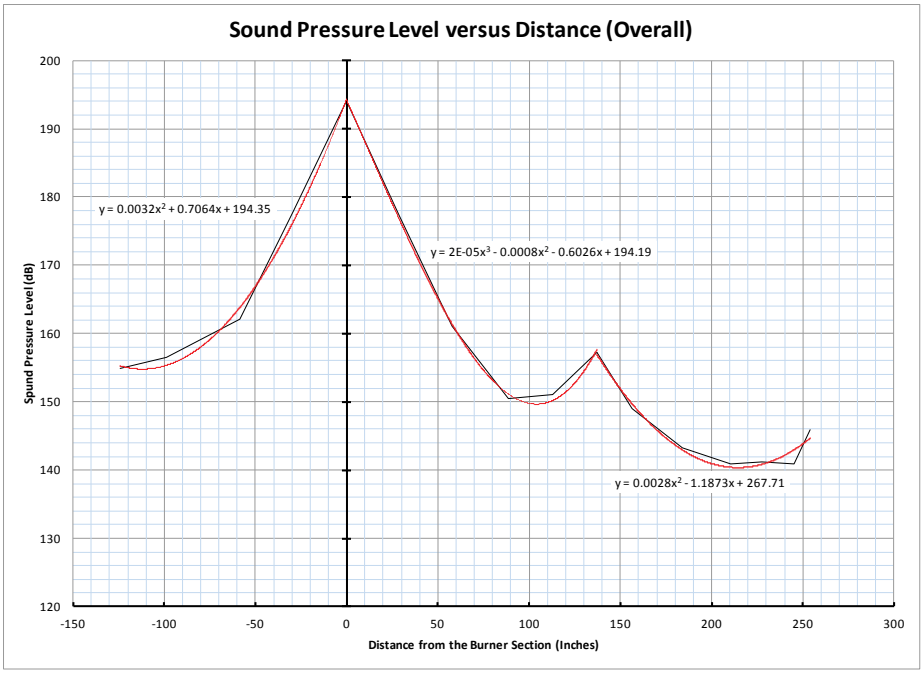

Figure 6.2.9 ScramJet Engines Internal Pressure Distribution

The least square fit equation was used to calculate the internal acoustic pressure along the length of the inlet, burner, and exhaust assembly. It was assumed that there are no pressure variations along the radial direction of the engine.

For the mixed mode propulsion, the analysis responses are root sum squared to obtain the results. Root sum squared was used to emulate the effect of the turbojet throttling down and the SCRAM jet throttling up.

The airframe will go thru heating during the supersonic acceleration phase and per the trajectory will experience temperature changes from ambient temperature to over 900°F within 220 Seconds. For the metallic skin, the material will undergo three major changes. The first change is the reduction of strength, which was addressed by the structural analysis. The second change was the thermal expansion and contraction, which was incorporated in the thermal analysis. The third was the reduction of stiffness, which can change both the overall and local stiffness, which had to be accounted by the dynamic analysis.

Titanium and Inconel were the two primary materials involved in this study. The Titanium alloy involved was Ti Beta 21S, in sheet-rib stiffened structure and honeycomb sandwich (Panel 3). The Inconel alloy involved was Inco 718 in honeycomb sandwich form (Panel 4).

Basic Ti Beta 21S properties were obtained from MMPDS-05 (Mil Handbook 5 replacement) (Ref. 8) and the GKN/Astech Aerospace Report (Ref. 9). ***Figures 6.2.10 and 6.2.11*** are from MMPDS-05 and ***Figures 6.2.12, 6.2.13***, and Table 6.2.2 are from the GKN/Astech Aerospace Report.

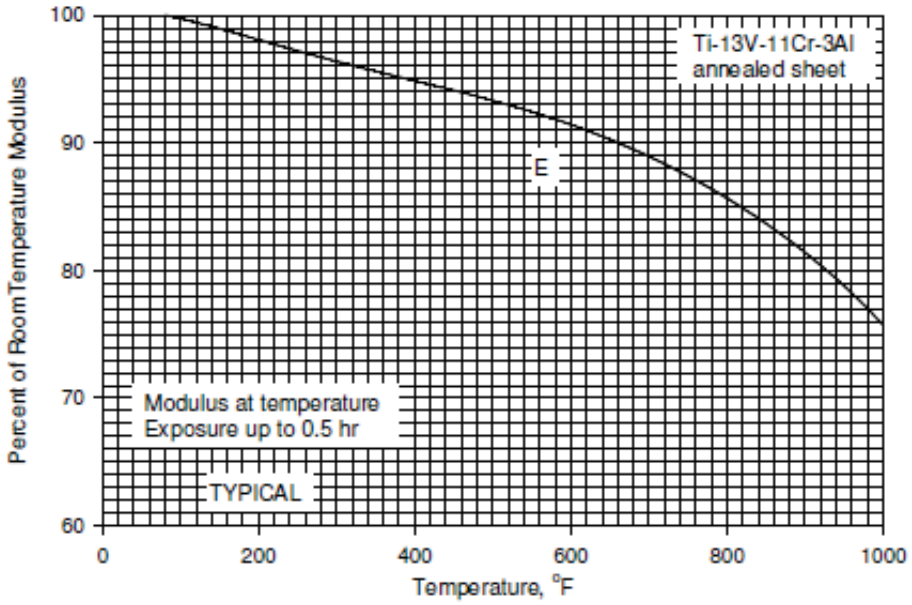

Figure 6.2.10 Temperature Effect on Tensile Modulus of Annealed Ti-13V-11Cr-3Al Alloy

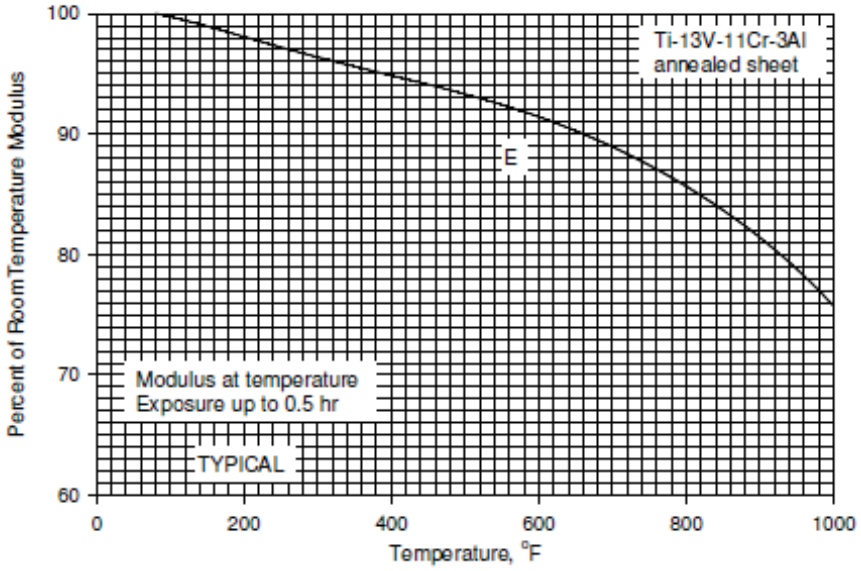

Figure 6.2.11 Temperature Effect on Tensile Modulus of Solution Treated and Aged Ti-13V-11Cr-3Al Alloy

Table 6.2.2 GKN Aerospace Report on Ti Beta 21S Sandwich Moduli

Elevated Temperature Moduli of Ti Beta 21S Sandwich							
	Flatwise Tension/Compression, psi			Shear, Longitudinal Ribbon Direction, psi			Shear, Transverse Ribbon Direction, psi
Temperature F	E'_c (c = 1.50)	E'_c (c = 0.65)	E'_c (c = 0.50)	G'_{cLong} (Plate)	G'_{cLong} (Beam Thick Faces)	G'_{cLong} (Bean Thin Faces)	G'_{cTrans}
70	469770	308100	250840	185230	221412	181450	84514
200	459435	301322	245322	181155	216541	177458	82655
300	455677	298857	243315	179673	214769	176006	81979
400	453328	297317	242061	178747	213662	175099	81556
500	450040	295160	240305	177450	212112	173829	80965
600	443933	291155	237044	175042	209234	171470	79866
700	433598	284376	231525	170967	204363	167478	78007
800	417156	273593	222746	164484	196614	161127	75049
900	391788	256955	209201	154482	184657	151329	70485
1000	356086	233540	190137	140404	167830	137539	64062
1100	308639	202422	164802	121696	145468	119212	55526
1200	246629	161753	131691	97246	116241	95261	44370

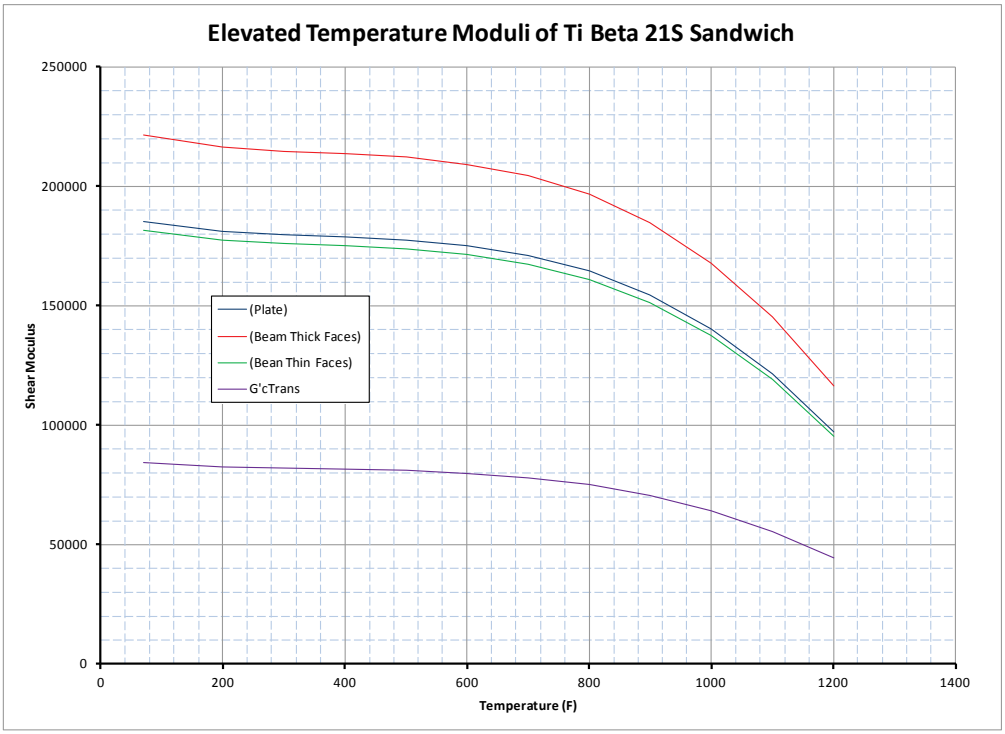

Figure 6.2.12 Elevated Temperature Shear Moduli of Ti Beta 21S Sandwich

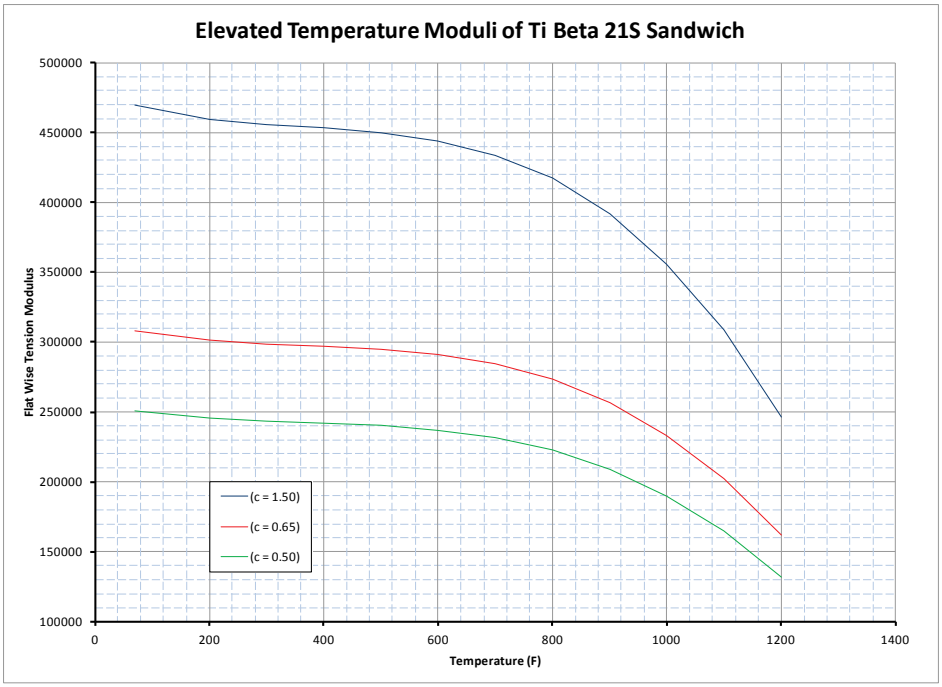

Figure 6.2.13 Elevated Temperature Flatwise Tension Moduli of Ti Beta 21S Sandwich

The results were then normalized, combined, and plotted in ***Figure 6.2.14***. A linear least square fitted equation was developed from the plot, and the equation was used to modify the material properties for the elevated temperature dynamic analysis.

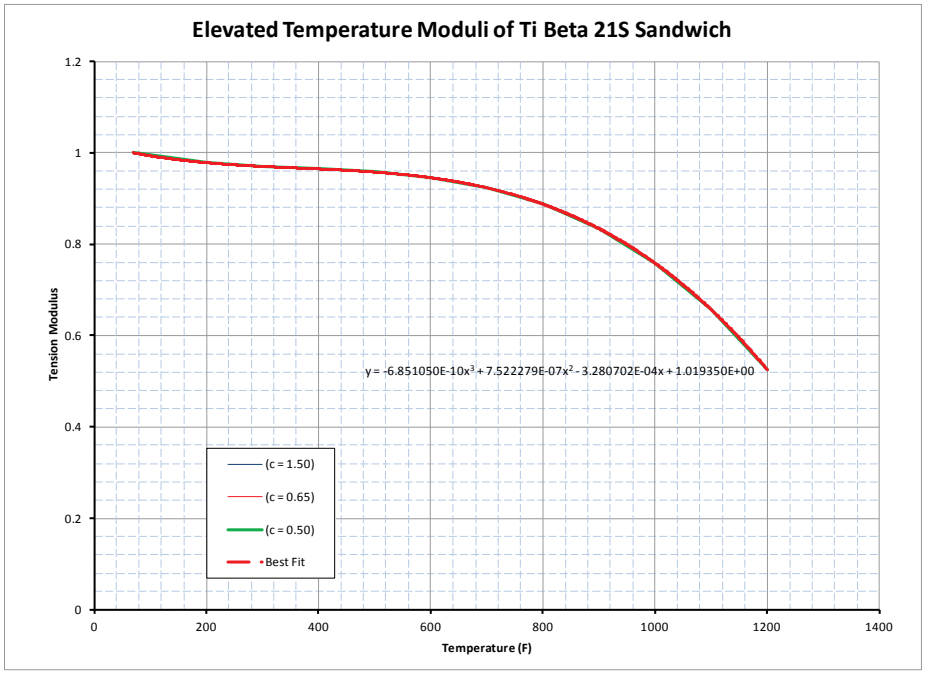

Figure 6.2.14 Normalized Elevated Temperature Flatwise Tension Moduli of Ti Beta 21S Sandwich

The linear best fit equation is listed in Equation 6.2.3. Given the panel temperature of Panel 1, plotted in ***Figure 6.2.15***, the normalized stiffness moduli was then be computed, and is presented in ***Figure 6.2.16***.

$$E_t = (6.85X10^{-10}*T^3 + 7.52X10^{-7}*T^2 - 3.28X10^{-4}*T + 1.019)* E_{rt}$$

Equation 6.2.3

Where
E_t: Moduli at temperature
T: Panel or material temperature in °F
E_{rt}: Moduli at Room Temperature

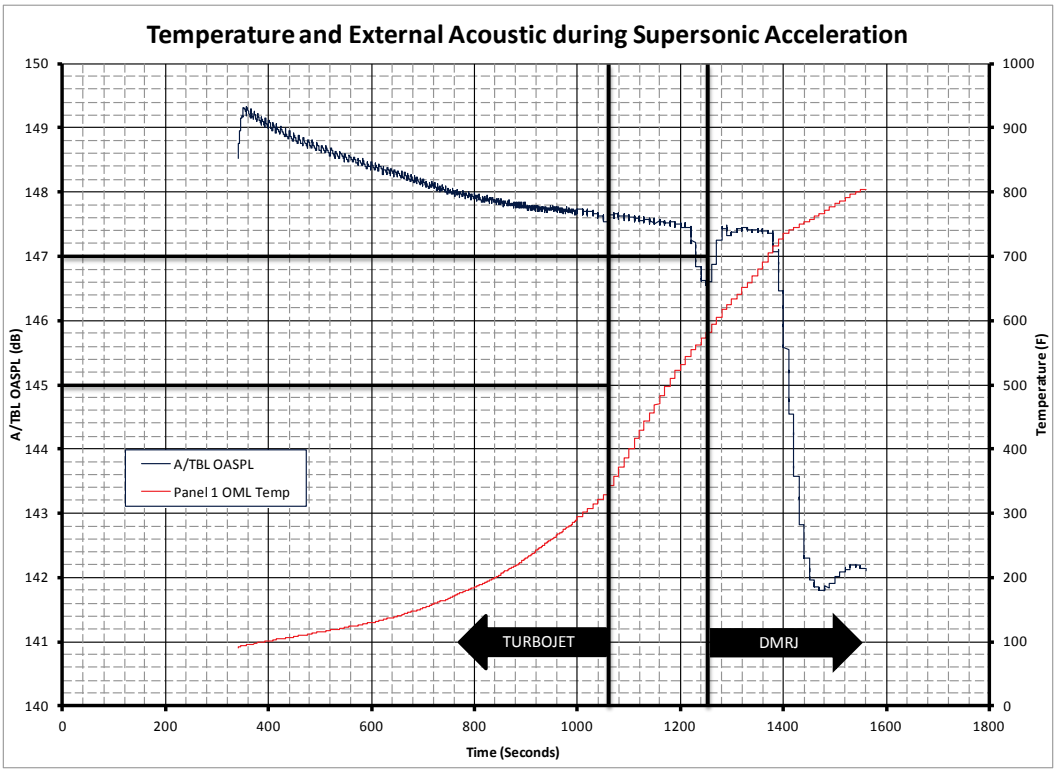

Figure 6.2.15 Temperatures and A/TBL OASPL Plot for Panel 1

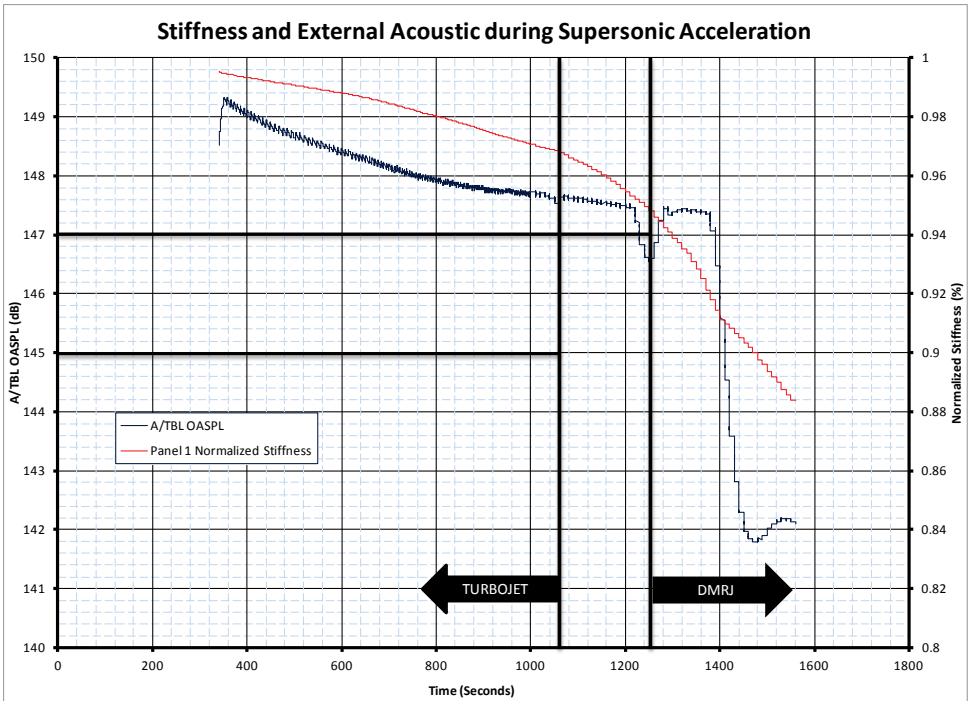

Figure 6.2.16 Normalized Stiffness and A/TBL OASPL Plot for Panel 1

The IN718 elevated temperature properties were treated in similar fashion. ***Figure 6.2.17*** represents the published modulus versus temperature plots for IN718 from GKN/Astech (Astech Design Allowables Manual ADAM-100, 1993). ***Figure 6.2.18*** illustrates the least square fit of the normalized moduli.

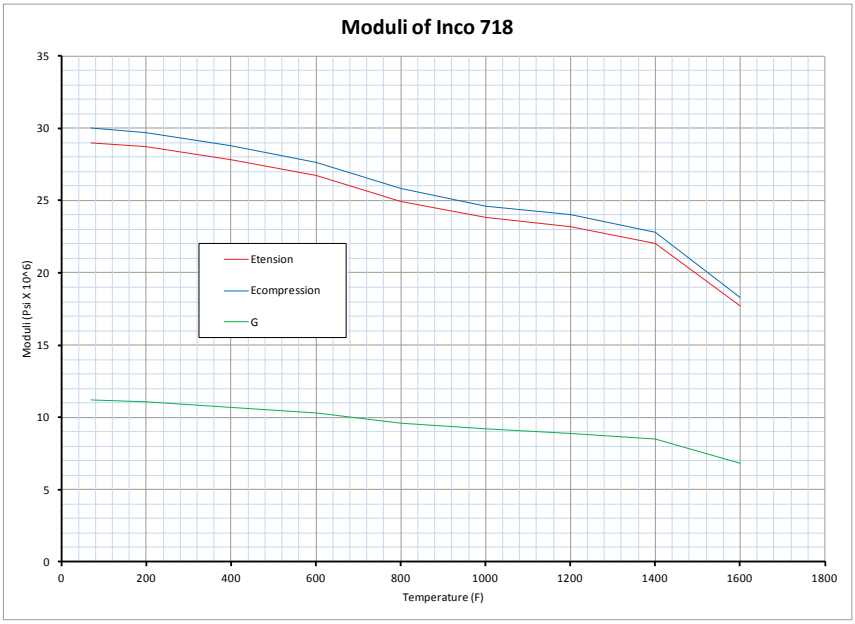

Figure 6.2.17 Elastic Modulus (E) Versus Temperature for Inconel 718

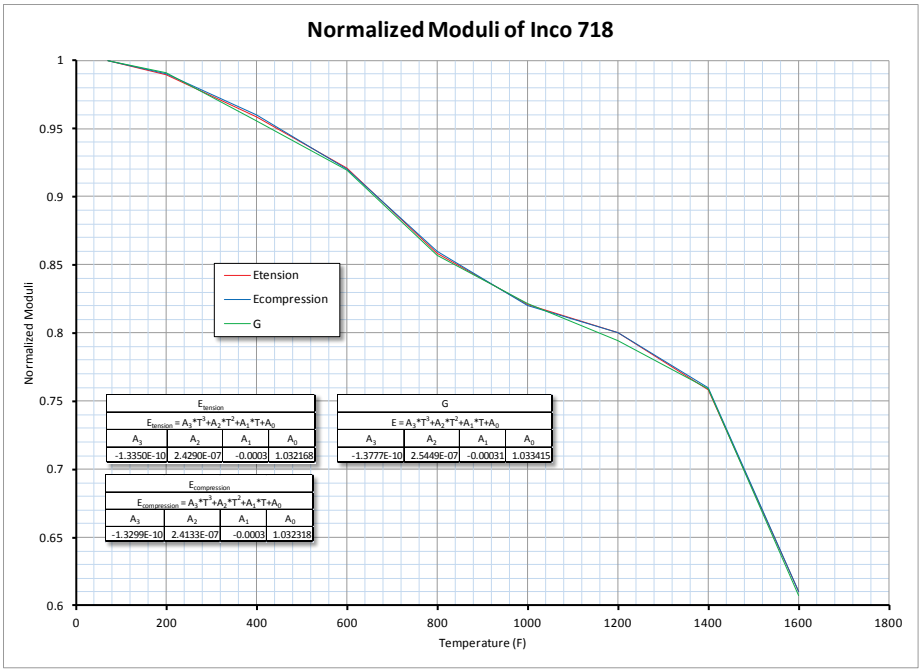

Figure 6.2.18 Normalized Moduli of Incomel 718

Table 6.2.3 Poisson's Ratio (μ) versus Temperature for Inconel 718

Elevated Temperature Moduli of Inconel 718				
Temperature F	$E_{tension}$ 10^6 Psi	$E_{compression}$ 10^6 Psi	G 10^6 Psi	μ
70	29	30	11.2	0.294

$E_{tension}$			
$E_{tension} = A_3*T^3+A_2*T^2+A_1*T+A_0$			
A_3	A_2	A_1	A_0
-1.3350E-10	2.4290E-07	-0.0003	1.032168

Equation 6.2.4

$E_{compression}$			
$E_{compression} = A_3*T^3+A_2*T^2+A_1*T+A_0$			
A_3	A_2	A_1	A_0
-1.3299E-10	2.4133E-07	-0.0003	1.032318

Equation 6.2.5

G			
$E = A_3*T^3+A_2*T^2+A_1*T+A_0$			
A_3	A_2	A_1	A_0
-1.3777E-10	2.5449E-07	-0.00031	1.033415

Equation 6.2.6

Knowing the temperature versus Mach Number relationship, the panel modulus can be calculated using the above equations and data. ***Figure 6.2.19*** plots the Elastic Modulus versus Mach Number, and ***Figure 6.2.20*** plots the elastic modulus versus trajectory flight time for Panel 4.

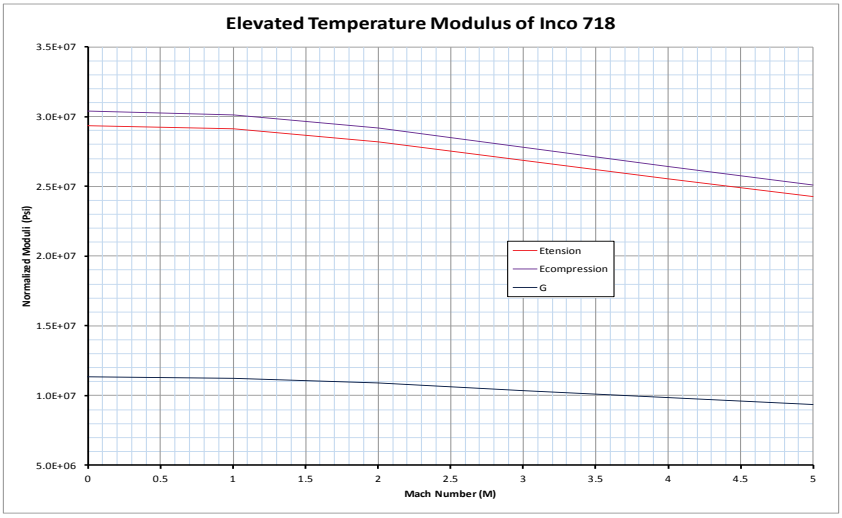

Figure 6.2.19 Elastic Modulus Versus Mach Number for Inconel 718

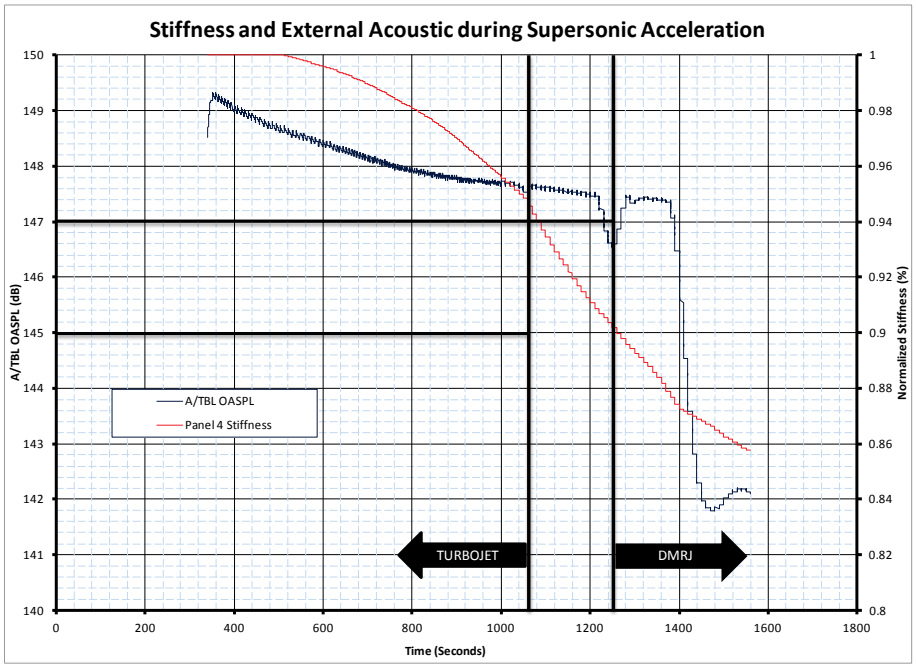

Figure 6.2.20 Panel 4 Elastic Modulus Versus Flight Time

Hypersonic Cruise External Excitation

The acoustic environments were developed primarily using the HCV mission trajectory, using similar methods and equations demonstrated in the Supersonic Acceleration section. ***Figure 6.2.21 through 6.2.23*** illustrate the results.

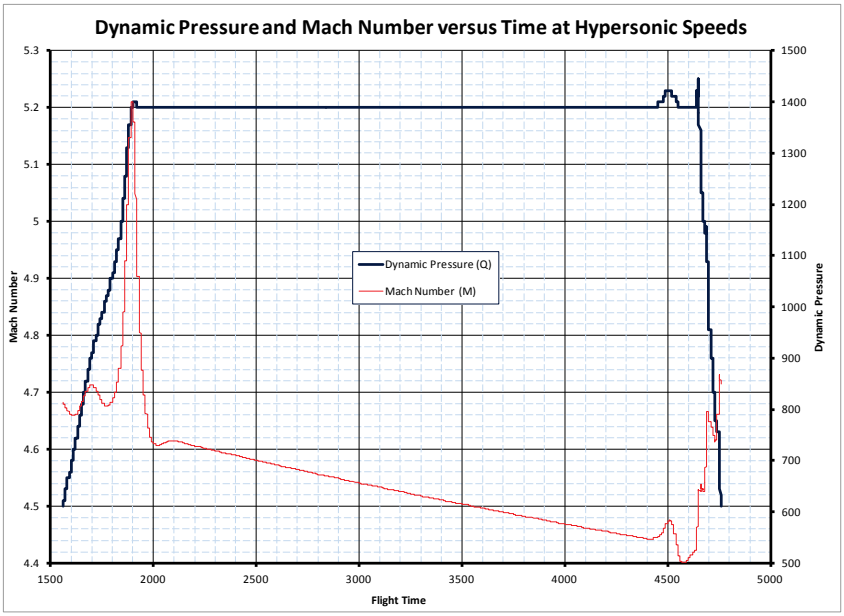

Figure 6.2.21 Dynamic Pressure (Q) and Mach Versus Flight Time

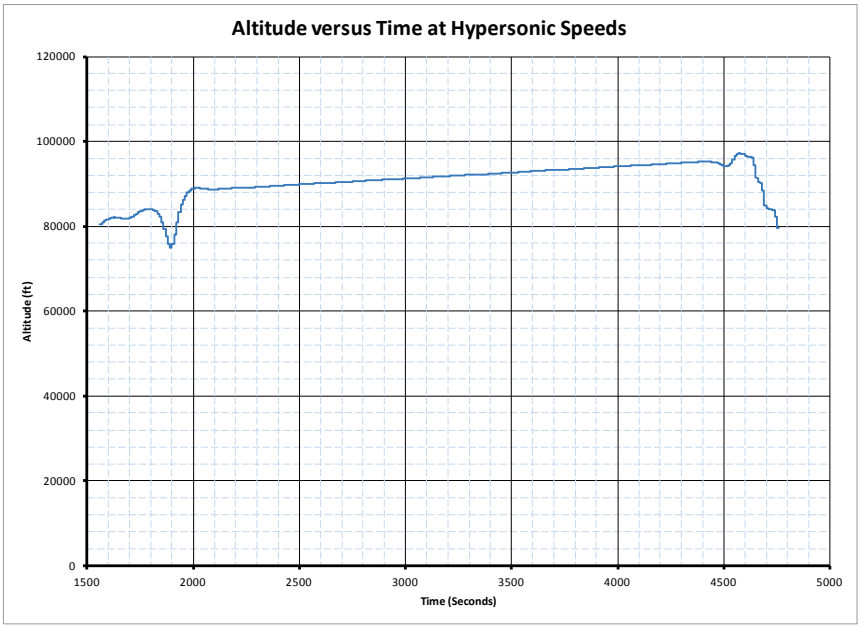

Figure 6.2.22 Altitude Versus Flight Time

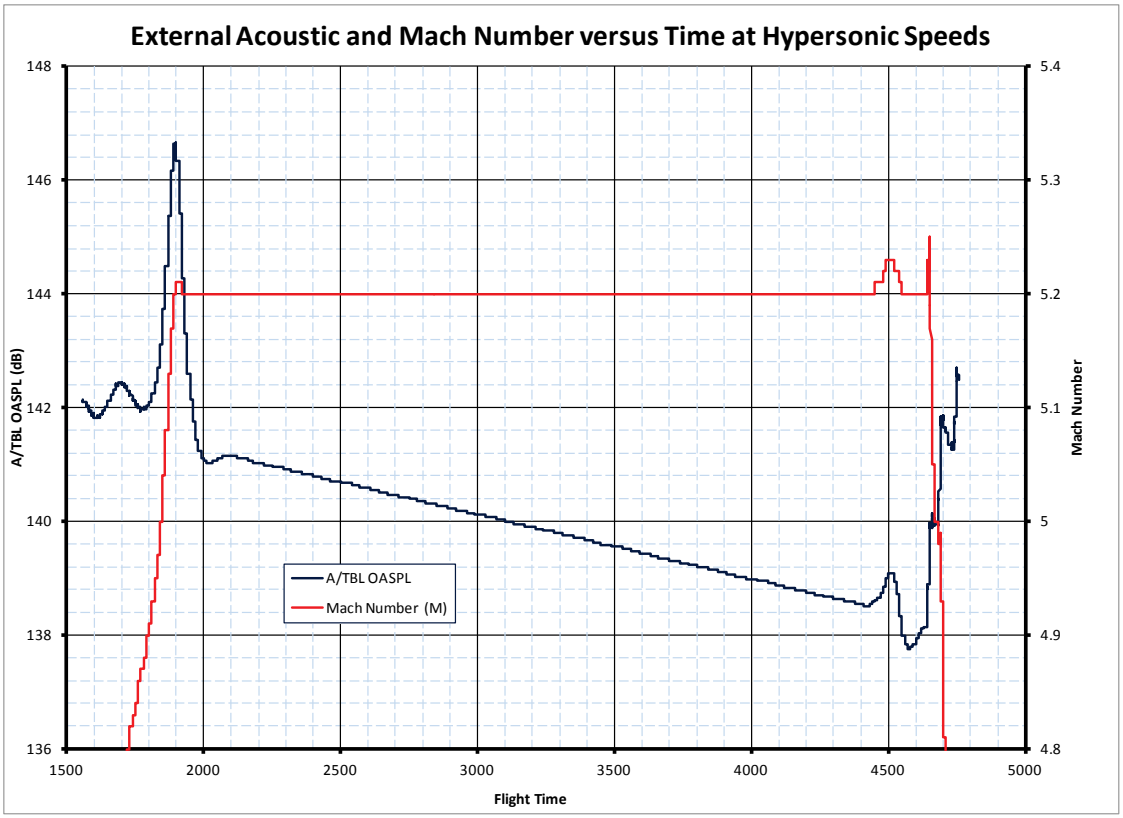

Figure 6.2.23 A/TBL Versus Flight Time for Hypersonic Cruise

The internal acoustic environments were the same environment as shown in the Supersonic Acceleration DMRJ excitation, which is primarily acoustic structural coupling.

A detailed analysis of the response of the aircraft structure had been made utilizing the finite element method. The response of the shell type structure to distributed random loads such as those produced by an acoustic environment is determined with a finite element modal solution.

MSC/Nastran was utilized for modal extraction and random response analysis. MSC/Patran was utilized for processing the modal results and the random response solution.

The Finite Element Model of the structure has the following sizing:

System Degrees of Freedom	-	125,000
Total Weight in lbs.	-	72,000

The un-deformed HCV structure is shown in ***Figure 6.2.24***.

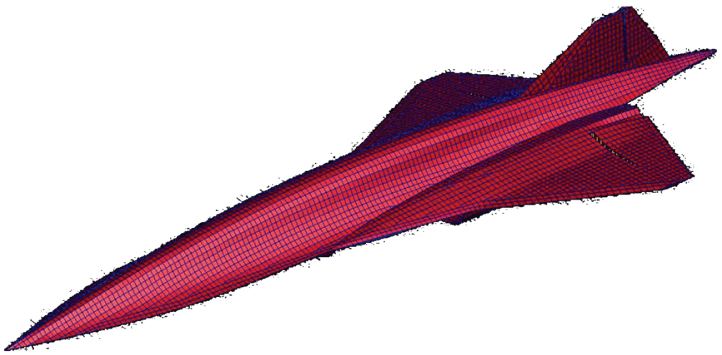

Figure 6.2.24 Un-deformed HCV Finite Element Model

A normal mode extraction was performed on the finite element model utilizing MSC/Nastran with the Lanczos method. Natural frequencies were extracted from 0.0 to 100.0 Hertz. In addition, an Effective Modal Mass calculation was performed to ensure that a sufficient number of Eigenvectors were extracted to accurately represent the modal participation of the model for all 3 axes (X-translation, Y-translation, Z-translation). An explanation of the Effective Modal Mass calculation is stated below. The natural frequencies from 0.0 to 10.0 Hertz are shown in Table 6.2.4.

Table 6.2.4 Real Eigenvalues Results

R E A L E I G E N V A L U E S

MODE	EXTRACTION	EIGENVALUE	RADIANS	CYCLES
1	1	9.431322E-04	3.071046E-02	4.887721E-03
2	2	1.584673E-01	3.980795E-01	6.335632E-02
3	3	7.447374E-01	8.629817E-01	1.373478E-01
4	4	1.574622E+00	1.254839E+00	1.997139E-01
5	5	2.263588E+01	4.757718E+00	7.572143E-01
6	6	1.575473E+02	1.255179E+01	1.997679E+00
7	7	1.648270E+02	1.283850E+01	2.043310E+00
8	8	1.689128E+02	1.299664E+01	2.068480E+00
9	9	2.332278E+02	1.527180E+01	2.430582E+00
10	10	3.798458E+02	1.948964E+01	3.101872E+00
11	11	4.552292E+02	2.133610E+01	3.395746E+00
12	12	5.133340E+02	2.265688E+01	3.605954E+00
13	13	5.302977E+02	2.302819E+01	3.665051E+00
14	14	5.794255E+02	2.407126E+01	3.831059E+00
15	15	6.904593E+02	2.627659E+01	4.182049E+00
16	16	7.518659E+02	2.742017E+01	4.364056E+00
17	17	1.384496E+03	3.720881E+01	5.921966E+00
18	18	1.442243E+03	3.797687E+01	6.044206E+00
19	19	1.483293E+03	3.851355E+01	6.129621E+00
20	20	1.727630E+03	4.156477E+01	6.615239E+00
21	21	1.890759E+03	4.348286E+01	6.920512E+00
22	22	2.184378E+03	4.673733E+01	7.438477E+00
23	23	2.268012E+03	4.762364E+01	7.579537E+00
24	24	2.289245E+03	4.784605E+01	7.614935E+00
25	25	2.320010E+03	4.816648E+01	7.665933E+00
26	26	2.654661E+03	5.152340E+01	8.200204E+00
27	27	2.747914E+03	5.242055E+01	8.342989E+00
28	28	2.924698E+03	5.408047E+01	8.607175E+00
29	29	3.055640E+03	5.527784E+01	8.797742E+00
30	30	3.066046E+03	5.537188E+01	8.812709E+00
31	31	3.201578E+03	5.658249E+01	9.005383E+00
32	32	3.353289E+03	5.790759E+01	9.216278E+00
33	33	3.435694E+03	5.861479E+01	9.328834E+00
34	34	3.496566E+03	5.913177E+01	9.411113E+00
35	35	3.691501E+03	6.075772E+01	9.669891E+00
36	36	3.742432E+03	6.117542E+01	9.736371E+00
37	37	3.761264E+03	6.132914E+01	9.760836E+00

The following is a ranking of the frequencies by Effective Modal Weight, Table 6.2.5.

Table 6.2.5 Effective Modal Weight Results

		Eff Modal Wt		
MODE	FREQUENCY	T1	T2	T3
12	3.61	0	2	27710
23	7.58	0	42	11492
31	9.01	0	46	6431
14	3.83	0	1	4694
7	2.04	0	1	2387
24	7.61	0	74	1679
21	6.92	0	19	1234
16	4.36	0	740	1077
26	8.20	0	37	1072
34	9.41	0	32	1062
30	8.81	0	269	690
13	3.67	0	121	657
33	9.33	0	16	566
32	9.22	0	262	531
1	0.00	18	0	432
22	7.44	0	175	313
29	8.80	0	174	265
15	4.18	0	1620	238
20	6.62	0	0	234
36	9.74	0	27	204
18	6.04	0	505	172
25	7.67	0	11	60
27	8.34	0	0	48
10	3.10	0	29988	36
11	3.40	0	4492	31
8	2.07	0	18	17
6	2.00	0	943	4
37	9.76	0	0	3
5	0.76	81	1	2
19	6.13	0	5	0
28	8.61	0	14	0
9	2.43	0	1595	0
35	9.67	0	48	0
4	0.20	71954	0	0
17	5.92	0	253	0
2	0.06	0	26	0
3	0.14	0	29610	0
	Total	72053	71167	63343

Note that Modes #12, #23, #31, #14, and #7 contribute a large percent of the total effective modal weight of the system for the out-of-plane T3 (Z-axis) direction. Plots of the dominant modes are shown in ***Figures 6.2.25 through 6.2.27.***

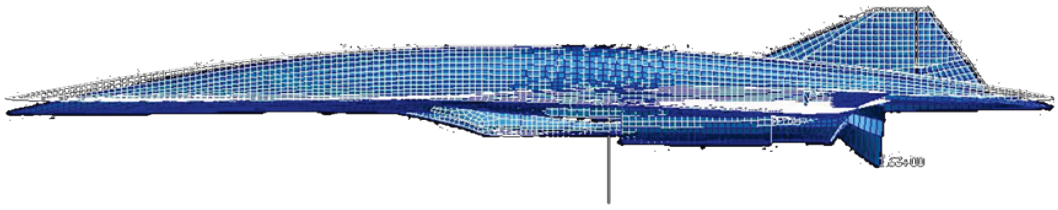

Figure 6.2.25 Mode 12 3.60 Hertz

Figure 6.2.26 Mode 23 7.57 Hertz

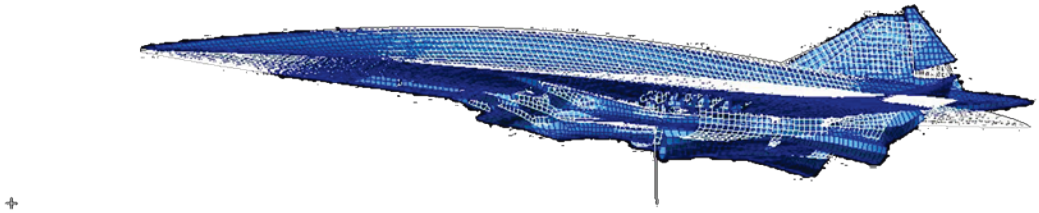

Figure 6.2.27 Mode 31 9.00 Hertz

Modal effective mass indicates the mass participation of each mode in each of the 6 rigid body motions (Translation T1 T2 T3 - Rotation R1 R2 R3) and the effective modal mass fraction is generally the most useful output. The modal effective mass was divided by total rigid body active mass.

The effective modal mass calculation will identify mode participations > 10 % Fraction. Ideally, one will calculate enough modes such that the cumulative modal effective mass fraction > 90% in each direction. Enough modes are also calculated to show when X-translation, Y-translation, Z-translation are distinctly active.

The coefficient vector is squared and divided by modal mass to give the modal effective mass values. The modal effective mass values are, in turn, divided by the total rigid body mass in each respective direction to give the modal effective mass fractions.

The modal effective weight shows modal participations in wt or mass units, and add toward the total active weight and mass for each direction. Total active mass is given by the diagonal terms on the 6x6 Total system rigid body mass matrix.

The equations defining the effective modal weight calculation are shown below:

The System Generalized Mass Matrix:

$$m = \Phi^T M \Phi$$

Equation 6.2.7

Where:

m= Generalized or Modal Mass
M= Total System Mass
r = *Unit displacement*
Φ= Eigenvector

The Coefficient Vector:

$$L = \Phi^T \quad M \quad r$$

Equation 6.2.8

The Modal Participation Factor Matrix:

$$\Gamma = L_i / m_{ii}$$

Equation 6.2.9

The Effective Modal Mass:

$$M_{eff,\ i} = L^2_i / m_{ii}$$

Equation 6.2.10

The Effective Modal Mass Fraction:

$$\text{Fraction} = M_{eff,\ i} / M$$

Equation 6.2.11

There is a strong relationship between the wave frequency and the finite element size when performing vibro-acoustic analysis. The approximation for the pressure field imposes requirements on the FEM mesh size.

For first order elements in MSC/Nastran (CQUAD4, CTRIA3, CTETRA), the element dimensions should be chosen such that the average element size is of the order of 6 times smaller than the acoustic wave.

An example of the acoustic wavelength calculation is shown below:

λ = c / f λ = Acoustic Wavelength
c = Speed of Sound (343 meters/sec)
f = Frequency
λ = (343 m/s) / 200 Hz = 1.715 m
λ /6 = 1.715 meters / 6 = 11.25 inches

For the MSC/Nastran full model, the average element mesh is between 10 thru 12 inches. Thus, the model mesh is sufficient for frequency excitation in the range of 1 Hertz thru 200 Hertz.

A random response analysis was performed for the full FEM of the structure. MSC/Nastran SOL 111 (modal complex frequency response analysis with random solution) was executed for the response solution.

The response solutions were divided into 5 distinct cases:

1. Unit pressure loading with full material properties
2. Unit pressure loading with temperature reduced material properties
3. DMRJ (Dual Mode Ram-Jet) loading with full material properties
4. DMRJ loading with temperature reduced material properties.
5. Turbojet loading with full material properties
6. Turbojet loading with temperature reduced material properties

Subsequently. the unit pressure loading for Case 1 and 2 was defined as a Power Spectral Density (PSD) PSI^2/Hz versus Frequency Power Spectral Density (PSD). The plot is shown in ***Figure 6.2.28***.

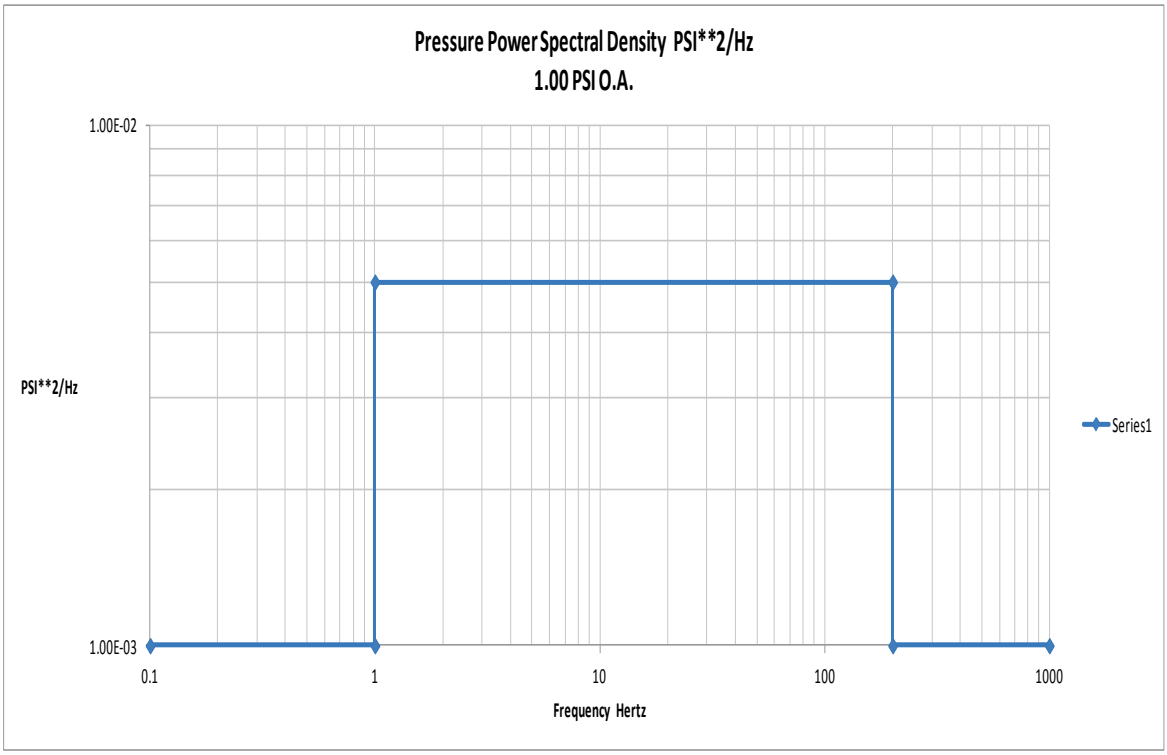

Figure 6.2.28 Unit Pressure Loading

Note that $psi_{rms} = \sqrt{\Delta f * PSD} = \sqrt{200\ Hz * 5.00 * 10^{-3}\ Psi^2/_{Hz}} = 1.00\ psi_{rms}$

Equation 6.2.12

The DMRJ input was in terms of a 1/3 octave band Sound Pressure Level (SPL) with an O.A. SPL of 193 dB. The SPL level was converted into a Pressure PSD utilizing the formula stated below:

$$PSD_{Pressure} = \frac{4.318 * P_0^2 * 10^{\left(\frac{dB}{10}\right)}}{f_c}$$

Equation 6.2.13

Where:
P_o= Reference Pressure: 2.9019E-9 psi
f_c = center band frequency

The Turbojet response analysis was executed by applying an Acceleration Power Spectral Density to the lumped masses which represented the weight of the four turbojet engines.

The G^2/Hz acceleration PSD (Overall 61.65 G_{rms}) is shown below.

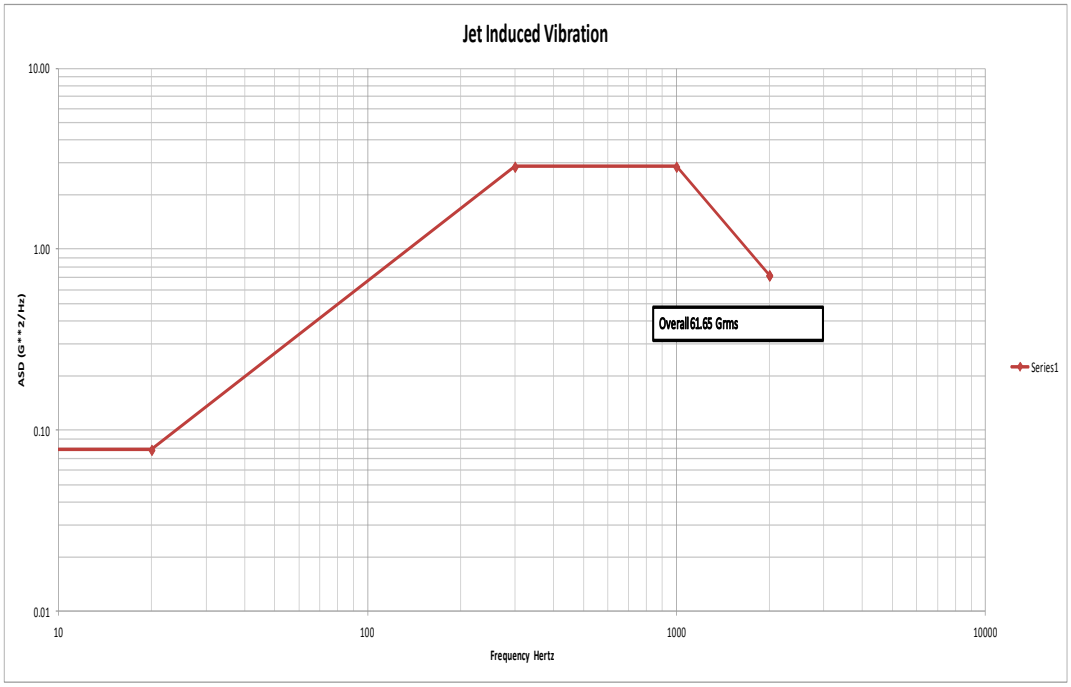

Figure 6.2.29 Turbojet Random Vibration Input

The random response analysis yielded response output for Panels 1-4:

Panel 1	Titanium Hat Section	
Panel 2	Titanium Hat Section	
Panel 3	Titanium Sandwich	0.018” ply / 0.375” core / 0.018” ply
Panel 4	Inconel 718 Sandwich.	0.025” ply / 0.750” core / 0.025” ply

The acceleration response, the displacement response, and the element internal forces were then recovered for Panels 1-4. Examples of Power Spectral Density plots showing the peak dominant natural frequencies are shown in ***Figures 6.2.30 through 6.2.32***.

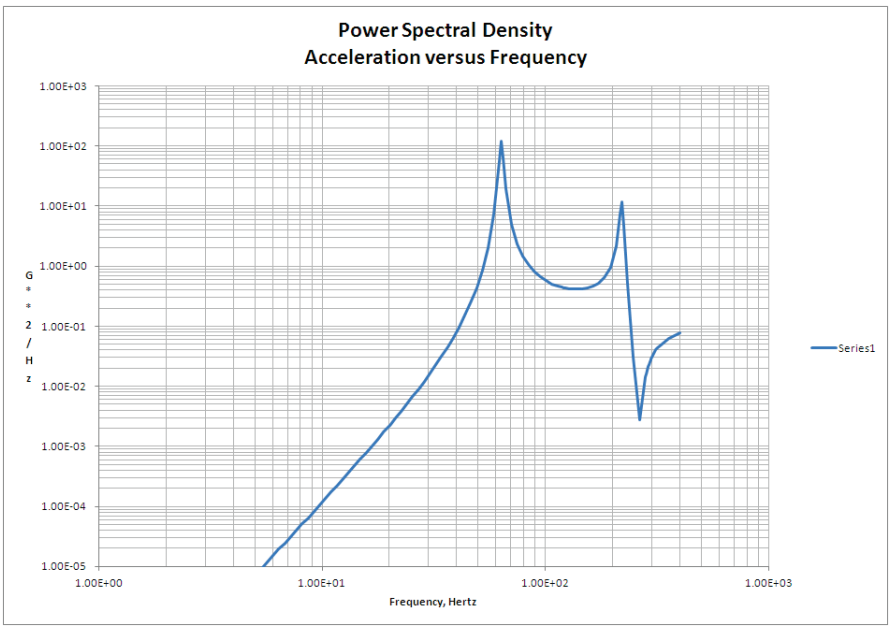

Figure 6.2.30 Acceleration Spectral Density Output

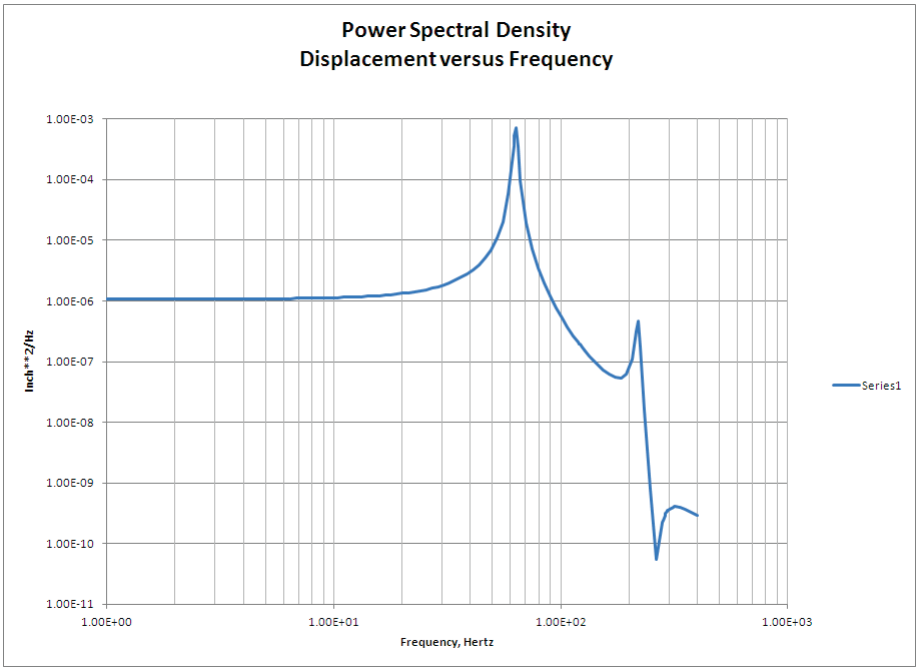

Figure 6.2.31 Displacements Spectral Density Output

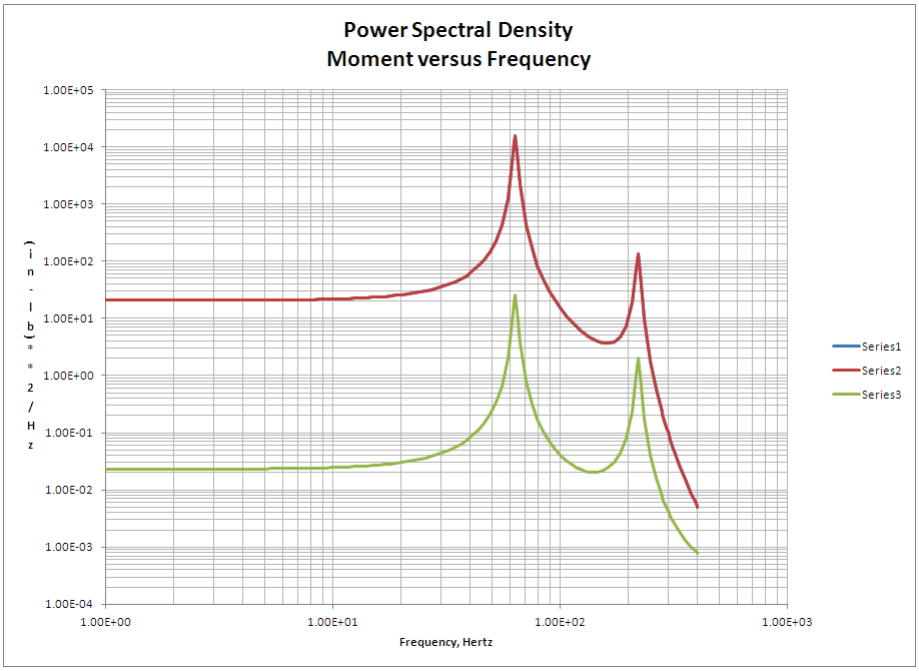

Figure 6.2.32 Moments Spectral Frequency Output

SEA Analysis

The finite element method is well-suited for determining the responses in lower mode order frequencies. However, for higher frequency analysis, the Statistical Energy Analysis (SEA) method must be utilized. The ESI Group software, VAONE (formerly known as AutoSea2), was utilized to determine the higher frequency response of the panels.

The ability of a fluctuating pressure field to excite structural response was determined by both the amplitude of the power spectrum and the spatial correlation characteristics.

The three pressure fluctuations available in AutoSea2 are:

1. Diffuse Acoustic Field
2. Propagating Wavefield
3. Turbulent boundary layer.

In addition, a mechanical input may be applied by defining a force or moment power spectrum. Any combination of excitations can be applied to the model simultaneously.

The structural SEA model was developed from the MSC/Nastran based HCV vehicle "half structure" FEM. The bulk data deck was imported into AutoSea2 and the structural panels were created from the existing FEM grid points and element definition. The elements modeled included the skin, internal frame and bulkhead supports, the fuselage, the wing, the inlet, and tail structures. Flat panel and singularly curved shell SEA subsystems were used. SEA acoustic cavities represented the internal air cavities. The SEA model is shown in ***Figure 6.2.33***.

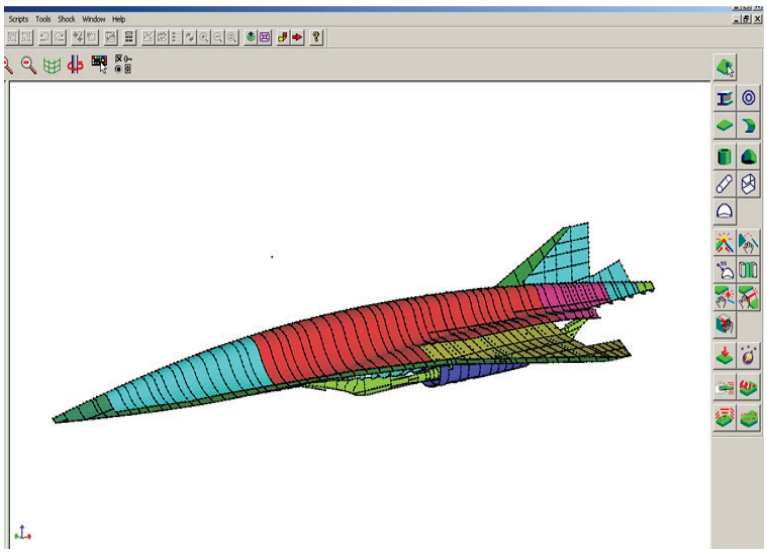

Figure 6.2.33 SEA Model

A Diffuse Acoustic Field (DAF) excitation was used to model flight at maximum dynamic pressure (max Q). The dynamic Q represented a Mach 5.2 condition (q=12.91 psi). For the turbulent boundary layer (TBL) excitation, conservative results were obtained by using the AutoSea2 default values for the TBL parameters:

$c_x(\omega)$, $c_y(\omega)$ ⟶ spatial correlation decay coefficients
$\kappa_x(\omega)$, $\kappa_y(\omega)$ ⟶ convection wave number
σ ⟶ convection velocity coefficient.

The loading for the AutoSea2 model is shown below in ***Figure 6.2.34***.

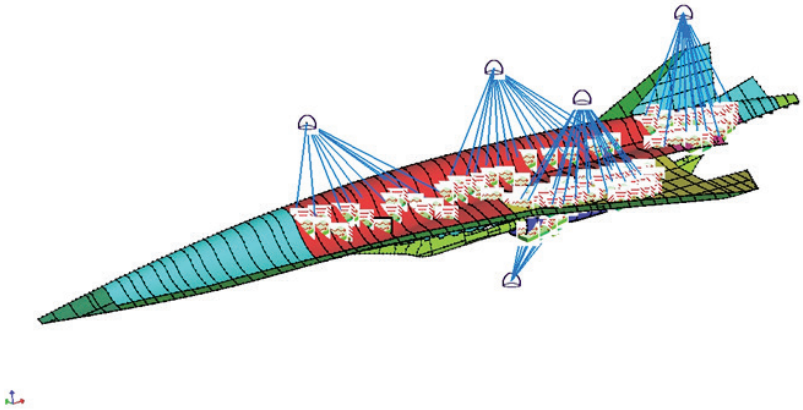

Figure 6.2.34 SEA Model Loading

Application of the environments to the SEA model resulted in spatial average prediction of the structural response for each SEA subsystem.

A plot of the structural responses, ***Figure 6.2.35***, for Panels 1-4 is shown below.

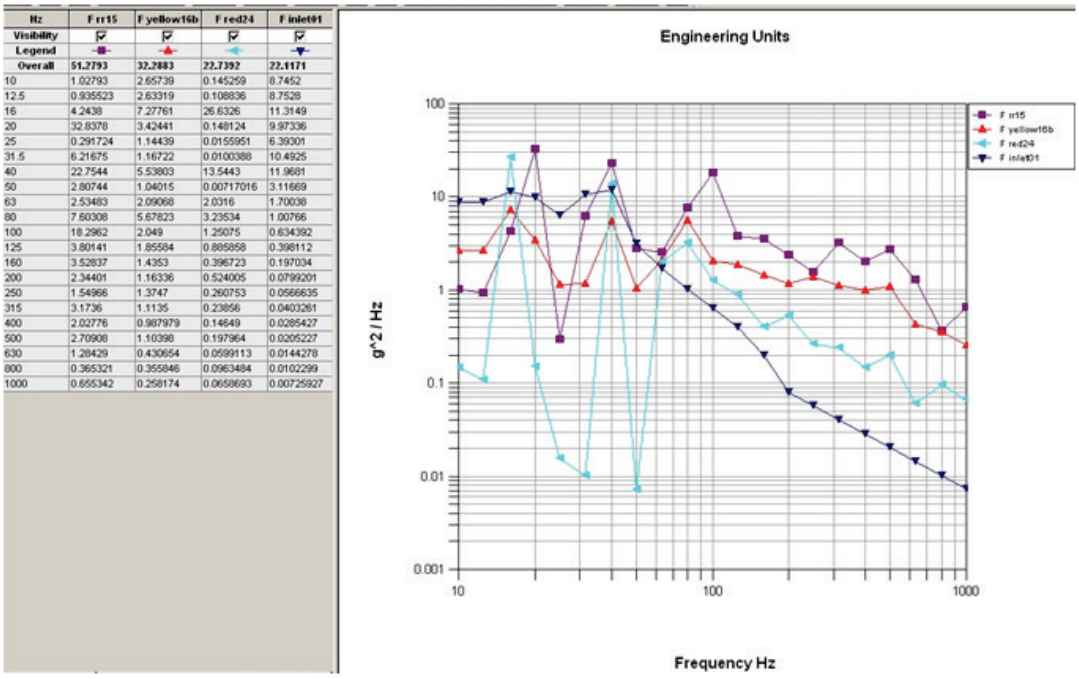

Figure 6.2.35 Structural Response of Panels 1-4

The solution domain for this analysis was a 1/3 octave band with a frequency range of 10 Hertz through 1000 Hertz.

The legacy HTV-3X FEM did not include the propulsion system as it was considered to be parasitic and non structural, and was only accounted for with mass points and rigid connections. The detailed acoustic analysis for the HCV vehicle required this propulsion system to be modeled in order to accurately predict the response. Using notional geometry from the legacy vehicle, the DMRJ section, inlet and exhaust region were meshed in MSC/Patran, as well as modeled stiffener regions and attachments, to allow integration into the vehicle FEM, as illustrated in ***Figure 6.2.36***.

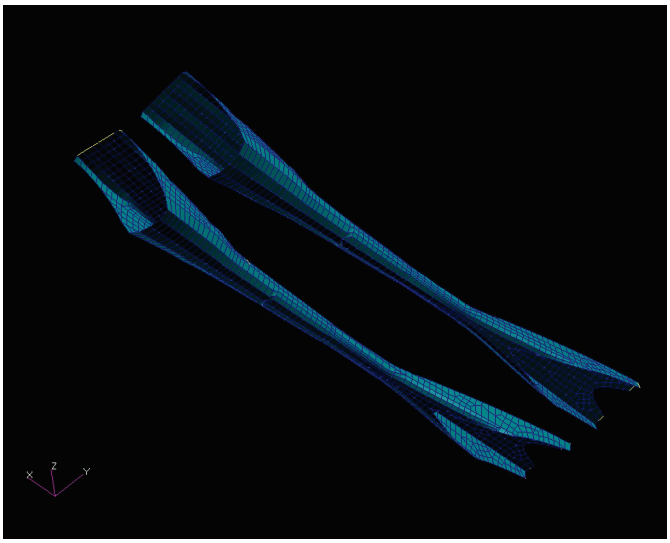

Figure 6.2.36 Propulsion System FEM

The inlet for the DMRJ engine was modeled in Autosea2 to provide for a more accurate spatial distribution of the engine noise source. The inlet FEM was extracted from the Full FEM model and then imported into AutoSea2. Flat panel and singularly curved panel subsystems were created for the inlet model, and SEA acoustic cavities represented the internal air cavities. The structural inlet subsystems (green) and the acoustic cavity subsystems (grey) are shown in ***Figures 6.2.37 and 6.2.38***.

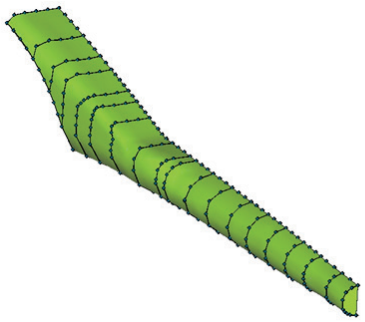

Figure 6.2.37 DMRJ SEA Model

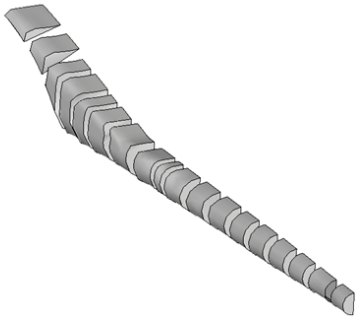

Figure 6.2.38 DMRJ Internal Acoustic Cavity Model

The input source excitation for the model was a diffuse acoustic field with an O.A. 193 dB sound pressure level (SPL). The plot of this input is shown in ***Figure 6.2.39***.

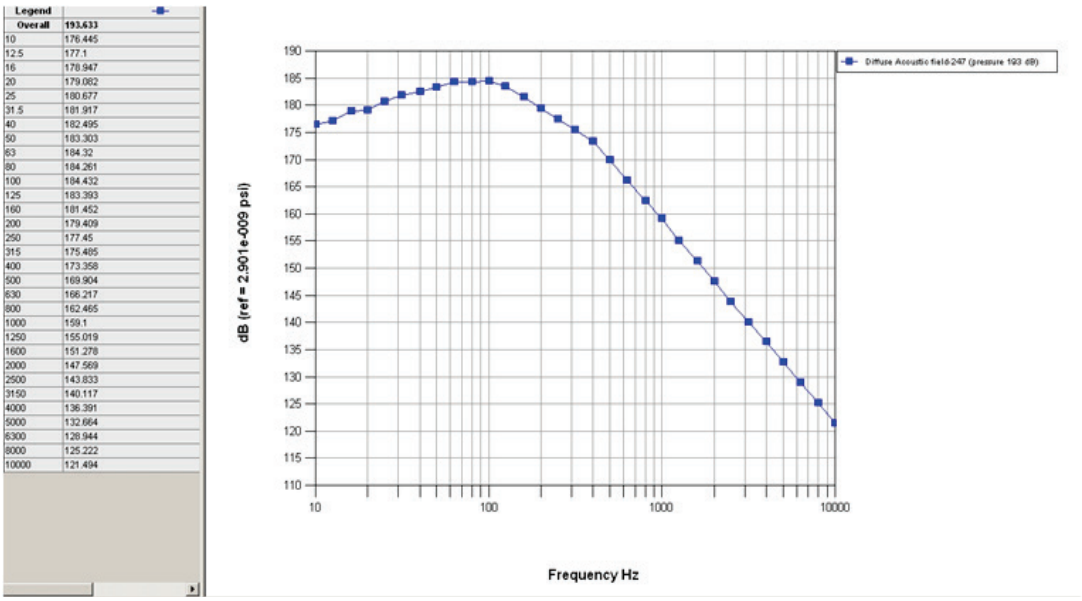

Figure 6.2.39 Input Acoustic Source

The SPL levels predicted for 4 different acoustic cavity locations ***(Figure 6.2.40)*** are illustrated in ***Figure 6.2.41***. The spatial distribution is apparent as cavity spatial position varies from input source. This SPL distribution was used in the MSC/Nastran FEM for modeling of the acoustic effects of the DMRJ engines.

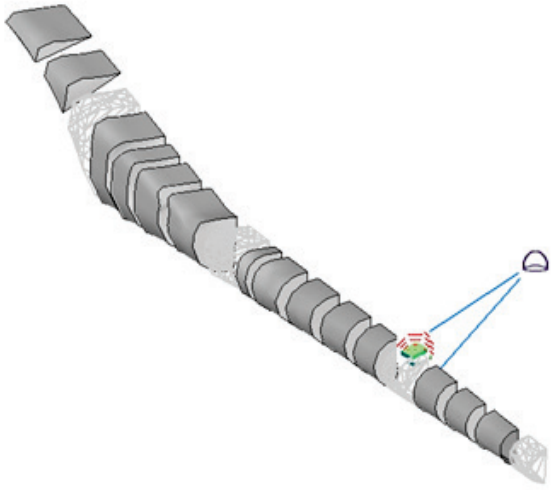

Figure 6.2.40 Acoustic Source Input to Acoustic Cavity

Hz	cavity05	cavity01	cavity11	cavity16
Visibility	☑	☑	☑	☑
Legend				
Overall	176.368	154.84	154.367	149.265
10	171.625	141.675	146.651	142.186
12.5	170.022	145.546	146.644	141.985
16	167.696	145.773	146.035	141.183
20	165.097	144.667	144.626	139.591
25	164.214	145.164	144.421	139.18
31.5	163.098	143.02	143.63	138.335
40	161.379	142.837	142.052	136.266
50	161.07	144.369	142.869	136.534
63	159.971	143.945	140.976	134.253
80	157.671	143.168	138.181	130.877
100	155.845	141.844	135.977	128.067
125	152.989	140.417	132.388	123.799
160	149.105	137.976	127.488	118.297
200	145.219	136.784	122.567	112.963
250	141.379	133.903	117.838	107.686
315	137.706	131.343	112.996	101.898
400	132.982	128.465	107.948	95.754
500	126.612	123.517	100.73	87.7367
630	121.298	117.366	94.2738	80.7161
800	115.803	110.766	87.0045	72.9109
1000	112.8	104.737	82.3764	67.6914
1250	103.412	97.9723	74.002	58.8112
1600	98.5136	91.4678	67.0891	51.2894
2000	94.744	85.1023	62.0095	46.8653
2500	96.8823	80.2578	64.3007	48.9513
3150	94.5065	74.1042	60.7909	46.0611
4000	83.4637	63.0815	49.2662	33.8594
5000	74.5558	53.4873	39.5503	23.2695
6300	66.0335	44.316	29.9786	12.6961
8000	57.646	36.3278	20.3123	1.8764
10000	49.7093	34.9192	11.0163	-8.61384

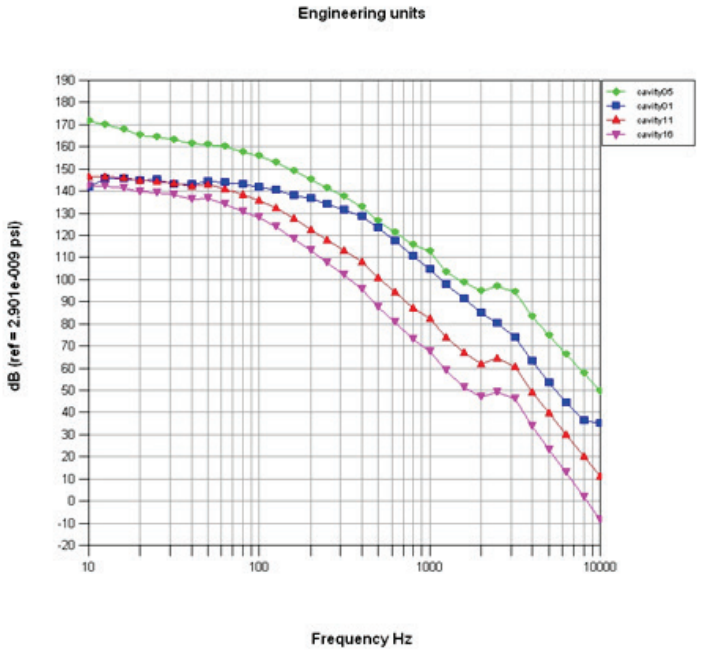

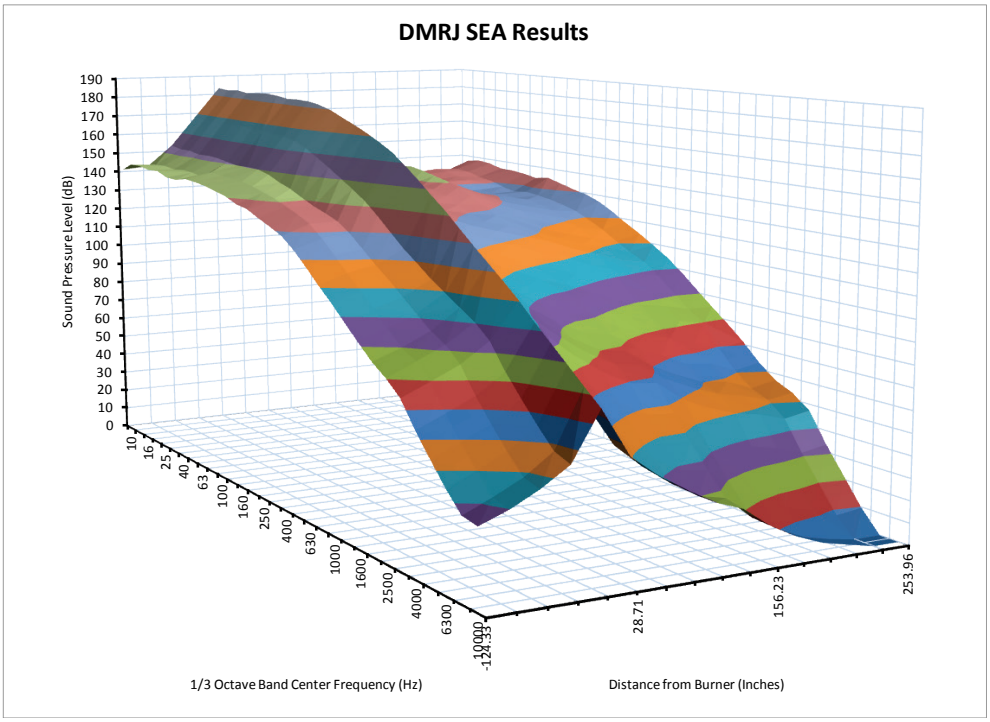

Figure 6.2.41 Acoustic Response of the DMRJ Acoustic Cavity Model

As a strong suggestion for future work includes, the vibro-acoustic assessments should be continued with updated and refined structural design information. As more detailed optimization of section properties become available, revised structural response predictions will be made.

The dynamic results were then combined based on different mission phases that the four HCV panels will experience. Element Root Mean Squared (RMS) load were extracted from the analysis echoing the element numbers being used by stress for their sizing analysis. These loads were intended to be combined with the thermal and maneuver loads. For straight and level flight plus flight maneuver below 1G, Equation 6.2.12 applies, and for flight maneuver loads above 1G, Equation 6.2.13 applies. Basically, for flight loads below 1G, the 3σ (99.7% occurrence) dynamic loads were directly added to the flight loads, whereas, during maneuver over 1G, due to the effect of increase damping while the structure are being loaded thus resulting in lower response, the 3σ dynamic loads are Root-Sum-Squared (RSS) with the maneuver loads. Figure 6.2.42 presents a visual illustration of the effect of the load combination

$$L_{Total} = \left(\frac{L_{Thermal} + L_{Static}}{\left| L_{Thermal} + L_{Static} \right|} \right) * \left(3 * L_{Dynamics} + \left| L_{Thermal} + L_{Static} \right| \right)$$

Equation 6.2.12

$$L_{Total} = \left(\frac{L_{Thermal} + L_{Static}}{\left| L_{Thermal} + L_{Static} \right|} \right) * \left(0.707 * 3 * L_{Dynamics} + \left| L_{Thermal} + L_{Static} \right| \right)$$

Equation 6.2.13

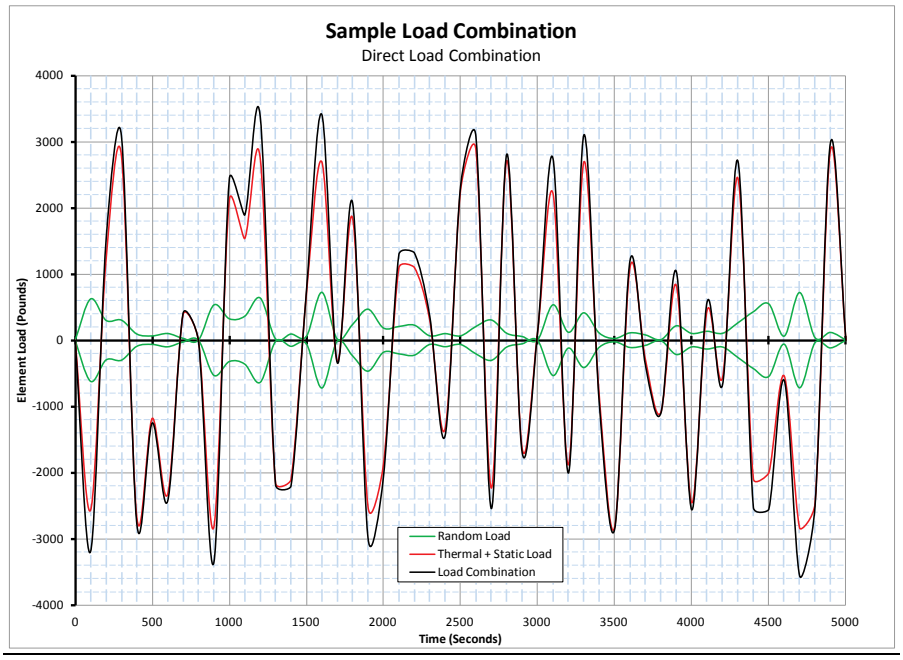

Figure 6.2.42 Sample Dynamic Load Combination

Transonic Phase:

The HCV acceleration from takeoff to Mach less than 1.25, occurs in approximately 400 seconds mission time. The temperature during this phase was generally considered to be at ambient for the study so no material modulus reductions were necessary. The propulsion energy source during this flight phase is only that of the turbojet. Moreover, the primary acoustic excitation was from the

external aero-acoustic and internal mechanical random vibration generated by the turbojet engines. There were propulsion acoustic coupling factors at the intake and exhaust nozzle, but the responses were covered by the random vibration event.

This load case utilizes external aero-acoustic excitation at room temperature, scaled to 149.3 dB. This was then combined with the random vibration analysis results for the turbojet to obtain the dynamic load for the transonic phase.

Supersonic Acceleration Phase:
The HCV undergoes some dramatic changes during the supersonic acceleration phase, which occurs at T= +400 to 1,250 seconds, in which the HCV accelerates from M = 1.25 to 3.5. The airframe will experience a dramatic temperature rise which will drive the material modulus to decrease, and the propulsion system also undergoes its propulsion mode transition in transforming form turbojet to scram jet propulsion. The load during this phase cannot be estimated as a single set and thus the results were separated into different phases, based upon the structural temperature and propulsion mode.

Supersonic Acceleration Phase, Ambient Temperature, Turbojet:
Also during this phase, the HCV accelerates from M=1.25 to 2.5, for a duration of 660 Seconds. The panel temperatures rise from approximately 80ºF to 140°F. The material modulus reduction is less than 2%. The primary propulsion system at this flight phase is turbojet and the primary acoustic excitation is from the external aero-acoustic and internal mechanical random vibration generated by the turbojet engines.

This load case utilizes external aero-acoustic excitation at room temperature, scaled to 142 dB and combining with (direct sum) the random vibration analysis results for the turbojet in order to obtain the dynamic load for the transonic phase.

Supersonic Acceleration Phase, Ambient Temperature, Dual Mode Propulsion:
During this flight phase, the HCV accelerates from M=2.5 to 2.6, for a duration of 20 Seconds. The panel temperatures rise from approximately 140 to 155°F. The material modulus reduction is less than 2.1%. The propulsion system is in dual mode, with both turbojet and scramjet operation. The primary acoustic excitation is from the external aero-acoustic, internal mechanical random vibration generated by the turbojet engines, and internal acoustic excitation from the scramjet.

This load case utilizes the RSS results from the turbojet and DMRJ, with direct summing with the external aero-acoustic excitation at room temperature, scaled to 142 dB.

Supersonic Acceleration Phase, Elevated Temperature, Dual Mode Propulsion:
During the mode transition phase, the HCV accelerates from M=2.6 to 3.5, for a duration of 170 Seconds. The panel temperatures rise from 155 to ~670°F. The material modulus reduction is approximately 10%. The propulsion system is in dual mode, with both turbojet and scramjet operation. The primary acoustic excitation is from the external aero-acoustic, internal mechanical random vibration generated by the turbojet engines, and internal acoustic excitation from the scramjet.

This load case utilizes the RSS results from the turbojet and DMRJ, and direct summing with the external aero-acoustic excitation, scaled to 142 dB. In all cases, the structure is hot, and the reduced stiffness HCV model was used.

Hypersonic Cruise Phase:
The HCV starts its cruise climb during the hypersonic cruise phase, which occurs at T= +1,250 to 4,550 Seconds, which the HCV cruises and slowly accelerates from M = 3.5 to 5.2 and maintained a constant Q cruise climb profile. The airframe temperature rises from ~670°F to over 920°F. The material modulus will decrease to ~86% of the room temperature modulus. The propulsion is now scram jet only, with the turbojet shut off at T=+1250 or Mach=3.5.

This load case utilizes the internal aero-acoustic results of the DMRJ, and direct summing with the external aero-acoustic excitation, scaled to 146.8 dB. In all cases, the structure is hot, and the reduced stiffness HCV model was used.

Descent to Landing Phase:
The HCV starts its cruise climb during the hypersonic cruise phase, which occurs at T> +4,550 Seconds, which the HCV de-accelerates from M = 5.2 to subsonic speed, while the airframe have been heat soaked at over 920°F for 3,300 Seconds. The material modulus will be ~86% of the room temperature modulus. The propulsion is now turbojet only, with the scramjet shut off at T=+4,550 (end of cruise phase).

This load case utilizes the internal random vibration results of the turbojets, and direct summing with the external aero-acoustic excitation, scaled to 146.8 dB. In all cases, the structure is hot, and the reduced stiffness HCV model was used.

The dynamic load combination results were then sent to the project stress analyst to combine with the thermal and maneuver loads, and final sizing of the structure.

Dynamic Analyses Conclusions
The DMRJ propulsion system, currently planned for hypersonic airframes, has a completely different acoustic spectrum than traditional turbojets or turbofans. ***Figure 6.2.43*** illustrates the typical turbojet or turbofan propulsion normalized spectrum as published in Military Standard 810G, along with the studied DMRJ acoustic spectrum.

The two spectrums clearly show the different acoustic characteristics of the two propulsion systems. The bulk of the energy of the typical jet engine is contained within the frequency band between 125 to 1,600 Hz, whereas, for the DMRJ, most of the energy is between 10 to 100 Hz.

For the typical jet engine, there is a clear frequency separation between the engine acoustic energy and the primary airframe frequencies (typically, for missiles, around 30 to 60 Hz), and for these design cases, the propulsion acoustics were not included in the primary and secondary structure design. On the other hand, the DMRJ acoustic spectrum presents a critical challenge to the airframe design, as the acoustic frequencies can couple with the airframe primary frequencies, and generate high dynamic airframe loads which must be accounted for early in the design of the hypersonic airframe.

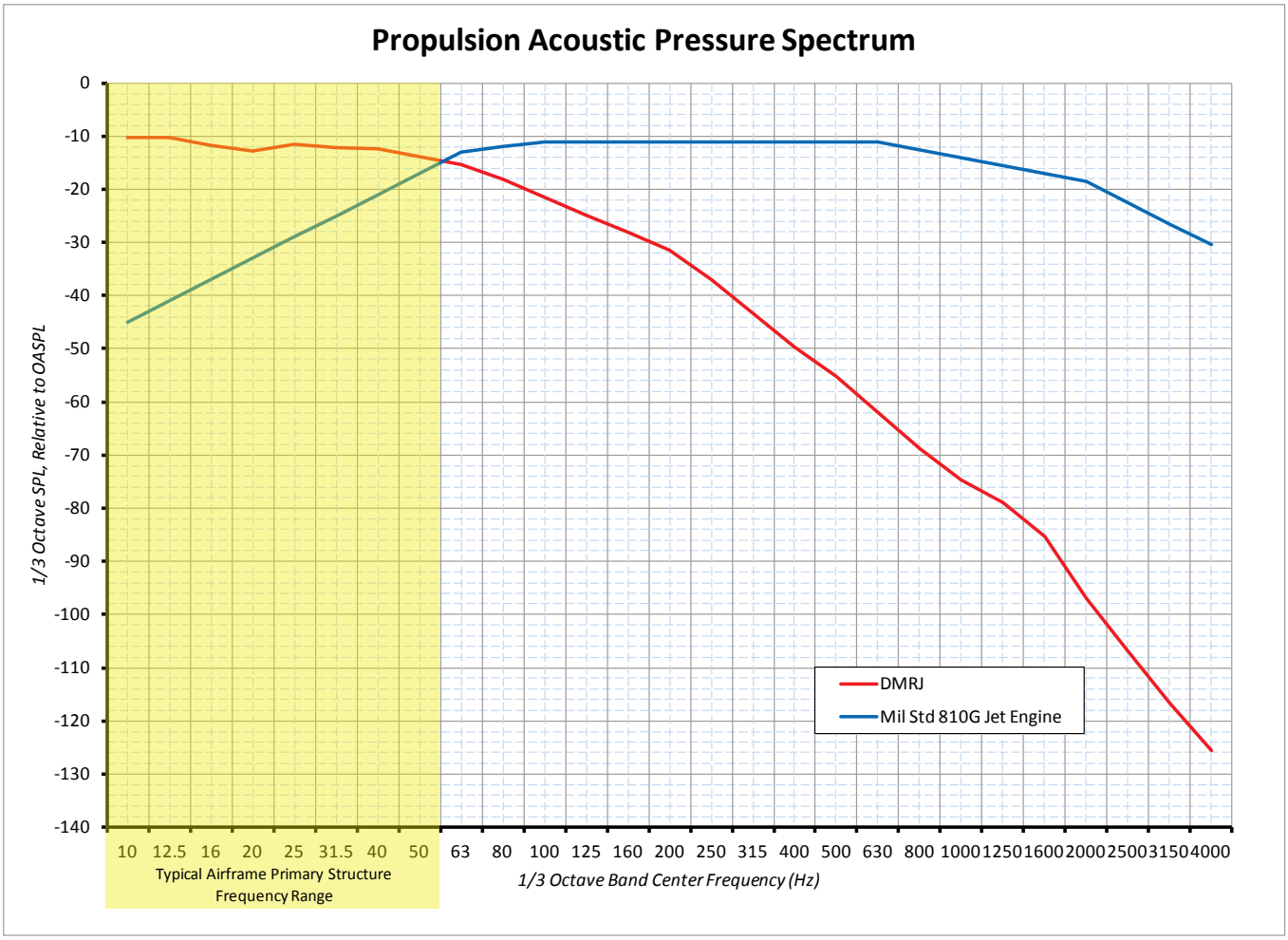

Figure 6.2.43 DMRJ versus Typical Mil Std 810G Jet Acoustic Pressure Spectrum

6.3 PANEL FLUTTER ANALYSES

A FEM based flutter analysis is a higher fidelity analysis used to validate an empirical model or provide better results.

In general, a FEM of the vehicle is developed to accurately represent the structure's modal characteristics, while an aerodynamic model is developed to represent those characteristics. The structural model is then splined onto the aerodynamic model, and then the response of the vehicle at multiple, usually transonic, Mach numbers.

Due to the nature of panels (having airflow on only one side), an aero factor of 0.5 is usually applied to the model.

The panel flutter effort consisted of FEMs and aero models (***Figures 6.3.1 through 6.3.4***) of the four panels. The FEMs were originally developed in ABAQUS to perform stress analysis but were modified and converted into MSC/Nastran that was required to work with Lockheed Martin's proprietary flutter analysis software, FAMAS. The Young's Modulus values were reduced to compensate for the expected temperature the panel will experience. Modal analyses were

performed, and mass, stiffness, and eigenvector matrices were extracted. An aero panel model was developed and run for various transonic and supersonic Mach numbers. The aero model uses Doublet-Lattice theory sub-sonically and ZONA51 theory supersonically and is solved using a p-k solution technique developed in a MATLAB-enhanced version of the Lockheed Martin FAMAS flutter solution code.

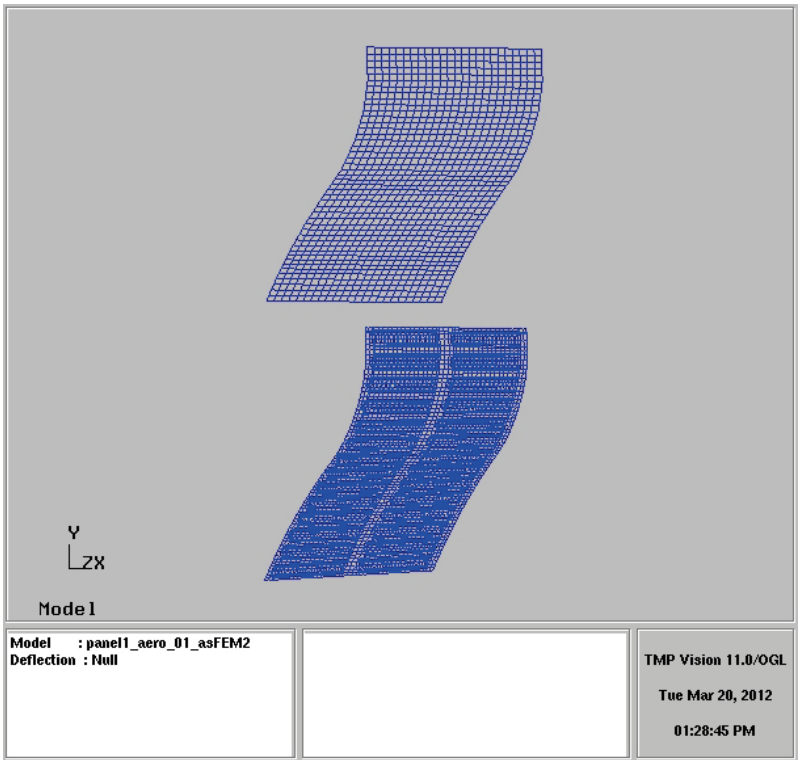

Figure 6.3.1 NASTRAN Aero Panel Model and FEM of Panel 1

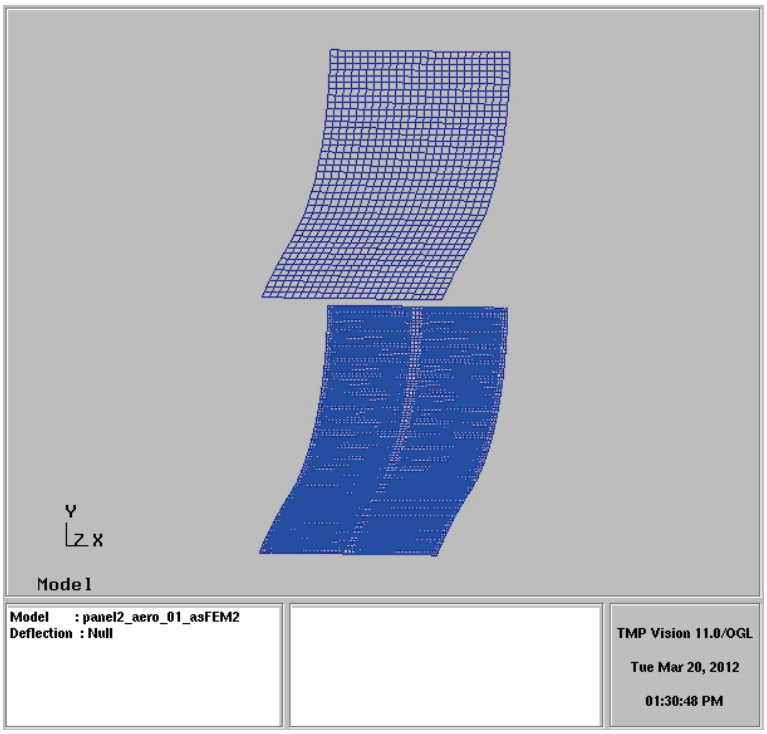

Figure 6.3.2 NASTRAN Aero Panel Model and FEM of Panel 2

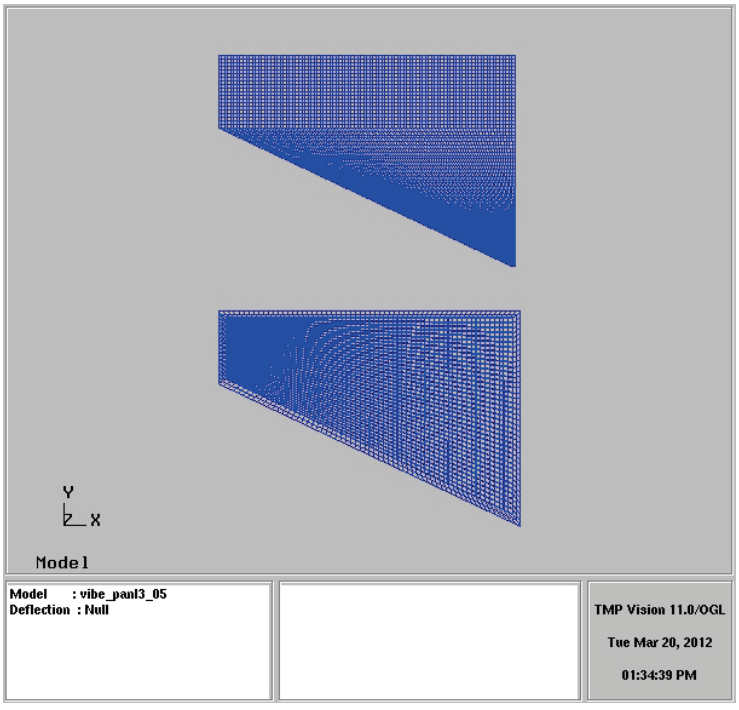

Figure 6.3.3 NASTRAN Aero Panel Model and FEM of Panel 3

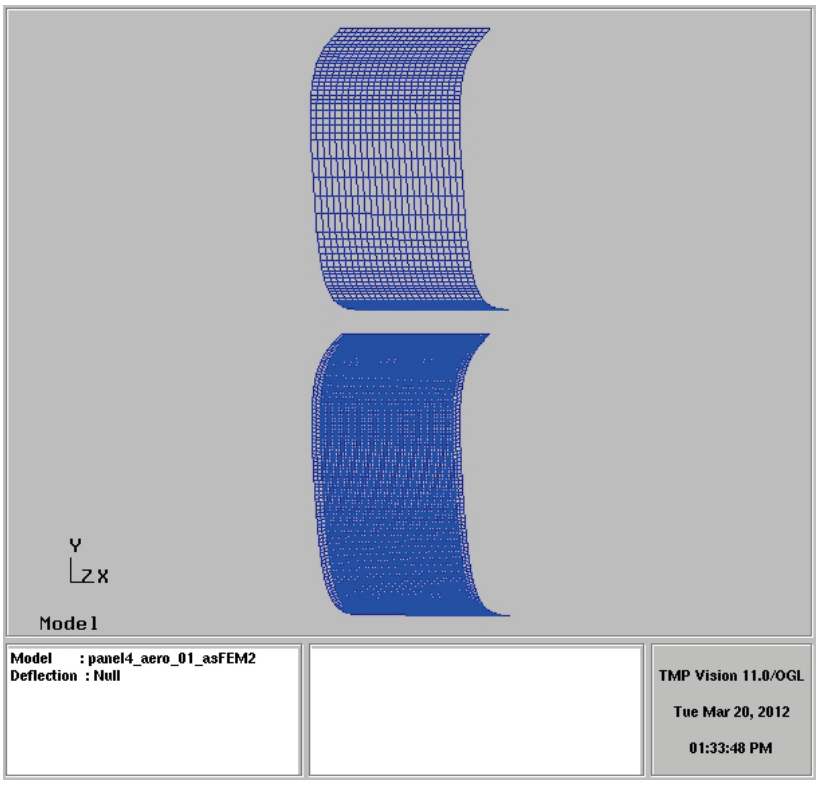

Figure 6.3.4 NASTRAN Aero Panel Model and FEM of Panel 4

All four panels were analyzed at Mach=0.8, 0.9, 1.1, 1.2, 2.0, and 3.0 for a baseline of reduced Young's modulus, clamped boundary conditions, and an aero factor of 0.5. All baseline cases were free from flutter in the flight regimes. Refer to ***Figure 6.3.5*** for a sample result. As the Mach 2.0 and Mach 3.0 appeared very stable, they were not analyzed in the trade studies listed below.

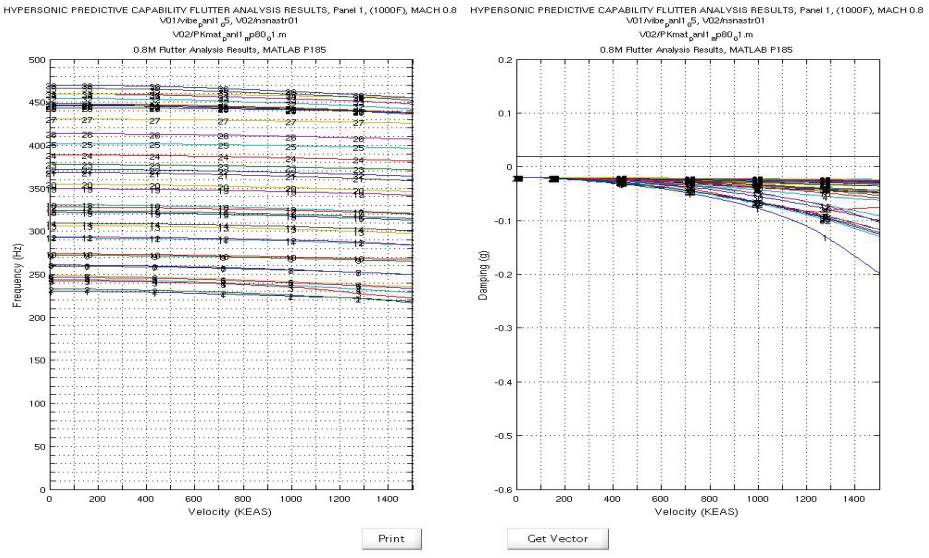

Figure 6.3.5 Panel 1 Baseline Flutter Analysis at Mach = 0.8

In addition to the baseline cases mentioned above, all panels at the transonic Mach numbers were subject to sensitivity studies compared to the baseline. The first study was to change the aero factor to 1.0, simulating a panel in the free stream. All panels at all Mach numbers were free from flutter in the flight regime.

The next sensitivity study was to set the boundary conditions to simply-supported (fixed in all three translation degrees of freedom only). Again, all panels at all Mach numbers were free from flutter in the flight regime.

In the next sensitivity study, all stiffeners from panels 1 and 2 were removed. This induced flutter in both panels. Panels 3 and 4 had their thicknesses reduced by 50%, but both were free of flutter at all Mach numbers within the flight regime.

The next study involves only Panel 1. The baseline includes a rigid attachment of the stiffeners to the panel back. This attachment stiffness was modified until flutter was seen, which occurred at Mach=0.8 at the relatively low 1000 lb/in per attachment.

In the final study, panel 4 has its aero factor modified until flutter was seen. The intent of this exercise was to simulate this panel, which will see exhaust impingement, in an in-flight condition. This occurred at an aero factor of 2.0, implying both sides of the panel saw twice as much aero loading as outside of the baseline panel.

A summary table of the flutter results is below (Table 6.3.1), where "No" means no flutter occurred up to 1500 keas, which is over twice the 644 keas value used in the empirical analysis.

Table 6.3.1 Summary of FEM-based Panel Flutter Results

Panel	Baseline values (all cases flutter free in flight regime)				Sensitivity studies					
	Temperature (°F)	Boundary conditions	Construction	Aero factor	Aero factor = 1.0	Simply supported	Stiffeners removed	Half thickness	Stiffener attachement stiffness	Excess aero factor (= 2.0)
1	1000	clamped	Ti w/stiffeners	0.5	No	No	322 keas	-	1117 keas	-
2	1000	clamped	Ti w/stiffeners	0.5	No	No	521 keas	-	-	-
3	1160	clamped	Ti honeycomb	0.5	No	No	-	No	-	-
4	1055	clamped	Inconel honeycomb	0.5	No	No	-	No	-	1227 keas

6.4 CFD BASED THERMAL EFFECTS MAPPING FOR TEMPERATURE INPUT

The Phase II program, as initially described in Section 5.3 of this report, required a higher fidelity, CFD approach for detailed thermal analysis of specific panels on the HCV where nonlinear effects are expected. This method also provides thermal maps for Mach < 3 which are not feasible using impact methods as done in Phase I. Additionally, the CFD approach is necessary to capture the three dimensional effects of the gap beneath the rudder, the rudder hinge line cove, rudder deflection and its effect on the flow field and thermal environment on the fuselage panel just below the vertical tail.

The technical approach planned to leverage a CFD model developed for the HTV3-X program, unfortunately, upon examination of the mesh near the surface of the vehicle, it was discovered that the mesh spacing was inadequate for accurate aero-thermal modeling. This force and moment study mesh used wall functions to approximate the boundary layer sub-layer and to reduce the size

of the boundary layer mesh. However, this is not the best approach for aerodynamic heating in a hypersonic boundary layer. Instead, a mesh which allowed accurate solution to the wall boundary was desired which requires a y+ < 1, or about 0.003 inch mesh spacing at the wall.

Structured meshes provide the best numerical accuracy in the boundary layer and for shock capture, however, development of a structured mesh around complex geometries is difficult, at best. For this reason, an attempt was made to build an unstructured mesh with a prism boundary layer. The Gridgen gridding tool now has an option where an unstructured mesh can be built on the surface of a vehicle and a tool to grow the volume grid automatically can be employed. This tool is still in the development stages but has been used extensively by the Lockheed Martin Aero Fort Worth group to develop unstructured grid for vehicles. The initial surface grid was accomplished; however, the volume grid had trouble with the fine spacing required for this vehicle to achieve good quantitative thermal results. Furthermore the gridding tool had difficulties with small gaps that were used to define the rudder cove and areas where a surface is deflected. At times Gridgen was able to grow a volume grid but the CFD program used found negative volume cells and was unable to run successfully.

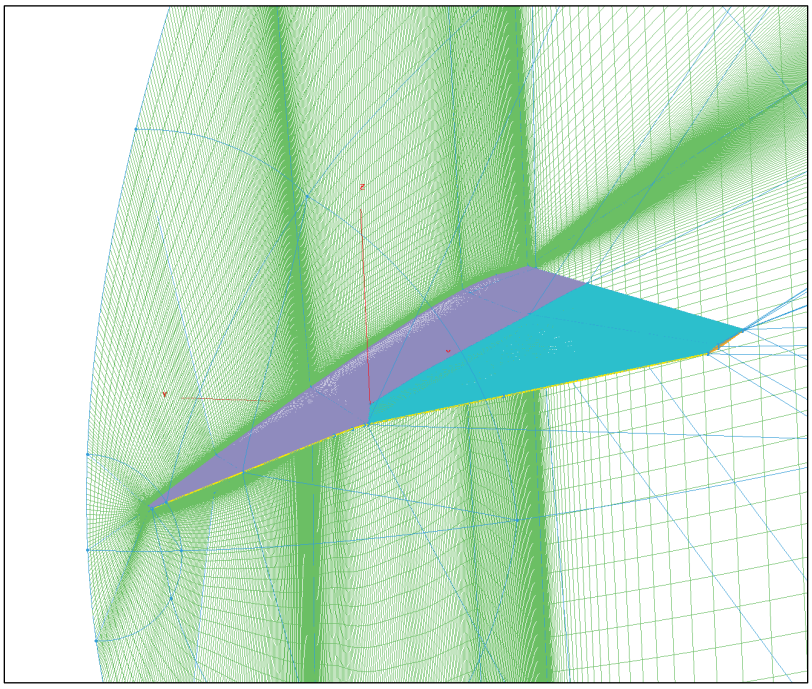

Figure 6.4.1 Structured Mesh Around the Vehicle Strake/Wing – 26M Cells

The vehicle model was simplified as an isolated strake and wing, since this would make the mesh construction straight forward and would have minimal impact on the environment for panel 3. Gridgen was used to build a block structured C-O mesh around the vehicle strake/wing as shown in ***Figure 6.4.1***. This model correctly accounts for both the mesh density needed in the boundary layer and wake to accurately predict aerodynamic and aero-thermal characteristics at the vehicle surface.

Mach 5.2 results for the strake/wing model were obtained using CFD++, a CFD code developed by Metacomp Technologies, Inc., and are illustrated in ***Figure 6.4.2***. The upper picture in the figure is for an angle of attack of 0° and the lower picture 2°. Both cases were modeled with an emissivity of 0.8. The results clearly show the nonlinear aerodynamic effects which could not be captured using impact methods, namely, the low pressure region emanating from the strake/wing intersection. The leading edge break in sweep induces a vortex structure and a resultant low pressure streak.

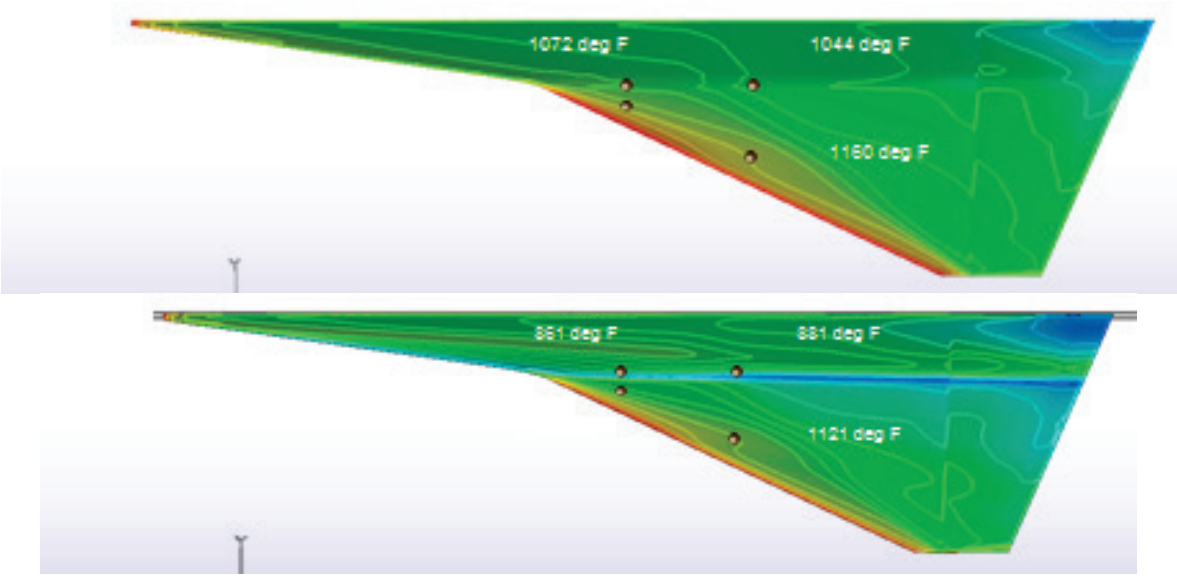

Figure 6.4.2 Isolated Strake/Wing Solutions at Mach 5.2. Angle of attack = 0° for Upper Picture and 2° for Lower, Emissivity = 0.8. Note Low Pressure Region Emanating From Leading Edge Break Due to Vortex Structure

In order to reduce complexity so that the entire vehicle could be meshed using the unstructured approach, the rudder cove and gap were removed. Additionally, the rudder was not deflected, allowing the model to take advantage of symmetry. Again, Gridgen was used to create the unstructured surface mesh and AFLR3, the hypermesh volume mesher, was used. This resulted in a mesh with 54 million cells and by looking at ***Figure 6.4.3***, it is apparent the difference in field mesh density from the structured strake/wing mesh in ***Figure 6.4.4***.

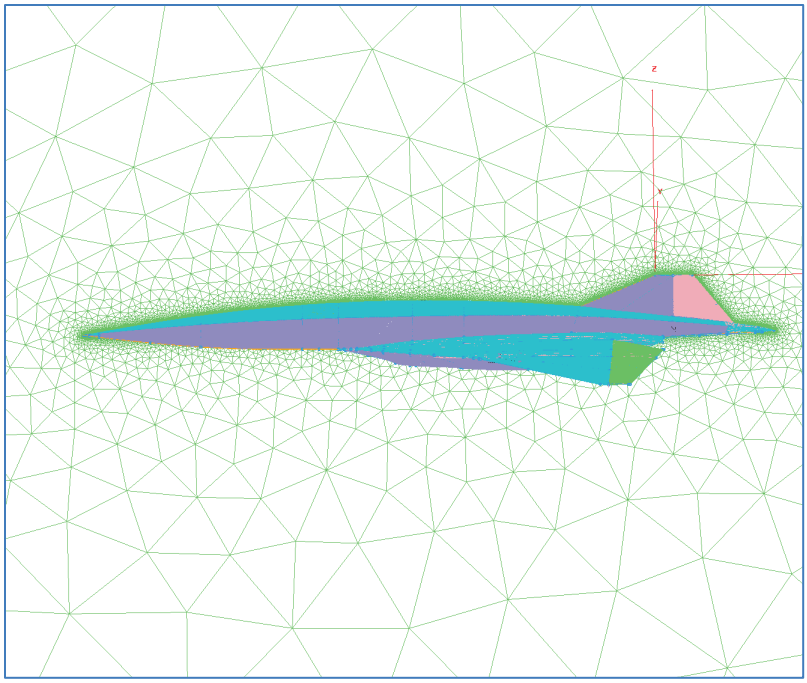

Figure 6.4.3 Unstructured Mesh Around Vehicle Without Rudder Cove or Gap. 54M Cells.

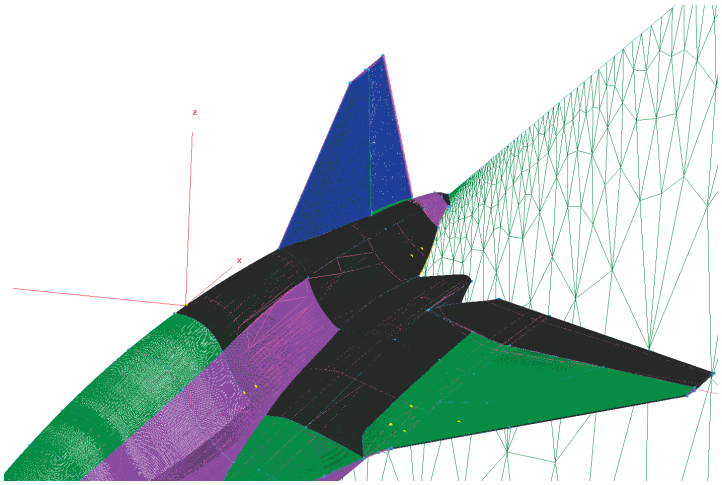

Figure 6.4.4 Surface Mesh Density is Equivalent to Corresponding Structured Mesh

Results for the simplified full vehicle model, again using CFD++, are shown in ***Figures 6.4.5 and 6.4.6***. ***Figure 6.4.5*** shows radiative equilibrium temperatures on the upper and lower surfaces of the HCV at Mach 5.2 and 0° angle of attack. Note the difference in solution smoothness as compared to the strake/wing solution in ***Figure 6.4.6***.

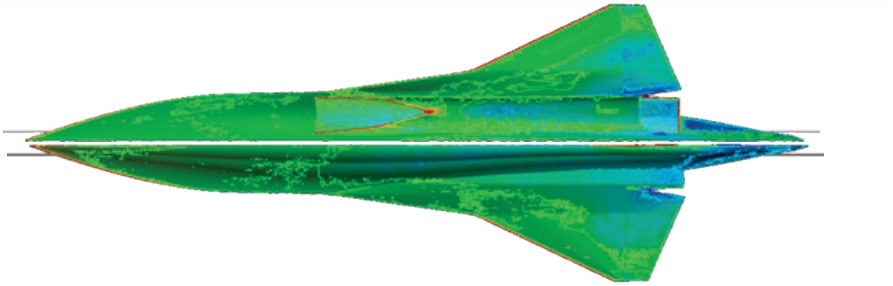

Figure 6.4.5 Mach 5.2 RET Maps on Upper and Lower Surfaces at 0° Angle of Attack

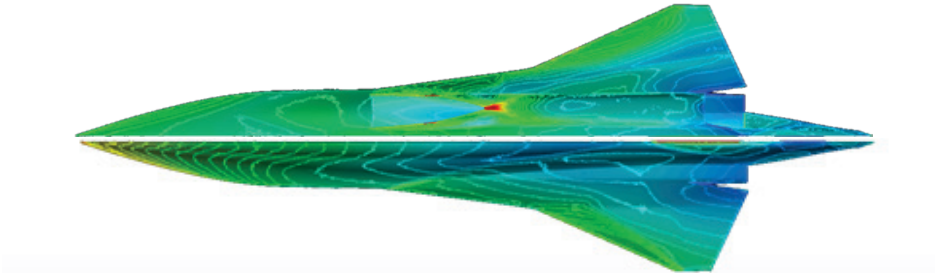

Figure 6.4.6 Mach 5.2 Pressure Distribution on Upper and Lower Surfaces at 0° Angle of Attack

CFD pressure and thermal loads had thus far been generated for panels 2-4. To compute results for panel 1, the rudder gap needed to be modeled. An isolated aft portion of the vehicle was modeled with the rudder gap included. The aft mesh size is 11.4 million cells. A significant difference in both temperatures and pressures was observed. The properly modeled rudder exhibited higher temperatures and pressures in the cove and gap areas. ***Figure 6.4.77*** through ***6.4.10*** illustrate the higher temperature environment of the cove in different views.

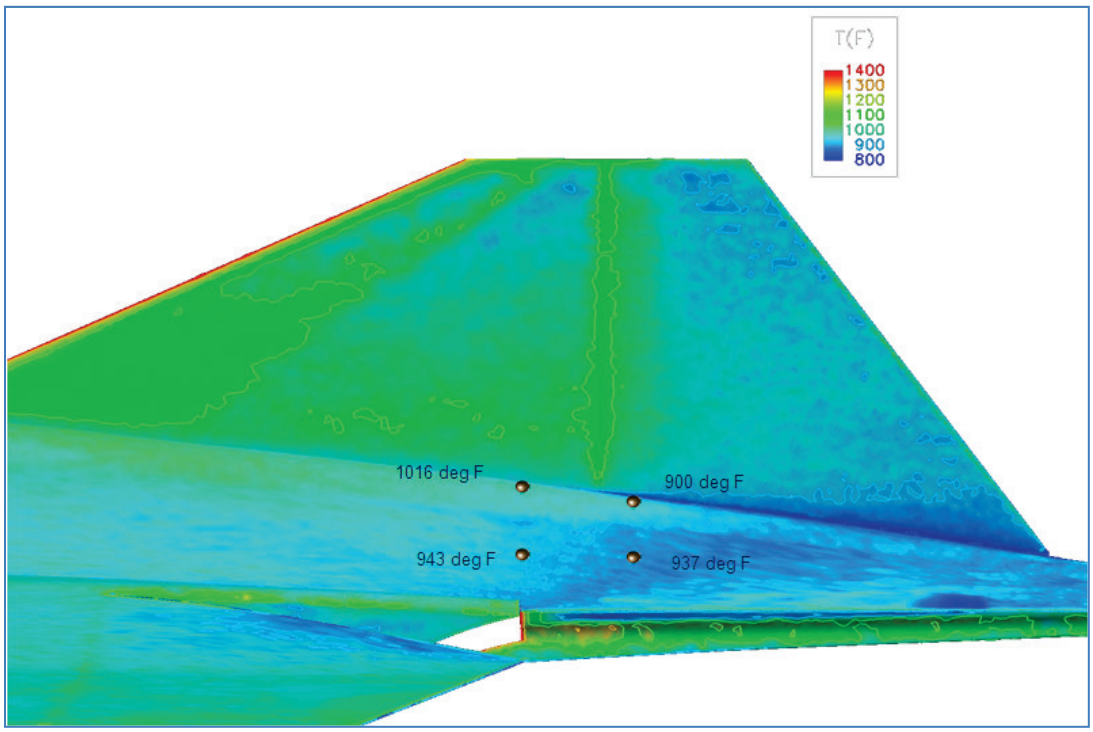

Figure 6.4.7 Mach 5.2 Radiative Equilibrium Temperatures With Rudder Cove and Gap Closed

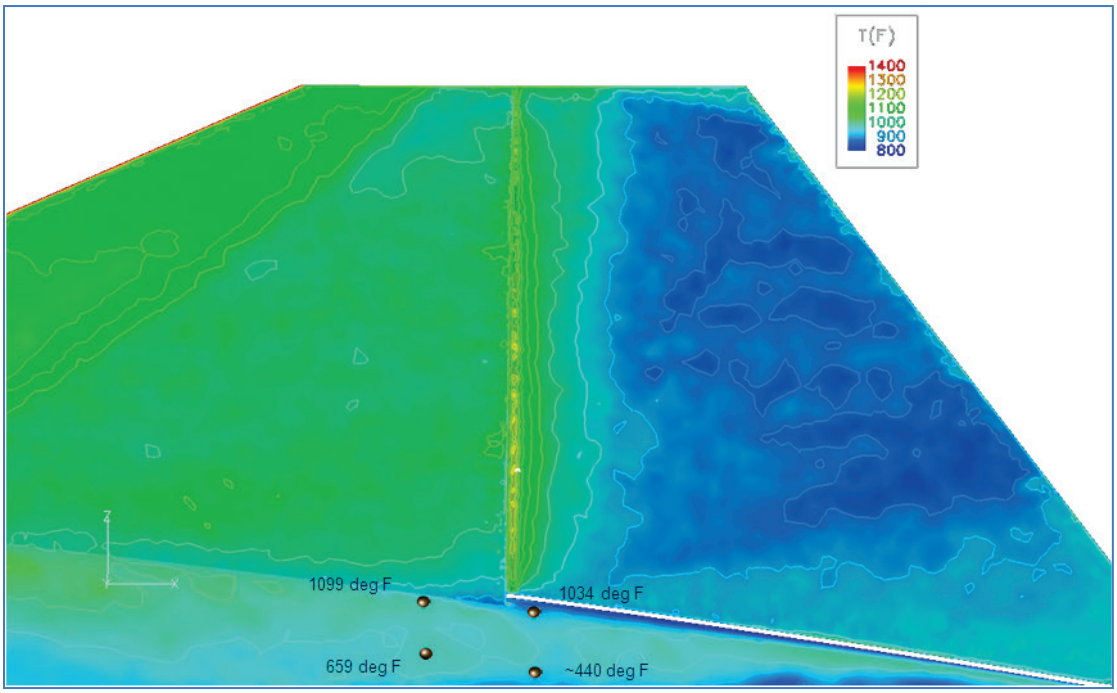

Figure 6.4.8 Mach 5.2 Radiative Equilibrium Temperatures With Rudder Cove and Gap Modeled

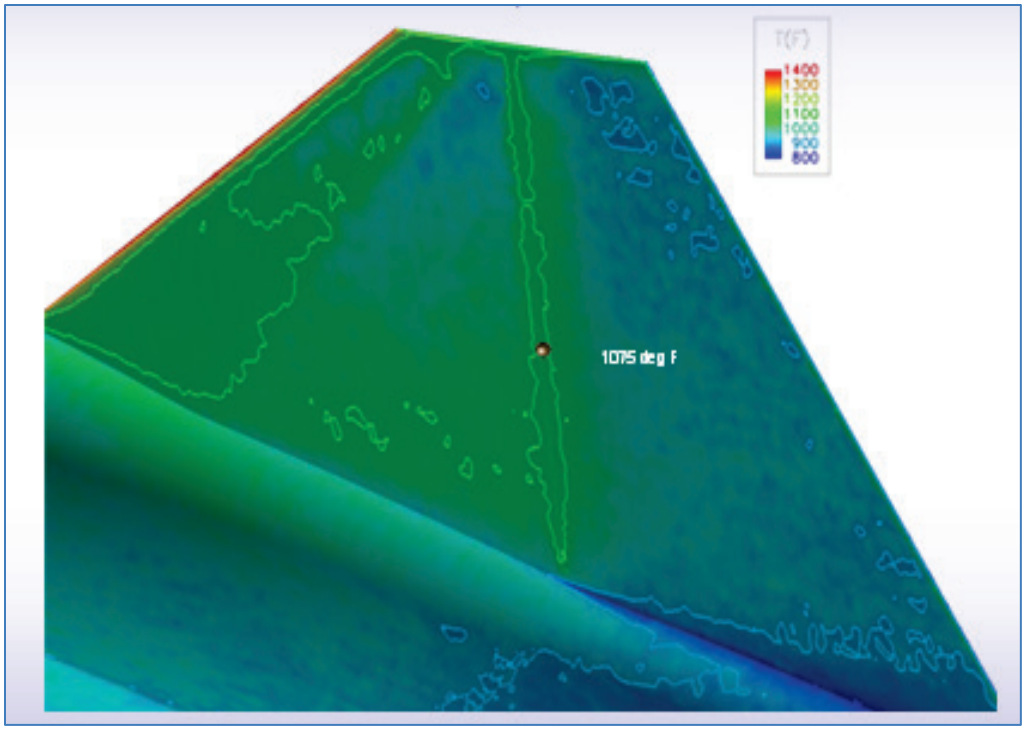

Figure 6.4.9 Mach 5.2 Radiative Equilibrium Temperatures With Rudder Cove and Gap Closed

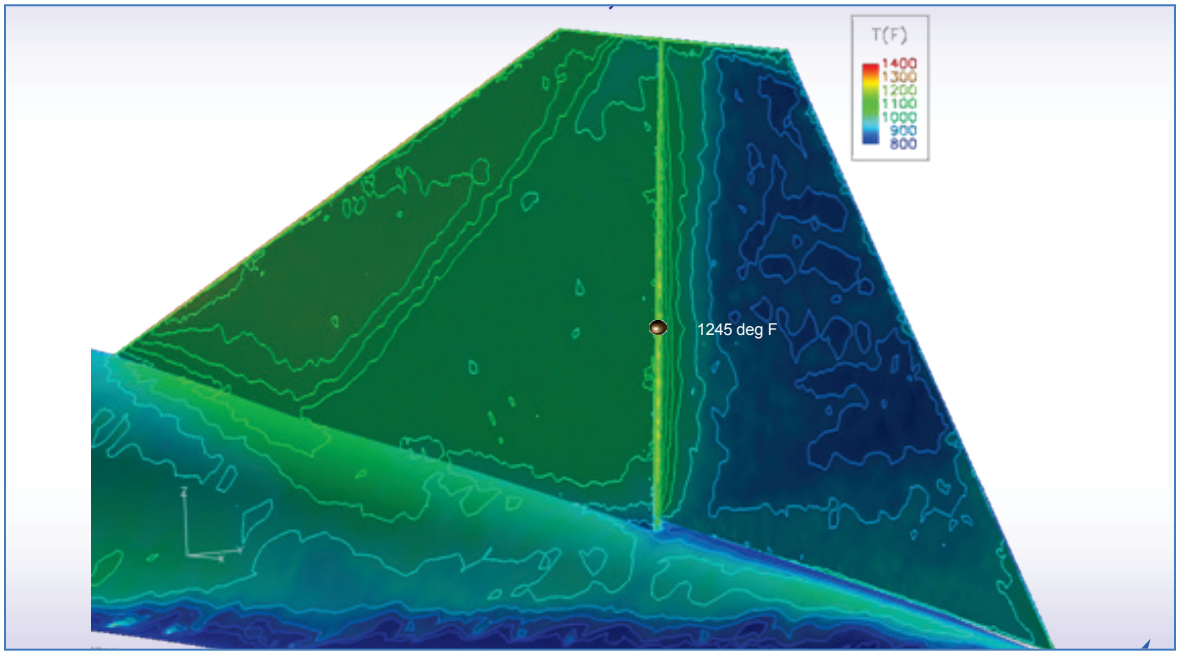

Figure 6.4.10 Mach 5.2 Radiative Equilibrium Temperatures With Rudder Cove and Gap Modeled

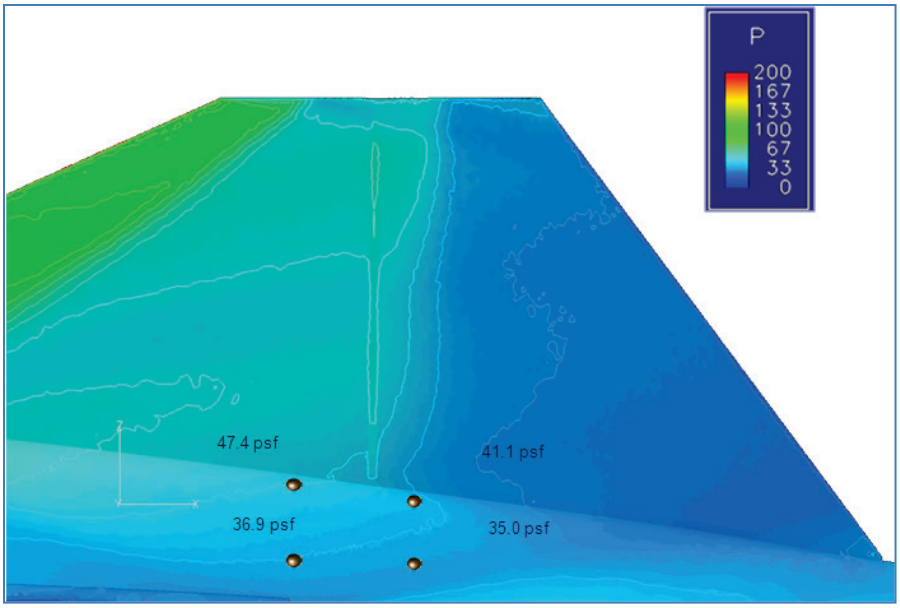

Figure 6.4.11 Mach 5.2 Surface Pressures With Rudder Cove and Gap Closed

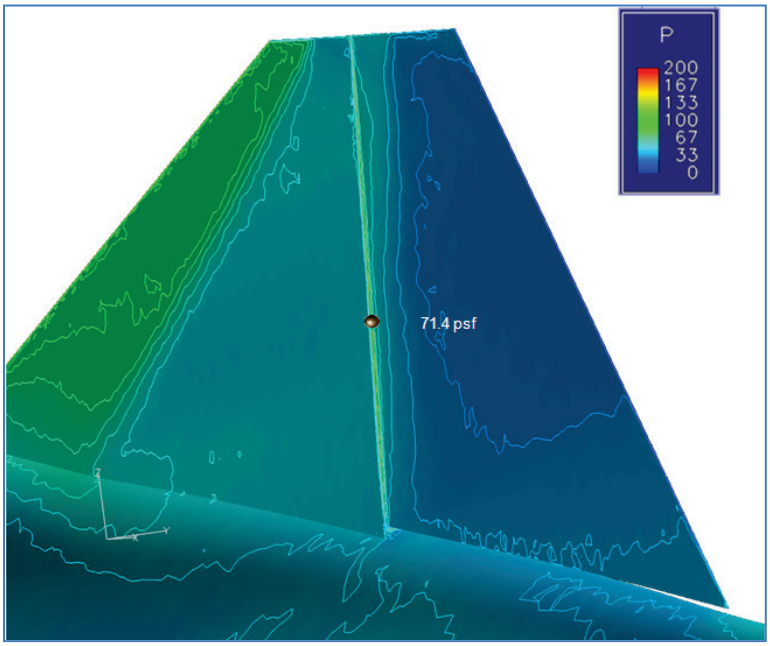

Figure 6.4.12 Mach 5.2 Surface Pressures With Rudder Cove and Gap Modeled

It was desirable to model the entire vehicle using a block structured mesh for the best solution quality, including all the complexities of the rudder cove, gap and deflection. In this case, one cannot take advantage of symmetry and the full vehicle must be modeled. This effort was undertaken, resulting in a mesh size of 216 million cells. This was the largest model constructed in ADP to date and resources to deal with such a large model were not available to solve the flow field. However, this resource bottleneck is planned to soon be relieved. In the mean time, Metacomp Technologies, Inc. verified the quality of the model by using their resources to execute a partial solution. The 216 million cell mesh is shown in ***Figures 6.4.13*** through ***6.4.15***.

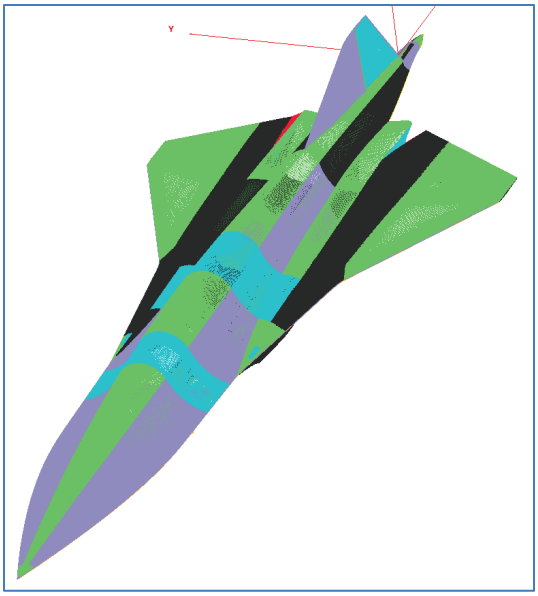

Figure 6.4.13 Surface Depiction of a 216 Million Cell Block Structured Mesh Which Includes Propulsion and Rudder Complexities

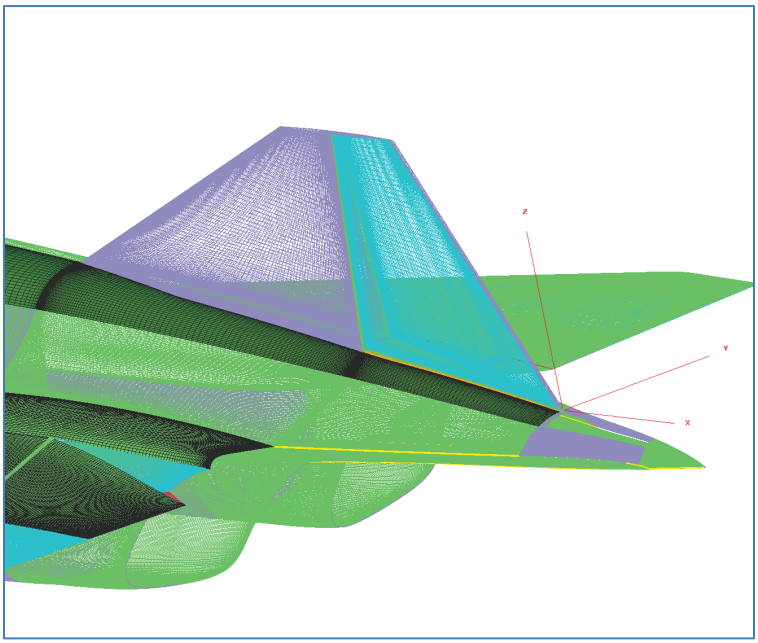

Figure 6.4.14 Aft Close Up of Surface Depiction of a 216 Million Cell Block Structured Mesh Showing Inclusion of Rudder Cove and Gap

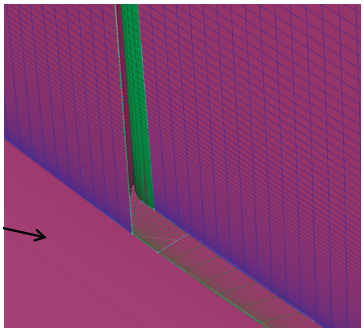

Figure 6.4.15 Rudder Cove Close Up

7.0 PANEL SERVICE LIFE ESTIMATION

In order to develop a reference service life load and thermal exposure spectrum, previous high speed vehicle program archives were examined, as well as interviews with personnel associated with these programs performed. Projected HCV service life spectrum input was derived from various internal LM as well as USAF sources. Conversations were held with:

- Jay Murphy (ex SR-71 pilot)
- Kent Burns (SR-71 program chief engineer, mid-1990s recertification program)
- Henry Combs (SR-71 chief of structures 1958 – 1962)
- Brian Kreimendahl (Lockheed ADP chief of stress mid 1990s)
- Fred Carmedy (chief Maintenance Officer of the SR-71 program, Beale AFB Mid-1990s recertification program)

The following documents were also reviewed:

- "U.S. Air Force White Paper on Long Range Bombers", March 1, 1999 document
- Long Range Strike Aircraft (LRSA) Studies (LM Internal), circa 2003

These documents do not represent the complete set of sources on the subject but were available during the course of the Phase II program. From these sources approximations on the design life of an HCV were attempted.

What was quite interesting was that no "formal" design life estimates for the SR-71/A-12 were ever performed as stated by both Mr. Jay Murphy and Mr. Henry Combs. Mr. Murphy stated that approx. 60% of the SR/A-12 platform design life was spent at Mach 3 and above, which was its high speed range.

Other pertinent points that were realized were that as far as design life at Mach ranges below Mach 3 there were no estimates available, and only that on the Mach 3.0+ missions the vehicle was quickly accelerated to Mach 3.0 to seal the joints to contain the fuel (as recorded in numerous sources, fuel leakage was a chronic issue over the course of the SR-71/A-12 design life).

The service life of the HCV was, for the purposes of study, considered to be very similar to that of the SR-71/A-12. With an average of 150 flight hours per year with 60% of those hours considered to be at its peak velocity range of Mach 3.0 and above, an estimate of 3,600 "hot" hours was assumed for the Mach 5.2 HCV after taking into consideration of an estimated 6,000 hour design life similar to the SR-71. In addition, a 30 year service life of the HCV platform was base-lined for purposes of this study and its spectrum development.

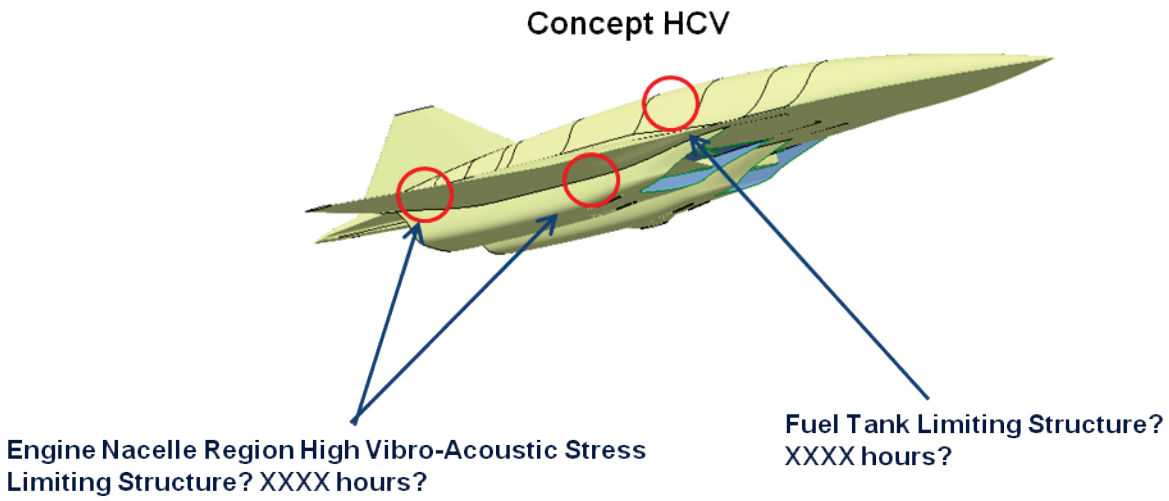

Figure 7.0.1 Concept HCV Limiting Structure Life Considerations

The conceptual HCV baseline trajectory of 5417 seconds was divided into the following generalized flight regimes:

1843 seconds (Takeoff and climb)	2734 seconds @ max Mach/temp. cruise condition = .77 hrs	840 seconds (descent and landing)

With the service life assumption of 3,600 "hot" hours, similar to that of the SR-71 design operations program: 3600 hr/.77 hot hrs. per flight = 4675 flights (total life) (design goal)

and this was rounded to 4700 flights (total life design goal) over a 30 year design life

As a "desired" design life, and for the purposes of the Phase II program, the goal was set at 4700 total flights. If the creep levels and fatigue life of the respective panels showed much less life achievable than the 4675 hrs., as they most likely were assumed to, then that panel or set of panels would have to be replaced after X amount of flights due to creep life and fatigue life constraints. The design factors illustrated above were used to develop the detailed service life spectrum as discussed in Section 7.1.

In addition, a more detailed, per a typical flight year, breakdown of "hot" hours for a conceptual HCV was performed so as to track temperature and acoustic level exposure for future panel test considerations.

These flight operation hours are summarized as follows:

With an estimate of 150 flight hours per year, and 60% of those flight hours considered to be flown on flight missions at the max Mach range (Mach 5.0-5.2) flights:

a) $\leq$90 "hot" (M5.0-5.2) flight hours per year and $\leq$70 lower Mach (<M5.0) flight hours per year

b) this would equate to 95 operational flights per year with 46 subsonic takeoff and landing proficiency flights

c) 141 takeoff and landing cycles with 95 “hot” landings per year

d) an assumption of 1/3 of total takeoff and landing cycles per year for proficiency qualifications per year of flight ops was made

e) 95 high acoustic cycles equating to ~130.3 hours/flight year, and these were subdivided into:

1) 34.7 high level external acoustic cycle hours/flight year

2) 104.0 high level internal acoustic cycle hours/flight year; with 90.7 hours at the airframe structure max temps (87%)

3) 8.4 combined high level internal/external acoustic cycle hours/flight year

A detailed spreadsheet of the assumptions and findings above was developed, and a sample of these results for Panel 1, are illustrated in ***Figure 7.0.2***.

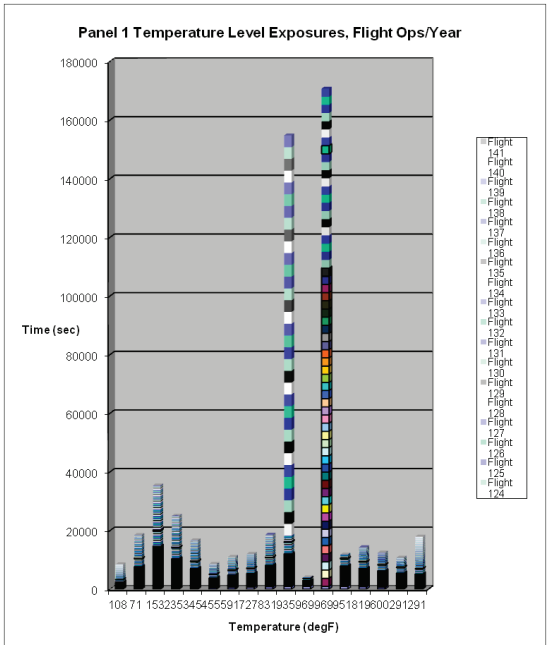

Figure 7.0.2 Panel 1 Temperature Level Exposures, Flight Operations Per Year

7.1 DEVELOPMENT OF HYPERSONIC VEHICLE LIFE SPECTRUM

A loads spectrum is critically necessary to perform a valid fatigue analysis. In this program, a spectrum was not available and one had to be generated with a minimum of supporting flight spectrum data available to the program. An attempt was made to create a conservative spectrum, and without an actual loads team to generate such a spectrum, we will not be able to determine how

conservative or un-conservative the generated spectrum actually is. To fully understand and be able to develop the spectrum correctly for an actual vehicle development program, a team of highly trained loads engineers would be needed for a period of years. For the purposes of the fatigue analysis performed here, it is assumed that the generated spectra are correct and used as valid spectra, as there is no other choice. However, this is not a desired position to be in, and proper spectra should be created if further studies are to be funded.

A description of how the spectra were generated for each panel follows, and an effort was made to keep a consistent approach for generating the spectra where possible. The common spectra methodology was maintained with the exception one check for Panel 1, which needed a modification due to the limitations of the tools used for analysis, and the spectrum for Panel 2, for which the loads are higher for the ascent condition than at the cruise condition, and therefore the loads for ascent are also used for descent. With only a cruise and an ascent/decent load case available, a few assumptions had to be taken based on observed or available data.

General Assumptions

1. Ascent lasts 1843 seconds (from the HCV derived spectrum).

2. Cruise lasts 2734 seconds (from the HCV derived spectrum).

3. Descent lasts 840 seconds (from the HCV derived spectrum).

4. The spectrum will be a single 1.5 hour flight spectrum repeated to get to a total life of 7050 hours (from the HCV derived spectrum)

5. Since only one load case is present for ascent or descent in the detailed Finite Element Model, the missing ascent or descent loads are assumed to be similar to the cruise case. This assumption should be conservative, as the mechanical loads only portion of the flight regime appear to be almost negligible with respect to the thermal loads (with the exception of Panel 2) and the reduced temperatures will result in higher material allowables. By assuming the cruise loads, the thermal loads are also added, and thus this should be a conservative assumption. Furthermore, once the analysis is performed, the properties for the analysis will be at the +1000°F temperature regime for the Inconel alloy and at the +900°F temperature regime for the Titanium alloy, which should also yield more conservatism. This assumption is not followed for Panel 2, and since the loads are higher for the mechanical load case, they are also used for the descent portion of the flight yielding a significantly more conservative spectrum for the Panel 2 acreage area.

6. Normally, on a sub-sonic/supersonic vehicle, there will be a certain number of analysis points sub-dividing a single maneuver into multiple sub-maneuvers that describe the maneuver at different time points from start to finish (time hacks per load case). This number is usually 8 or 10 to adequately describe a fatigue load case in a spectrum and the load case is typically a flying maneuver such as a turn, pull-up, etc. Not knowing how the load cases affect the hypersonic vehicle and assuming that the hypersonic vehicle is not likely to perform many maneuvers, it is assumed that most of the load cycles present in the

vehicle occur during take-off and landing, as that's where the atmosphere is likely to interact more with the vehicle. It is also assumed that during hypersonic cruise, the atmosphere is fairly stable at high altitude, and therefore, nothing significant is occurring that in turn acts like a load case for the vehicle. With these assumptions in mind, it will be assumed that during take-off and landing, a "maneuver" or "load case" occurs every fifteen seconds, and that a typical 10 time hacks per load cycle will be acceptable to describe the event. Furthermore, since we have no information as to how the event takes place over time, it will be assumed that the 10 time hacks will yield 5 fully reversed load cycles (5 cycles is the highest number of cycles that can be achieved with the 10 data points assumed, as you only have max-min cycles) per load event (excluding temperature, as the temperature will not oscillate). Therefore, the thermal stresses will provide a mean for the cycles to occur over. As a result, there will be a load event every 15 seconds of the ascent or descent portion of the flight regime that yields 5 fully reversed load cycles oscillating about a thermal stress mean.

7. High cycle fatigue is usually not considered for generating a loads spectrum. However, from the high cycle fatigue analysis performed, some of the panels have very large dynamic loads in the 10 to 20 Hz. range. The dynamic loads tend to usually yield random vibrations. Not knowing how that translates into a loads spectra and how the loads will affect the panels, a sinusoidal 10 Hz. signal with a 1 sigma dynamic stress is assumed to exist for the entirety of the flight. A 1 sigma dynamic stress is assumed for the service life calculation, as the spectrum is supposed to be a typical spectrum for the vehicle's life, and not a worst case spectrum, as that is too severe.

8. For ascent cycles, round 843 seconds to 850 seconds. This yields 616 mechanical cycles, which is then rounded up to 620 cycles.

9. For ascent and cruise dynamic cycles, there are 4577 cycles. This is rounded down to 4550 seconds. At a rate of 10 cycles per second, this yields 45500 cycles.

10. For descent mechanical cycles, there are 840 seconds. This is rounded up to 850 seconds. This gives 283 cycles, which is also rounded up to 290 cycles.

11. For descent dynamic cycles, following the same assumptions as general assumption 8 but using a rate of 10 cycles per second, yields 8500 dynamic cycles.

12. The maximum-principal stress dictates the stress amplitude in the spectrum, as cracks will begin to form perpendicular to the maximum-principal direction.

13. All stress and fastener loads will be taken directly from the FEM.

14. For Panel 1, the fastener load is large enough by itself to force the material around the fastener hole to significantly exceed the ultimate stress allowable near the fastener area when utilizing the Titanium +900°F data. As a result, the crack initiation life is zero hours of flight as the material fails. In reality, for this particular load case, the allowable should be higher as the temperature is only approximately 485°F. For that check only, the stresses for

descent were modified to be those at cruise for the descent portion of the flight as a test case to try and improve the fatigue life.

15. For Panel 2, the acreage and the doubler have inverse stress levels for the two load cases (one is highest in the tension load case, and the other is highest in the compression load case), and therefore 2 different spectra are will be created.

Panel 1 Spectrum:

Thermal only cruise stress: 40ksi
Thermal + mechanical cruise stress: 41ksi
Thermal + mechanical + 3σ cruise stress: 43ksi
Estimated Thermal + mechanical + 1σ cruise stress: 42 ksi

Thermal only descent stress: 79ksi
Thermal + mechanical descent stress: 79ksi
Thermal + mechanical + 3σ descent stress: 81ksi
Estimated Thermal + mechanical + 1σ descent stress: 80 ksi

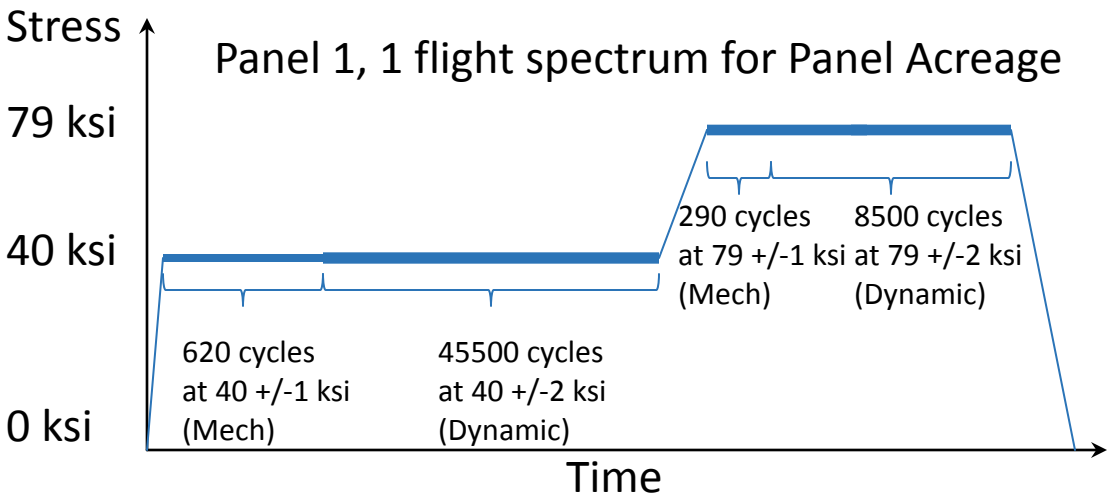

Figure 7.1.1 Single Flight Spectrum for Panel 1 Acreage

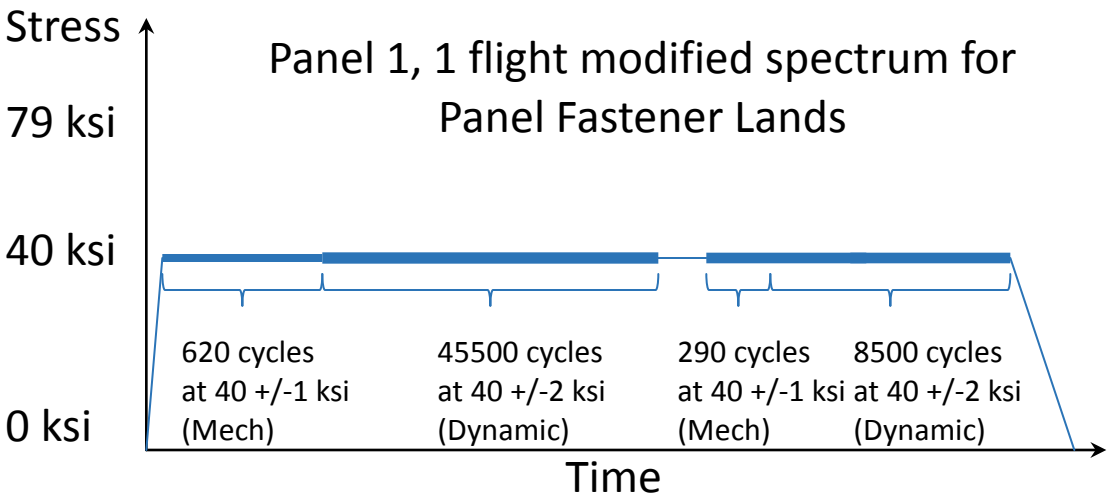

Figure 7.1.2 Single Flight Spectrum for Panel 1 Fastener Lands

Panel 2 Spectrum Acreage:
Thermal only cruise stress: 7ksi
Thermal + mechanical cruise stress: 8ksi
Thermal + mechanical + 3σ cruise stress: 13ksi
Estimated Thermal + mechanical + 1σ cruise stress: 10 ksi

Thermal only ascent stress: 1ksi
Thermal + mechanical ascent stress: 19ksi
Thermal + mechanical + 3σ ascent stress: 21ksi
Estimated Thermal + mechanical + 1σ ascent stress: 20 ksi

Panel 2 Spectrum Doubler (land):
Thermal only cruise stress: 32ksi
Thermal + mechanical cruise stress: 38ksi
Thermal + mechanical + 3σ cruise stress: 40ksi
Estimated Thermal + mechanical + 1σ cruise stress: 39 ksi

Thermal only ascent stress: 1ksi
Thermal + mechanical ascent stress: 19ksi
Thermal + mechanical + 3σ ascent stress: 21ksi
Estimated Thermal + mechanical + 1σ ascent stress: 20 ksi

For descent, since the vehicle will be hot, apply the 32 ksi thermal stress and cycle with the +/- 18 ksi mechanical stress from the ascent load case.

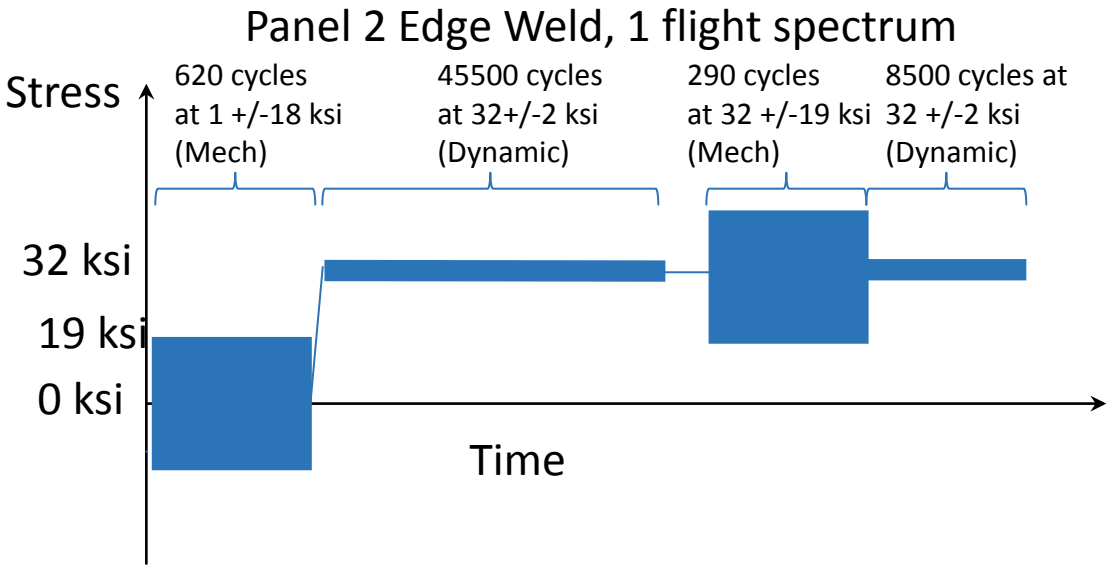

Figure 7.1.3 Single Flight Spectrum for Panel 2 Edge Weld

Panel 3 Spectrum:
Thermal only cruise stress: 10ksi
Thermal + mechanical cruise stress: 12ksi
Thermal + mechanical + 3σ cruise stress: 17ksi
Estimated Thermal + mechanical + 1σ cruise stress: 13 ksi

Thermal only descent stress: 40ksi
Thermal + mechanical descent stress: 42ksi
Thermal + mechanical + 3σ descent stress: 61ksi
Estimated Thermal + mechanical + 1σ descent stress: 48.5 ksi

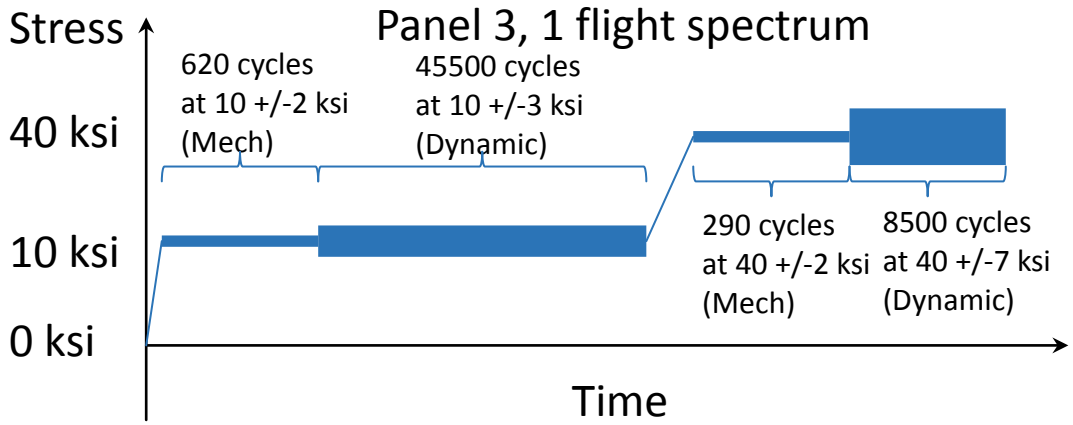

Figure 7.1.4 Single Flight Spectrum for Panel 3

Panel 4 Spectrum:
Thermal only cruise stress: 38ksi
Thermal + mechanical cruise stress: 39ksi
Thermal + mechanical + 3σ cruise stress: 35ksi
Estimated Thermal + mechanical + 1σ cruise stress: 41 ksi

Note that since there is actually a decrease in stress from the high frequency vibration, the 3ksi decrease is assumed to be the range in stress for the Estimated Thermal + mechanical + 1σ cruise stress.

Thermal only descent stress: 15ksi
Thermal + mechanical descent stress: 15ksi
Thermal + mechanical + 3σ descent stress: 45ksi
Estimated Thermal + mechanical + 1σ descent stress: 25 ksi

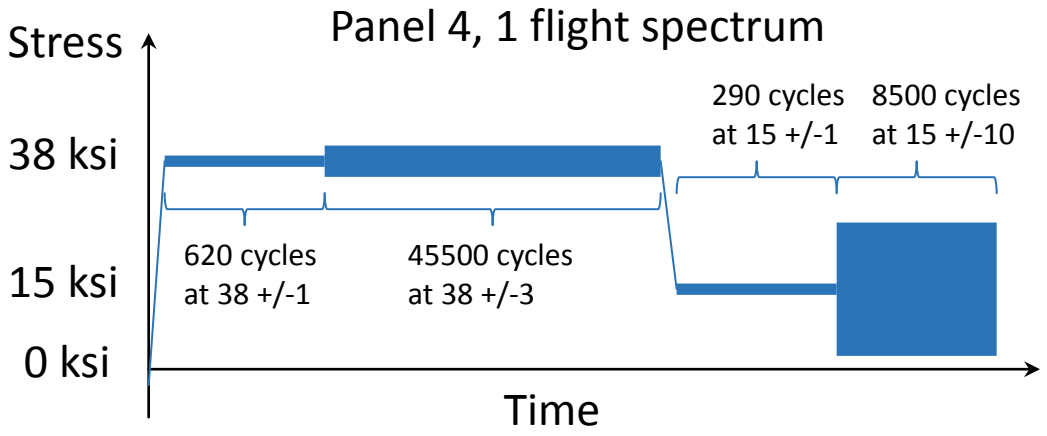

Figure 7.1.5 Single Flight Spectrum for Panel 4

7.2 PANEL CREEP LIFE ANALYSES

In order to estimate panel lifetime based on creep concerns, time and stress at temperature are required. The maximum tensile stresses in each panel usually do not occur at the highest temperatures, which provides some creep relief. However, usage of the peak tensile stresses at the hot load cases even proved to be overly conservative. Some local averaging of the stresses was required in order to reduce the peaking affects in the results in some areas. This is a reasonable assumption given that any local creep would lead to redistribution of the loading. Illustrated in ***Figure 7.2.1***, the red box indicates the region elements averaged to obtain the stress value used in the creep analysis. This region represents the highest tensile stresses in the panel, discounting artificial stresses at fastener locations which are calculated independently as a bearing stress.

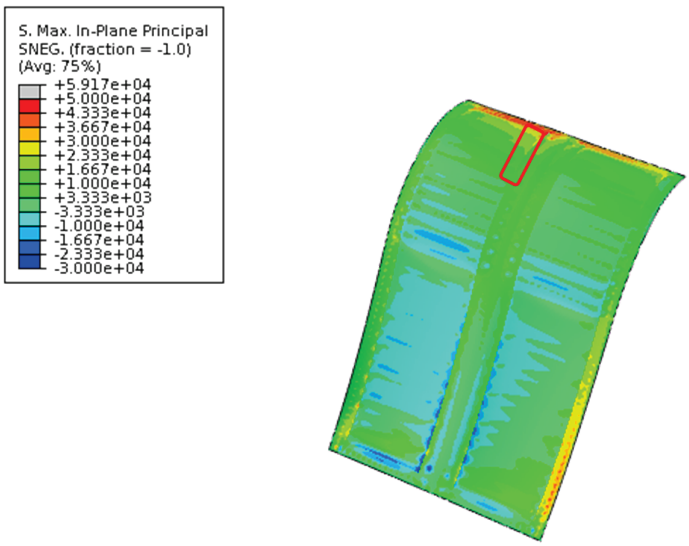

Figure 7.2.1 Panel 1 Max Tensile Stress Zone Averaging

Once an averaged maximum tensile stress at hot conditions was determined, the material appropriate creep data curves were used to determine lifetime. These charts utilized the Larson-Miller parameter approach assuming a 0.1% creep strain limit. The 0.1% limit was chosen based on the most available data for that creep limit. However, a 0.2% limit is considered standard for many designs and could be justified here to increase the predicted lifetimes. The Larson-Miller Parameter refers to a temperature and time at stress parameter that can be correlated to the log of the applied stress. The parameter P is described as:

$$P = T\,(20+\log t)\times 10^{-3}$$

Equation 7.2.1

Where: T is the Temperature in °F
And t is the time at the corresponding stress (hours)

The Panel 1 averaged stresses are on the order of 15 ksi at the maximum temperature level of 970°F. This stress level was plotted to find the Larson-Miller Parameter in ***Figure 7.2.2***. Three anneals of the Ti-6-2-4-2 alloy were looked at as alternatives, with each providing a different lifetime prediction.

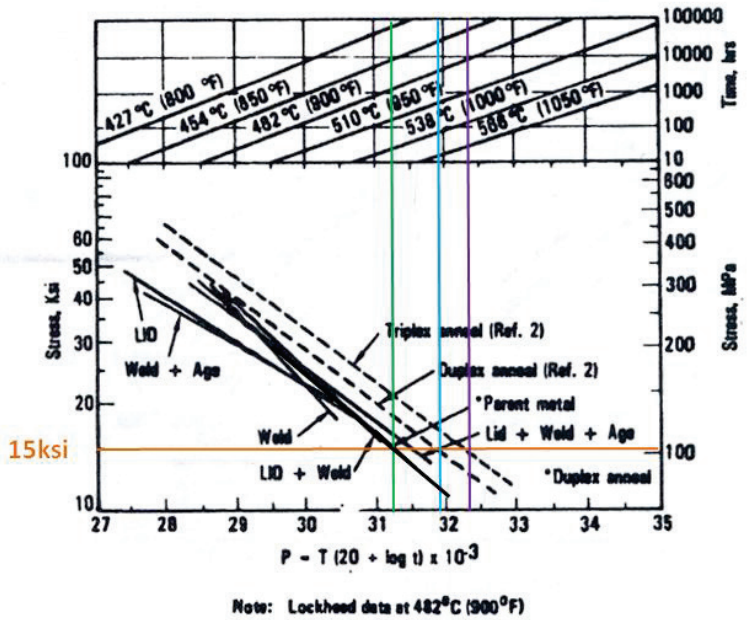

Figure 7.2.2 Panel 1: Larson-Miller Presentation for 0.1% creep of Ti-6-2-4-2 Alloy Sheet at 15ksi Stress Level

Using the associated parameter for each anneal, and assuming the stress and temperature combination presented, the following lifetimes can be estimated for Panel 1.

Assuming 15 ksi stress @ 970°F:

- Parent Metal P value = 31.2
  - 0.1% creep life of 65 hours
- Duplex Anneal P value = 31.9
  - 0.1% creep life of 200 hours
- Triplex Anneal P value = 32.4
- 0.1% creep life of 450 hours

These results dictated that Panel 1 will need to be replaced during the vehicle lifetime. The frequency of replacement is dependent on the specific anneal chosen.

Using the data already seen in ***Figure 7.2.2***, the maximum temperature of Panel 2 is relatively low (765°F), and the max stress at this temperature is also relatively low (8 ksi before averaging). Thus, creep was not considered to be a concern for Panel 2 (>100,000 hours). Panel 2 has a creep life that meets the lifetime requirements of the vehicle without needing replacement.

Panel 3, near the leading edge of the wing, is one of the highest temperature environments on the entire vehicle. Efforts were made to reduce the maximum stress at temperature as best as possible, down to approximately 5 ksi. However, as shown in ***Figure 7.2.3*** (extrapolated to these low stresses) the resulting Larson-Miller parameter was still very high, implying a short lifetime at elevated temperatures. Lacking sufficient data related to Titanium honeycomb core creep, only the face-sheets and support assembly were able to be evaluated for creep for the Panel 3 design.

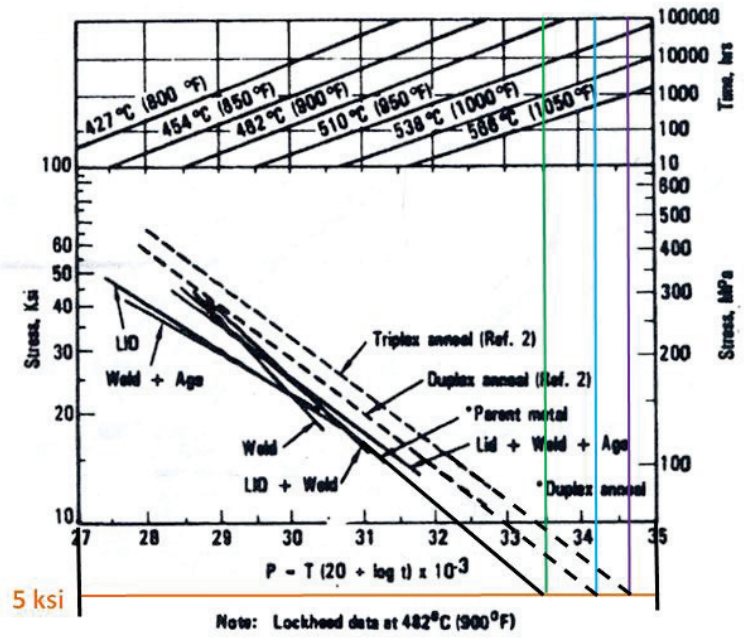

Figure 7.2.3 Panel 3: Larson-Miller Presentation for 0.1% Creep of Ti-6-2-4-2 Alloy Sheet at 5ksi Stress Level

Using the associated parameter for each anneal, and assuming the stress and temperature combination presented, the following lifetimes were estimated for Panel 3.

Assuming 5 ksi stress (averaged similar to Panel 1) @ 1093°F, the chart data must be extrapolated to get an idea of the creep life:

- Parent Metal P value = 33.5
  - 0.1% creep life of 38 hours
- Duplex Anneal P value = 34.1
  - 0.1% creep life of 95 hours
- Triplex Anneal P value = 34.6
  - 0.1% creep life of 190 hours

These results dictated that Panel 3 would need to be replaced during the vehicle lifetime, and Panel 3 is in fact the most creep limiting panel. The frequency of replacement is dependent on the anneal chosen.

Panel 4 is the engine fairing and although it sees relatively high temperatures and stress, the IN718 material choice provides adequate margin for creep life. The Larson-Miller data for IN718 is shown in Figure 7.2.4 and is extrapolated down to 14 ksi. Lacking sufficient data related to Inco honeycomb core creep, only the face-sheets and support assembly were able to be evaluated for creep in Panel 4.

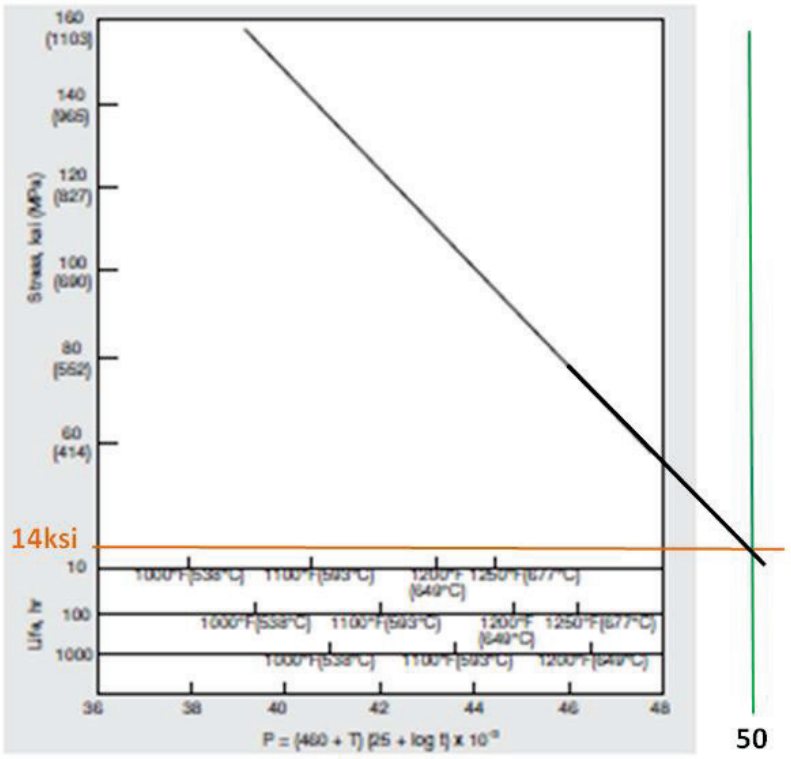

Figure 7.2.4 Panel 4: Larson-Miller Presentation for 0.1% Creep of IN718 Alloy Sheet at 14ksi Stress Level

In using the standard alloy sheet anneal, the following lifetime was estimated

Assuming a 14 ksi stress (averaged similar to Panel 1) @ 1070°F and extrapolating the data:

- Parent Metal P value = ~50
  - 0.1% creep life of > 100,000 hours
  - Note: This panel also shows acceptable life without stress averaging

Panel 4 has a creep life that meets the lifetime requirements of the vehicle without needing replacement.

7.3 PANEL FATIGUE LIFE ANALYSES

Fatigue analysis is a well understood and developed field for traditional sub-sonic / supersonic vehicles. However, even in those vehicle types, some simplifying assumptions have to be made to be able to complete the design of the vehicles. This is particularly true in areas that have high thermal gradients and very thin ligaments, such as metallic screens. There is also a general lack of data for high temperature material properties in many metals, perhaps with the exclusion of some Titanium alloys, Inconel alloys, and other high heat resistant materials. However, the way that heat data is normally acquired is at some constant pre-set temperature, and the potential perceived effects of the material re-annealing every flight and eliminating damage (as is suspected of Titanium) has not been captured to date. If there is such a benefit from annealing during flight, it would make many portions of the vehicle statically sized and provide a more optimized design.

The current fatigue analysis tools are very powerful to solve current problems and could be modified to tackle some of the problems that a hypersonic vehicle analysis will encounter. Currently, it is assumed that constant temperature properties are adequate for vehicle sizing. However, for a hypersonic vehicle, the temperatures experienced during takeoff, landing, and cruise are very dissimilar, as are the stresses seen in each environment. With the current analysis approaches, the analyst is forced to use a constant temperature curve for sizing, while in reality each environment should have its own material property curve and the applied stresses should create damage based on the proper material allowable. There is likely to be research needed to investigate how the damage accumulates and transitions into the different temperature regimes, but as a first step, modifying the tools to be able to continue damage without any second order effects would be a step in the right direction. In addition, if there is a benefit from annealing every flight, this method could easily capture that effect with a simple code modification. For the study performed for this program, such software is not available, and therefore the worst constant temperature curves obtained were used for the entire flight regime, which should be conservative.

With this tool of the future, the way spectra are generated might also need modifications. Somehow, temperature, pressures, and thermal gradients, at a minimum, would need to be captured. This might mean that the traditional FEM used for structure might not apply anymore, as the thermal gradients the vehicle experiences upon ascent might be critical for some components (honeycomb stiffened structure, and perhaps all attachment points/joints of the structure). This is another area of study for the future and the computing power needed to address this problem will have to be significantly higher and include significantly more detail in the FEM.

In conventional aircraft, the joints of parts is where most problems arise for fatigue analysis as they are usually fastened and have stress concentration factors that significantly reduce part life. Welding is an alternative method of joining that proposes to eliminate some of the stress concentration factors. However it has been found to be traditionally unreliable as the consistency in the welds varies too much and many times un-uniformity introduces the flaws that allow for fast crack-growth and end up significantly reducing component life. For a fully optimized vehicle design, welding should be incorporated. However, that means that a large investment for many years will need to be performed to fully create and quantify a welding process that's fully reliable and that gives similar properties to the parent material. To the author's knowledge, only Electron Beam welding is accepted as being that consistent. The need for a vacuum to perform such welds limits the use on vehicle assemblies. Perhaps titanium deposition could be expanded to make complex 3-D assemblies instead of just parts and reduce the welding issue. In this instance again, we encounter space limitations.

Furthermore, the effect of sonic fatigue and the interaction of low cycle fatigue should be explored further, as there could be an affect at high temperature that we are not aware of. Normally, these loads are considered to not interact. However, in this study, there is a significant structural response at frequencies as low as 10 Hz, which cease to be high cycle. Some testing for low cycle fatigue is done at frequencies as high as 10 Hz in a test lab environment, and not knowing how to intermix the two loading environments, a conservative assumption was taken for this study.

Investment needs in order of perceived importance can be listed as:

1. Effects of material re-annealing every flight for crack growth and crack initiation

2. Damage interaction at different temperatures from crack growth and crack initiation
3. Analysis tool modifications
4. Welding process development
5. Interaction for crack growth and crack initiation under low cycle and high cycle fatigue environments
6. FEM modifications

Lockheed Martin's Integrated Metallic Durability and Damage Tolerance Analysis Toolset (IMAT for short, internal analytical tool) (Ref. 10) was used to perform both the crack initiation and crack growth analysis. As a result of some of the material needs for the software, and due to the fact that some of the data was not available for the materials at temperature, some simplifying assumptions had to be performed. Furthermore, no crack-retardation was assumed as the spectrum is not high fidelity.

The assumptions made for the analysis are as follows:

1. Only stress-life data is available for the materials. This data is converted to strain-life by dividing stress by the Young's modulus (E) of the high temperature material.
2. Assumed that the monotonic stress-strain curve is the same as the cyclic stress-strain curve.
3. A cyclic proportional limit was assumed based on how the stress-life curves flatten out at 1 million cycles.

The strain-life data for Ti-6Al-2Sn-4Zr-2Mo was obtained from (Kaneko, 1982) NASA Contractor Report 166006 (Ti-6Al-2Sn-4Zr-2Mo Structural Development), October 1982 (Ref. 5), for a thickness of 0.04 in. and a temperature of 900ºF (page 33 and 53). The only data for Ti-6-2-4-2 that was found was for an R value of 0.1 (R=min. stress/max stress=stress ratio), and the software code needs an R value of -1.0 as it computes the other R values to perform the analysis. As a result, the R = -1.0 curve is estimated and provided to the software so as to not have an un-conservative analysis. Parameters from Ti-6Al-4V were used as a starting point for the Ti-6-2-4-2 curve fit.

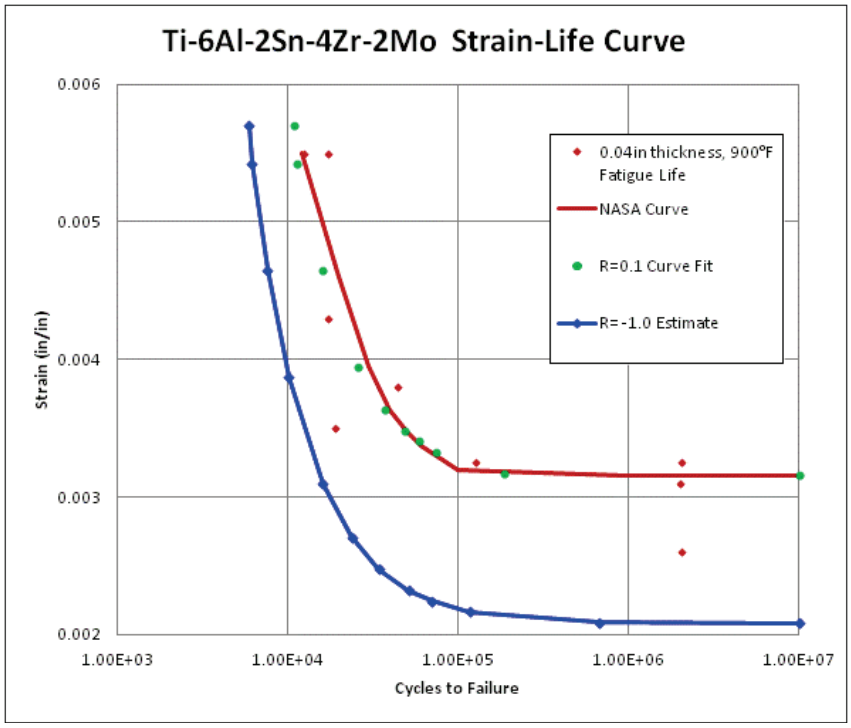

Figure 7.3.1 Ti-6Al-2Sn-4Zr-2Mo Strain-Life Curve, Kt=1.0, Temp=900°F, R=0.1, -1.0

Similarly, for Inconel 718, the strain-life data is obtained from MIL-HDBK-5J (Handbook, 2003, pp. 6-69)

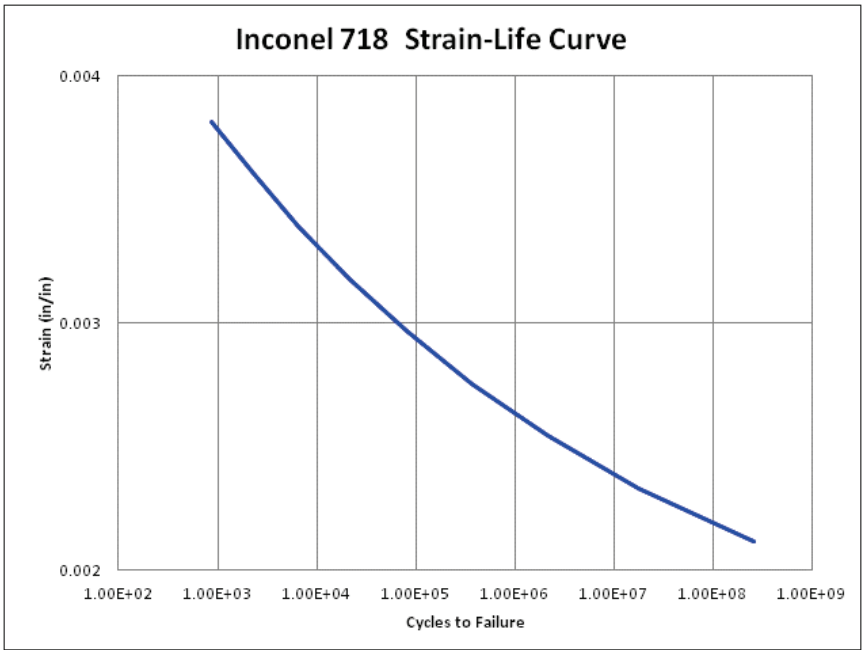

Figure 7.3.2 Inconel 718 Strain-Life Curve, Kt=1.0, Temp=1000°F, R= -1.0

For Inconel 718, a complete set of da/dN (crack growth rate per load cycle) vs. Delta K (stress intensity factor range) was found (Henkener, 1994). However, for Ti-6Al-2Sn-4Zr-2Mo, only one curve at R=0.1 was found (Kaneko, 1982). Similar to the crack initiation data, some curve fitting was performed to obtain a family or R value curves, and the initial parameters from Ti-6Al-4V were also used as a starting point for the curve fit.

The da/dN data for Ti-6Al-2Sn-4Zr-2Mo is obtained from NASA report (Kaneko, 1982, p.61) for a thickness of 0.04 in. and a temperature of 900ºF. The only data for Ti-6-2-4-2 that was found was for an R value of 0.1. In order to obtain a family of R curves, parameters from Ti-6Al-4V were used as a starting point for the Ti-6-2-4-2 curve fit.

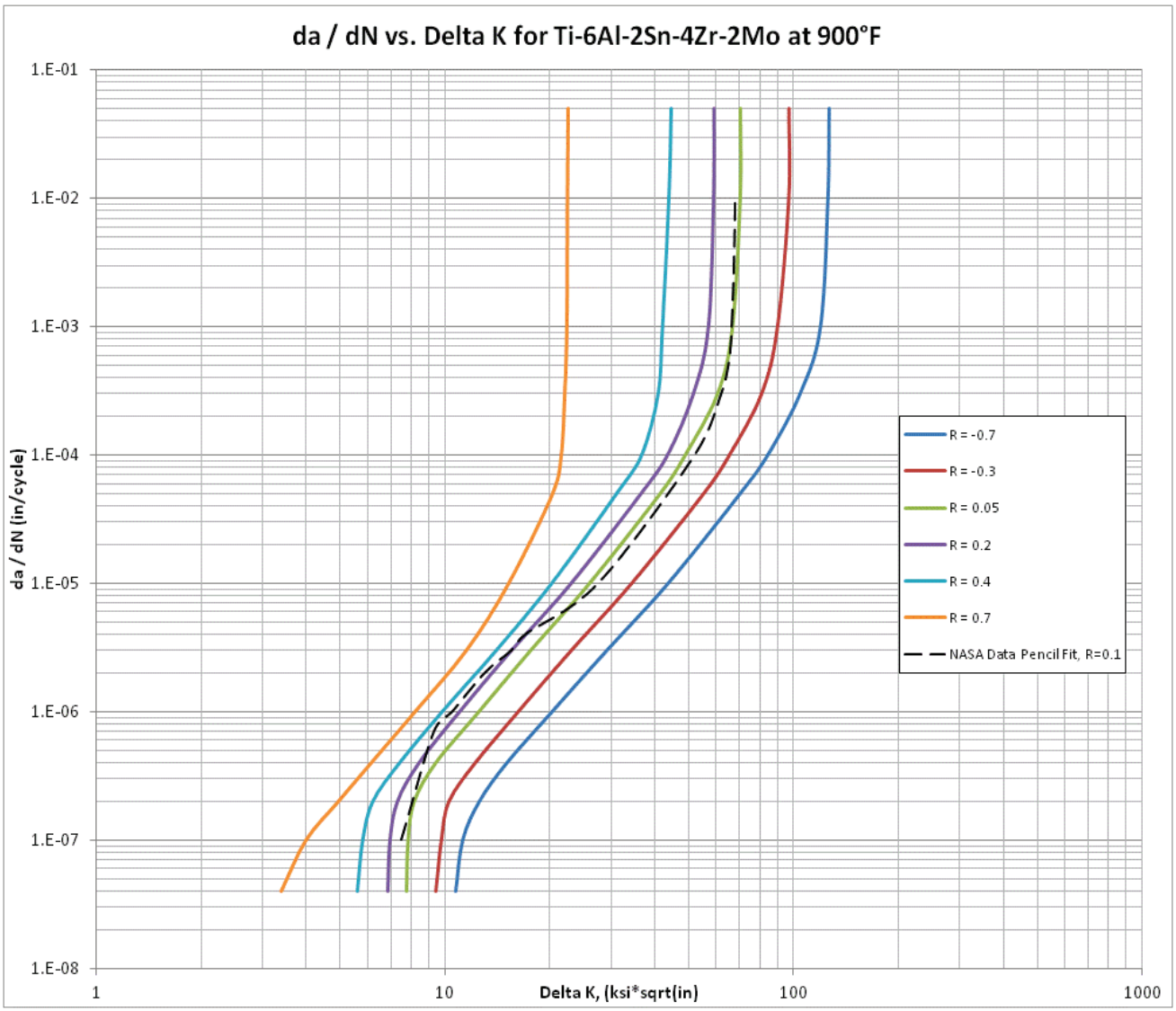

Figure 7.3.3 Ti-6Al-2Sn-4Zr-2Mo da/dN vs. °K Curves, Temp=900°F

Similarly, for Inconel 718, the da/dN data is obtained from the FLAGRO manual (Henkener, 1994, p.33) (Ref. 11). However, unlike that for titanium, an equation describing the entire family of curves was provided with fitting factors. The curves used for the analysis are presented in ***Figure 7.3.4***.

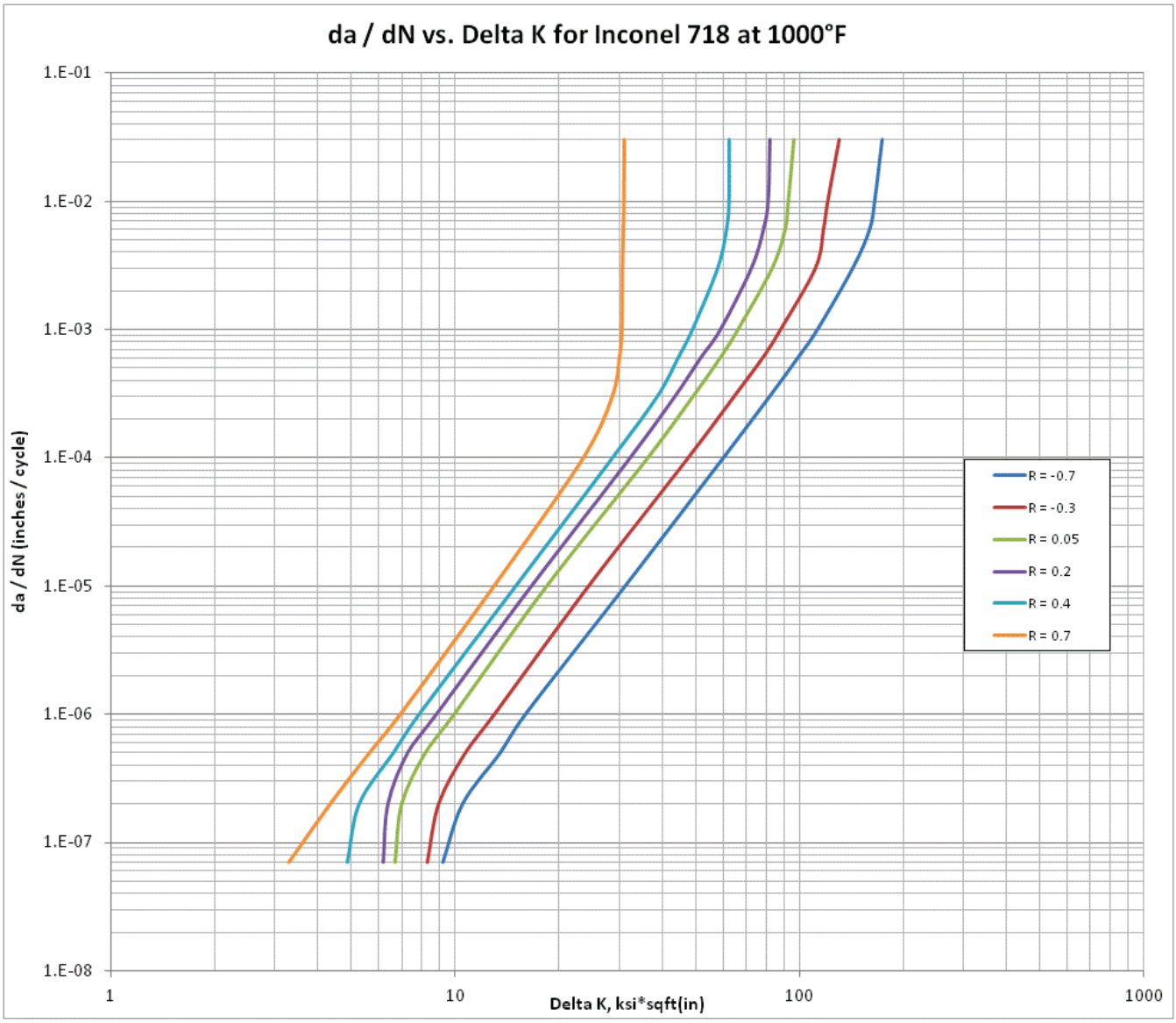

Figure 7.3.4 Inconel 718 da/dN vs. °K Curves, Temp=1000°F

A fatigue (Crack Initiation using LOOPIN) and fracture (Crack Growth) analysis for the critical areas in each panel was performed per the U.S. Air Force's (USAF) Durability Criteria for failure per JSSG 2006 (United States Department of Defense, 30 October 1998) (Ref. 12) and U.S. Navy (USN) criteria (Ref. 13) with the spectra defined in section 7.1 and not the 50% and 90% spectra as defined by the USAF and USN. Per the USN durability criteria, the fatigue analysis is performed in a pristine material that is cycled until a crack the size of 0.01 inches long is created, and this indicates failure of the part. However, the USN criteria tends to use fairly severe spectra, and this

approach has served them well in the past for sizing vehicles. Per the USAF durability criteria, a 0.01 in x 0.01 in. flaw is assumed at the critical location on the part being sized at time t=0 seconds, and the part is cycled until failure occurs as the stress in the part exceeds the residual strength.

For the facture analysis, the USN damage tolerance criteria uses a 0.01 in. x 0.01 in. flaw and it is assumed to be at the critical location on the part being sized at time t=0 seconds. The part is cycled until failure occurs because the stress in the part exceeds the residual strength. Per the USAF damage tolerance criteria, a 0.05 in. x 0.05 in. flaw is assumed at the critical location on the part being sized at time t=0 seconds, and the part is cycled until failure occurs because the stress in the part exceeds the residual strength. For some of the thin skins in this study, the 0.05" flaw is significantly larger than the panel thickness, and it becomes a through crack. Perhaps some new NDI techniques (such as a pressure test) can be evaluated to remove through cracks and lower the minimum crack size for the analysis for the very thin areas of the panels. For the analysis, the way a vehicle like this would build a spectrum is more likely to match what the USAF would do (probably run and maintained by the USAF as well), and as a result, the USAF results have a better application with regards to criteria. Since in the approach undertaken here, the USN damage tolerance criteria is the same as the USAF durability criteria due to only having one spectrum, the USN damage tolerance criteria will not be discussed in the following analysis. In addition, a scatter factor of 2.0 was used for the fracture analysis, while a scatter factor of 4.0 was used for the fatigue analysis.

In the following analysis, the life estimates are outputs of the software code and are not easily described. Also, it is assumed that if a panel is hot-formed, the final machining of the panel will take place after hot-forming.

Panel 1

The stress data, load cases, and basic stress assumptions are provided in the following section.

Compression Sizing Case

Result File: Pan1d_60020M5C_C_SL02
Max Temp: 803.5 F @M5.2 Cruise
Sizing: Ti6242 Baseline, Fastened Edges and Stiffeners
Fastener Pitch: 1.0” Fast Diam: 0.25”
Skin t: 0.06” Doubler t: 0.09”

	Thermal Only	Therm + Mech	Therm + Mech + 3σ Dyn
% of LIMIT Allow	64%	67%	71%
Max/Min Prin Stress (ksi)	+40/-58	+41/-60	+43/-62
Max Fastener Force (lbs)	2500	2500	2500
Max Bearing (ksi)	35.4	35.4	35.4

Result File: Pan1d_60126M2D_T_SL02
Max Temp: 485F @M2 Descent

	Thermal Only	Therm + Mech	Therm + Mech + 3σ Dyn
% of LIMIT Allow	59%	60%	60%
Max/Min Prin Stress (ksi)	+79/-42	+79/-42	+81/-41
Max Fastener Force (lbs)	3400	3400	3500
Max Bearing (ksi)	48.1	48.1	49.6

Figure 7.3.5 Panel 1 FEM Stress Results

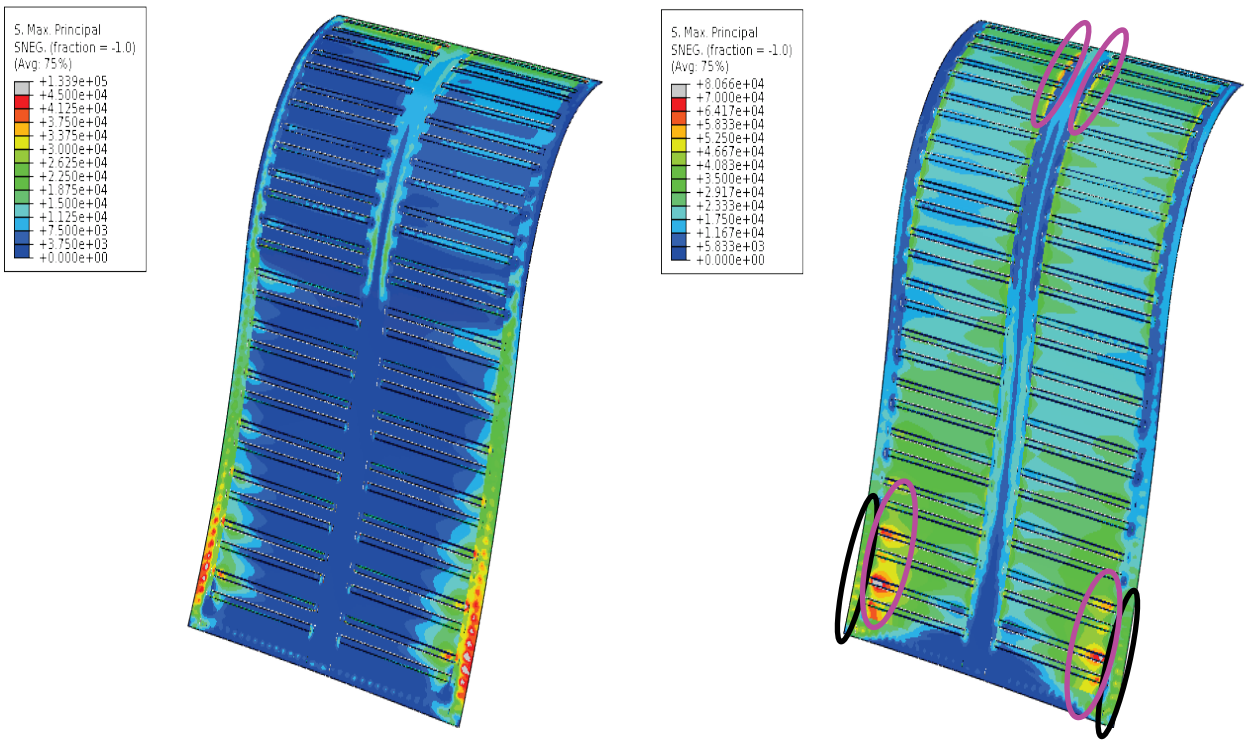

Figure 7.3.6 FEM Maximum Principal Stresses for the Compression Sizing Case (left) and the Tension Sizing Case (right)

The FEM also has the following assumptions:

1. Two inch wide land area where fasteners attach
2. Land thickness is 0.15 inches

The following assumptions were made for the analysis:

1. The fastener attaches at the center of the land area.
2. For the acreage control point, a semi-elliptical surface flaw is assumed for the crack-growth analysis.
3. For the fastener control point, a corner elliptical surface flaw at the fastener hole is assumed for the crack growth analysis.
4. The doubler and the skin are machined from one piece, otherwise, the minimum countersink requirement for the fasteners is not met. Also, the transition from the thick land to the skin will be gentle and will try to minimize stress risers.

From the FEM, the peak stress in the acreage is 81 ksi. For the control point, a homogeneous stress of 81 ksi. is applied to the control point.

1) With a peak stress of 81 ksi., a short life of 3200 hours is obtained for the areas of the panel circled in hot pink, based on the USN durability criteria and the 0.06" skin thickness assumption.
2) With a peak stress of 81 ksi., the panel is satisfactory for life based on the USAF durability criteria and the 0.06" skin thickness assumption.
3) For the USAF damage tolerance criteria, a short life of 1000 hours is obtained for the areas of the panel circled in hot pink.

There are various ways to mitigate the local effects of these short life areas. For the areas circled in hot pink, if the stress can be reduced to 53ksi. by either thickening (i.e., a local thickness of up to 0.092 inches) or panel modifications that redistribute load away from the areas of concern, then the panel acreage will meet the life requirement of 7050 hrs. established for this project.

The FEM stress in land area is 28ksi.. The fastener load of 3500 lbs includes the 3 sigma dynamic loads and the thermal only fastener load is 3400 lbs.. Therefore, the 1 sigma dynamic load is estimated to be 3433 lbs..

1) With a bypass stress (general stress in the part not being introduced because of the fastener load. In this case the general stress around the fastener load is that derived from the FEM results) of 28 ksi and a fastener load of 3433 lbs., a short life of 0.0 hours was obtained based on the USN durability criteria and a short life of 450 hours was obtained based on the USAF durability criteria for the areas of the panel circled in black.

Due to the significantly short estimated life in the areas circled in black in ***Figure 7.3.6***, the land area in those locations was thickened up to 0.18 inches to reduce the bypass stress.

2) Using the spectrum of ***Figure 7.1.1***, with a bypass stress of 23.4 ksi and a fastener load of 3433 lbs., a short life of 0.0 hours was obtained based on the USN durability criteria for the areas of the panel circled in black.
3) Using the spectrum of ***Figure 7.1.1***, with a bypass stress of 23.4 ksi and a fastener load of 3433 lbs., the panel is satisfactory for life based on the USAF durability criteria and the 0.18 in. fastener land thickness assumption.
4) Using the spectrum of ***Figure 7.1.1***, with a bypass stress of 23.4 ksi and a fastener load of 3433 lbs., the panel is satisfactory for life based on the USAF damage tolerance criteria and the 0.18 in. fastener land thickness assumption.

Since the life based on the USN durability criteria is still 0.0 hours, being purely based on the stress around the hole nearing 200 ksi. (including the effects of the fastener countersink and the fastener hole itself), which is significantly above the ultimate strength of the material at 900°F. As a result, the spectrum was modified to that shown in ***Figure 7.1.***. Utilizing that spectrum, the life based on the USN durability criteria improved to 1050 hours. However, the short life here was likely due to the lack of the tool to be able to incorporate the differences in material properties with respect to the flight profile stresses.

The remaining fastener lands should be satisfactory for life at the currently modeled 0.15 in. thickness. The fastened stiffeners were not evaluated for life, as the model was not set up for retrieving those fastener loads easily. However, those fasteners in the stiffeners should not be seeing large loads, and as a result, only some of them will need to have thicker lands. Furthermore, the minimum fastener countersink requirements should be accounted for in future skin sizing, as this will dictate how thick the skin will be in the areas where the stiffeners attach to the skins using fasteners. The use of welding in this application would be a wise thing to do to keep the vehicle lightweight. However, very few welding techniques on Titanium are currently considered as acceptable design practice, with electron beam welding being the one that is considered robust and acceptable. This welding method is being employed on the Joint Strike Fighter.

Panel 2

The stress data, load cases, and basic stress assumptions are provided in the following section.

Compression Sizing Case

Result File: P2b_60014M5C_C_S01
Max Temp: 765 F @M5.2 Cruise

Tension Sizing Case

Result File: P2b_60172M1A_S01
Max Temp: 80 F (uniform) @M1 Ascent

Sizing: Ti6242 Baseline, E Beam Welded Edges, Spot Weld Stiffeners

Spot Weld Pitch: 1.0″ Weld Diam: 0.25″
Skin t: 0.07″ Doubler t: 0.14″
Hat t: 0.05″

	Thermal Only	Therm + Mech	Therm + Mech + 3σ Dyn
% of LIMIT Allow	56%	56%	61%
Max/Min Prin Stress (ksi)	+7/-42	+8/-43	+13/-43
Max Fastener Force (lbs)	500	600	600
Max Bearing (ksi)	4.6	5.5	5.5

	Thermal Only	Therm + Mech	Therm + Mech + 3σ Dyn
% of LIMIT Allow	1%	16%	20%
Max/Min Prin Stress (ksi)	+1/-1	+19/-5	+21/-5
Max Fastener Force (lbs)	150	150	150
Max Bearing (ksi)	1.5	1.5	1.5

Figure 7.3.7 Panel 2 FEM Stress Results

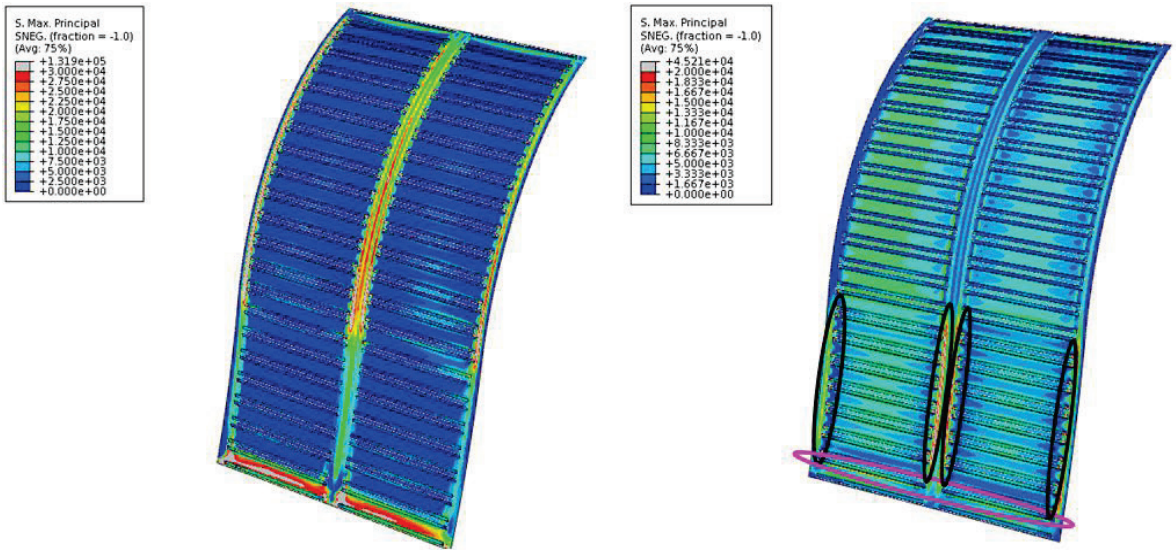

Figure 7.3.8 Panel 2 FEM Maximum Principal Stresses (in psi) for the Compression Sizing Case (left) and the Tension Sizing Case (right)

The FEM also has the following assumptions:

1. 2.15 inch wide land area where panel is welded to the substructure
2. Land thickness is 0.21 inches

The following assumptions are made for the analysis:

1. The analysis is run with the pristine material properties and a 10% life knockdown is applied to account for the potential weld knockdowns.
2. The Electron Beam (EB) weld is made perpendicular to the panel's OML and the weld zone is approximately 0.25 inches wide.
3. The doubler and the skin are machined from one piece, otherwise, the crack grows too fast into a through thickness crack, limiting the part life even further (the through thickness crack will grow at a faster rate than a quarter-elliptical crack under the same spectrum. Also, the transition from the thick land to the skin will be gentle and will try and minimize stress risers. This transition will limit the stresses shown in the FEM for the areas circled in black, and these areas will therefore not be analyzed, as the stress risers shown in the FEM are fictitious.
4. For the acreage durability control point, a semi-elliptical surface flaw is assumed for the crack-growth analysis.
5. For the acreage damage tolerance control point, a corner elliptical surface flaw is assumed for the crack-growth analysis, as a gradient is needed to be applied to the control point to show it good for life.
6. For the edge weld control point, a corner elliptical surface flaw is assumed for the crack growth analysis. Also, since the weld in the FEM is represented by a single node attachment, and the high stress area is only approximately half an inch wide, with an EB weld width of approximately a quarter inch width, the peak stress should decrease by approximately 33% (i.e. high stress FEM zone increases from 0.5 inches to 0.75 inches).
7. For the spot weld control point, a semi-elliptical surface flaw is assumed for the crack-growth analysis.

From the FEM, the peak stress in the acreage is 21 ksi, and it occurs where the stiffeners meet the thicker doubler. For the control point, a homogeneous stress of 21 ksi is applied.

1. Applying a constant cross-section stress of 21 ksi, a full life is obtained based on the USN durability criteria and the 0.07" skin thickness assumption.
2. Applying a constant cross-section stress of 21 ksi, the panel is satisfactory for life based on the USAF durability criteria and the 0.07" skin thickness assumption.
3. For the damage tolerance check, the 0.07" skin does not show full life for the area circled in hot pink. Since the assumption has been made that the panel will be machined and that a gentle transition area will be present in this location, an even more gentle transition will be engineered for this region and the thickness at this location will at a minimum be 0.14" thick, which does show full life for the analysis based on the USAF damage tolerance criteria. The thickness here could also be slightly thinner (~0.11"), but the thickness was not optimized. On a prototypical design level effort, multiple iterations between the stress group and the DaDT group would occur.

The peak FEM stress in the doubler area for the compression case was 21 ksi (as shown in ***Figure 7.3.8***), while for the tension case it was 39 ksi. Since the assumption for the spectrum on Figure 7.1.3 was made that the thermal stress of 32 ksi from the cruise case would be combined with the 19 ksi mechanical load from the ascent case would be combined, the resulting stress to use in this analysis needed to be modified to 51 ksi. Also, the FEM has a single line of nodes to represent the EB weld, and this results in a high intensity (for stress) weld width of approximately 0.5 inches wide. Since the weld width in reality is approximately 0.25 inches, this should result in a high stress zone of approximately 0.75 inches, which lowered the peak stress of 51 ksi to 34 ksi.

1) Applying a constant cross-section stress of 34 ksi, a full life is obtained based on the USN durability criteria and the 0.21" skin thickness assumption.
2) Applying a constant cross-section stress of 34 ksi, the panel is satisfactory for life based on the USAF durability criteria and the 0.21" skin thickness assumption.
3) Applying a constant cross-section stress of 34 ksi, the panel only shows a life of 2500 hours based on the USAF damage tolerance criteria and the 0.21" skin thickness assumption. However, if a stress gradient (representative of the observed stresses) is applied to decelerate the crack, then the life of the part is computed at 8000 hours.
    a. Note: EB welding might not be the best method to weld this part. The weld is too narrow for the application and welding the panel to the substructure will become troublesome. A Fusion weld would perhaps be better in this location as it could easily be made to be approximately 0.5 inch wide, and the resulting lower stresses from the extra weld width could mitigate the potentially reduced life of a fusion weld versus an EB weld.

From the FEM, the peak spot weld load is 600 lbs., which is dominated by the out-of plane (pull-off) force in the weld. For the control point, a 600 lbs. was applied as a pure pull-off load (out of plane), as the software was only designed to perform the analysis for a Mode 1 crack. However, this is conservative as growing the crack in Mode 1 is a faster way of failing a piece of material than growing a crack through the shear loading required for a Mode 2 crack that should be used for the analysis.

1) In applying a constant load of 600 lbs., a full life is obtained based on the USN durability criteria and a 0.25" spot weld diameter assumption.
2) In applying a constant load of 600 lbs., the panel is satisfactory for life based on the USAF durability criteria and a 0.25" spot weld diameter assumption.
3) In applying a constant load of 600 lbs., the panel is satisfactory for life based on the USAF damage tolerance criteria and a 0.25" spot weld diameter assumption.

Panel 3

The stress data, load cases, and basic stress assumptions are provided in the following section.

Compression Sizing Case

Result File: Pan3a_M52A_LC60076_S02
Max Temp: 1093 F @M5.2 Cruise

Tension Sizing Case

Result File: Pan3A_M20D_LC60041_S02
Max Temp: 702 F @M2 Descent

Sizing: Ti B21S Core and Ti 6242 Sheet Baseline, Fastened Edges

Fastener Pitch: 1.5″ Fast Diam: 0.25″
Skin t: 0.018″ Doubler t: 0.058″
Core H: 0.65″

	Thermal Only	Therm + Mech	Therm + Mech + 3σ Dyn
% of LIMIT Allow	27%	27%	51%
Max/Min Prin Stress (ksi)	+10/-14	+12/-14	+17/-33
Max Fastener Force (lbs)	300	310	600
Max Bearing (ksi)	6.6	6.8	13.2

	Thermal Only	Therm + Mech	Therm + Mech + 3σ Dyn
% of LIMIT Allow	38%	40%	58%
Max/Min Prin Stress (ksi)	+40/-27	+42/-26	+61/-31
Max Fastener Force (lbs)	450	450	700
Max Bearing (ksi)	10.0	10.0	15.4

Figure 7.3.9 Panel 3 FEM Stress Results

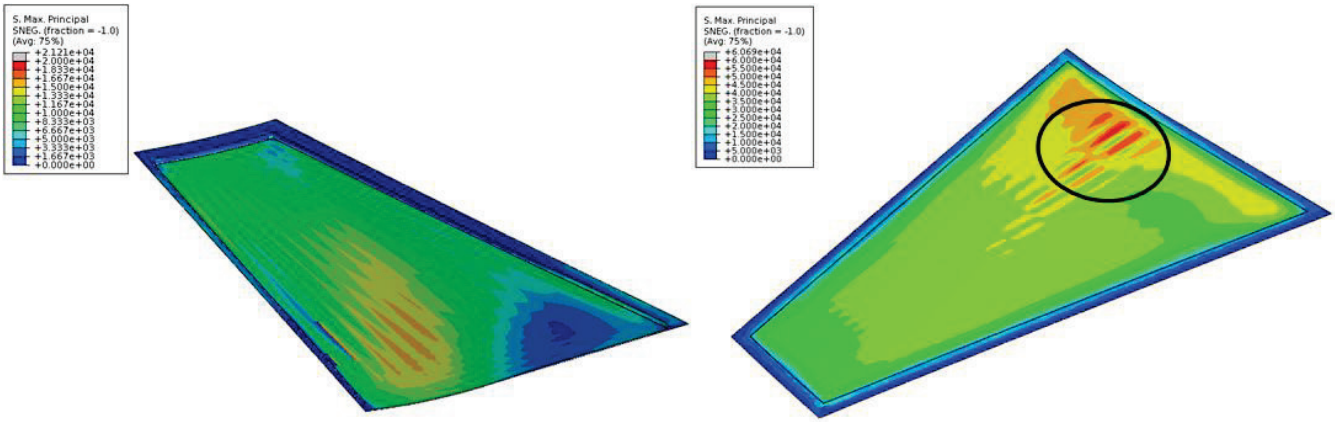

Figure 7.3.10 Panel 3 FEM Maximum Principal Stresses (in psi) for the Compression Sizing Case (left) and the Tension Sizing Case (right)

The FEM also has the following assumptions:

1. 1.5 inch wide land area where fasteners attach
2. Land thickness is 0.058 inches

The following assumptions were made for the analysis:

1. The fastener attaches at the center of the land area.
2. The land area should be 0.115 in. thick for countersink requirements. This again probably means that the outer skin is machined.

3. The fastener pitch was reduced from 1.5” to 1.0” at the fasteners with high load.
4. For the acreage control point, a semi-elliptical surface flaw is assumed for the USAF durability crack-growth analysis.
5. For the acreage control point, a through thickness flaw is assumed for the USAF damage tolerance crack-growth analysis.
6. For the fastener control point, a corner elliptical surface flaw at the fastener hole is assumed for the crack growth analysis.
7. The doubler and the skin are machined from one piece, otherwise, the minimum countersink requirement for the fasteners is not met. Also, the transition from the thick land to the skin will be gentle and will try and minimize stress risers.

From the FEM, the peak stress in the acreage is 61 ksi. However, 48.5 ksi was used for the analysis, as that was more representative of a 1 sigma load that represents a more typical load and not a worst case load for the fatigue analysis. For the control point, a homogeneous stress of 48.5 ksi was applied.

1) Applying a constant cross-section stress of 48.5 ksi, a full life was obtained based on the USN durability criteria and the 0.018” skin thickness assumption.
2) Applying a constant cross-section stress of 48.5 ksi, the panel is satisfactory for life based on the USAF durability criteria and the 0.018” skin thickness assumption.
3) For the damage tolerance check, the 0.018” skin was too thin, and the smallest crack that can be assumed was a 0.05” through thickness crack. A damage tolerance check on the 0.018” thick skin, and a 48.5 ksi stress yielded a life of 1600 flight hours. Since the assumption that the OML skin was to be machined had been made, it was then possible to locally increase the thickness in the area circled in black in Figure to 0.025”. At this new thickness, the peak stress should decrease to 35ksi, which resulted in a full life part utilizing the USAF damage tolerance crack-growth analysis methodology.

The peak FEM stress in the doubler area for the tension case was 16 ksi (which included thermal, mechanical + 3 sigma loading) and 9 ksi (including only thermal and mechanical loading), and the doubler thickness was 0.058”. The load that was to be used for the analysis assumed a 1 sigma dynamic contribution, which yielded 5.75 ksi for a 0.115 inch doubler thickness. The fastener load was 360 lbs from the descent case (450 lbs. + ((700 lbs.-450 lbs.)/3) / 1.5) for a 1” fastener spacing.

1) In applying a bypass stress of 5.75 ksi and a fastener load of 360 lbs., a full life was obtained based on the USN durability criteria and the 0.115” doubler thickness assumption.
2) In applying a bypass stress of 5.75 ksi and a fastener load of 360 lbs., the panel was found satisfactory for life based on the USAF durability criteria and the 0.115” doubler thickness assumption.
3) In applying a bypass stress of 5.75 ksi and a fastener load of 360 lbs., the panel was found satisfactory for life based on the USAF damage tolerance criteria and the 0.115” doubler thickness assumption.

There were no checks performed on the core. However, the FEM showed a maximum normal stress on the core of 200 psi. As such, it was expected that the bond/weld from the core to the skin would be satisfactory for life, as well as the core itself.

Panel 4

The stress data, load cases, and basic stress assumptions are provided in the following section.

Compression Sizing Case

Result File: P4c_60041M5C_C_SL02
Max Temp: 1073 F @M5.2 Cruise

Tension Sizing Case

Result File: P4c_60062M2D_T_S02
Max Temp: 268 F @M2 Descent

Sizing: Inco617 Core and Inco718 Sheet Baseline, Fastened Edges

Fastener Pitch: 1.0″ Fast Diam: 0.25″
Skin t: .025″ Doubler t: 0.125″
Core H: 0.75″

	Thermal Only	Therm + Mech	Therm + Mech + 3σ Dyn
% of LIMIT Allow	25%	35%	50%
Max/Min Prin Stress (ksi)	+38/-16	+39/-20	+35/-30
Max Fastener Force (lbs)	1050	1050	1900
Max Bearing (ksi)	10.7	10.7	19.4

	Thermal Only	Therm + Mech	Therm + Mech + 3σ Dyn
% of LIMIT Allow	12%	11%	32%
Max/Min Prin Stress (ksi)	+15/-18	+15/-17	+45/-18
Max Fastener Force (lbs)	800	750	1000
Max Bearing (ksi)	8.2	7.7	10.2

Figure 7.3.11 Panel 4 FEM Stress Results

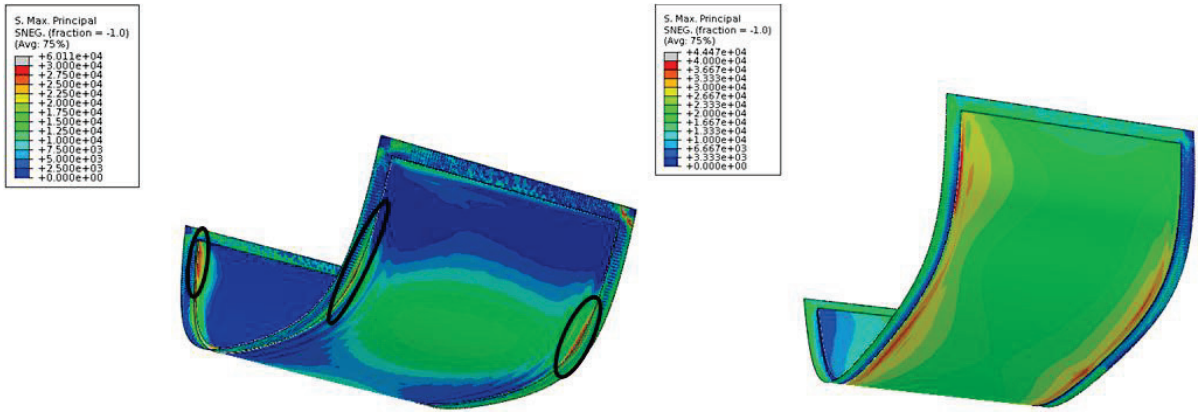

Figure 7.3.12 Panel 4 FEM Maximum Principal Stresses (in psi) for the Compression Sizing Case (left) and the Tension Sizing Case (right)

The FEM also has the following assumptions:

1. 2.5 inch wide land area where fasteners attach
2. Land thickness is 0.125 inches

The following assumptions were made for the analysis:

1. The fastener attaches at the center of the land area.
2. The land area should be at least 0.15 inch thick for countersink requirements for a 0.25 inch fastener. This assumes that the outer skin is to be machined.
3. For the acreage control point, a semi-elliptical surface flaw was assumed for the USAF durability crack-growth analysis.
4. For the acreage control point, a through thickness flaw was assumed for the USAF damage tolerance crack-growth analysis.
5. For the fastener control point, a corner elliptical surface flaw at the fastener hole was assumed for the crack growth analysis.
6. The doubler and the skin are assumed to be machined from one piece, otherwise, the minimum countersink requirement for the fasteners was not met. Also, the transition from the thick land to the skin will be gentle and will try to minimize stress risers.

From Section 7.1, the peak stress in the acreage is 41 ksi.

1) In applying a constant cross-section stress of 41 ksi, a full life is obtained based on the USN durability criteria and the 0.025" skin thickness assumption.
2) In applying a constant cross-section stress of 41 ksi, the panel is satisfactory for life based on the USAF durability criteria and the 0.025" skin thickness assumption.
3) For the damage tolerance check, the 0.025" skin is too thin, and the smallest crack that can be assumed is a 0.05" through thickness crack. A damage tolerance check on the 0.025" thick skin and a 41.0 ksi stress level yields a life of 3 flight hours. Since the assumption that the OML skin was to be machined had been made, it was then possible to locally increase the thickness in the areas circled in black in ***Figure 7.3.12*** to 0.05". At this new thickness, the peak stress should decrease to 20.5ksi, which results in a full life part utilizing the USAF damage tolerance crack-growth analysis methodology.

The peak FEM stress in the doubler area for the tension case was 25 ksi (including thermal, mechanical,+ 3 sigma loading) and 12 ksi (includes only thermal and mechanical loading), and the doubler thickness is 0.125". The load to be used for the analysis assuming a 1 sigma dynamic contribution yielded 10.25 ksi for a 0.2 inch doubler thickness. The fastener load was 1340 lbs from the cruise condition (1050 lbs + ((1900 lbs-1050 lbs)/3)) for a 1" fastener spacing.

1) In applying a bypass stress of 9.8 ksi and a fastener load of 1340 lbs., a full life was obtained based on the USN durability criteria and the 0.21" doubler thickness assumption.
2) In applying a bypass stress of 9.8 ksi and a fastener load of 1340 lbs., the panel was satisfactory for life based on the USAF durability criteria and the 0. 21" doubler thickness assumption.
3) In applying a bypass stress of 9.8 ksi and a fastener load of 1340 lbs, the panel was satisfactory for life based on the USAF damage tolerance criteria and the 0. 21" doubler thickness assumption. The thicker doubler was only needed in the areas with the high fastener loads, and therefore, the weight gain should be limited.

There were no checks performed on the core. However, the FEM shows that the maximum normal stress on the core was 170 psi. As such, it was expected that the bond/weld from the core to the skin should be satisfactory for life, as well as the core itself.

7.4 SONIC FATIGUE ANALYSES

Sonic fatigue analysis was performed on Panel 1 and 4, to determine the dynamic life of the panels.

In order to perform sonic fatigue analysis, the high cycle fatigue properties needed to be obtained. The Lockheed Martin F-22 program had provided the non-propriety IN718, which were an accumulation and compilation of both commercial and non-propriety corporate data. The data is shown in ***Figure 7.4.1***.

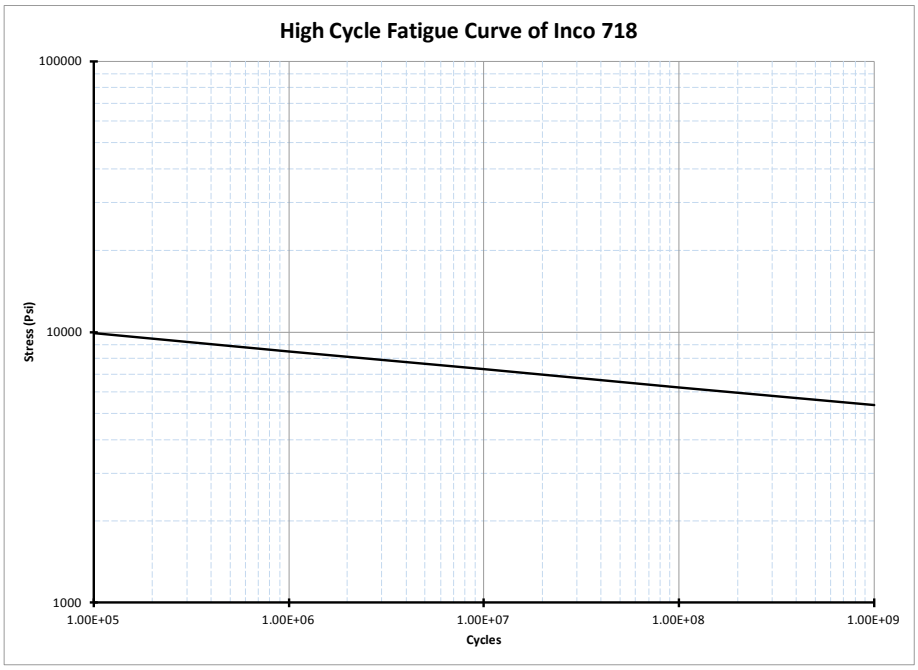

Figure 7.4.1 Inconel 718 High Cycle Fatigue Data

There was a series lack of non-propriety fatigue data for Titanium Beta S. For the sonic fatigue exercise, the Lockheed Martin F-35 program supplied Titanium 6-2-2-2 Alloy S/N Curve, as shown in ***Figure 7.4.2***.

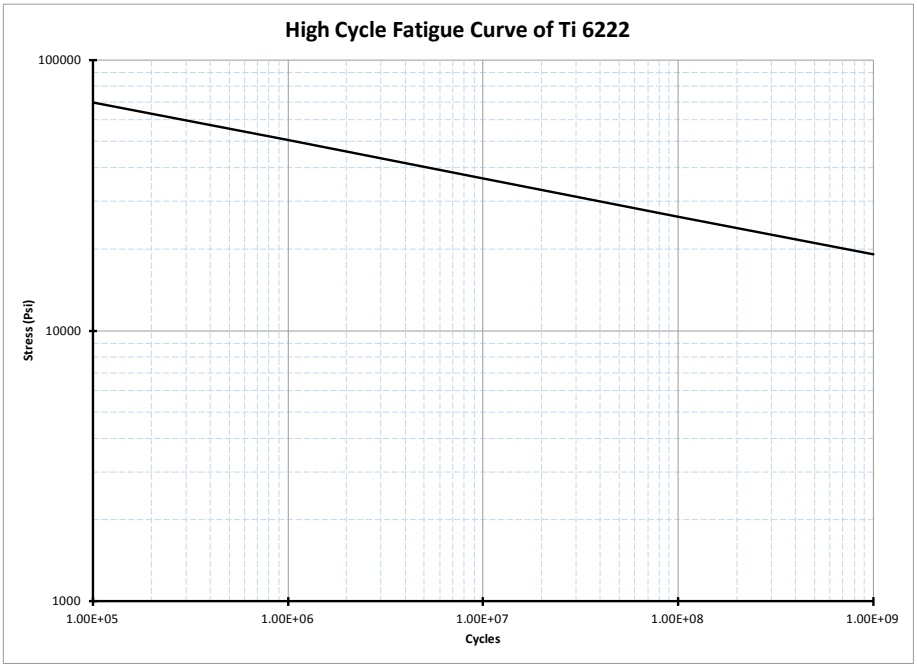

Figure 7.4.2 Titanium 6-2-2-2 High Cycle Fatigue Data

The data were plotted using $Stress_{rms}$ versus cycles, not $Stress_{peak}$ versus cycles.

Dynamic stresses were calculated similar to the methods used to determine the dynamics load. The FEM of the HCV was analyzed using different random vibration and acoustic excitation, and the correct conditions were combined to obtain the dynamic stress at each mission phase.

A second HCV Statistical Energy Analysis (***Figure 7.4.3***) was performed to determine the dynamic response of said panels. The results indicate 80% of the panel responses are below 200 Hz, which the FEM is good for. This would mean the sonic fatigue analysis could under estimate the panel life. To mitigate the effect of under-estimation, the stress input were increased by 20% to counter the effect. ***Figure 7.4.4 and 7.4.5*** present the analysis results.

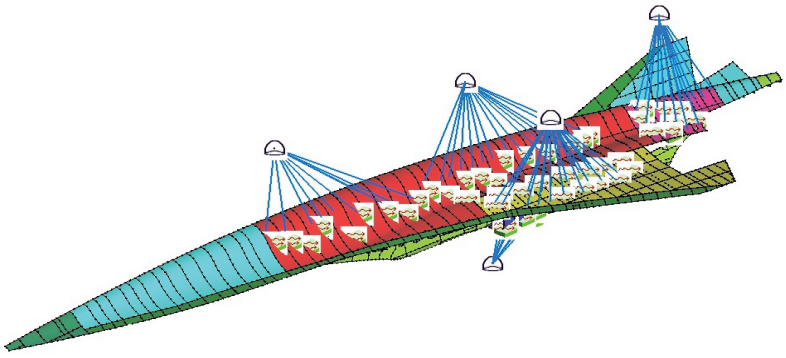

Figure 7.4.3 Sonic Fatigue SEA Model

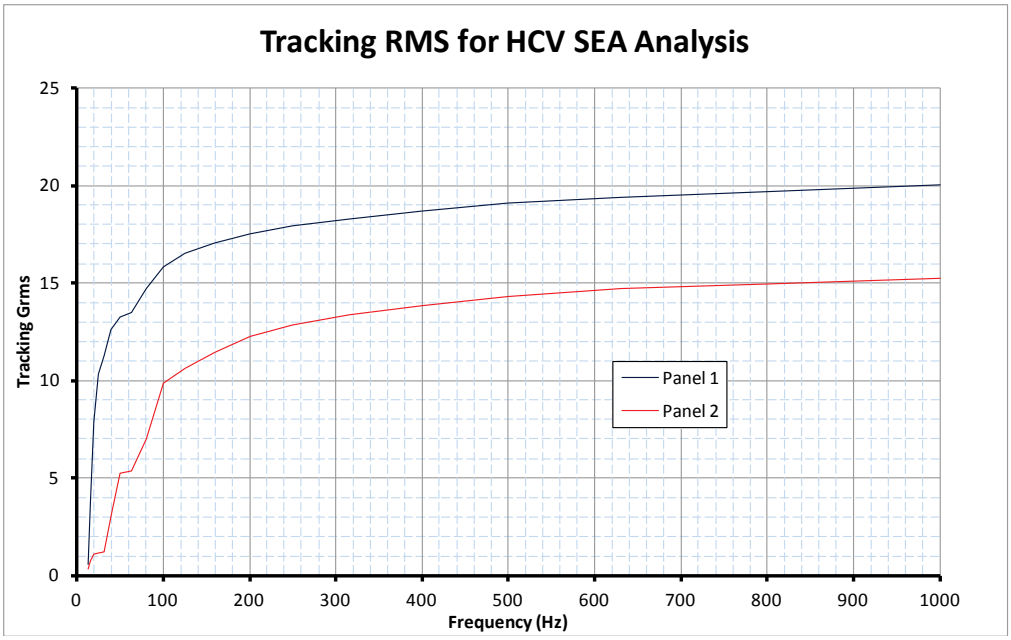

Figure 7.4.4 Panel Responses – Tracking G_{rms}

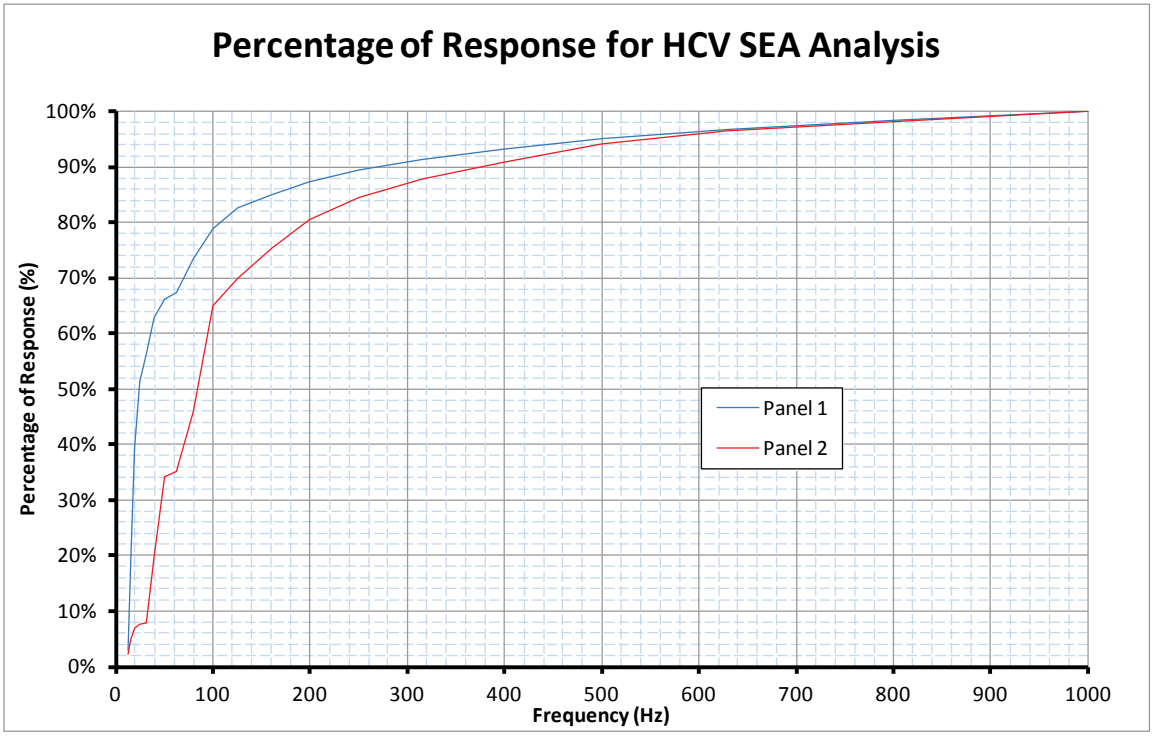

Figure 7.4.5 Panel Normalized Responses

High cycle fatigue can be estimated using the formula listed in Equation 7.4.1.

$$N = \left(\frac{S_{mean}}{S_{apply}} \right)^{B}$$

Equation 7.4.1

Where:

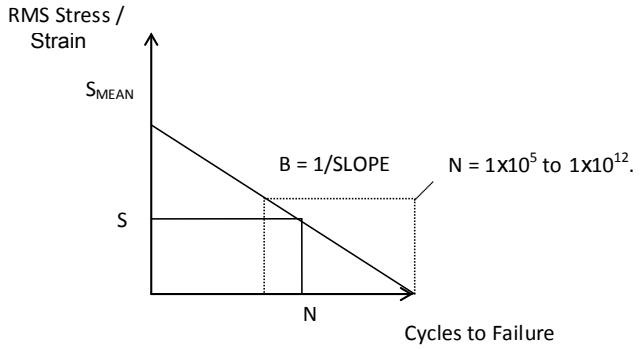

S_{Mean}:	Published Mean Stress, defined by: $S_{Mean}=S*N^{1/B}$
B:	1/Slope of the SN Curve
S_{apply}:	Apply RMS Stress

In this case, the IN718 and Ti 6-2-2-2 high cycle fatigue data were supplied with S_{Mean} and B. After estimating the number of cycles using Equation 7.4.1, a conservative life estimation is based upon the assumption of keeping all the stress cycles applied at 200 Hz. For a more accurate estimation, Rayleigh distribution can be used for dynamic load cycle accumulations, but this was not able to be used in this analysis.

Panel 1

Using the results directly from the supersonic acceleration, dual mode and DMRJ phase, the panel had essentially zero life. The S_{Apply} were so high that no cycle life can be expected. ***Figure 7.4.6*** illustrates the sonic fatigue analysis results using the Panel 1 dynamics stresses, as shown, where the minimum cycle is approximately 3,000 cycles or 14.5 Seconds. For the purpose of the design study, the S_{Apply} were reduced to the Panel 4 level, and Panel 1 thereafter had a sonic fatigue life of 1,100 Hours.

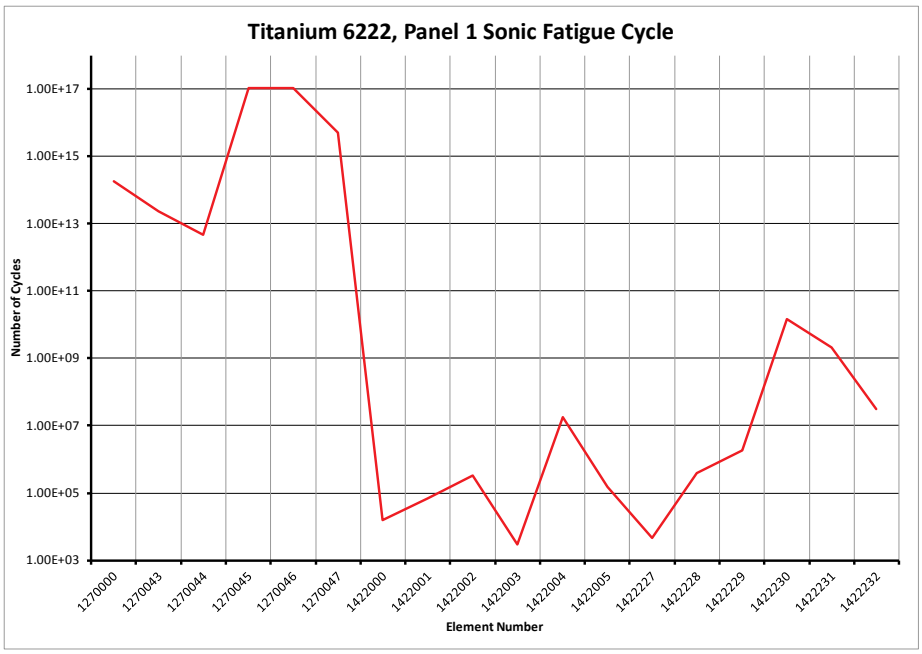

Figure 7.4.6 Panel 1 Sonic Fatigue Analysis Results

Panel 4

The sonic fatigue results for Panel 4 are illustrated in ***Figure 7.4.7***. Due to the lower dynamic stresses at Panel 4, even during SCRAM jet operation, the panel has unlimited life.

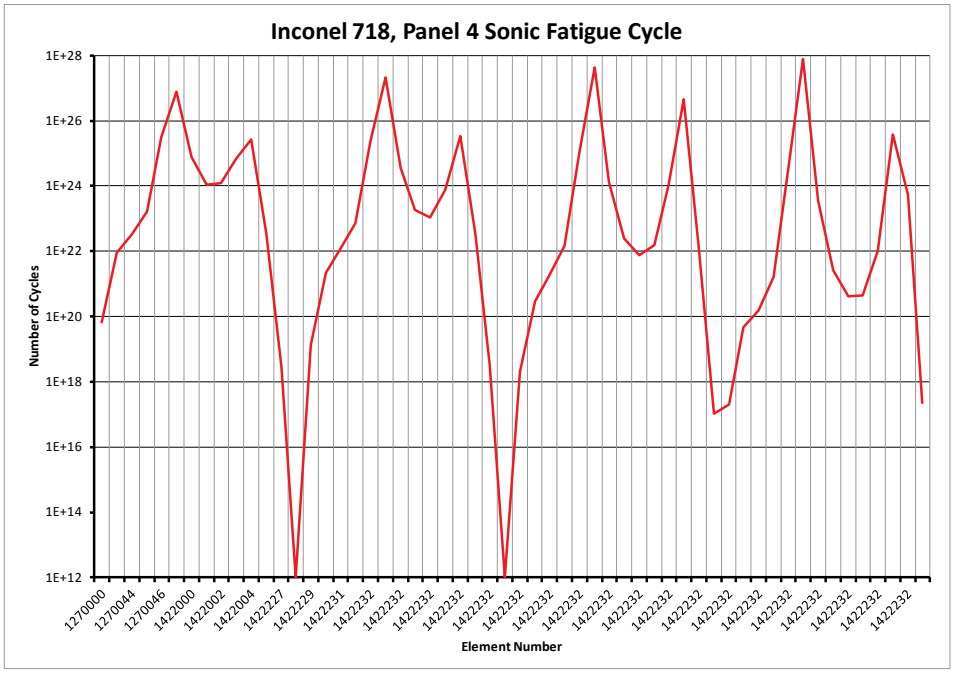

Figure 7.4.7 Panel 4 Sonic Fatigue Analysis Results

8.0 PANEL DESIGN SUMMARY

The final sizing details for each panel are summarized below.

8.1 PANEL 1

An illustration of the design and assembly of Panel 1 is found in ***Figure 6.1.1.1***. The sizing of the components was completed through various stages of the project from basic stress sizing on through the incorporation of dynamic loading followed up by creep and fatigue considerations. The final sizes and dimensions for Panel 1 are as follows:

- Titanium 6-2-4-2S alloy; MIL-T-9046, Type III, Comp. G, Duplex Annealed
- Skin thickness = 0.060”
- Edge doubler width = 2.0” doubler assumed to be integral to skin, tapered to skin thickness
- Edge doubler total thickness (including skin) = 0.150” (0.180” locally for some regions)
- Hat stiffener sheet thickness = 0.032”
- Hat stiffener pitch = ~4”
- Hat design layout: illustrated in ***Figure 8.1.1***
- Perimeter fastener pitch = 1.0”
- Stiffener fastener pitch = 1.0”
- Fasteners are 0.25” diameter (AM2154 IN718)

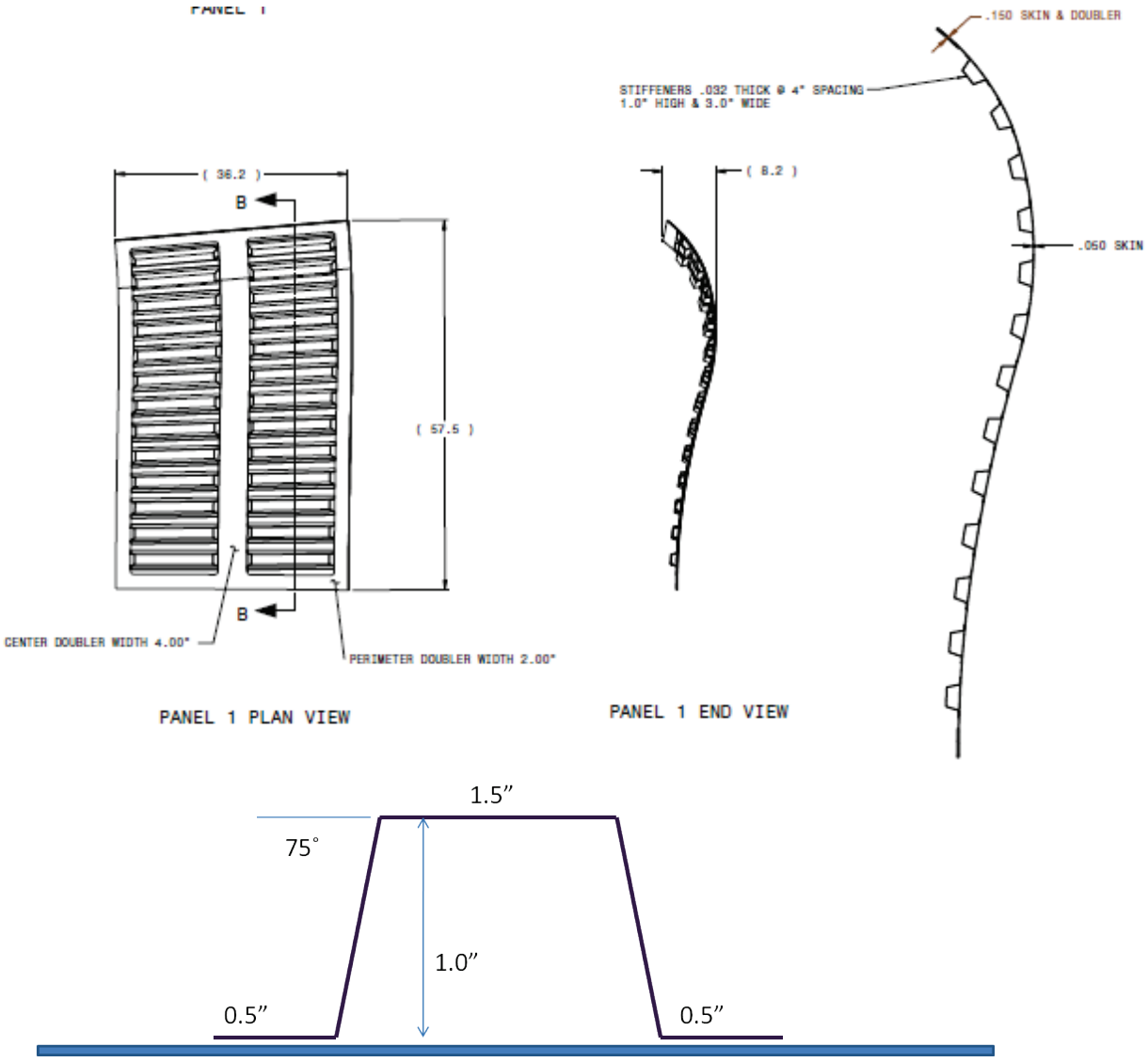

Figure 8.1.1 Panel 1 Dimensions and Hat Siffener Details

8.2 PANEL 2

An illustration of the design and assembly of Panel 2 is shown in ***Figure 6.1.4*** with similar construction to Panel 1 (***Figure 6.1.1.1***). One key difference to note from the Panel 1 design is that Panel 2 uses welded attachments in place of discrete fasteners. This is due to the fuel tank region location of Panel 2. Small ¼" spot welds were assumed to connect the stiffeners to the skin while a continuous beam weld attaches the perimeter edges to the substructure. The final sizes and dimensions for Panel 2 are as follows:

- Titanium 6-2-4-2S alloy; Specification: MIL-T-9046, Type III, Comp. G, Duplex Annealed
- Skin thickness = 0.070"
- Edge doubler width = 2.15" (doubler assumed to be integral to skin, tapered to skin thickness)

- Edge doubler total thickness (including skin) = 0.210”
- Hat stiffener sheet thickness = 0.050”
- Hat stiffener pitch = ~4”
- Hat design layout: illustrated in ***Figure 8.2.1***

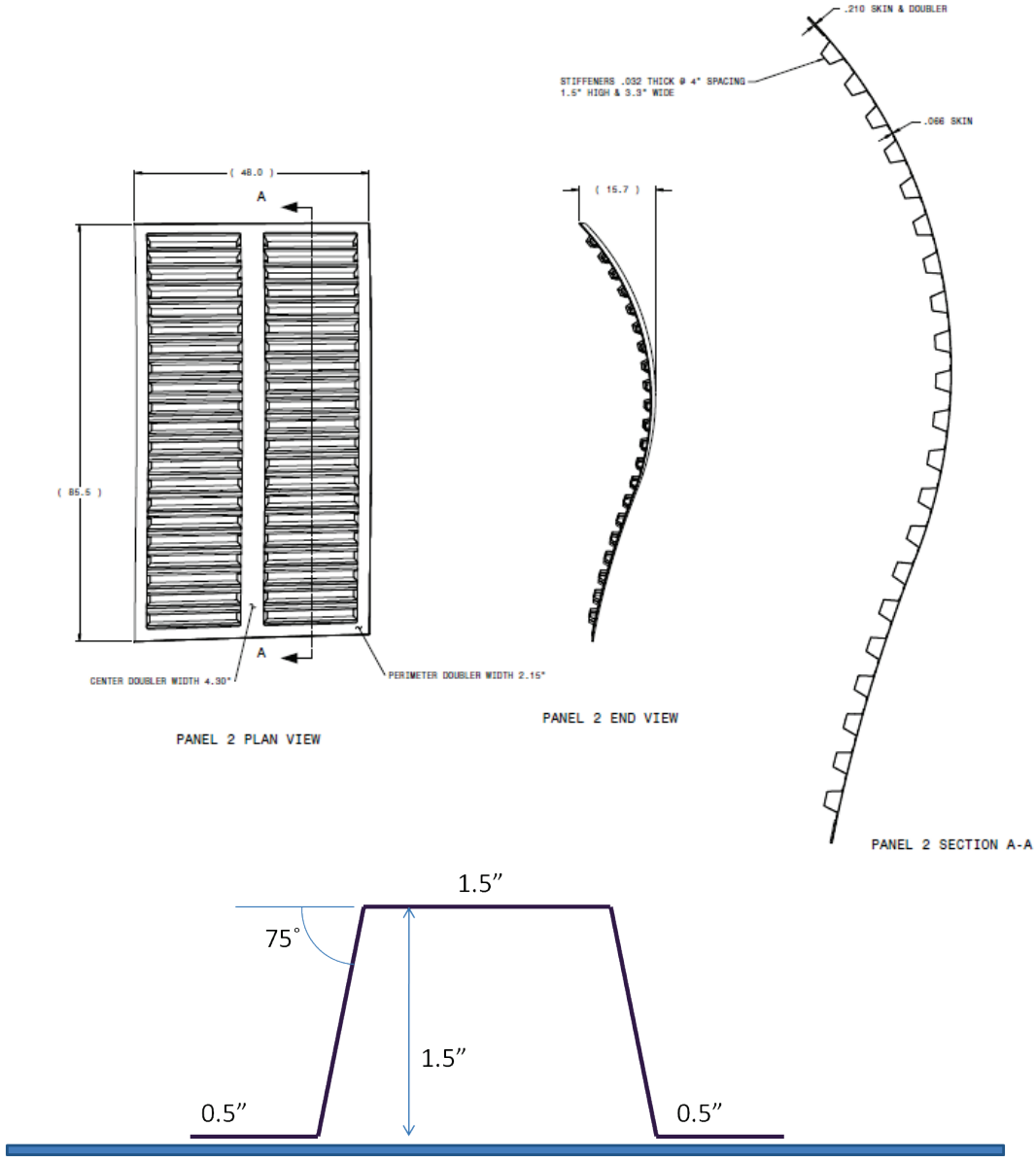

Figure 8.2.1 Panel 2 Dimensions and Hat Stiffener Details

- Stiffener spot weld pitch = 1.0”
- Perimeter weld thickness = 0.25”

8.3 PANEL 3

Panel 3 is of sandwich core construction, and the baseline gauges were dictated by an available configuration already in process at a Titanium sandwich panel vendor. The details outside of core thickness and facesheet thicknesses were sized by these studies. A frame is welded to the sub assembly, and the sub assembly is attached to substructure with fasteners. The final sizes and dimensions for Panel 3 are as follows:

- Ti 6-2-4-2S material facesheets, Ti B21S honeycomb core: cell size .375", foil size .007 in. thick, estimated core weight density = .8562 lbs/ft**2
- Facesheet thickness = 0.018" (0.025" locally if machined facesheet, at high stress location)
- Facesheet doubler at attachment edges = 0.115" (assumes machined facesheet, or frame thickness)
- Frame added to design to act as doubler for attachments and to transfer load into assembly
- Frame thickness = 0.050"
- Core thickness = 0.65"
- Fastener pitch = 1.5" (with 1.0" pitch locally at high load regions)
- Fasteners are 0.25" diameter (AM2154 Inco 718)

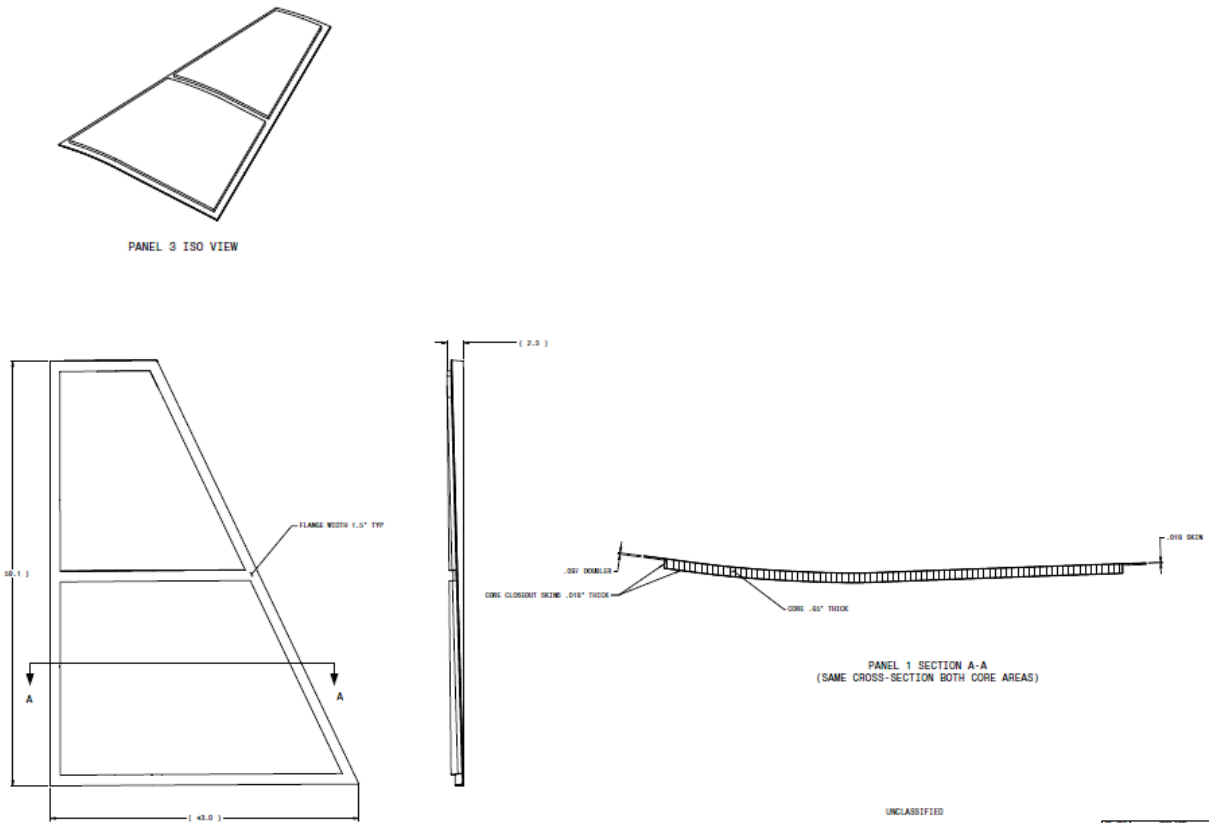

Figure 8.3.1 Panel 3 Detail

8.4 PANEL 4

The generalized design and assembly of Panel 4 is shown in ***Figure 6.1.7***. This panel is of sandwich core construction. A frame is welded to the sub assembly, and the sub assembly is attached to substructure with fasteners. The final sizes and dimensions for Panel 4 are as follows:

- IN617 material facesheets, IN718 honeycomb core: cell size .375", foil size .007 in. thick.
- Facesheet thickness = 0.025" (0.050" locally if machined facesheet, at high stress location)
- Facesheet doubler at attachment edges = 0.15" and 0.21" locally at highly loaded fasteners (assumes machined facesheet, or frame thickness)
- Frame added to design to act as doubler for attachments and to transfer load in to assembly
- Frame thickness = 0.100"
- Core thickness = 0.75"
- Fastener pitch = 1.0"
- Fasteners are 0.25" Diameter (AM2154 IN718)

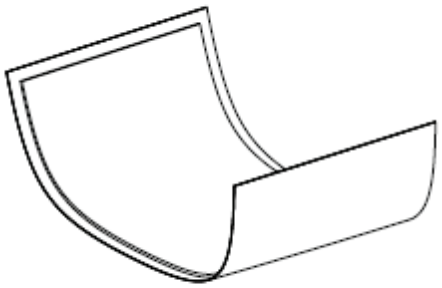

PANEL 4 ISO VIEW

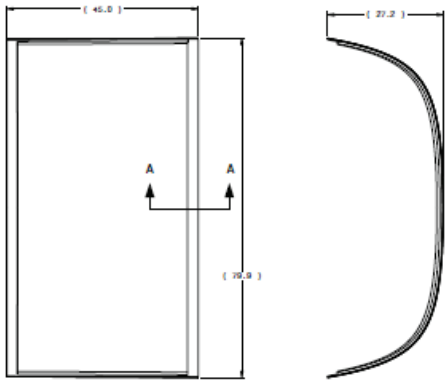

PANEL 4 PLAN VIEW

PANEL 4 END VIEW

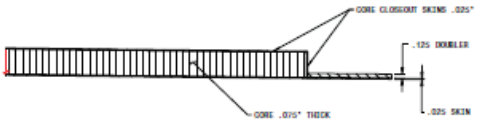

PANEL 4 SECTION A-A
(TYPICAL CORE PANEL CROSS-SECTION)

Figure 8.4.1 Panel 4 Detail

9.0 BULKHEAD F.S. 1554 (F.S. 518) DETAILED ANALYSES UNDER COMBINED ENVIRONMENT LOADING

The F.S. 518 bulkhead from the HTV-3X model was a limiting bulkhead due to the extreme temperature gradients present, as well as carrying wing bending loads. The corresponding 1554 bulkhead in the HCV was selected for further study for these same reasons. A machined plate, integrally stiffened approach was base-lined and this is illustrated in Figure 9.0.***1*** and ***9.0.2***. This bulkhead would consist of multiple regions joined together. The full bulkhead was analyzed as a singular unit for preliminary sizing. Due to the complex nature of the geometry and loading, HyperSizer was not used for initial sizing similar to the panels analyses.

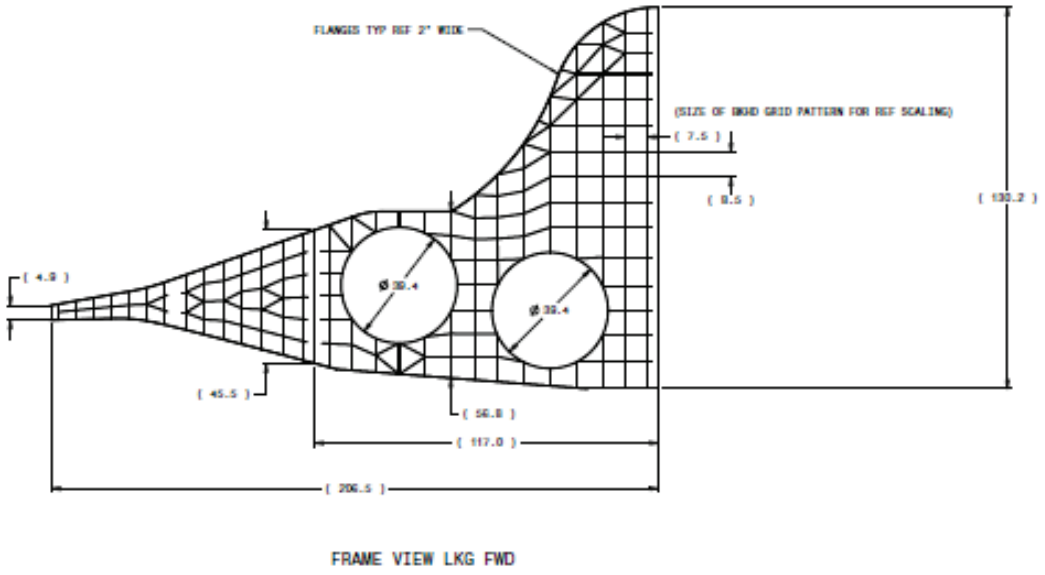

Figure 9.0.1.5 F.S. 1554 Bulkhead Geometry With Dimensions

The bulkhead basic geometry was imported into Abaqus as simplified 2D shell elements for the bulkhead panel region, and 1D elements for all stiffeners, both interior and around the perimeter. This allowed for ease of sizing iterations and layout modifications.

The highest loads on the F.S. 1554 bulkhead were thermally induced. Therefore, the limiting thermal case was chosen for analysis. At Mach 5.2 the exterior of the vehicle is extremely hot, as well as are the interior cut-outs where the engines are passing through. To compound the hot thermal effects within this bulkhead there are also two much cooler regions. One is at the center-line where the fuel is located, and there is one outboard in the wing inside a cooled compartment in order to accommodate the landing gear tire. These hot and cold regions are illustrated in the thermal mapping shown in ***Figure 9.0.3***, where red zones indicate temperatures near 1000°F and blue zones indicate regions at approximately 300°F.

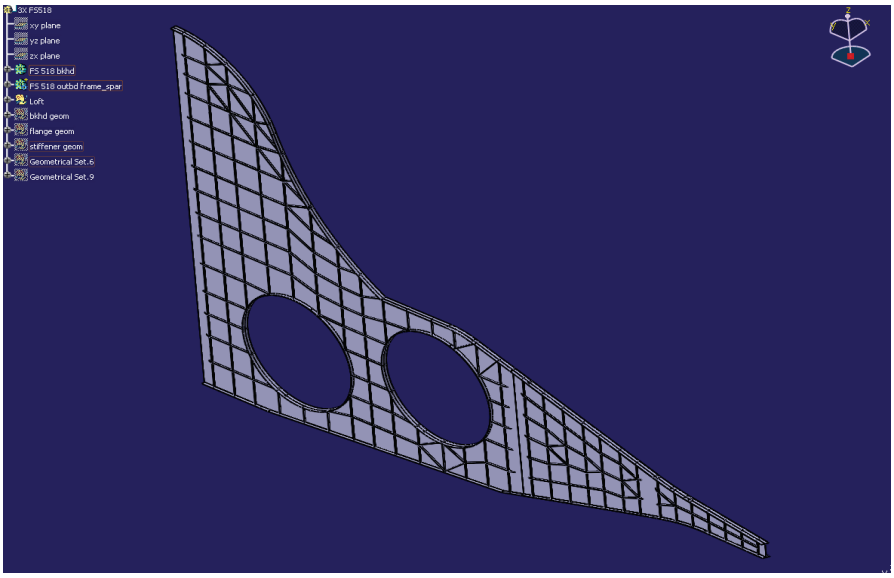

Figure 9.0.2 F.S. 1554 Bulkhead Geometry

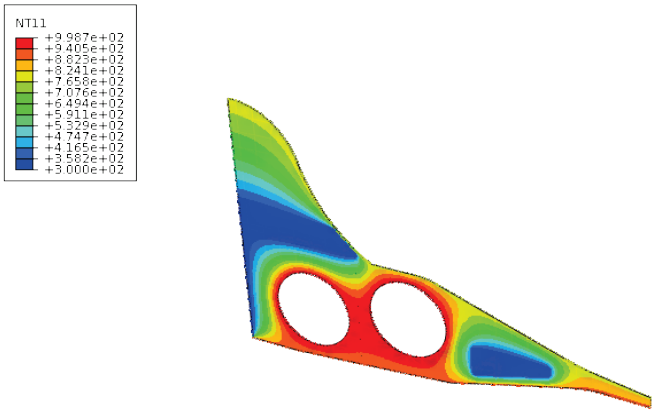

Figure 9.0.3 F.S. 1554 Bulkhead Temperatures at Mach 5.2

Using the temperatures of this limiting thermal case, a structural case was analyzed based on the thermal expansion. The bulkhead boundary conditions are symmetry at the centerline, and constrained from moving in and out of plane at the keel intersections and skin attachments. The thermal expansion results are shown below in ***Figure 9.0.4*** for the baseline stiffener layout.

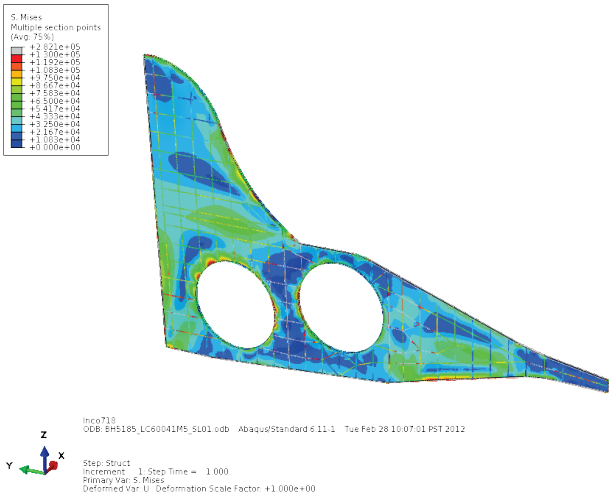

Figure 9.0.4 Baseline Bulkhead Thermal Stress

The stress results showed that the panel webs are nearly adequate. However, the caps that run along the periphery, as well as the internal stiffeners, were all over their stress limits after multiple sizing iterations. The thermal "force fight" is not straightforward to mitigate as additional material often renders the problem worse. A layout with half the previous stiffener spacing was also tried with slightly improved results, as shown in ***Figure 9.0.5***.

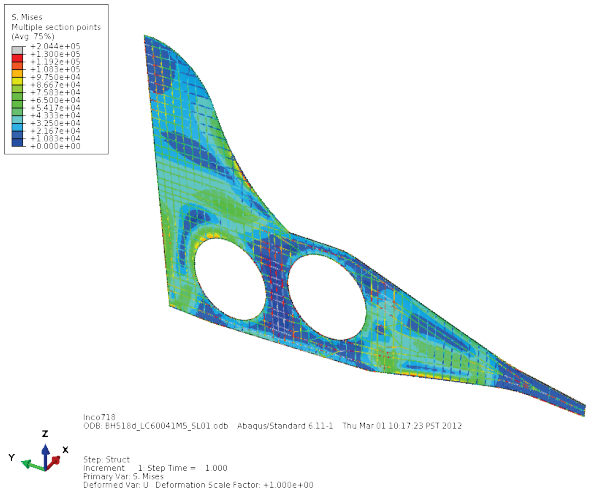

Figure 9.0.5 Half Spacing Bulkhead Thermal Stress

The results in this case were slightly improved yet still far from within stress limits. Due to project time constraints this bulkhead sizing exercise was not closed. Moreover, a new design approach that focuses heavily upon high temperature gradients is the suggestion for future work in this area.

10.0 TEST PLANNING

During the course of the detailed design phase structural test considerations and early strategies were formulated. These were based upon the analyses and simulation issues to that date, and were also in consideration of the "gaps" in said analyses that were being experienced.

A generalized summary is listed below:

Panel 1: Ti 6-2-4-2S skin stringer construction of dual curvature.

a) The replication/simulation of the various flight phase acoustic was considered extremely critical to the validity of a structural test in determining either static response behavior or service life prediction estimates.

b) The abrupt temperature field variations per the movement of the adjoining control surface area were deemed highly integral to the "softness" of the panel.

c) The attachment method (baseline –fastener) boundary condition simulation is equally vital to simulation of the adjoining panel displacement conditions.

Panel 2: Ti 6-2-4-2S skin stringer construction of dual curvature

a.) As this structural panel temperature field and elastic qualities will be highly dependent upon the state of the internal residual fuel level, the gradual thermal differentiation is vital to performance accuracy.

b.) This structural skin was considered likely to be tension critical (initially) upon skin expansion.

c.) Panel 2 will be in constant "force fights" between fuel floor and the expansion of the outer fuel tank skin, and the boundary condition of the welded joint is highly integral to the value of the test simulation.

Panel 3: Ti 6-2-4-2S/Beta 21S composition sandwich

a.) As the Panel 3 location adjoins a different material (projected) leading edge, accurate representation of the thermal shock factors is vital.

b.) Panel 3 is the most flat panel of all four panels under study and in a flutter wing zone so the potential of "lifting up" of the edges is a critical area where testing could be used to validate simulation/prediction.

c.) The HCV upper wing skin area is considered as highly compression critical and the simulation of heated boundary condition compressive running loads, along the entire panel perimeter, is critical to the test simulation for panel survivability.

Panel 4: IN718 composition sandwich.

a.) Combined acoustic and thermal loading is paramount to an accurate assessment of its service life as well as for comparison to static response and service life prediction results.

b.) The accurate simulation of the acoustic field energy is critical for understanding the response of the panel.

c.) A varying of the temperature fluctuations/cycles in phase with the acoustic energy emission from the DMRJ would serve as excellent resultant data for panel FEM calibration.

10.1 HYPERSONIC PANEL THERMAL-DYNAMICS TESTS

Figure 10.1.1 and ***Figure 10.1.*** below show the locations of all four panels, and the related dynamic environments.

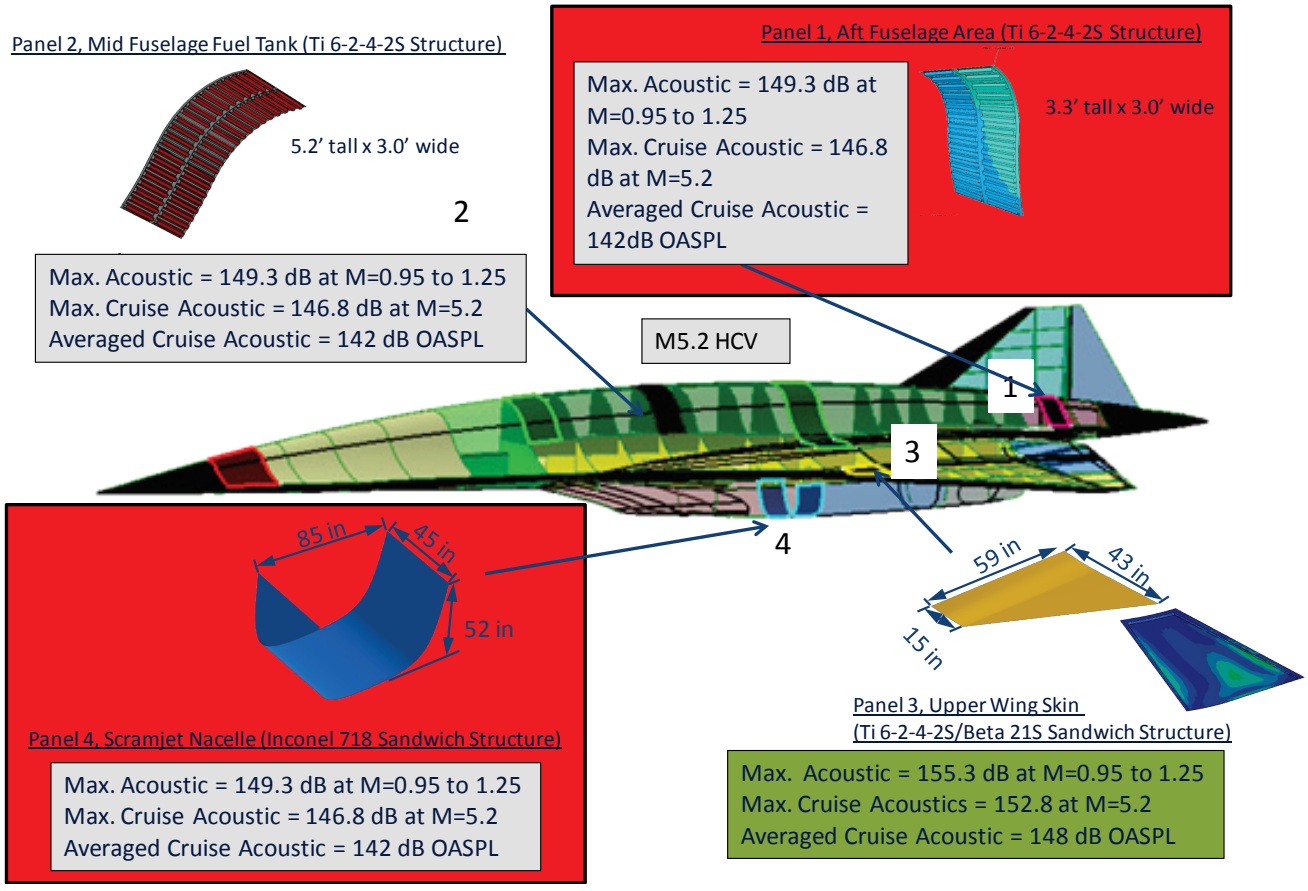

Figure 10.1.1 Maximum External Acoustic Distribution Levels

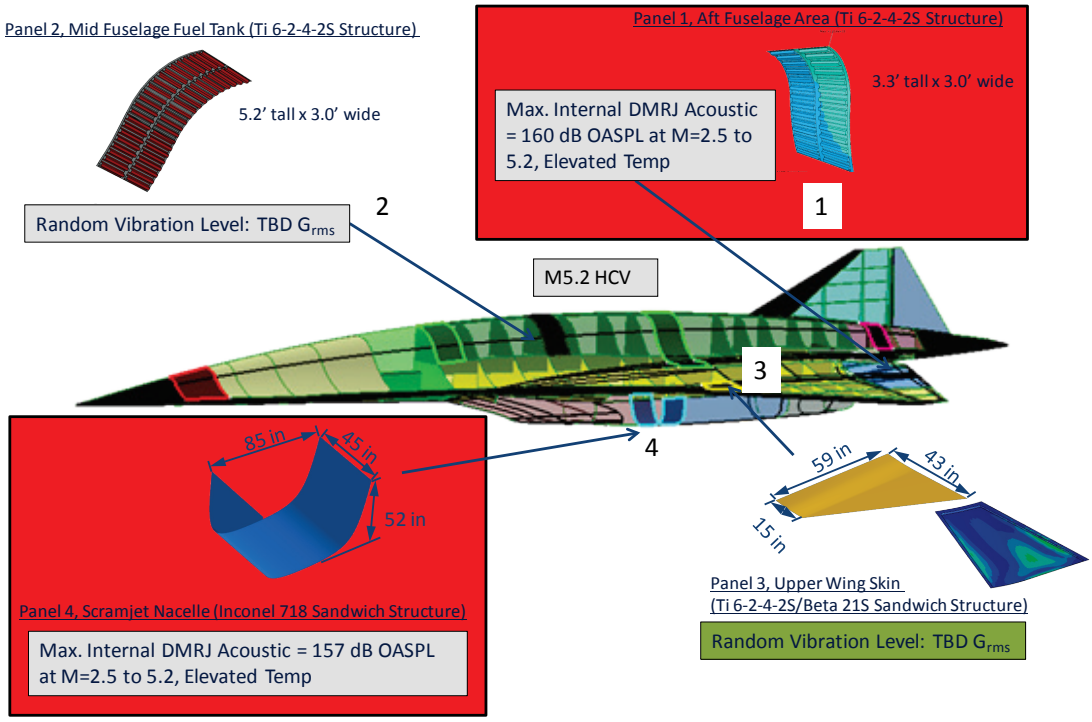

Figure 10.1.2 Maximum Internal Acoustic Distribution Levels

Two panels were selected as the primary panels for dynamics based testing. Panel 1, located above the engine, at the aft section of the fuselage was selected because of its location, which is exposed to the worse dynamic environment caused by the propulsion system. Panel 4, located near the inlet at roughly the mid-point of the fuselage, was selected due to its exposure to the inlet shock and acoustic environment.

The internal acoustic results indicate a different story. Panels 1 and 4 are exposed to very high internal acoustic during the supersonic acceleration and hypersonic cruise phase, and most of the time, the material are at elevated temperature. The levels shown in ***Figure 10.1.1 and Figure 10.1.2*** are predicted flight environments, with 0 dB margin included in the results. What is considered worse is that, while the external acoustic were normally dominated by an acoustic spectrum, which the energy peaked around 200 to 1,600 Hz, the internal acoustic spectrum energy is mainly distributed at the low frequency (structural frequency) range.

The external acoustic were governed by the results defined in previous chapters. For Panels 1 and 4, the maximum external acoustic test level is 149.3 dB OASPL during transonic (room temperature) and 142 dB OASPL, with a short spike at 146.8 dB OASPL during cruise (elevated temperature). The acoustic pressures spectral distribution is shown in Figure 10.1.3.

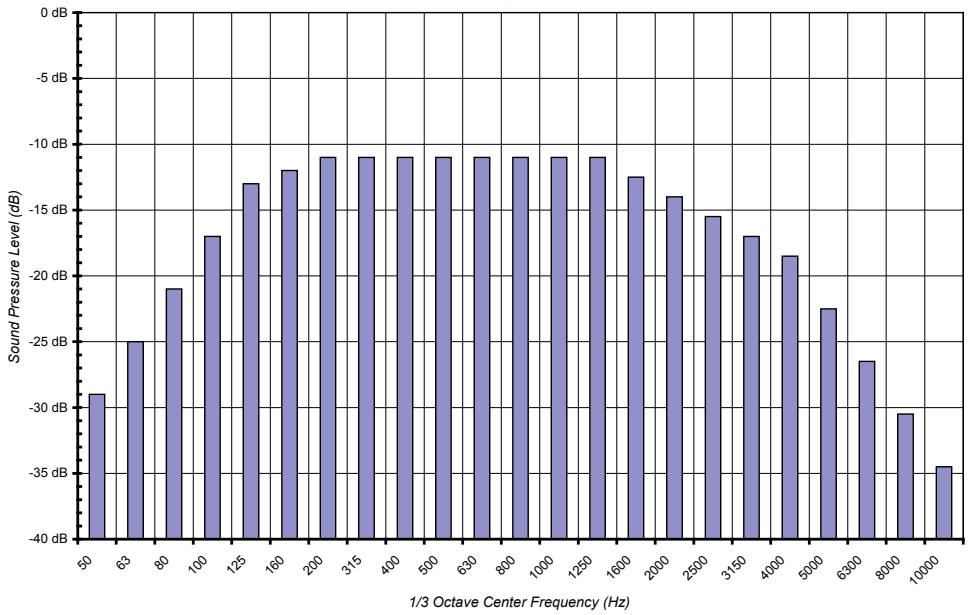

Figure 10.1.3 Acoustic Pressures Spectral Distribution

Turbojet Environment

The turbojet environments can be simulated by a shaker test. The panels shall be subjected to the vibration environment in both room temperature and elevated temperature (takeoff, supersonic acceleration, and de-accelerating – landing). The exposure time for Panel 1 is -3 dB @ 600°F for 300 Seconds, and -0 dB @ room temperature for 1,000 seconds per mission. The exposure time for Panel 4 is -3 dB @ 700°F for 300 Seconds, and -0 dB @ room temperature for 1,000 seconds per mission.

DMRJ ScramJet Environment

The SCRAM jet environments for Panel 1 is 160 dB and for Panel 2 is 157 dB OASPL. The exposure time for Panel 1 is -3 dB @ 600°F for 300 seconds and -0 dB @ 930°F for 3,600 seconds per mission. The exposure time for Panel 2 is -3 dB @ 700°F for 300 seconds and -0 dB @ 1,100°F for 3,600 seconds per mission.

The SCRAM jet environment can be quite difficult to simulate in an acoustic chamber, although the preference are to test the panels in the acoustic environment at elevated temperature. There are two major challenges, the magnitude and spectral distribution. The magnitude shown in previous section is very high, and finding an acoustic facility that can accommodate can be challenging. A major bulk of the acoustic energy, as shown in ***Figure 10.1.3***, is at low frequency, which is extremely difficult to simulate using the current state of the art testing equipment.

An alternative method to simulate the environment is to perform an initial thermal acoustic test at lower level (-6 to -10 dB, broad band or tonal), obtain the responses, and perform a random vibration shaker test. This would means longer testing, by might be the only method due to the limitation of the current state of the art acoustic test equipment. This method is only valid if the material response and life response linearly.

10.2 PANEL 1

Figure 10.2.1 illustrates the Panel 1 test specimen and its relationship between the internal and external dynamic test. The test specimen is projected to be a 4' X 3' ribbed stiffened panel, and two specimens shall fit into a 4' X 6' fixture that simulates the HCV primary structure interfaces. Ideally, the interface should also approximate the stiffness of the surrounding structures, but for a development test program, a stiff interface should suffice.

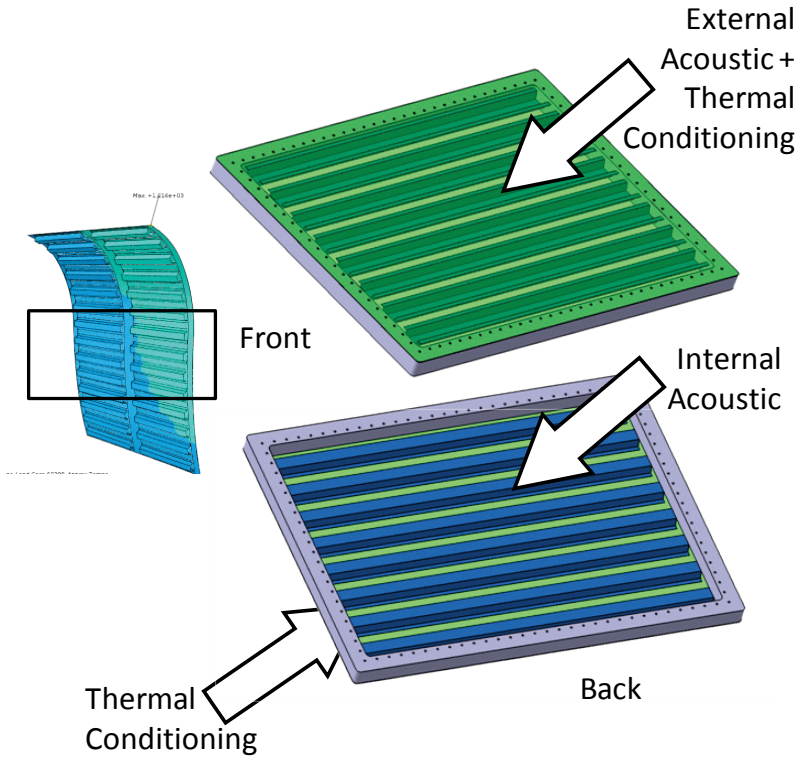

Figure 10.2.1 Panel 1 Suggested Test Specimen

The Panel 1 suggested testing parameters are summarized as follows:

Test Section: 4 ft X 3 ft per frame (as illustrated in Figure 10.2.1), 2 frames

Test Boundary Condition: Support Frame Simulated Primary Aircraft Structures: Attach bulkhead and adjoining panels.

Max. Test Temperature: (969ºF – 1000ºF)

Test Input: Driven by Dynamics Loading

a.) External acoustic
b.) Internal acoustic
c.) Random vibration

Test Type: Thermal-Acoustic Test, Thermal-Vibration Test

a.) External Acoustic
b.) Internal Acoustic (Tonal)

Projected Test Chamber: Combined Environment Acoustic Chamber (CEAC), Air Force Research Lab, Wright Patterson Air Force Base, Ohio.

1. Acoustic Tunnel
2. Acoustic Chamber

Projected "Gaps" Mitigated by Tests:
Panel Survivability
- External Acoustic and Vibration Only
- Not with Tonal Internal Acoustics

Acoustic Coupling Factor
- Acoustic Test Only

Projected "Gaps" Not Expected to be Mitigated by Tests:
The true effects of the boundary conditions as the tests will be limited to a scale panel. As such, the test will not include the effects of the adjoining panels on the vehicle scale.

10.3 PANEL 2

Panel 2 consists of a hat stiffened panel measuring 62" tall by 36" wide and represents an upper fuselage skin with fuel containment. The panel is supported by a central bulkhead and would require bulkhead closeouts both fore and aft and a dummy floor and wall would be required in order to allow simulated fuel pressurization. The panel is buckling critical due to thermal force fights. The test temperature for the panel is 819^0F and combined mechanical and thermal induced running lodes are shown below.

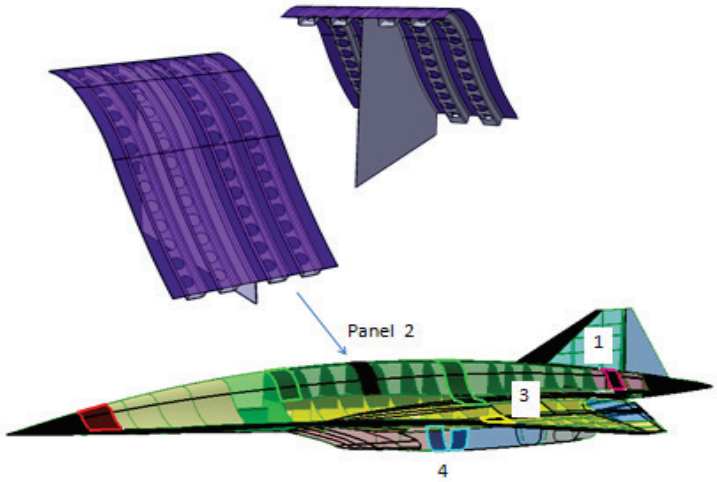

Figure 10.3.1 Panel 2 for Test Planning

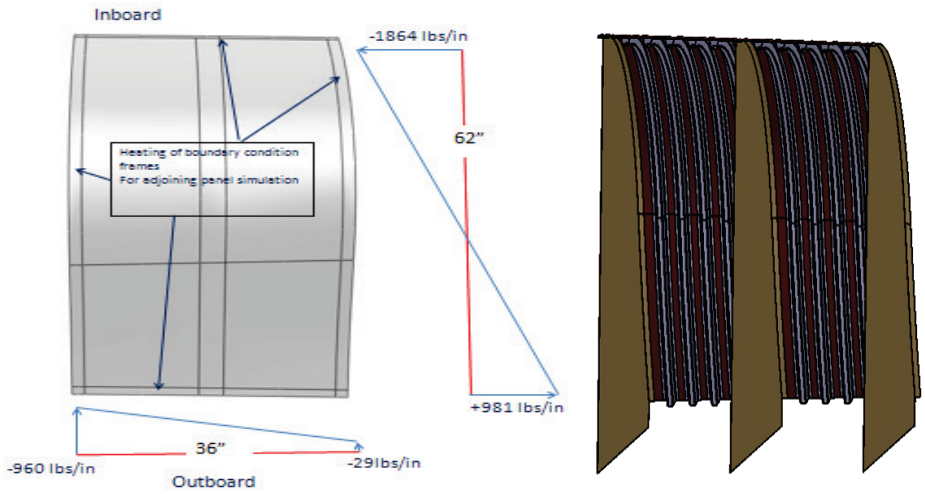

Figure 10.3.2 Panel 2 Generalized Structural Loading Pattern

Two options for testing this panel were identified consisting of either complex test using the NASA Combined Loads Test System (COLTS) facility to test an upper fuselage structural element consisting of two book-ended panels and support structure in combined bending and torsion or a simplified panel test using standard picture frames and a multi axis load reaction frame. Pressurization of both panel test configurations will require the design and fabrication of a containment box to back up the test panel.

The first option consisting of an upper fuselage component would require adaptation to the COLTS D frame test fixture and additional work would be required for development of the heating capability using quartz lamp heaters.

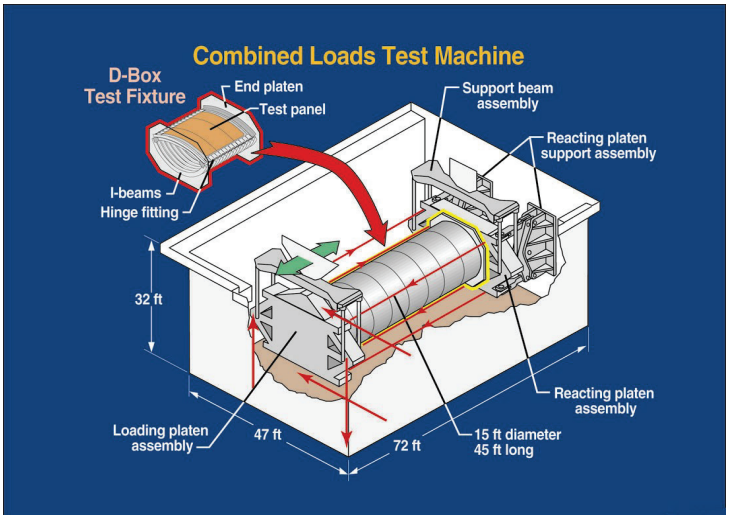

Figure 10.3.3 Panel 2 NASA LaRC COLTS Facility

The second option, consisting of a panel and limited back up structure, could be tested in most multi-axis test facilities using picture frame loading methods and four hydraulic jacks for application of the running loads.

Both configurations would require construction of additional load introduction bays to provide for heating uniformity and loads introduction to the test section. In the case of picture frame loading the picture frame hardware may require heating in order to avoid inducing non representative boundary condition loads.

The internal fuel tank pressurization of 10 psi would be simulated in both cases. However, exterior pressure loads would not be simulated in either test option.

Instrumentation would consist of load, displacement, temperature, pressure, and strain measurements. Each hydraulic actuator will be monitored for applied or reacted load, load train temperature at the load cell interface, and stroke. Loads should be monitored at all hydraulic actuators or in the case of the COLTS facility each load actuator driving the load platens. All load cells should be monitored for temperature as an additional precaution. Displacement of the test panel should be monitored in a minimum of six locations for characterization of panel displacement.

Strain measurement should consist of a minimum of twenty rosette strain measurements that would allow for monitoring panel crippling and buckling of the skin, stiffeners, and bulkheads. An additional eight back to back axial strain measurements would allow for minimal strain correlation at the load introduction points. At a test temperature of 819^0F strain measurements will require significant experimentation prior to installation on the test article in order to insure that measurements are obtained.

Pressure measurements would be required for control of the internal simulated fuel level and to maintain simulated fuel pressurization. Pressure measurements will need to be made remotely as to prevent thermal drift of the transducers. Surface pressure due to aerodynamic load may be partially compensated for but fuel pressurization of this panel should dominate the load case. If hydrocarbon fuel is used, provisions for operation of the test in an inert environment and secondary containment must be made.

Temperatures appear to be relatively uniform across the face of the test panel and the thermal profile should be controllable using a minimum of five control zones arrayed from the top to the bottom of the test panel. Each zone would consist of six quartz lamp heaters and all six would be slaved to a single weld-on control thermocouple. Provisions should be made for back up control thermocouples for each zone. This would result in six control thermocouples and an additional twelve data channel thermocouples for backups and alarms. Additional thermocouples will be required for monitoring and controlling thermal loads in the mechanical load introduction fixtures. Jack train temperatures should also be monitored near the load cell interfaces to address concerns of loads drift due to thermal effects. In all there could be as many as 36 to 48 data channels dedicated for temperature monitoring and at least 20 control channels required for panel surface temperature and load introduction hardware.

To summarize, the Panel 2 suggested testing parameters are summarized as follows:

Test Section: 3 ft X 3 ft per Frame, 2 frames

Test Boundary Condition: Support frame simulated with the primary attach bulkheads and forward and aft adjoining panels.
Max. Test Temperature: (819ºF – 850ºF)

Test Input: Driven by transient thermal input

a.) Apply aero loading in sequence
b.) Simulate fuel burn down rate
c.) Simulate heating and boundary condition motion
d.) Simulate internal tank pressure per relief valves

Test Type: Thermal/aero pressure-per altitude test incorporating:

a.) External Aero
b.) Internal cooling
c.) Fuel floor expansion vs. outer panel expansion

Projected Test Chamber(s): NASA COLTs Langley Research Center (LaRC), Hampton, Va..

1.) The facility offers up to full fuselage test capability
2.) The facility also has the ability to simulate a fuel burn-down rate over a large area.

Projected "Gaps" Mitigated by Tests:

Panel Service Life Output

- Effects of the fuel "sink" upon the structural skin temperature
- Provides fuel effects on a "hot" skin on a material level

Projected "Gaps" Not Expected to be Mitigated by Tests:

Limited to the scale of the panel so the test will not fully capture the effects of fuel slosh over an entire tank volume along with vapor pressure effects.

10.4 PANEL 3

Panel 3 consists of an upper wing skin that will experience primarily compressive loads and a maximum temperature of 1118ºF. Loads consist of both up-bending and torsion of the wing combined with thermal expansion. The panel boundary conditions will be a significant challenge with this panel and may require construction of a full depth wing box for the most accurate testing, and would most likely be required for a flight vehicle program. Stiffness and thermal loads at the adjacent points and leading edge will be challenging to match and must accurately simulate those boundary conditions.

Many options were examined for the testing of Panel 3 and these are described throughout this section. In the end, a high speed flow test was deemed as critical to capturing the required structural response as is deemed critical to a panel in this vehicle location. The test parameters are summarized at the end of this section.

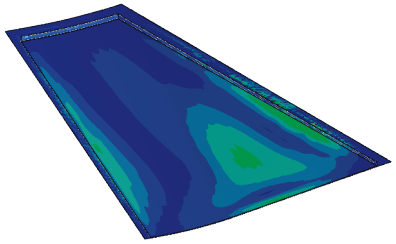

Figure 10.4.1 Panel 3 for Test Planning

Testing of a full depth wing box provides additional insight into the structural interaction through not only the initial skin panel but also the sub-structure and adjacent load introduction and reaction hardware. However, testing as a panel will require significant work to develop a picture frame interface for loads reaction and introduction and may require thermal matching at the test fixture interfaces. Refer to the combined mechanical and thermal running loads diagram as illustrated below.

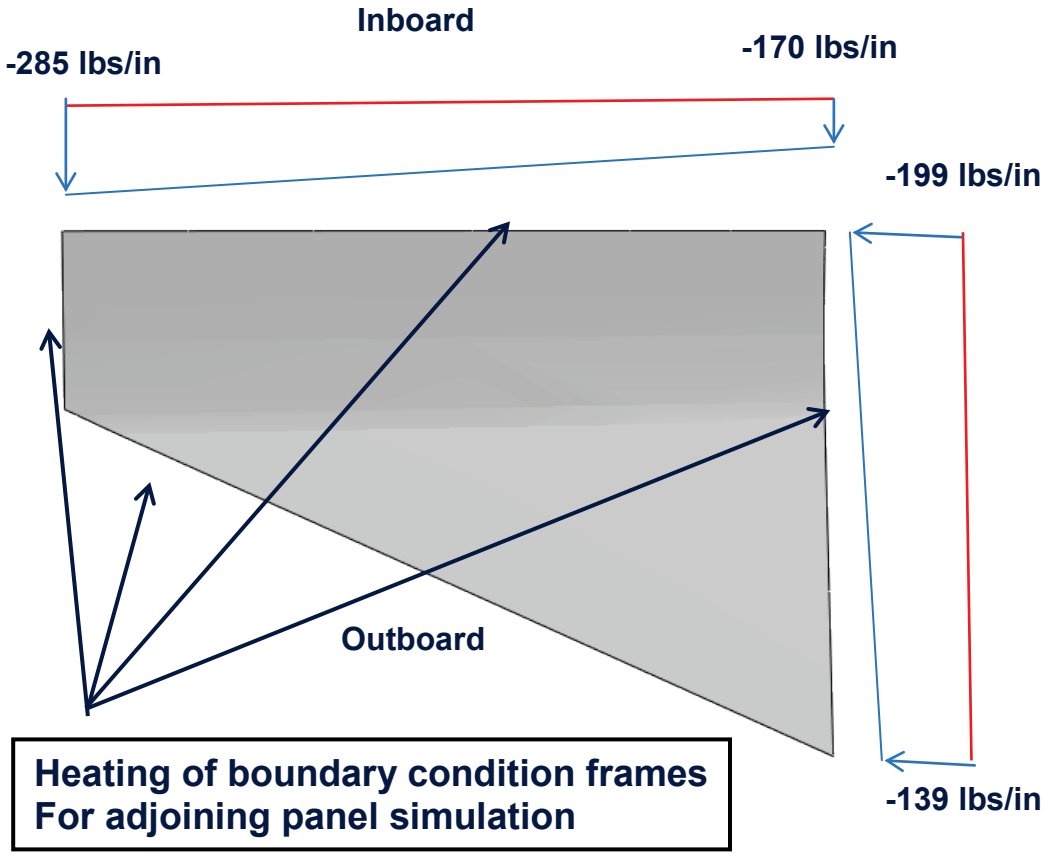

Figure 10.4.2 Panel 3 Generalized Structural Loading Pattern

Thermal loads can be introduced through five heater banks slaved to individual control thermocouples. Approximately twenty six lamps will be required for this test. As a panel, this testing at temperature will require surface heating using quartz lamps and careful consideration of

the restraint hardware thermal conditions at the test temperature. Steady state thermal distribution will require tuning the restrain and load introduction hardware temperatures in addition to maintaining a steady state surface temperature profile.

Thermal mapping using thermography may provide some confirmation of thermal gradients over the surface of the test panel and the loading and restraint hardware interfaces. Thermocouples would be welded to the test panel surface for the purpose of discreet temperature control zones. Overall panel surface temperature gradients will vary from that of the modeled distribution by up to 25ºF to 50ºF in some places due to lamp geometry and convection effects. Load application will be accomplished through heated attachment fittings with thermally isolated load cells. Calibration of the load cells at temperature and monitoring of the load cell temperature during testing is required for monitoring thermal induced load drift.

Option 1) Use of the COLTS facility (***Figure 10.3.3***) may be possible with either a full depth wing box structure or through the use of the D-box test fixture testing only the skin panel. Heating the test specimen will be a challenge to the COLTS facility due to the test temperature of 1118ºF. Fuel pressurization effects would need to be included in the test planning and should be possible with this facility. Use of fuel or a simulated fuel for fill and drain thermal variation testing and or static volume testing is an additional issue requiring use of an inert test environment and secondary containment for the working fluid.

Option 2) Use of a multi-axis reaction frame and construction of picture frame restraints and load introduction fixtures would also allow for pressurization effects if a secondary close out to the test specimen was fabricated to back up the skin panel. Sealing and thermal compensation would need to be addressed as would the stiffness of the reaction and load introduction fittings. Stability of the frame test approach is also a concern due to the complexity of the load reactions and support points. Similar wing box testing was undertaken at lower temperatures at the Lockheed Rye Canyon test facility in the 1960's for development testing of the SST wing root joint at temperature. The multi-axis or MUAX test frame is still in use in the Palmdale mechanical test lab. Significant work would be required for development of the loads introduction and reaction hardware and would likely include active heating of the interface hardware.

Option 3) Use of the NASA Dryden Flight Loads Lab (FLL) facility at the Dryden Flight Research Center (DFRC) would require attachment of a full depth wing box to their strong back fixture in the test chamber. While an inert environment is easily achieved with this facility, secondary containment and or use of a working fluid is problematic. The floor of the test cell contains structural channels for the purpose of mounting hydraulic actuators and running lines. Containment of a working fluid may be the biggest issue. The test could be conducted using two jacks for introduction of torsion and bending loads to a full depth wing box, additional loads may be required in plane and can react to the strong back fixture in the for aft axis while an additional reaction structure would be required in the transverse axis parallel to the strong back frame. The thermal profile capabilities of the FLL should be more than capable of supporting sustained temperature of 1118ºF. DFRC also has substantial in house instrumentation research capability critical to testing at temperature and may offer a unique paring of test and instrumentation capabilities.

Figure 10.4.3 NASA DFRC Flight Load Laboratory

Option 4) The magnitude of the applied and reacted loads would require development of a considerably more substantial reaction frame for the AFRL combined acoustic thermal test facility. This option however allows for acoustic excitation of the test panel while under thermal and mechanical load not available elsewhere. Some consideration for orientation of the test article must be taken into account as a working fluid would not provide the proper pressure distribution if the panel is mounted in a vertical plane for testing. Rotation of the heating structure to an overhead position in order to allow for horizontal testing of the panel would require extensive modification of the existing test facility. The thermal requirements of the test would not be an issue due to the significant heating capability already in place at the AFRL facility.

Option 5) The NASA LaRC 8' Tunnel was looked at based on a request for simulation of Q effects combined with mechanical and thermal loads. It was determined that test duration would be limited to lengths of 60 seconds or less making heating and operation of a loads test impractical. One possible exception to this determination would be the potential for a specific carve out test to address leading edge heating and loading under high Q. Some interest was expressed in evaluation of edge effects and local area buckling or panel edge buckling effects for Panel 2. While full panel testing appears to be impractical, a specific test of a leading edge section containing expansion joints and adjacent wing skins and backup structure would appear to be appropriate for testing in

the NASA LaRC 8' tunnel. This would allow for investigation of leading edge expansion joint effects documented within the X-15 program. While this is beyond the scope of the planned panel testing listed above it would appear to be feasible at this facility. Additional work would be required for characterization of this structural detail as this area of the structure was not addressed in the initial phases of this contract.

Refer to the NASA LaRC 8' Tunnel facility capability matrix in Table 10.4.1:

Table 10.4.1 NASA LaRC 8' Tunnel Test Parameters

Mach Number	**4**	**5**	**7**
Stagnation Pressure, psia	**50 to 310**	**90 to 530**	**600 to 3500**
Stagnation Temperature, deg. R	**1640**	**2350**	**2500 to 3650**
Dynamic Pressure, psf	**525 to 3100**	**350 to 2000**	**320 to 1900**
Reynolds Number, 10^6 /ft	**0.87 to 5.09**	**0.44 to 2.58**	**0.3 to 3.0**
Altitude Simulation, k-ft	**47 to 85**	**65 to 100**	**80 to 120**
Heating Rate, BTU/$ft^{1.5}$ – sec	**7.0 to 17.0**	**10.5 to 25.3**	**20 to 48**

Initial estimates for instrumentation of this panel consist of a minimum of four load control channels for a panel test and significantly more for the COLTS facility. Four stroke channels would be required for gross displacement under applied loads. Additional load and stroke channels may be required due to specific facility requirements.

Instrumentation would consist of load, displacement, temperature, pressure, and strain measurements.

Additionally stroke for each actuator for monitoring of gross displacement under load should be provided for.

Displacement of the test panel should be monitored in a minimum of six locations for characterization of panel displacement. Strain measurement should consist of a minimum of twelve rosette strain measurements on the face of the test panel that would allow for monitoring panel crippling and buckling of the skin, additional strain measurements would be required for monitoring stiffeners, and bulkheads. An additional eight back to back axial strain measurements would allow for minimal strain correlation at the load introduction points. At a test temperature of

1118ºF strain measurements will require significant experimentation prior to installation on the test article in order to assure strain data is obtainable. High failure rates of strain channels are expected. This uncertainty alone may justify the use of optical strain measurement methods such as optical metrology in specific areas of interest.

As with the test outlined for Panel 2, temperatures appear to be relatively uniform across the face of the test panel and the thermal profile should be controllable using a minimum of five control zones arrayed from fore to aft of the test panel. Each zone would consist of an increasing number of quartz lamp heaters and all would be slaved to a single weld on control thermocouple for each zone. Provisions should be made for back up control thermocouples for each zone. This would result in six control thermocouples and an additional twelve data channel thermocouples for backups and alarms. The number of data channels will be similar to that of Panel 2.

To summarize, the Panel 3 suggested testing parameters are summarized as follows:

Test Section: 15 in. x 59" section

Test Boundary Condition: Support frame simulated leading edge and wingbox aircraft structure

Max Test Temperature: (1118ºF – 1125ºF)

Test Input: Driven by High Speed Flow Concerns

- Edge Heating from area aft of leading edge
- Surface smoothness variation per flight
- Differential LE material on outboard edge must be simulated

Test Type: High Speed Flow for BL Determination

- External acoustic levels should be replicated
- Post buckling strength capability data would be invaluable

Projected Test Chamber: NASA LaRC 8' tunnel, Hampton, Va.

- Has the capability for the q level and temperature
- Can simulate both ascent and descent flight conditions

Projected "Gaps" Mitigated by Tests:

- Will provide an estimate of the boundary layer transition point
- Will provide flow characteristics over simulated panel surface roughness (loss of coating, ablation, etc.)

Projected "Gaps" Not Expected to be Mitigated by Tests:
Limited to the scale of the panel so the test will not necessarily, unless the leading edge structure is incorporated, include the effects of the leading edge and its rate of thermal energy "pass-through"

10.5 PANEL 4

Figure 10.5. shows the projected Panel 4 test specimen and its relationship between the internal and external dynamic test. The test specimen is 4' X 6' ribbed stiffen panel, and two specimens shall fit into an 8' X 6' fixture that simulates the HCV primary structure interfaces. Ideally, the

interface should also approximate the stiffness of the surrounding structures, but for a development test program, a stiff interface should suffice.

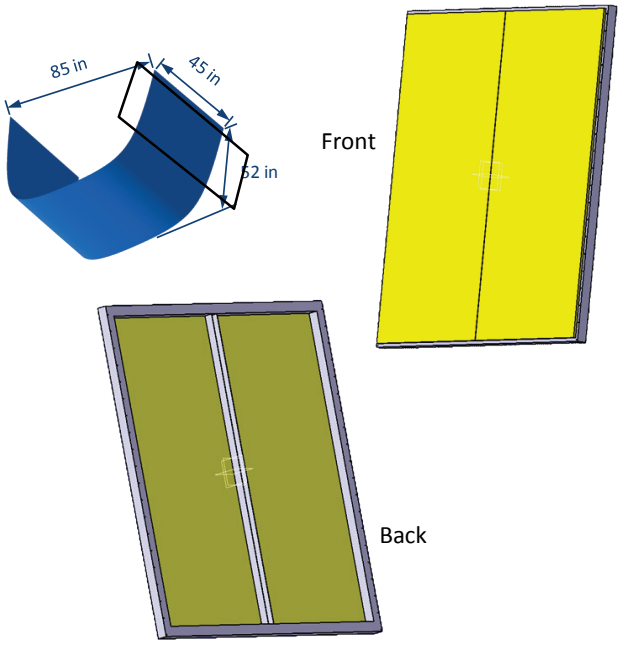

Figure 10.5.1 Panel 4 Suggested Test Specimen

The summary of Panel 4 suggested testing parameters, similar to that for Panel 1, is as follows:

Test Section: 4 ft X 6 ft per Frame, 2 frames

Test Boundary Condition: Support Frame Simulated Primary Aircraft Structures: frame attach method

Max Test Temperature: (1090ºF – 1250ºF)

Test Input: Driven by Dynamics Loading

- External acoustic
- Internal acoustic

Test Type: Thermal-Acoustic Test

- External Acoustic
- Internal Acoustic (Tonal)

Projected Test Chamber: Combined Environment Acoustic Chamber (CEAC), Air Force Research Lab, Wright Patterson Air Force Base, Ohio.

- Acoustic Tunnel
- Acoustic Chamber

Projected "Gaps" Mitigated by Tests:
Panel Survivability
- External Acoustic and Vibration Only

Acoustic Coupling Factor
- Acoustic Test Only

Projected "Gaps" Not Expected to be Mitigated by Tests:
The true effects of the boundary conditions as the tests will be limited to a scale panel. As such, the test will not include the effects of the adjoining panels on the vehicle scale.

As a summary to the projected testing strategy for Panels 1-4, consideration was given to whether design margin, per the static response margins results, would be totally alleviated through the execution of panel testing exercises per the methodology as outlined. ***Figure 10.5.2*** illustrates some thoughts on these test considerations. As an overall statement to the considerations outlined in ***Figure 10.5.2***, which are agreed to be wholly subjective and at the same time, argumentative, the test simulation is only as good as how accurate the boundary conditions are simulated around the test specimen.

		Static Response Margins Results							
Criteria		**Panel 1**		**Panel 2**		**Panel 3**		**Panel 4**	
		Untested	**Margin Est. Improved Through Test?**		**Margin Est. Improved Through Test?**		**Margin Est. Improved Through Test?**		**Margin Est. Improved Through Test?**
Limit Stress	test to limit	0.29		0.50		0.42		0.50	
Ultimate Stress	test to ult./failure	0.25		0.33		0.29		0.30	
Bearing Stress		0.71		0.96		0.91		0.90	
Local Buckling/Stability (LIMIT)		0.02		0.69		N/A		N/A	
Panel Buckling (Ultimate)		0.20		0.29		0.56		0.69	
Waviness Check		0.011" (<0.020")		0.007" (<0.020")		0.006" (<0.020")		0.004" (<0.007")	

High value added per test

some value added but whether margin estimates are improved is questionable

general thought is that margin estimates will not improve

Figure 10.5.2 Panel 1-4 Static Response Design Margins and Testing Thoughts

11.0 PHASE I GAPS SUBSTANTIATED AND VERIFIED IN PHASE II PANEL DESIGN AND ANALYSES

Throughout this project various data have been found to be lacking which would likely be available, or need to be made available, for an actual flight vehicle program. From a detailed hypersonic panels lifetime prediction standpoint, these areas lacking data can best be illustrated by starting with the ideal analysis process.

The Ideal Analysis Cycle for a Hypersonics Flight Program:

1. CFD Analysis performed for the entire flight envelope
2. Thermal data of full vehicle available in FEM map able format (assumes preliminary sizes and any required data from CFD, etc)
3. Materials group to set guideline stress limits based on using these materials at the temperatures derived in thermal model. Limits based on creep, fatigue, etc.
4. Loads Model Run with Baseline Sizes using loads group input and thermal model data (Abaqus Loads Model Ideally)
5. HyperSizer runs on locations of interest based on Loads Model data, using limits from the materials group.
6. Vehicle loads model re-run with HyperSizer sizing results
7. Dynamics model created and run with HyperSizer results
8. Abaqus Sub-Models built and analyzed with the latest Loads+Dynamics Model data and HyperSizer sizes as the starting point, with thermal data either from the Loads Model or direct from thermal model (should be the same). The need to keep to the same stress limits identified by materials group, as well as displacement / stability criteria is paramount.
9. Use sub model data to perform creep analysis.
10. Re-run sub-model with any changes required from creep and fatigue analyses
11. Additional: Re-Run thermal model with final sizes to check for large changes – projected for pre-Phase III program
12. Additional: Verify loads used by re-running Loads Model with final sizes – projected for the pre-Phase III program

Following this analysis outline, the main items lacking on this program level were:

1. Creep data at temperatures of interest, limits identified up front
2. Detailed HCV Thermal Model Results for pertinent vehicle and trajectory. At the time of report publication this is being mitigated by Lockheed Martin internal work.
3. Integrated Abaqus Loads Model for better sub-modeling capability (due to starting with legacy data)

Some other concerns outside of the standard analysis procedure also became evident in this exercise. Two main topics that fall under this classification were: 1) mitigation of thermal gradient loads, and 2) dynamic loads caused by this type of engine. Mitigation assumptions were required on the dynamics loading in order to show acceptable results for Panel 1. An upfront strategy would need to be designed into the vehicle in order to reduce these effects on a future vehicle, such as damping and decoupling when possible. High thermal gradient regions should also be identified as soon as possible from the initial thermal model results in order to start developing mitigating design strategies as soon as possible, such as decoupling parts if possible.

Likewise, during the course of the Phase II program it was readily apparent that "gaps" in the current capability of analyses for hypersonic vehicle structure, some that were first identified during the Phase I project, were exemplified and exploited during the design and analyses tasks of the Phase II program. In addition, new "gaps", or shortfalls in the current simulation and analyses field, were identified. Some of these are and will continue to be considered highly, highly critical to the design process of hot structure for future hypersonic platforms. These are as listed below, and the individual panel or panels that the "gap" or shortfall was most closely associated with during the analyses and simulation tasks of the Phase II program, are in parentheses:

1) Interaction of the fasteners to hole contact, which could be a big determiner of the eventual thermal gradient across the panel along with the overall boundary conditions of the panel (applicable to Panels 1, 3, 4)
2) Ascertaining the flow field variance at an inflection point such as projected rough spots or protrusions within a panel (Panel 1)
3) Capturing the effects of the internal structure heat sink characteristics, and sub-structure motion, and the effects upon the skin temperature and stiffness (Panel 2)
4) Capturing the adequate flutter margin for a relatively flat panel in a highly critical flutter region with reduced stiffness characteristics (Panel 3) – for repeated on-demand hypersonic flight
5) The connectivity of the analyzed acoustic field and its translation to the test environment for highly sonic fatigue critical structure (Panels 1 and 4)
6) Accurate combination of the acoustically induced random vibration loads with the thermally and aero induced load set (Panels 1 and 4)
7) Interaction of the panel coating material and its break down upon repeated cyclic exposure (Panels 1-4)
8) The effect of sonic fatigue induced weakening of adjoining panels (assumptions to be made) (Panels 1 and 4)
9) Assumptions needed on varying emissivity levels based on coating application (analysis in the "as-manufactured" state) (Panels 1-4)
10) Need to make assumptions on material stiffness and "breakdown" versus repeated cyclic exposure (Panels 1-4)
11) Interaction of the coating and its break down upon repeated cyclic exposure (Panels 1-4)
12) Modeling of the thermal transfer around a fastener (or weld joint) (Panel 2)
13) Assumptions on the overall creep rate (for steady state conditions) versus cyclic thermal degradation (Panels 1-4)
14) Comparison of global FEM coarse grid results and eventual sizing per sub-level FEMs of individual components (Panels 1-4)
15) Post buckling performance for flight return and through descent phase loading (Panels 1 and 3)
16) Cool-down effects of internal structure and sensitivity analyses on descent flight so as to cool landing gear structure for impact (Panels 1 and 4)
17) Interaction of the DMRJ acoustic field transmission through internal structure and its effects upon the static response prediction of OML panels. Are there sound energy mitigation techniques available and how is the energy transmission cut when panels are to be in close proximity to the wall(s of the DMRJ propulsion source? (Panels 1 and 4)

18) The contribution of a sandwich core to the creep life of a sandwich panel sheet under the combined environment. Are facesheet material creep property data sufficient for creep life estimates on metallic sandwich panels in the hypersonic environment? On the Phase II program the lack of this data required the assumption that the facesheet creep material data was adequate for sonic for creep life, and this could be highly inaccurate. (Panels 3 and 4)

As was discussed in the Phase I report, the X-33 program revealed a critical relationship between project flight goals and predictive uncertainty. An allocated amount of TPS panel creep deformation was defined for each flight of the X-33 during its 15 flight test demonstration cycles such that the TPS panels would approach their limits as the vehicle reached the end of its design life. The Phase II program findings are similarly detecting uncertainty in these results and not only for creep design considerations but also for acoustic and pressure loads and issues such as panel flutter. A quick program decision on an HCV program, if such a flight program or similar one is developed, could lead decision makers to conclude that an HCV vehicle might have a useful life of only a few flights, or many more than 100, depending on unknowns. These are additional examples of the significant effect that predictive gaps have on perceptions of overall program risk.

12.0 CONCLUSIONS AND SUMMARY

The detailed design and analyses steps for four individual outer mold line panels of a Mach 5+ conceptual level design vehicle have been completed, illustrating the current state of the art in the design and analyses tasks for such structure. In addition, test plan considerations and strategies have been outlined for the Phase III program.

Through the course of the Phase II project it was very apparent that the LM design and analysis process continued to experience various knowledge gaps that have posed areas of uncertainty where conservative assumptions are presently required to mitigate, and usually to the detriment of the vehicle structural weight budget. Knowledge gaps that were first uncovered during the Phase I program through the investigation of previous high speed programs continued to plague the detailed design efforts for hypersonic vehicle structure. To illustrate further, the HTV-3X Mach 6+ demonstrator program schedule and cost environment was understood to be severely limited. As a result, the design approach could not include significant weight margin for structural predictive uncertainty. On a future HCV type program, this will most likely continue to be the case.

As displayed on a number of hypersonic vehicle airframe programs, and most likely for those in the near future, the reduction of current design practice conservative weight margins will require a heavy reduction of thermal, acoustic, and mechanical loading simulation tool solution and assumption uncertainty. Even state-of-the-art structural testing will not reduce all of the uncertainly in analyses and simulations but will, nonetheless, provide much insight on the structural micro-level. However, structural testing will only supplement uncertainty on the macro-level, and system level simulation will remain as the preferred “more economical” approach as system level testing is expensive and will continue to be expensive.

Aircraft industry companies will continue to use simplified coarse grid type vehicle models for conceptual level and preliminary design level analyses, and for rapid turnaround in these levels of analyses. The key here is not so much to increase the number of simulations able to be conducted within a day by orders of magnitudes (which creates storage space issues), but to make these simplified models and simulations “smarter” as aircraft companies are assumed to continue to use simple models and simulations for rapid design turnaround and maturation. The LM design and analysis flow would greatly benefit from advanced simulation capabilities being developed through the Structural Sciences Center at the AFRL. Closer ties and collaborations between academia, government agencies, and industry should be formed soon to develop the simulation capabilities that will eventually be needed to field these platforms.

13.0 REFERENCES

1.) “Hypersonic Predictive Capability - Phase I report”, Zuchowski, Brian, Lockheed Martin Aeronautics Doc. No. FZM-9932, September 30, 2010.

2.) Mil-Hdbk-5J, Metallic Materials and Elements for Aerospace Vehicle Structures, Department of Defense Handbook, 2003

3.) MIL-A-8860B, Aircraft Strength Rigidity

4.) NASA report CR-2801, “Design Procedures for Flutter-Free Surface Panels.”

5.) Kaneko, R. S. (1982). *Ti-6Al-2Sn-4Zr-2Mo Structural Development*, *NASA Contractor Report (CR) 166006.*

6.) AFRL-RB-WP-TR-2010-3068, V1

7.) MIL-STD-810G, Department of Defense Test Method Standard: Environmental Engineering Considerations and Laboratory Tests (31 OCT 2008)

8.) MMPDS MMPDS-05, Metallic Materials Properties Development and Standardization (MMPDS) Handbook

9.) Astech Design Allowables Manual ADAM-100, (1993)

10.) Lockheed Martin Aeronautics. (2005). *FZM-8966. IMAT v2.3 System Description*

11.) Henkener, J.A. (1994, June). Derivation of Crack Growth Properties of Materials for NASA/FLAGRO *2.0, Document Number, JSC-26254.* Houston, Texas: NASA Lyndon B. Johnson Space Center.

12.) U.S. Air Force’s (USAF) Durability Criteria for failure per JSSG 2006 (United States Department of Defense, 30 October 1998)

13.) U.S. Navy (USN) Durability Criteria for failure per MIL-A-8866C, Military Specification: Airplane Strength and Rigidity Reliability Requirements, Repeated Loads, Fatigue, And Damage Tolerance (20 May 1987)

APPENDIX A: HCV EXTERNAL LOAD CASE SET

Thermal case Description	Load Case ID	State Variables				Landing Gear Position
		% Fuel (non-dim)	n_z (g's)	M (non-dim)	h (ft)	
M1.0 Ascent	MP2000M0419F1000	1.000	2.000	0.419	0.000	Gear Up
M1.0 Ascent	MP2000M1134F0952	0.952	2.000	1.134	0.000	Gear Up
M1.0 Ascent	MP2000M1243F0883	0.883	2.000	1.243	0.000	Gear Up
M1.0 Ascent	MP2000M1368F0877	0.877	2.000	1.368	0.000	Gear Up
M2.0 Ascent	MP2000M1510F0814	0.814	2.000	1.510	0.000	Gear Up
M2.0 Ascent	MP2000M1674F0775	0.775	2.000	1.674	0.000	Gear Up
M2.0 Ascent	MP2000M1861F0742	0.742	2.000	1.861	0.000	Gear Up
M2.0 Ascent	MP2000M2079F0714	0.714	2.000	2.079	0.000	Gear Up
M2.0 Ascent	MP2000M2335F0689	0.689	2.000	2.335	0.000	Gear Up
M3.0 Ascent	MP2000M2632F0665	0.665	2.000	2.632	0.000	Gear Up
M3.0 Ascent	MP2000M2966F0642	0.642	2.000	2.966	0.000	Gear Up
M3.0 Ascent	MP2000M3343F0621	0.621	2.000	3.343	0.000	Gear Up
M4.0 Ascent	MP1875M3768F0594	0.594	1.875	3.768	0.000	Gear Up
M4.0 Ascent	MP1750M4246F0559	0.559	1.750	4.246	0.000	Gear Up
M5.0 Ascent	MP1625M4785F0538	0.538	1.625	4.785	0.000	Gear Up
M5.0 Ascent	MP1500M5374F0533	0.533	1.500	5.374	0.000	Gear Up
M5.0 Ascent	MP1500M5546F0528	0.528	1.500	5.546	0.000	Gear Up
M5.0 Ascent	MP1500M5546F0507	0.507	1.500	5.546	0.000	Gear Up
M5.0 Ascent	MP1500M5546F0427	0.427	1.500	5.546	0.000	Gear Up
M5.0 Ascent	MP1500M5546F0332	0.332	1.500	5.546	0.000	Gear Up
M5.0 Ascent	MP1500M5546F0090	0.090	1.500	5.546	0.000	Gear Up
M1.0 Ascent	MN1000M0332F1000	1.000	-1.000	0.332	0.000	Gear Up
M1.0 Ascent	MN1000M1059F0952	0.952	-1.000	1.059	0.000	Gear Up
M1.0 Ascent	MN1000M1161F0883	0.883	-1.000	1.161	0.000	Gear Up
M1.0 Ascent	MN1000M1276F0877	0.877	-1.000	1.276	0.000	Gear Up
M1.0 Ascent	MN1000M1409F0814	0.814	-1.000	1.409	0.000	Gear Up
M2.0 Ascent	MN1000M1563F0775	0.775	-1.000	1.563	0.000	Gear Up
M2.0 Ascent	MN1000M1737F0742	0.742	-1.000	1.737	0.000	Gear Up
M2.0 Ascent	MN1000M1941F0714	0.714	-1.000	1.941	0.000	Gear Up
M2.0 Ascent	MN1000M2179F0689	0.689	-1.000	2.179	0.000	Gear Up
M3.0 Ascent	MN0733M2456F0665	0.665	-0.733	2.456	0.000	Gear Up
M3.0 Ascent	MN0467M2769F0642	0.642	-0.467	2.769	0.000	Gear Up
M3.0 Ascent	MN0200M3120F0621	0.621	-0.200	3.120	0.000	Gear Up
M4.0 Ascent	MN0200M3517F0594	0.594	-0.200	3.517	0.000	Gear Up

Thermal case Description	Load Case ID	State Variables				Landing Gear Position
		% Fuel	n_z	M	h	
		(non-dim)	(g's)	(non-dim)	(ft)	
M4.0 Ascent	MN0200M3963F0559	0.559	-0.200	3.963	0.000	Gear Up
M5.0 Ascent	MN0200M4466F0538	0.538	-0.200	4.466	0.000	Gear Up
M5.0 Ascent	MN0200M5016F0533	0.533	-0.200	5.016	0.000	Gear Up
M5.0 Ascent	MN0200M5197F0528	0.528	-0.200	5.197	0.000	Gear Up
M5.0 Ascent	MN0200M5197F0507	0.507	-0.200	5.197	0.000	Gear Up
M5.0 Ascent	MN0200M5197F0427	0.427	-0.200	5.197	0.000	Gear Up
M5.0 Ascent	MN0200M5197F0332	0.332	-0.200	5.197	0.000	Gear Up
M5.0 Ascent	MN0200M5197F0090	0.090	-0.200	5.197	0.000	Gear Up
M0.3 Hot Landing	MP2000M0419F0000	0.000	2.000	0.419	0.000	Gear Up
M2.0 Descent	MP2000M1134F0000	0.000	2.000	1.134	0.000	Gear Up
M2.0 Descent	MP2000M1243F0000	0.000	2.000	1.243	0.000	Gear Up
M2.0 Descent	MP2000M1368F0000	0.000	2.000	1.368	0.000	Gear Up
M2.0 Descent	MP2000M1510F0000	0.000	2.000	1.510	0.000	Gear Up
M2.0 Descent	MP2000M1674F0000	0.000	2.000	1.674	0.000	Gear Up
M2.0 Descent	MP2000M1861F0000	0.000	2.000	1.861	0.000	Gear Up
M3.0 Descent	MP2000M2079F0000	0.000	2.000	2.079	0.000	Gear Up
M3.0 Descent	MP2000M2335F0000	0.000	2.000	2.335	0.000	Gear Up
M3.0 Descent	MP2000M2632F0000	0.000	2.000	2.632	0.000	Gear Up
M3.0 Descent	MP2000M2966F0000	0.000	2.000	2.966	0.000	Gear Up
M4.0 Descent	MP2000M3343F0000	0.000	2.000	3.343	0.000	Gear Up
M4.0 Descent	MP1875M3768F0000	0.000	1.875	3.768	0.000	Gear Up
M5.0 Descent	MP1750M4246F0000	0.000	1.750	4.246	0.000	Gear Up
M5.0 Descent	MP1625M4785F0000	0.000	1.625	4.785	0.000	Gear Up
M5.0 Descent	MP1500M5374F0000	0.000	1.500	5.374	0.000	Gear Up
M5.0 Descent	MP1500M5546F0000	0.000	1.500	5.546	0.000	Gear Up
M0.3 Hot Landing	MN1000M0332F0000	0.000	-1.000	0.332	0.000	Gear Up
M2.0 Descent	MN1000M1059F0000	0.000	-1.000	1.059	0.000	Gear Up
M2.0 Descent	MN1000M1161F0000	0.000	-1.000	1.161	0.000	Gear Up
M2.0 Descent	MN1000M1276F0000	0.000	-1.000	1.276	0.000	Gear Up
M2.0 Descent	MN1000M1409F0000	0.000	-1.000	1.409	0.000	Gear Up
M2.0 Descent	MN1000M1563F0000	0.000	-1.000	1.563	0.000	Gear Up
M2.0 Descent	MN1000M1737F0000	0.000	-1.000	1.737	0.000	Gear Up
M2.0 Descent	MN1000M1941F0000	0.000	-1.000	1.941	0.000	Gear Up
M3.0 Descent	MN1000M2179F0000	0.000	-1.000	2.179	0.000	Gear Up
M3.0 Descent	MN0733M2456F0000	0.000	-0.733	2.456	0.000	Gear Up

Thermal case Description	Load Case ID	State Variables				Landing Gear Position
		% Fuel (non-dim)	n_z (g's)	M (non-dim)	h (ft)	
M3.0 Descent	MN0467M2769F0000	0.000	-0.467	2.769	0.000	Gear Up
M4.0 Descent	MN0200M3120F0000	0.000	-0.200	3.120	0.000	Gear Up
M4.0 Descent	MN0200M3517F0000	0.000	-0.200	3.517	0.000	Gear Up
M4.0 Descent	MN0200M3963F0000	0.000	-0.200	3.963	0.000	Gear Up
M5.0 Descent	MN0200M4466F0000	0.000	-0.200	4.466	0.000	Gear Up
M5.0 Descent	MN0200M5016F0000	0.000	-0.200	5.016	0.000	Gear Up
M5.0 Descent	MN0200M5197F0000	0.000	-0.200	5.197	0.000	Gear Up
M1.0 Ascent	GP1371M0458F0952	0.952	1.371	0.458	0.000	Gear Up
M1.0 Ascent	GP1854M1059F0952	0.952	1.854	1.059	0.000	Gear Up
M1.0 Ascent	GP1884M1161F0883	0.883	1.884	1.161	0.000	Gear Up
M1.0 Ascent	GP1890M1276F0877	0.877	1.890	1.276	0.000	Gear Up
M1.0 Ascent	GP1882M1409F0814	0.814	1.882	1.409	0.000	Gear Up
M2.0 Ascent	GP1867M1563F0775	0.775	1.867	1.563	0.000	Gear Up
M2.0 Ascent	GP1775M1737F0742	0.742	1.775	1.737	0.000	Gear Up
M2.0 Ascent	GP1680M1941F0714	0.714	1.680	1.941	0.000	Gear Up
M2.0 Ascent	GP1592M2179F0689	0.689	1.592	2.179	0.000	Gear Up
M3.0 Ascent	GP1501M2456F0665	0.665	1.501	2.456	0.000	Gear Up
M3.0 Ascent	GP1421M2769F0642	0.642	1.421	2.769	0.000	Gear Up
M3.0 Ascent	GP1354M3120F0621	0.621	1.354	3.120	0.000	Gear Up
M4.0 Ascent	GP1302M3517F0594	0.594	1.302	3.517	0.000	Gear Up
M4.0 Ascent	GP1255M3963F0559	0.559	1.255	3.963	0.000	Gear Up
M5.0 Ascent	GP1213M4466F0538	0.538	1.213	4.466	0.000	Gear Up
M5.0 Ascent	GP1176M5016F0533	0.533	1.176	5.016	0.000	Gear Up
M5.0 Ascent	GP1140M5197F0528	0.528	1.140	5.197	0.000	Gear Up
M5.0 Ascent	GP1111M5197F0507	0.507	1.111	5.197	0.000	Gear Up
M5.0 Ascent	GP1088M5197F0427	0.427	1.088	5.197	0.000	Gear Up
M5.0 Ascent	GP1070M5197F0332	0.332	1.070	5.197	0.000	Gear Up
M5.0 Ascent	GP1056M5197F0090	0.090	1.056	5.197	0.000	Gear Up
M5.0 Ascent	GP1044M5197F0090	0.090	1.044	5.197	0.000	Gear Up
M1.0 Ascent	GP0629M0458F0952	0.952	0.629	0.458	0.000	Gear Up
M1.0 Ascent	GP0146M1059F0952	0.952	0.146	1.059	0.000	Gear Up
M1.0 Ascent	GP0116M1161F0883	0.883	0.116	1.161	0.000	Gear Up
M1.0 Ascent	GP0110M1276F0877	0.877	0.110	1.276	0.000	Gear Up
M1.0 Ascent	GP0118M1409F0814	0.814	0.118	1.409	0.000	Gear Up
M2.0 Ascent	GP0133M1563F0775	0.775	0.133	1.563	0.000	Gear Up
M2.0 Ascent	GP0225M1737F0742	0.742	0.225	1.737	0.000	Gear Up

Thermal case Description	Load Case ID	State Variables				Landing Gear Position
		% Fuel	n_z	M	h	
		(non-dim)	(g's)	(non-dim)	(ft)	
M2.0 Ascent	GP0320M1941F0714	0.714	0.320	1.941	0.000	Gear Up
M2.0 Ascent	GP0408M2179F0689	0.689	0.408	2.179	0.000	Gear Up
M3.0 Ascent	GP0499M2456F0665	0.665	0.499	2.456	0.000	Gear Up
M3.0 Ascent	GP0579M2769F0642	0.642	0.579	2.769	0.000	Gear Up
M3.0 Ascent	GP0646M3120F0621	0.621	0.646	3.120	0.000	Gear Up
M4.0 Ascent	GP0698M3517F0594	0.594	0.698	3.517	0.000	Gear Up
M4.0 Ascent	GP0745M3963F0559	0.559	0.745	3.963	0.000	Gear Up
M5.0 Ascent	GP0787M4466F0538	0.538	0.787	4.466	0.000	Gear Up
M5.0 Ascent	GP0824M5016F0533	0.533	0.824	5.016	0.000	Gear Up
M5.0 Ascent	GP0860M5197F0528	0.528	0.860	5.197	0.000	Gear Up
M5.0 Ascent	GP0889M5197F0507	0.507	0.889	5.197	0.000	Gear Up
M5.0 Ascent	GP0912M5197F0427	0.427	0.912	5.197	0.000	Gear Up
M5.0 Ascent	GP0930M5197F0332	0.332	0.930	5.197	0.000	Gear Up
M5.0 Ascent	GP0944M5197F0090	0.090	0.944	5.197	0.000	Gear Up
M5.0 Ascent	GP0956M5197F0090	0.090	0.956	5.197	0.000	Gear Up
M0.3 Hot Landing	GP1558M0365F0000	0.000	1.558	0.365	0.000	Gear Up
M2.0 Descent	GP2529M1059F0000	0.000	2.529	1.059	0.000	Gear Up
M2.0 Descent	GP2619M1161F0000	0.000	2.619	1.161	0.000	Gear Up
M2.0 Descent	GP2671M1276F0000	0.000	2.671	1.276	0.000	Gear Up
M2.0 Descent	GP2699M1409F0000	0.000	2.699	1.409	0.000	Gear Up
M2.0 Descent	GP2710M1563F0000	0.000	2.710	1.563	0.000	Gear Up
M2.0 Descent	GP2561M1737F0000	0.000	2.561	1.737	0.000	Gear Up
M2.0 Descent	GP2396M1941F0000	0.000	2.396	1.941	0.000	Gear Up
M3.0 Descent	GP2237M2179F0000	0.000	2.237	2.179	0.000	Gear Up
M3.0 Descent	GP2062M2456F0000	0.000	2.062	2.456	0.000	Gear Up
M3.0 Descent	GP1905M2769F0000	0.000	1.905	2.769	0.000	Gear Up
M4.0 Descent	GP1768M3120F0000	0.000	1.768	3.120	0.000	Gear Up
M4.0 Descent	GP1659M3517F0000	0.000	1.659	3.517	0.000	Gear Up
M4.0 Descent	GP1560M3963F0000	0.000	1.560	3.963	0.000	Gear Up
M5.0 Descent	GP1470M4466F0000	0.000	1.470	4.466	0.000	Gear Up
M5.0 Descent	GP1388M5016F0000	0.000	1.388	5.016	0.000	Gear Up
M5.0 Descent	GP1311M5197F0000	0.000	1.311	5.197	0.000	Gear Up
M5.0 Descent	GP1246M5197F0000	0.000	1.246	5.197	0.000	Gear Up
M5.0 Descent	GP1195M5197F0000	0.000	1.195	5.197	0.000	Gear Up
M5.0 Descent	GP1155M5197F0000	0.000	1.155	5.197	0.000	Gear Up

Thermal case Description	Load Case ID	State Variables				Landing Gear Position
		% Fuel	n_z	M	h	
		(non-dim)	(g's)	(non-dim)	(ft)	
M5.0 Descent	GP1123M5197F0000	0.000	1.123	5.197	0.000	Gear Up
M5.0 Descent	GP1098M5197F0000	0.000	1.098	5.197	0.000	Gear Up
M0.3 Hot Landing	GP0442M0365F0000	0.000	0.442	0.365	0.000	Gear Up
M2.0 Descent	GN0529M1059F0000	0.000	-0.529	1.059	0.000	Gear Up
M2.0 Descent	GN0619M1161F0000	0.000	-0.619	1.161	0.000	Gear Up
M2.0 Descent	GN0671M1276F0000	0.000	-0.671	1.276	0.000	Gear Up
M2.0 Descent	GN0699M1409F0000	0.000	-0.699	1.409	0.000	Gear Up
M2.0 Descent	GN0710M1563F0000	0.000	-0.710	1.563	0.000	Gear Up
M2.0 Descent	GN0561M1737F0000	0.000	-0.561	1.737	0.000	Gear Up
M2.0 Descent	GN0396M1941F0000	0.000	-0.396	1.941	0.000	Gear Up
M3.0 Descent	GN0237M2179F0000	0.000	-0.237	2.179	0.000	Gear Up
M3.0 Descent	GN0062M2456F0000	0.000	-0.062	2.456	0.000	Gear Up
M3.0 Descent	GP0095M2769F0000	0.000	0.095	2.769	0.000	Gear Up
M4.0 Descent	GP0232M3120F0000	0.000	0.232	3.120	0.000	Gear Up
M4.0 Descent	GP0341M3517F0000	0.000	0.341	3.517	0.000	Gear Up
M4.0 Descent	GP0440M3963F0000	0.000	0.440	3.963	0.000	Gear Up
M5.0 Descent	GP0530M4466F0000	0.000	0.530	4.466	0.000	Gear Up
M5.0 Descent	GP0612M5016F0000	0.000	0.612	5.016	0.000	Gear Up
M5.0 Descent	GP0689M5197F0000	0.000	0.689	5.197	0.000	Gear Up
M5.0 Descent	GP0754M5197F0000	0.000	0.754	5.197	0.000	Gear Up
M5.0 Descent	GP0805M5197F0000	0.000	0.805	5.197	0.000	Gear Up
M5.0 Descent	GP0845M5197F0000	0.000	0.845	5.197	0.000	Gear Up
M5.0 Descent	GP0877M5197F0000	0.000	0.877	5.197	0.000	Gear Up
M5.0 Descent	GP0902M5197F0000	0.000	0.902	5.197	0.000	Gear Up
Pre-takeoff M0.0	TP2003M0000F1000	1.000	0.000	0.011	0.000	Gear Down
Pre-takeoff M0.0	TP2002M0000F1000	1.000	0.000	0.011	0.000	Gear Down
M0.3 Hot Landing	TP2003M0000F0000	0.000	0.000	0.011	0.000	Gear Down
M0.3 Hot Landing	TP2002M0000F0000	0.000	0.000	0.011	0.000	Gear Down
M1.0 Ascent	LP2003M0450F1000	1.000	1.000	0.450	0.000	Gear Down
M1.0 Ascent	LP2002M0450F1000	1.000	1.000	0.450	0.000	Gear Down
M0.3 Hot	LP2003M0450F0000	0.000	1.000	0.450	0.000	Gear

Thermal case Description	Load Case ID	State Variables				Landing Gear Position
		% Fuel (non-dim)	n_z (g's)	M (non-dim)	h (ft)	
Landing						Down
M0.3 Hot Landing	LP2002M0450F0000	0.000	1.000	0.450	0.000	Gear Down
Pre-takeoff M0.0	SP1003M0000F1000	1.000	0.000	0.011	0.000	Gear Down
M0.3 Hot Landing	SP1003M0000F0000	0.000	0.000	0.011	0.000	Gear Down

APPENDIX B: PRELIMINARY DESIGN PANEL TRADE STUDY INPUT AND ASSUMPTIONS

PANEL 1

- RET map shows max of ~900°F
- Trade stiffened sheet and honeycomb panel concepts at:
  - Ambient Temperature
  - 400°F
  - 900°F (use 1000°F props if 900°F props are unavailable)
  - max/min edge loadings per HCV mechanical/thermal combined loading results
  - trade between material props in Hypersizer database (preference as listed):
    1. Ti 6-2-4-2S sheet
    2. Ti 6-4 sheet
    3. IN 718 sheet
    4. IN 600 alloy (sheet)
    5. IN 617 honeycomb sandwich construction
    6. Ti Beta 21S sheet

PANEL 2

- RET map shows max of ~1000°F
- Trade stiffened sheet and honeycomb panel concepts at:
  - Ambient Temperature
  - 400°F
  - 900°F (use 1000°F props if 900°F props are unavailable)
  - max/min edge loadings per HCV mechanical/thermal combined loading results
  - assume 10psi tank pressure at all temperatures and in combination with the edge loading condition
  - trade between material props in Hypersizer database (preference as listed):
    1. Ti 6-2-4-2S sheet
    2. Ti 6-4 sheet
    3. IN 718 sheet
    4. IN 600 alloy (sheet)
    5. IN 617 honeycomb sandwich construction
    6. Ti Beta 21S sheet

PANEL 3

- RET map shows max of ~1100°F (at leading edge of panel in the chord-wise direction)
- Trade stiffened sheet and honeycomb panel concepts at:
    - Ambient Temperature
    - 400°F
    - 800°F
    - 1100°F (use 1200°F props if 1100°F are unavailable)
    - max/min edge loadings per HCV mechanical/thermal combined loading results
    - assume 10psi tank pressure at all temperatures and in combination with the edge loading condition
    - trade between material props in Hypersizer database (preference as listed):
        1. IN 718 sheet
        2. IN 600 alloy (sheet)
        3. IN 617 honeycomb sandwich construction
        4. Ti 6-2-4-2S
        5. Ti Beta 21S

PANEL 4

- RET map shows max of 1100°F but as it's in close proximity to the scramjet engines it will be higher (for Hypersizer trade assume 1200°F at equilibrium)
- Trade stiffened sheet and honeycomb panel concepts at:
    - Ambient Temperature
    - 400°F
    - 800°F
    - 1200°F (use 1300°F props if 1200°F props were unavailable)
    - max/min edge loadings per HCV mechanical/thermal combined loading results
    - assume 10psi tank pressure at all temperatures and in combination with the edge loading condition
    - trade between material props in Hypersizer database (preference as listed):
        1. IN 617 honeycomb sandwich construction
        2. IN 718 honeycomb sandwich construction

F.S. 1554 BULKHEAD

- HTV-3X data showed max of 1200°F – 1300°F due to the engines (for Hypersizer trade assume 1200°F at equilibrium)
- Trade structural bulkhead materials at:
    - Ambient Temperature
    - 400°F
    - 800°F
    - 1200°F (use 1300°F props if 1200°F props were unavailable)
    - max/min edge loadings per HCV bulkhead similar web elements loading results
    - trade between material props in Hypersizer database (preference as listed):
        1. IN 718 sheet
        2. IN 600 alloy (sheet)

APPENDIX C: PANEL AEROSMOOTHNESS REQUIREMENTS

LOCATION	FORWARD FACING STEP (INCH)	AFT STEP (INCH)	GAP (INCH)	WAVINESS (INCH)	Flatness Height/Length)
			NOSE/CHINES		
FALCON	None Allowed	0.05	0.055	0.004	<0.050
NASP	None Allowed	<0.1	0.3 on sliding joints for CTE motion	125 RMS	<0.050
X-33	0.03	0.05	0.055	0.004	
			WINDWARD– MIDBODY		
FALCON	0.04	0.04	0.075	0.007	<0.050
NASP	<0.020	0.04	0.3 on sliding TPS joints	250 RMS	<0.050
X-33	0.04	0.075	0.075	0.007	
			LEEWARD-MIDBODY		
FALCON	0.1	0.15	0.1	0.02	<0.050
NASP	0.15	0.15	0.3 on sliding joints	250 RMS	<0.050
X-33	0.1	0.15	0.1	0.02	
			WINDWARD-CANTED FIN		
FALCON	None Allowed	0.05	0.03	0.004	<0.050
NASP	None Allowed	<0.1		125 RMS	<0.050
X-33	0.03	0.05	0.03	0.004	